Weather Route Optimization for Oceanic Vessels

Master of Science Thesis

F.J. Aendekerk

The development of an industrial application of a MATLAB-based weather routing system, starting from performance measurements, aiming at finding the most economical and environmentally friendly routes.

Cover picture: Mineral Nippon, CMB Group [28]

TU Delft

Weather Route Optimization for Oceanic Vessels

Master of Science Thesis

by

F.J. Aendekerk

to obtain the degree of Master of Science
at Delft University of Technology.

Student number: 4180011
Project duration: May 1, 2017 – March 19, 2018
Supervisors: Dr.ir. H.G. Visser
Dr.ir. S. Hartjes
Dr.ir. M. Voskuijl

This thesis is confidential and cannot be made public until January 31, 2020.

TU Delft

Preface

In the wake of the economical crisis of 2008, the shipping industry changed from a very profitable industry to a struggling one, aiming to optimize vessel operations in order to survive. Theories regarding route optimization based on weather and oceanic currents exist, but only few reliable industrial applications can be found. This, together with nowadays global environmental concerns, is where the roots of this project, aiming at developing a route optimization tool for seagoing vessels, based on real-life vessel data, short-term weather forecasts and oceanic currents and monthly averaged sailing conditions can be found. Due to the huge amount of fuel burned by seagoing vessels, achieving just a fraction of fuel savings already results in a significant reduction of global greenhouse gas production.

The concept of weather routing is not new, but the results that can be achieved by using it are not widely documented. In order to quantify this, a weather route optimization tool has been developed. The availability of detailed hindcast datasets made it possible to incorporate monthly averaged sailing conditions in the optimization process, influencing the decision on which route to take when weather forecasts are not available anymore.

Analysis of different ratios between forecasts, monthly averaged conditions and taking the shortest path to describe the sailing environment, led to the conclusion that forecasts are more reliable than sailing according to the monthly averages or taking the shortest path, as long as these forecasts are available. When no forecasts are available, using monthly averages as reference environment is favored over taking the shortest path.

While evaluating randomly selected routes, it became clear that the usage of these monthly averaged sailing conditions can reduce the fuel consumption by 0.59 %, where the total effect of applying weather route optimization is found to be approximately 3.18 %. Due to the limited number of simulations performed and the unstructured nature of the data distribution, the 95 % confidence interval of the expected fuel savings ranges from 2.54 % to 4.02 %.

When assuming the achieved savings are approximating reality, application of weather route optimization on the entire CMB fleet, containing close to 100 vessels, leads to a CO_2 emission reduction almost 80 thousand metric tonnes per year. This is the result of a fuel consumption reduction of 23.5 thousand tons, which would roughly saves 9.35 million US Dollar in bunker costs.

Acknowledgments

With this thesis, I terminate my time as aerospace student, ready to continue developing myself in the real world. This is a suitable time to mention some of the most important persons that helped me to get to this point. Without them, this project would not have been possible.

First of all, I would like to thank Dr.ir. H.G. Visser, my supervisor from Delft University of Technology, for his knowledge when mine was insufficient. Thank you for your guidance and for being there whenever I needed advice or help.

To Ir. Roy Campe Rayco and Quintana-Diaz, my colleagues at CMB, thank you for all the fruitful discussions on weather routing and all the time we spent together.

I would also like to thank Gianandrea Mannarini, scientist at Centro Euro Mediterraneo sui Cambiamenti Climatici and developer of VISIR, a route optimizer for small vessels, for sharing his knowledge concerning weather route optimization with me. The tools and articles he provided me with made it easier for me to complete this project, especially during the early stages.

Ir. Maarten Milis and Toon Hendrikx, who have been supporting me throughout my entire time as fellow student in Delft, thank you for the fun times and cooperation, it has been an honor to complete my studies with you guys around.

To my parents, Ir. Peter Aendekerk and Patricia Kuykx; thank you for everything you have ever done for me. I truly am grateful for your support throughout my educational journey and especially for raising me to become the person I am today.

Jules Jordens and Ir.arch. Arno Maes, thank you for not running away during my endless talking about my thesis; it definitely helped me to strengthen my confidence and understanding during this project.

Last but not least, Sarah Verstreken; I don't know how to thank you for everything you have done for me the last year. You're the best that ever happened to me. You motivate me in every aspect of life, I love you.

F.J. Aendekerk
Antwerpen, March 2018

Contents

List of Figures

List of Tables

1 Introduction

Companie Maritime Belge (CMB) is a Belgian shipping company founded in 1895, operating passenger vessels between Antwerp and Congo. With the independence of Congo and increasing popularity of travel by plane, the company shifted its focus from passenger vessels to dry bulk and container vessels in the sixties, terminating its passenger services in 1972. Today, CMB operates container vessels, dry bulk carriers and chemical tankers [17].

In 2008, the entire landscape of the shipping industry changes due to the economical crisis. Before the crisis, profits on the transported cargo were high, making fast arrival the main goal of the ship operators. After the crash, the main goal became limiting the losses, rather than making as much profit as possible. Fuel management became important, not only to lower operational expenses, but also to reduce greenhouse gas emissions. In 2017, about 740 thousand metric tons of bunkers were consumed by the CMB fleet [1]. Following Nurmi's approach [64], which makes use of the relative constant carbon content of the fuels used, the CO_2 emissions from the CMB fleet are estimated to be 2.34 million tons annually.

It is clear that saving a small percentage of fuel will have a massive impact on fuel costs and CO_2 production. Ship or engine design is something CMB is not (yet) working on, but managing the vessel's operations is done from the CMB headquarters in Antwerp. Choosing the right routes and speeds to sail, can potentially result in a significant decrease in fuel consumption and subsequently improve cost-effectiveness while, at the same time, reduce greenhouse gas emissions. The objective of this research project is to reduce both operating costs and emissions by optimizing the sailing routes for the CMB fleet, based on global current and weather forecasts.

Route optimization for oceanic vessels is a multi-disciplinary problem: it asks for a mathematical ship model, models describing external influences on a ship and reliable weather and current predictions. In addition, it will require a grid-like model that can be used to simulate sailing from point A to point B, as well as optimization algorithms, capable of finding the best expected routes.

There are several approaches to deal with weather routing, as shown in chapter 2, but most of them are theory-focused. Software tools provided by commercial partners to optimize a sailing route are only available at high prices and usually, these companies do not provide their users with the methods used. Another drawback of using a market solution is their vessel models; these require either a lot of specific parameters or are too general, plus they do not account for fouling effects, explained in more detail in chapter 3.

Because of the previously mentioned reasons, the question arose if it would be possible to create an in-house developed route optimization tool, based on weather forecasts and hindcasts, designed for CMB's specific needs. This is the research objective, formulated in the most general way. Depending on the commercial solution presented, weather routing service providers claim between 2 % and 10 % decreased fuel consumption, but without guarantees on these numbers and only very specific examples to validate their numbers, their potential fuel consumption reductions are not very reliable. This gives rise to the first question that will be investigated: *"What are the actual gains of applying weather route optimization strategies when industrial*

conditions, in combination with real vessel data are incorporated in the optimization process?"

CBM's vessels typically perform long voyages, sometimes taking more than two months to complete (e.g. transporting raw materials from Brazil to be processed in China or shipping finished products from China to the East coast of the United States). Usually, weather routing is only applied for the part of the voyage where weather forecasts are available, but with the amount of weather hindcast data available nowadays, it might be possible to determine seasonal or monthly averaged weather and transition towards these values to build a better, more reliable weather routing model. To deal with these routes, the second research question has to be answered: *"What are the optimal influence ratios of weather forecasts, monthly averaged weather and following geodetic routes, to reduce the average fuel consumption the most?"*

Part I
Literature Review

To answer the research questions posed in chapter 1, a multi-disciplinary approach is required. Since the optimal heading and vessel speed are to be found, route optimization can be seen as an optimal control problem. Paraphrasing H.G. Visser on control problems from Course AE4447 - Aircraft Performance Optimization" p.43 [86] and applying the weather routing problem to it, the following things are at least required to build a functional weather routing application:

- A mathematical model: Model describing vessel behavior. This goes from relations between speed and consumption or propeller revolutions and engine setting, to the effect of wind, waves or currents on the consumption.

- Physical constraints: For weather routing, these are related to the vessel and the sailing conditions, but also to the globe's topology and the market-focused constraints, like target arrival time, requested heavy weather avoidance, ...

- Identify performance indicator(s), usually by means of (an) objective function(s): In this case, this can be the fuel consumed, the emissions produced, the required time to reach the target, the total cost of the voyage, ...

- A description of the task: Sail from A to B within a certain time frame, optimizing the required indicator(s) defined above.

Taking this as starting point, the industrial application of weather routing can be represented as a combination of the modules identified in figure 1.1. The remainder of this part will focus on state-of-the-art solutions for each of these modules. By answering the research questions, other interesting characteristics, like weather routing influence on safety (or which cost increases are encountered when choosing a less hazardous route) can be answered.

Chapter 2 will focus on already applied methods to weather routing as well as algorithms showing a lot of potential to achieve good results. Then, in chapter 3, performance prediction methods for seagoing vessels will be discussed, both in perfect and disturbed environmental conditions. Chapter 4 will discuss the available weather forecast models and to wrap up this part, chapter 5 covers the most important conclusions that can be drawn from the literature review.

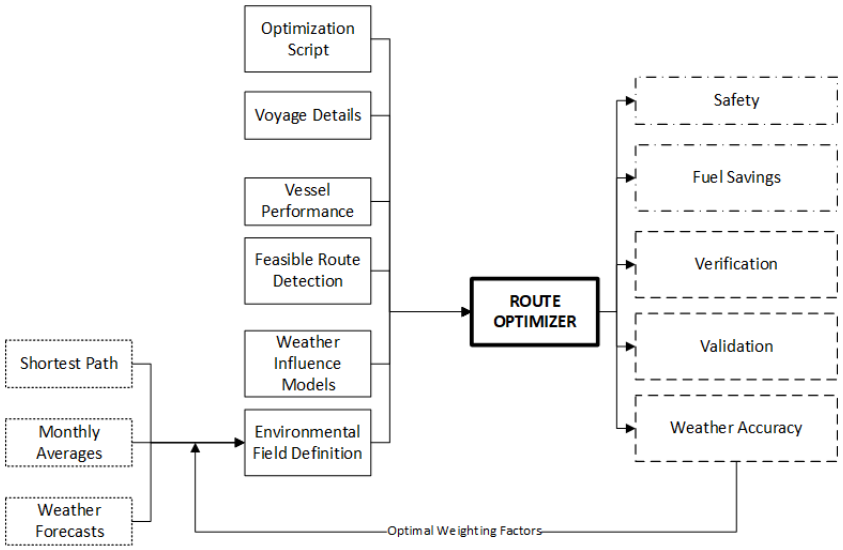

Figure 1.1: Schematic module representation of a weather route optimization tool.

In this figure, the full border lines represent modules, the dotted border lines sub-modules, the dashed lines outputs that are only of interest during the development of the tool and the dash-dotted border lines mark the most important outcomes.

2

Optimization Methods for Weather Routing

The roots of weather routing trace back to 1855, when Maury suggested the usage of ship log based charts, describing winds and currents, to find better sailing routes for (wind-powered) vessels [57]. This was the main routing tool used, until R.W. James proposed his isochrone method in 1957 [45]. From this point in time, several attempts have been made to find optimal sailing routes. Driven by minimal time, minimal fuel consumption and/or minimal costs, the different approaches used can be divided in three main categories, namely the isochrone methods (section 2.1), the methods using calculus of variation (section 2.2) and dynamic programming methods (section 2.3).

2.1. Isochrone Methods

An isochrone is a line of equal time, like an isobar is a line of equal pressure. In case of vessel routing, it represents locations reachable in the same time, as shown in figure 2.1. Based on weather forecasts, distances covered in a certain time step depend on vessel heading, resulting in unsymmetrical isochrones.

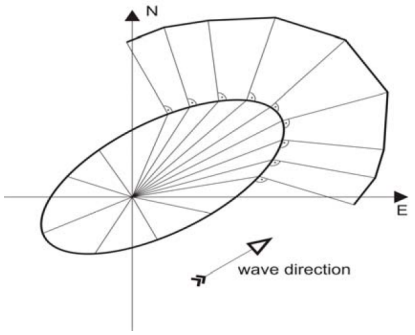

Figure 2.1: Graphical representation of isochrone method, visualized by Szalapczymska and Smierzchalski [81]

The original isochrone method, proposed by R.W. James in 1957 [45], made use of hand calculations to find the fastest arrival times, making use of the maximum attainable vessel speed and reducing that speed according to weather charts. When one isochrone is completed, locations on the isochrone that look promising are selected as new starting points, from which new isochrones are constructed. The outer boundary of the new isochrones is used for the next time step and the process is repeated until the destination is almost reached.

In 1989, H. Hagiwara modifies the original isochrone method, simplifying algorithmic implementation. The algorithm can be described as follows:

1. Simulate movement in all discretized directions for time step Δt and store location reached.

2. From the previously reached locations, new reachable positions are calculated for the next time step. Making use of great circle distances, the points within a selected subset that are furthest away from the origin are stored for this time step.

3. Connect these points to define the isochrone at time step two, the reachable positions in proximity to the great circle between starting and target point are to be used for the next step.

4. Repeat the previous two steps to define a new isochrone.

5. When the isochrone line approximates the target position, start from the closest reachable position to the target and manually calculate the next step.

6. Trace back which intermediate reachable points were used to construct the point on the final isochrone approximating the target position, reconstructing the optimal time route.

From the description above, it becomes clear that Hagiwara's modified isochrone method is a recursive algorithm, making it closely related to the so-called dynamic programming methods. These methods are discussed in more detail in section 2.3. The proposed method is very fast, but only allows for voyage time optimization and lacks the tools to efficiently optimize for minimal fuel consumption. A basic model involving a penalty function is proposed to estimate a fuel-optimal solution, but engine settings are kept constant and heading is the only independent variable used. An intermediate stage of the calculation of a route between the Netherlands and the United States is shown in figure 2.2.

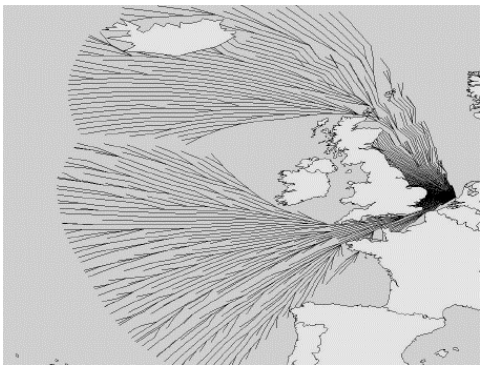

Figure 2.2: Intermediate result of Hagiwara's modified isochrone method [31]

Three years after Hagiwara published his modified isochrone method, M. Klompstra [47] comes up with a model focusing on minimal fuel consumption by incorporating variation of vessel speed as control variable: the isopone method. In this method, the state space is extended from two to three dimensions, including time as state variable.

By extending the state space, it becomes possible to determine isopones, positions attainable in the three-dimensional state space using the same amount of fuel. Figure 2.3 shows a graphical representation of these isopones, as shown in Klompstra's own work. Note that a limit to the time must be set to ensure the model does not approach infinity.

In order to compute the isopones, the state space is discretized. The loss in accuracy by doing so is marginal, knowing weather predictions come in a discretized format. Then, for each heading and time within the discretized system, the position attained after consuming a specified amount of fuel is calculated. Connecting these points results in a barrel-like surface defined in space, which is called the isopone. After calculating this discretized isopone, the isopone is converted to a continuous boundary and then reconverted to a discretized form to initiate the next loop, using equally spread points, based on great circle descriptions.

Despite being theoretically elegant and accurate, as it uses time as independent variable and attained position as dependent variable (which is what happens in reality), this method is not practically applied. As stated by S. Wei and P. Zhou [87], the method is very complex, especially when dealing with land masses, and could

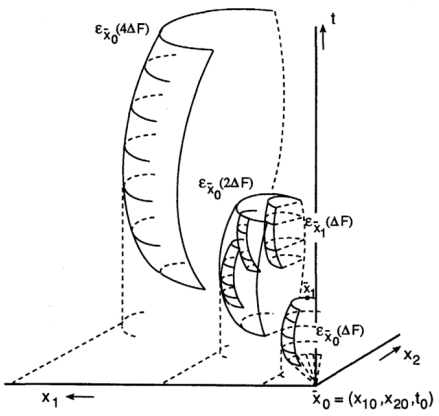

Figure 2.3: Graphical representation of the isopone method by Klompstra, showing energy fronts (isopones) in the three-dimensional space state. [47]

therefore only be efficiently used for the open sea parts of the route. SPOS, a weather routing service offered by MeteoGroup [77] used to apply this method for route optimization, but abandoned it due to operational difficulties, as stated by Weintrit et al. [88].

In 2007, Szłapczyńska et al. [81] modify Hagiwara's modified isochrone method even further by automating land avoidance. A potential reachable point is accepted or rejected by a bitmap based algorithm that checks the potential route for landmasses. By automatically detecting and avoiding land, another step is taken in order to automate the entire weather routing process.

2.2. Calculus of Variations

A second group of methods addressing route optimization, define the objective function as a continuous problem, focusing on minimization by solving (numerical) differential equations. All these methods use speed or engine setting and/or heading as control variables and apply an objective function suiting their specific needs.

Haltiner and Hamilton (1962) [32] are the first ones to propose a method to solve the minimal-time ship routing problem making use of calculus of variation. They solve the Euler-Lagrange equations, assuming constant engine settings.

In 1965, Bleick and Faulkner [12] demonstrate the above method to be feasible for open sea routes and a static environment, but identify difficulties with the complexity and influence of the boundary conditions. In addition, they present a FORTRAN-based code, capable of solving the Euler-Lagrange equations numerically, which shows that it is possible to make software-aided routing decisions.

In 1975, S.J. Bijlsma [11] introduces intermediate arrival/departure points in the Euler-Lagrange equations, making it computationally more efficient. He describes the equations of motion of a vessel as:

$$\begin{aligned} \dot{x} &= V(t, lon, lat, \theta) \cdot cos(\theta) + S_x\big(t, lon, lat\big) \\ \dot{y} &= V(t, lon, lat, \theta) \cdot sin(\theta) + S_y\big(t, lon, lat\big) \end{aligned} \tag{2.1}$$

Where V is speed, depending on time t, position is defined as (lon,lat), heading is denoted as θ and oceanic currents are split up in components S_x and S_y.

From these equations, a generic integral to minimize time is set up (see equation 2.2). Defining $\vec{u}(t)$ as a set of control functions and $\vec{x}(t)$ as vessel position, this is similar to the control problem of Bolza, which is treated in more detail by many sources, for example by H.G. Visser [86].

$$J = \int_{t_0}^{t_1} f_0\big(t, \vec{x}, \vec{u}(t)\big)\, dt \tag{2.2}$$

The focus, however, still lies on time optimization (environmental fields influence speed at predefined engine settings) for open sea parts of a route, and assumptions concerning fuel management make this model inaccurate for cost and emission optimizations and the final results look similar to the results achieved by H. Hagiwara in 1989 with the isochrone method as shown in figure 2.4.

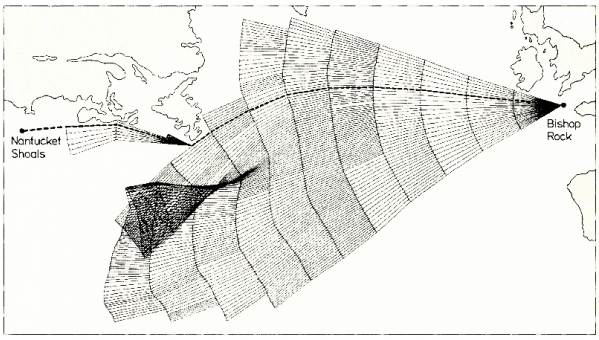

Figure 2.4: Bijlsma's weather routing approach for the open sea part between Bishof Rock and Nantochet Shoals. Note that the kink in the curve next to Newfoundland must be manually implemented in the code. [11]

Papadakis and Perakis (1990) [67] tackle ship routing in a slightly different way, solving initial value problems and boundary value problems. Evaluation of speed as function of time and direction is used to find minimal voyage times, but once again, minimal time is considered rather than fuel efficiency. Varying the engine settings can help to reduce the fuel consumption, but remains a trial and error process and the authors do not manage to prove that the proposed route is truly the most efficient one attainable under the specified conditions.

2.3. Dynamic Programming

Dynamic programming often makes use of Bellman's Principle of optimality. Citing R. Bellman [8] to explain the principle in the most elementary way:

> *"An optimal policy has the property that, whatever the initial state and initial decisions are, the remaining decisions must constitute an optimal policy with regard to the state resulting from the first decision."* ~ R. Bellman in "Dynamic Programming" page 83. [8]

A policy can be seen as a certain decision making process and an optimal policy the policy that gives the optimal result. In other words, the optimal decisions made are only a feasible solution if they can lead to an optimal solution in the end.

Dynamic programming methods dealing with weather routing apply this principle on grid-based routes, calculating time required, fuel consumed, emissions produced,... for a lot of small, potential parts of a voyage. The final result is reached by super-positioning of optimal pieces, while maintaining a clear overview on how intermediate results were obtained.

2.3.1. Greedy Algorithms

Greedy algorithms, are closely related to dynamic programming and are often applied in shortest path finding. One of the most known greedy algorithms is the A-start (A*) algorithm, which solves the shortest path problem according to equation 2.3. P. Hart et al. [33] discuss the A* algorithm for the first time in 1968. By including a heuristic function in the weight assigned to a node, the algorithm gives priority to investigating solutions indicating more potential.

$$J(n) = f(n) + g(n) \tag{2.3}$$

Where J is the cost at node n, f the cost required to reach n and g a heuristic function which guesses the remaining cost [33].

Actually, the A* algorithm is a generalization of the Dijkstra Algorithm, which makes use of a heuristic function equal to zero to find shortest paths. As explained by D. Ostrowski [66], the A* algorithm will not necessarily find the optimal solution due to the approximation induced by the heuristic function. It is, however, much faster than Dijkstra's method because only a subspace of the entire domain is searched.

Dijkstra designed his algorithm in 1956 (and published his work in 1959 [20]) to demonstrate the potential of a revolutionary computer, in such a way anyone would understand it, by building a simplified network of roads between 64 cities in the Netherlands, finding the shortest path from any city to another one [26].

As explained in [20], the algorithm finds the shortest path between two points on a (weighted) graph. In other words, it finds the shortest path between two arbitrary nodes in a network of nodes, connected by edges carrying a certain weight or cost. For weather routing, this could be the time needed to advance from one node on the globe to another, or the amount of fuel burned between two nodes. The algorithm works as follows:

1. Set the cost to reach any node other than the starting node to infinity and floating number. Set cost to 0 at the initial node and label as permanent.

2. Select the initial node as active node and calculate the cost to reach each of its neighboring nodes.

3. In case the newly calculated cost is lower than the current value, replace the old value by the new one (any solution will overwrite the initial infinity values).

4. When all nodes are evaluated, set the temporary node linked to the lowest cost as active node and repeat steps 2 till 4. Since the temporary node containing the lowest cost can never be reached passing through a higher cost node, this node can be labeled as permanent.

5. When the target point is labeled permanent, trace back where this shortest path originated from. This can be done by storing the previous node in the sequence at the moment a node is set to permanent.

The most famous applications of Dijkstra's algorithm are probably (computer) network routing [29], disease propagation tracing [39] and last but not least, it's application in GPS systems worldwide, including Google Maps [21].

2.3.2. 2-D Dynamic Programming

C. De Wit presents his two dimensional dynamic programming (2DDP) method in 1990, starting from a fixed time frame and predefined grid to select a route [19]. To find the best route, the number of propeller revolutions is kept constant, and vessel heading is the only real control variable. The number of propeller revolutions is indirectly a control variable, since its value is varied to match with the arrival time, but it is not changed within the journey. It is an easily understandable method that can be summarized as follows:

1. Build a grid between initial and target location.

2. Set the initial propeller rpm very low, ensuring the target will not be reached within the allowed time frame.

3. Based on the selected propeller rpm, calculate in a Dijkstra-like way how long it would take to reach the target location by calculating the time required for each grid movement and using superposition.

4. If target is reached within the selected time frame, identify the route and propeller rpm as optimal.

5. When arrival is not in time, increase propeller rpm and go back to step 3.

Following this approach, a solution similar to the isochrone method, combined with required %MCR (engine setting as % of the maximum continuous rating) determination for optimal fuel consumption is found. In theory, the assumption of constant %MCR seems logical, since speed and consumption are approximately related with a third power curve, and %MCR is linear with the consumption. However, by maintaining a constant engine setting, the number of options considered is limited. In terms of fuel consumption, it could, for example, be more beneficial to speed up a little at the beginning of a voyage to arrive at a critical point before bad weather arrives there, then slightly slow down for the remaining part of the voyage.

2.3.3. 3-D Dynamic Programming

The 2DDP method discussed above is the starting point for the three dimensional dynamic programming (3DDP) method developed by Wei and Zhou [87]. This approach eliminates the big drawback of the 2DDP method, by incorporating the two main control variables of a seagoing ship in the model, namely the ship heading and the ship speed. To be able to do this, weather routing is tackled in a way similar to the 2DDP method, but the time is added as third dimension (similar to the isochrone and isopone method). By doing this, it is possible to specify a minimal consumption required to reach a grid point (longitude,latitude) within a certain time (t). For each admissible location within a specified time frame, the minimal fuel consumption to get there is saved and used for that specific point in the next loop. A step-by-step procedure is given below:

1. Take the initial point and time to determine the state (X), position (P) and set the active stage (k) to 1.
2. For any potential state X^*, calculate potential fuel consumption F^* and time required to reach a grid position P on stage k+1, using each speed defined in set U (for example, speeds between 5 and 20 kts are considered with an interval of 0.5 kts). Reject solutions that violate time constraint for stage advancement, geographical constraints, safety constraints, ...
3. For each position P at stage k+1, identify the heading, speed and position of stage k requiring the least amount of fuel consumption. The required time and path followed are used as starting point in the next loop.
4. Set stage k+1 as active stage and repeat the previous two steps until the final stage is reached.
5. Trace back the route taken.

Arrival time is treated as a floating number between predefined times, allowing for various speed settings.

In their paper [87], Wei and Zhou present a case-study, showing an additional fuel saving of 5.1 % with respect to the 2DDP method. This is, however, based on a weather situation where the 2DDP method performs worst. The authors provide a second case study, where bad weather does not have a big impact on the state of the ocean. In this case, fuel gains by using the 3DDP compared to the 2DDP method are marginal.

2.4. Conclusions on Optimization Methods for Weather Route Optimization

Apart from the methods discussed throughout the preceding part of this chapter, several other methods have been looked at. The DIRECT algorithm (**di**viding **rect**angles) by D.R. Jones et al. [46] is applied to weather routing by E. Larsson and M.H. Simonsen [51], but has been excluded due to its exponential convergence time for increased mesh size, which is critical in order to accurately model currents and when evaluating long distance trips, which are often sailed by CMB's vessels.

Approaches similar to B. Sridhar's solution to minimal contrail formation for aerospace applications, as presented in [79] by B. Sridhard et al. or in S. Hartjes et al. in [34], are also identified as infeasible as they operate in a relatively static environment and make use of either a function-based environmental description or require complex non-linear programming solutions and interpolated algebraic field descriptions or pseudo-spectral methods (GPOPS [72] is used by S. Hartjes et al., for example). Unavailability of detailed function-wise coast-line and ocean depth descriptions make it impractical to attempt to apply maneuver optimality

algorithms as provided by Q. Gong et al. [70] .

From the three different main approaches used for weather route optimization of ocean going vessels, dynamic programming is identified as preferred approach. Isochrone methods are computationally efficient, but are focused on time optimization and do not provide sufficiently accurate tools to redefine the objective function for different purposes, like fuel, cost or emission optimization.

Whereas the calculus of variation and optimal control theory methods are mathematically elegant, the many discrete operators are involved in the process, like the environmental forecasts, required ocean depth and coastlines, make it very complicated to design a route optimizer that operates on a global level. For open sea parts of a voyage, these methods could prove more useful.

From the dynamic programming methods, the 3D dynamic programming method seems the superior method, because it is using time as independent variable and controlling the position reached by variations in both speed (or %MCR, interchangeable) and heading. Based on a grid describing space and time, the fuel required to move from one location in time and space to another one will be calculated by means of an objective function and the optimal solution will be constructed using a Dijkstra-like algorithm.

3

Vessel Performance

Another module required to develop a functional weather routing optimizer, is a module capable of predicting the performance of the vessel for which an optimal route has to be found. Whereas CFD models would result in the most accurate results, as discussed by MARIN [73], its application is not achievable within CMB at the time being [14]. First of all, the exact hull shape of vessels is not always known. For container vessels, the shape above the waterline changes according to the loading condition and apart from this, fouling effects, discussed in more detail in section 3.2.1 cannot be accounted for.

The remaining two methods to deal with performance, namely theory-focused models, discussed in section 3.1 and data collection methods, treated in section 3.2 are both focused on ideal sailing conditions and require models to fine-tune performance figures, correcting data according to less favorable sailing conditions. Models describing these corrections are summarized in section 3.3.

3.1. Theory-Focused Performance Models

Three different theory-based performance models will be discussed, namely:

- International Tank Towing Conference (ITTC)
- Holtrop and Mennen
- Hollenbach

3.1.1. International Tank Towing Conference (ITTC)

The ITTC is an international NGO related to the International Maritime Organization, focused on hydrodynamics and vessel performance [40]. A conference is held every three years and at the end of each conference, research subjects of interest for the next conference are listed. Three models have been modeled for the Maersk Niagara, a vessel build in 2008 and operating at the same trade for 6 years already, namely the ITCC-1957 [78], ITCC-1978 [25] and ITTC-2011 [44] model.

Each of the models is based on the same principle: measure the resistances of a model in a tank towing test and scale this up for the real vessel. The original model from 1957 is the baseline for the other models, which modify the parameters used to better match actual measurements. The main equations for the 1957 model can be found in equations 3.1 till 3.3. The total frictional coefficient of the model is calculated as follows:

$$C_{M_{tot}} = \frac{R_{M_{measured}}}{\frac{1}{2}\rho_w V_M^2 S_M} \tag{3.1}$$

Where $R_{M_{measured}}$ is the resistance of the model, measured in a towing tank, ρ_w the density of the water, V_M the speed of the model and S_M the wetted surface of the model. Subtracting the calculated frictional resistance C_{F_M} from the measured one results in the so-called residuary resistance coefficient C_R. The calculated

frictional resistance of the model is calculated using equation 3.2.

$$C_{FM} = \frac{0.075}{\left(\log^{10}(Re_M) - 2\right)^2} \tag{3.2}$$

Where Re_M is the model's Reynolds number. The calculated friction resistance of the real ship C_{FR} can be calculated using the same equation, but replacing the model's Reynolds number with the actual one. Now, the total resistance coefficient for a smooth ship C_{FS} can be calculated using equation 3.3:

$$C_{FS} = C_{FS} + C_R + C_A \tag{3.3}$$

In this final equation, C_A represents a coefficient taking ship surface roughness into account. ITTC-57 recommends using a value of 0.0004 in case this coefficient is unknown.

In the ITTC-1978 model, a better equation for the roughness allowance coefficient C_A is used and an equation for the air resistance coefficient C_{AA} is presented. A form factor is also included in the model. More details on the form factor can be found in [58]. The 2011 model slightly adapts the model friction coefficient equation. More details on each of the models can be found in the references provided.

3.1.2. Holtrop-Mennen

J. Holtrop and G.G.J. Mennen propose an alternative method to predict the fuel consumption of vessels in 1978, calculating the total resistance experienced while sailing through water [37].

Seeing the success of their method, J. Holtrop and G.G.J. Mennen re-evaluate their method using more measurement data, improving the vessel types that can be analyzed and adapting their empirical relations [38]. In corporation with MARIN, J. Holtrop decided to improve the Holtrop-Mennen method even further [36]. Increasing complexity of the empirical equations, even more vessel configurations could be used (e.g. twin-screw configurations were included here).

To model the resistance of the Maersk Niagara, the excel calculator "Estimacion de la resistencia por el metodo de holtrop y mennen" by C. Estacio Gomez (in Spanish) [27] is used.

3.1.3. Hollenbach

K.U. Hollenbach [35] made use of 15 years of data available from the Vienna Towing Tank to provide an even better estimation of power predictions. Apart from a best fitting regression model, a minimal consumption curve designers could possibly achieve is also given. Just like Holtrop-Mennen, the method functions well for maritime designers during the preliminary phase, but can be used for performance modeling as well. The total resistance coefficient is expressed in equation 3.4. For more details on the model coefficients, the reader is referred to [35] or appendix A.1.

$$\begin{aligned} C_R = C_{R_{base}} C_{R_{Fn,crit}} d_1 L^{d_2} \left(\frac{T}{B}\right)^{a_1} \left(\frac{B}{L}\right)^{a_2} \left(\frac{L_{os}}{L_{WL}}\right)^{a_3} \left(\frac{L_{WL}}{L}^{a_4}\right) \left[1 + \left(\frac{T_A - T_F}{L}\right)\right]^{a_5} \cdot \\ \cdot \left(\frac{D_P}{T_A}\right)^{a_6} (1 + N_R)^{a_7} (1 + N_{Br})^{a_8} (1 + N_{Bo})^{a_9} (1 + N_{Thr})^{a_{10}} \end{aligned} \tag{3.4}$$

Using C_R as total resistance coefficient, $C_{R_{base}}$ as base resistance, $C_{R_{Fn,crit}}$ the resistance coefficient at critical Froude number, T the average draft, which is the mean of the aft draft T_A and front draft T_F, B the breadth of the ship, L the total length, L_{os} distance between aft water line and must frontal point of the vessel, L_{WL} the length of the waterline, D_P the propeller diameter and coefficients with subscript a and d as tabulated in [35].
The strength of Hollenbachs method is that it does not only present an expected performance curve, but also a curve discussing the best possible result (which is a good reference for designers) and a worst case performance curve. The curves are visualized in the succeeding section.

3.1.4. Theoretical Model Comparison

To compare the different methods discussed in the previous section, all methods are applied to an existing vessel, the Maersk Niagara. The exact dimensions of this vessel are known, and sea trial and tank towing test data is available. The resulting graph is shown in figure 3.1. A big difference between the different methods can be seen. Note that for the Hollenbach method, propeller efficiency is assumed to be 0.70 and total mechanical efficiency is estimated at 0.97.

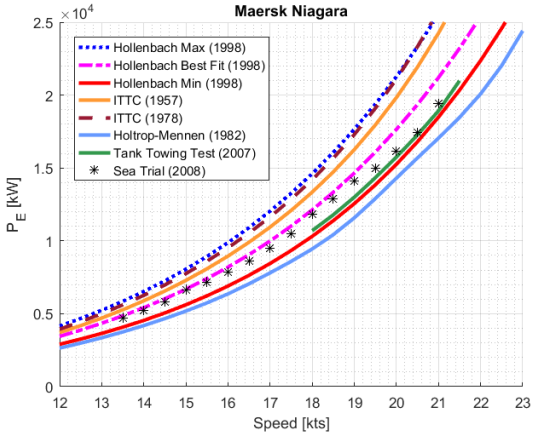

Figure 3.1: Graphical representation of different power prediction methods

The most realistic data available is the data provided during the sea trials, since actual measurements are used rather than mathematical models. For now, assume the sea trial data is the actual performance of the Maersk Niagara; the mean value of the Hollenbach prediction method seems to be the best approximation for speeds up to 19 knots, after which the sea trial data moves closer to the minimal achievable data of (again) the Hollenbach method. This makes sense, knowing the design speed of the vessel decided before the 2008 economical crisis, was set much higher than operational speeds of today. The differences between the different outcomes of the Hollebach method, the sea trial data and the actual operational data obtained by CMB itself will be discussed in the next section.

3.2. Data Analysis Performance Models

To maintain an overview of the performance of the fleet, all captains send a detailed performance report every day at noon. This report, called a noon report, includes the amount and different types of fuel consumed, speed sailed, weather conditions, currents, engine settings, average propeller revolutions, ... The interface is shown in figure 3.2.

These reports are used as input of an internally developed program called Fleet Performance Monitoring (FPM) by F. Aendekerk [2], designed for performance analysis of the entire CMB fleet. Simultaneously with this project, FPM is further developed, aiming to have a proper interference between the performance monitoring tool and the weather route optimizer.

Knowing FPM is designed for real-time performance analysis, it is chosen to calculate performance curves within this tool. FPM automatically analyses all the vessels at night and stores the relevant values outside the program. The values of the ship of interest can be reloaded in any MATLAB environment and can thus be used for the weather route optimizer.

3.2.1. Fleet Performance Monitoring - Basics

To gain more understanding in how FPM works, the reader is referred to [1]. In this project, it is assumed that the values produced by FPM are correct. A brief summary of FPM will be presented in this section to show

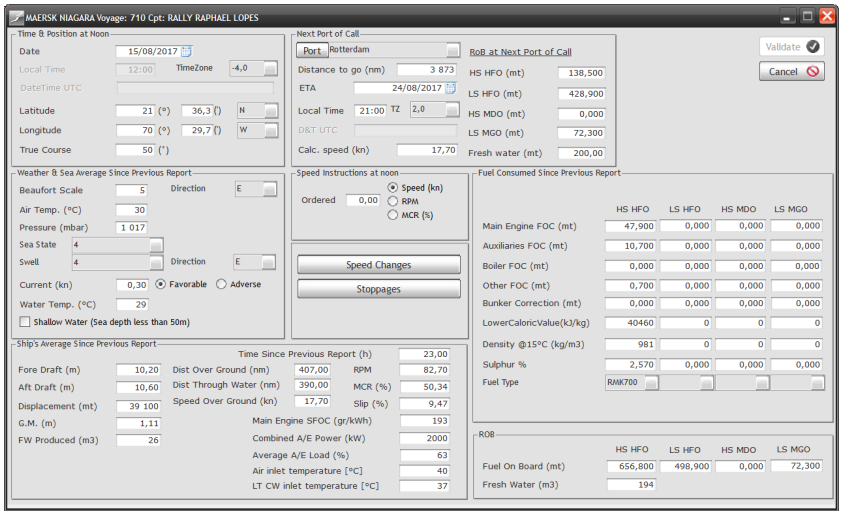

Figure 3.2: Noon Report user interface, needs to be completely filled in every noon by each captain.

the strength of using the tool.

The 5 most important tools provided within FPM are:

1. Data gathering: this is done by making the right call to an SQL server
2. Data filtering: Specified by the user, most severe conditions are usually not taken into account, days containing a commence or end of sea passage are usually omitted,...
3. Data normalization: The filtered data is converted to ideal sailing conditions with standard fuel (LHV: 42700 kJ/kg).
4. Post-processing: Performance curves are generated, errors are monitored, numbers to include in contracts are provided, ...
5. Fouling detection: hull condition is monitored over time, from which decisions to clean hulls or plan dry-docks are made.

Going from step 1 to step 3 is visualized in figure 3.3.

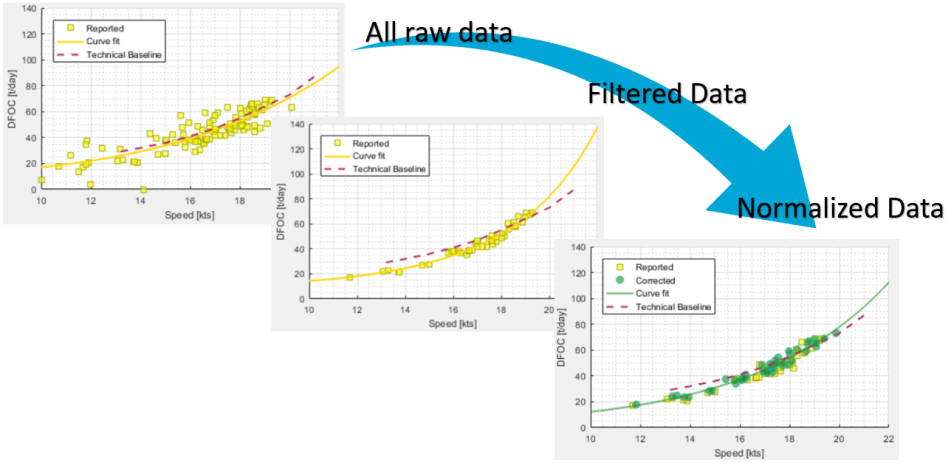

Figure 3.3: Graphical overview of FPM's application of filtering and normalization.

As shown in figure 3.4 curve produced by FPM are close to the sea trial results and transition from close to Hollenbach's best fit at low speeds towards the minimum achievable solution of Hollenbach at higher speeds.

This makes sense, knowing the vessel was designed to operate at high speeds, which was the standard before the economical crisis of 2008.

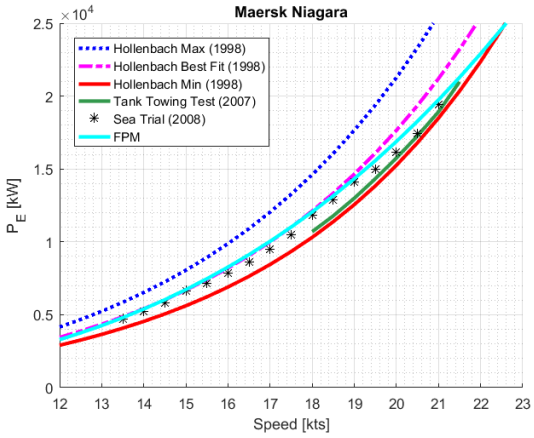

Figure 3.4: Quality indication of FPM curve of the Maersk Niagara

At this moment, it is important to introduce fouling, which can be seen as any unwanted attachments to the hull of a vessel, usually in the form of mussels or sea weeds. This can severely reduce the hydrodynamic performance of the vessel, causing up to 30 % increased fuel consumption [2]. Figure 3.5 shows the change in performance over time of the Mineral Subic, a CMB vessel that was severely affected by fouling last year.

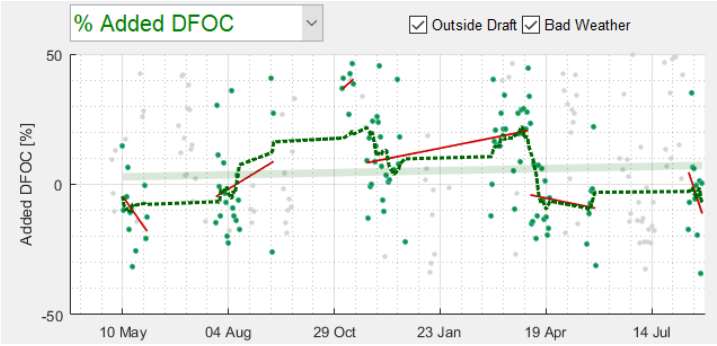

Figure 3.5: Relative consumption over time, compared with best fitting performance curve generated by FPM. Idle periods in July 2016, October 2016 and March 2017. Green dots represent noon reports accepted by all filters, grey dots are points not passing the filters of FPM, green lines are trend lines over time, red lines are trend lines over periods without idle periods of more than 14 days or cleanings.

From these figures, it can be seen that the idle period in October 2016 decreased performance, after which it was immediately decided to clean the vessel, which reduced the consumption back to the level of before the idle period. A similar story can be seen in April 2017, where another cleaning was necessary.

3.3. Environmental Influences

The above sections deal with vessel performance under ideal circumstances when it comes down to the environment. There are several factors influencing the real performance of vessels. The main environmental contributors are:

- Wave resistance
- Wind resistance
- Oceanic currents

3.3.1. Wave Resistance

Oceanic waves are the biggest contributor to the additional resistance experienced by seagoing vessels due to the sailing environment [45]. Luo et al. [52] state that the average added wave resistance $\overline{R_{AW}}$ depends on the wave height ζ, directional wave spectrum $S_\zeta(\omega,\theta_{wave})$, wave frequency ω and a ship specific response function $R_{AW}(\theta,\omega)$ as shown in equation 3.5.

$$\overline{R_{AW}} = 2\int_0^\infty \int_0^{2\pi} \frac{R_{AW}}{\zeta^2} \cdot S_\zeta \cdot d\theta_{wave} \cdot d\omega \tag{3.5}$$

This equation is internationally accepted by the ISO 15016 standard [42] (see Annex D, where it is worked out in more detail), but requires a ship specific response function, based on an accurate CAD model for each vessel and not freely available software ShipX from MARINTEK [54]. Therefore, the ISO 15016 standard provides another, more general model, presented in equation 3.6 and 3.7. This equation is based on Kreitner's formula for added wave resistance [48] and is, according to the ITTC of 2005, still a viable model [43].

$$\overline{R_{AW}} = \frac{1}{16} \cdot \rho_{sw} \cdot H_s^2 \cdot B \cdot \sqrt{\frac{B}{L_{WL}}} \tag{3.6}$$

$$R_{AW} = \left[\frac{2}{3} + \frac{1}{3} cos(\theta_{wave})\right] \cdot \overline{R_{AW}} \tag{3.7}$$

With total added wave resistance R_{AW}, sea water density ρ_{sw}, significant wave height H_s, ship breadth B, waterline length L_{WL} and θ_{wave} the incidence angle of the waves relative to the sailing direction.

This method only takes length and breadth of the vessel into account, and does not provide extremely accurate results; however, it can be used as a decent approximation of added resistance through waves. As the focus of this research project lies on route optimization rather than wave resistance prediction, it is decided that this model will be sufficiently accurate to be included in the route optimizer. Decent object-oriented programming will make it possible to replace this model when it appears to be of insufficient accuracy.

3.3.2. Wind Resistance

A first model dealing with wind resistance on vessels, is proposed by Isherwood in 1973 [41]. According to Isherwood, the wind influence parallel to the sailing direction can be estimated using equation 3.8:

$$R_{wind} = \frac{1}{2} C_x \rho_{air} V_{wind}^2 A_T \tag{3.8}$$

Where R_{wind} is the total resistance generated by the wind, C_x the resistance coefficient in longitudinal direction and A_T the transverse projected area above the water line.

To estimate the total resistance, the resistance coefficient is calculated using the following empirical resistance coefficient formula:

$$C_x = a_0 + a_1 \frac{2(A_L + A_{SS})}{L_{oa}^2} + a_2 \frac{2A_T}{B^2} + a_3 \frac{L_{oa}}{B} + a_4 \frac{S}{L_{oa}} + a_5 \frac{C}{L_{oa}} + a_6 M \tag{3.9}$$

Where A_L is the lateral projected area, A_T the transverse projected area, A_{SS} the lateral projected area of the superstructure, L_{oa} the overall length, B the breadth, S the length of the perimeter of the lateral projection, excluding waterline and slender bodies, C the distance between the bow and the centroid of the lateral projected area and M the number of groups of masts/kingposts seen from the side, not accounting for the bridge. all "a" components are empirical dimensionless numbers found by regression, documented in Isherwood for every ten degrees of wind direction relative to the vessel.

Whereas Isherwood shows his model to be the best available empirical model at the time being, there are several limitations to his method. Looking at figure 3.6, it becomes clear that different placement and number of containers make variables S and C hard to define, making it hard to apply this model on big scale within an industrial environment, where a lot of different configurations are used.

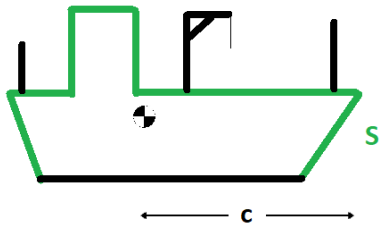

Figure 3.6: Description of variable coefficients S and C, used in Isherwood's wind correction model

Another method is proposed by Blendermann [13], who investigated wind influence on vessels in a semi-empirical way in 1996, making use of scaled models in a towing tank. With tests on 15 different type of vessels, he created formulas to estimate wind influence on each vessel type. From his equations, it can be seen that the force coefficient in sailing direction mainly depends on the wind direction, the frontal and longitudinal projected area above the water line and three vessel-type specific parameters, namely the cross-force parameter, the longitudinal resistance coefficient and the lateral resistance coefficient. The main coefficients influenced by the wind are:

$$C_X = \frac{X}{q \cdot A_F} \quad , \quad C_Y = \frac{Y}{q \cdot A_L} \tag{3.10}$$

$$C_N = \frac{N}{q \cdot A_L \cdot L_{oa}} \quad , \quad C_K = \frac{K}{q \cdot A_L \cdot H_M} \tag{3.11}$$

Where C_X is the wind induced resistance coefficient in sailing direction, C_Y the resistance coefficient in lateral direction, C_N the yawing coefficient, C_K the rolling coefficient, A_F frontal projected area above the waterline, A_L lateral projected area above the waterline, L_{oa} overall vessel length, H_M the reversal of the aspect ratio ($H_M = \frac{A_L}{L_{oa}}$) and the dynamic pressure q.

To calculate the coefficients, a similar approach to Isherwood is used, but more data is used and more recent vessels are used as reference. Equations 3.12 till 3.15 describe Blendermann's approach.

$$C_X = -C_{D_l} \cdot \frac{A_L}{A_F} \cdot \frac{cos(\epsilon)}{1 - \frac{\delta}{2} \cdot \left(1 - \frac{C_{D_l}}{C_{D_t}}\right) \cdot sin^2(2\epsilon)} \tag{3.12}$$

$$C_Y = C_{D_t} \cdot \frac{sin(\epsilon)}{1 - \frac{\delta}{2} \cdot \left(1 - \frac{C_{D_l}}{C_{D_t}}\right) \cdot sin^2(2\epsilon)} \tag{3.13}$$

$$C_N = \left[\frac{s_L}{L_{oa}} - 0.18 \cdot \left(\epsilon - 90^o\right)\right] \cdot C_Y \tag{3.14}$$

$$C_K = \kappa \cdot \frac{s_H}{H_M} \cdot C_Y \tag{3.15}$$

Where C_{D_l} is the longitudinal resistance coefficient, C_{D_t} the lateral resistance coefficient, A_F frontal projected area above the waterline, A_L lateral projected area above the waterline, ϵ the incidence angle of the wind relative to the sailing direction, δ the cross-force parameter, s_L the longitudinal arm, s_H the vertical moment arm and κ the rolling moment factor. A detailed description of the coefficients can be found in appendix A in table A.2.

Oil Companies International Marine Forum (OCIMF) demonstrate yet another method, using a combination of parameters and graphs to determine the wind resistance [65]. This method is almost the same as Blendermann's method [13], but uses tabulated values for the resistance coefficient.

M. Haddara and C. Guedes Soares [30] compare Isherwood's method, Blendermann's approach, the above mentioned OCIMF solution and the Gould method (not discussed here). They are in favor of using Blendermann's approach, but conclude there is no "best method" to deal with wind resistance. Their final statement sums up wind predictions pretty well. Directly citing from [30] :

> *"Generally speaking the comparative study indicates that there is no general agreement between the methods used for the estimation of wind forces on ships. The experimental results obtained by Blendermann are the most comprehensive and reliable among the four methods."*
> ~ M. Haddara and C. Guedes Soares in "Wind Loads on Maritime Structures" page 209.

3.3.3. Oceanic Currents

A third and last environmental influence is the current experienced by the evaluated vessel. N. Bialystocki et al. [10] reason that current can be seen as a moving block of water the vessel is emerged in, allowing to add the current and its direction to the vessel's movement. N. Kristensen [49] draws the same conclusion. Where weather influences convert the environment to a resistance or increased consumption, currents are evaluated to modify the sailing speed of the vessel. Note that, for wind corrections, speed over ground is still used. For sailing speed corrections, equation 3.16 will be used:

$$V_{tw} = V_{OG} + V_c \cdot cos(\theta_c) \tag{3.16}$$

Where V_{tw} is the speed through water, V_{OG} the speed over ground, which is reported by the vessels, V_c the speed of the current and θ_c the incidence angle of the current. This can be assumed when the sailing speed is much larger than the current speed. Based on the Global Real-Time Ocean Forecast System (GRTOFS) [24], which is based on the HYCOM model [16], downloaded from the NOAA server on October 1, 2017 [62], this is a valid assumption, as the average current reported is 0.23 $\frac{m}{s}$ and the maximum value found is 2.5 $\frac{m}{s}$, much lower than typical operational speeds of vessels.

3.4. Conclusions on Vessel Performance

For the performance under ideal conditions, using FPM data is the best available method because it provides real-time performance rather than theoretical results, including potential performance deterioration in the calculations.

For the environmental influence models, following choices have been made:

- Wave resistance: Adapted Kreitner model. This model was chosen because the all required parameters are available for every CMB vessel.
- Win resistance: Blendermann model, which seems to be performing best according to M. Haddara and C. Guedes Soares [30]. In addition, these parameters are also available for any CMB vessel.
- Oceanic currents: Speed modification assuming the vessel is emerged in continuous water flow.

To ensure flexibility in the methods used and enable easy replacement, separate functions for the correction models will be build with power required to overcome as output. By doing so, any module can either be disabled by forcing a zero as output, or be replaced by any other model that can be converted to required power.

4

Weather and Current Forecast

Models to deal with the influence of the sailing environment on vessel performance have been identified, but the values used to define the environment have to come from somewhere. This chapter will discuss the available weather and current data forecasts and how these will be processed to an operational format.

4.1. Wind and Wave Predictions

The first required forecast provides wind and wave predictions. Since a part of the waves is generated by the wind, wind and waves will be threated together. The National Oceanic and Atmospheric Administration (NOAA) provides a model simulating wind and waves for the upcoming eight days [61]. With the massive increase in computational power due to the supercomputer upgrade from January 2016 (going from 0.776 petaflops to 5.78 petaflops) [63], the latest stable release of the Wavewatch III model, version 5.16, has increased accuracy. Wavewatch III is based on Tolman's model from 1989 [85], which originally was designed at Delft University of Technology to accurately present hindcast wind and wave data. The method of forecast acquisition is placed outside the scope of this project, but the forecasts will not be blindly trusted. More information concerning forecast accuracy can be found in section 4.3.

To create an operational program, the data is automatically gathered using an executable created by MATLAB's application compiler [82]. This executable stores the available forecasts on a local server every night. The data format used by NOAA is a grib2 format, a compressed format designed for weather data transfer. To process this format, B. Schlining's "NC Toolbox" [74] could be used, but due to Java library interference, the toolbox is not usable for compiled scripts [75], which is required to ensure proper software functioning for an extended period of time.

MATLAB has build-in functions for NetCDF formatted files (the format used for oceanic current forecasts) available, which function well within a runtime compiler environment. Therefore, it was decided that a Linux-based application, wgrib2 [22], is simulated on Windows 10 using cygwin [5], converting the unreadable grib2 files to NetCDF format, which can be handled by MATLAB. Processed data is stored for an extended period of time to facilitate verification and validation in a later state of the project, which is discussed in more detail in chapter 11. The wind and wave data is visualized in figures 4.1 and 4.2, where land is created using the M_Map package of R. Pawlowicz et al. [68]. Being able to produce charts of the numerical data shows that the interpretation of the fully numerical weather datasets does not contain errors.

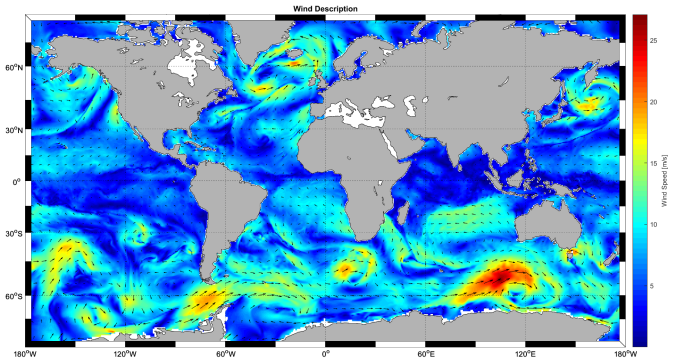

Figure 4.1: Wind prediction and direction, provided by NOAA's Wavewatch III model, visualized in MATLAB

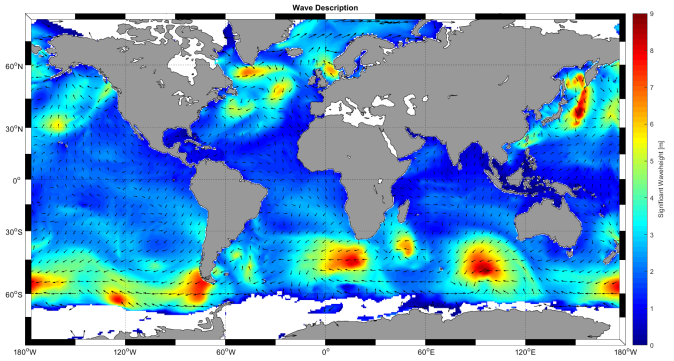

Figure 4.2: Significant waveheight prediction, provided by NOAA's Wavewatch III model, visualized in MATLAB

4.2. Current Predictions

The third and last discussed external influence on the vessel is the current, which is provided by NOAA's Global Real-Time Ocean Forecast System (GRTOFS) [62]. Again, forecasts up to eight days are available, but this time, the data is already provided using NetCDF. Using a similar approach to the one described for wind and waves, data is stored on the local servers. One dataset per day will be downloaded, which has a resolution 0.08 degrees by 0.054 degrees. An example forecast is shown in figure 4.3.

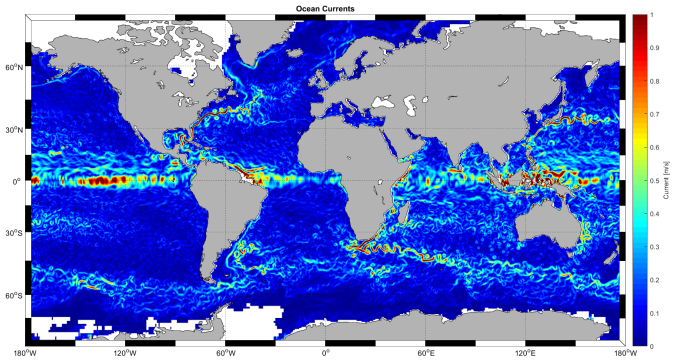

Figure 4.3: Oceanic current, provided by NOAA's GRTOFS model, visualized in MATLAB

4.3. Monthly Averages

With the amount of data and processing power available nowadays, it becomes possible to create maps describing expected seasonal weather. These seasonal averages used to be available for free, provided by the European Centre for Medium-Range Weather Forecasts [69], but is now subjected to a subscription fee. Therefore, it was decided that the hindcast data available through the NOAA servers will be used to create monthly averages to deal with reduced weather forecast reliability. This research aims at finding optimal influence ratios between weather forecasts, monthly averages and shortest paths, making the monthly averages a key component.

Wind and wave hindcasts are available starting in March 2005, and oceanic current data starts from 1993. This allows for averaging of 11 and 24 full years, respectively. Looking at the standard deviations, reliability statements can possibly be made, which can be incorporated in the weather routing, adding seasonal average weights inversely proportional to the standard deviation.

The results of averaging the wind, waves and current over the 11 and 24 year period on monthly basis results in smoother conditions than originally expected. For the wind and waves, a 3-hour interval hindcast of 4 017 days has been included in the averaging process, using a total of 32 136 global wind and wave hindcasts, each containing 720x311 data points, equaling a total of 7 195 893 120 points. Current hindcast from 1993 till 2016 is reported every 5 days, thus resulting in 1 728 global models containing 1080x481 data points, resulting in a total of 897 661 440 points used. To deal with this amount of data, the original data files are partitioned and restructured. The final values found are summarized in table 4.1 and results of the month June are visualized in figures 4.4 till 4.6.

Table 4.1: Monthly Averages: stored parameters

Parameter	Unit	Matrix size	Mean value	Mean standard deviation
Wind: u-component	$[\frac{m}{s}]$	720x311	0.3864	4.5433
Wind: v-component	$[\frac{m}{s}]$	720x311	0.1293	4.5784
Wind: speed	$[\frac{m}{s}]$	720x311	7.7040	2.981
Waves: significant height	$[m]$	720x311	2.5942	0.8707
Waves: direction	$[deg]$	720x311	215.480	22.651
Current: u-component	$[\frac{m}{s}]$	1080x481	0.0048	0.1059
Current: v-component	$[\frac{m}{s}]$	1080x481	0.0046	0.1020
Current: speed	$[\frac{m}{s}]$	1080x481	0.1620	0.0827

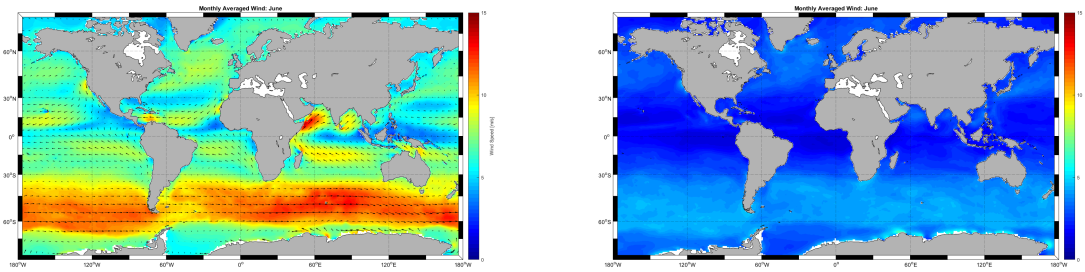

(a) Average speed and direction

(b) Standard deviation of wind speed

Figure 4.4: Monthly averaged wind characteristics

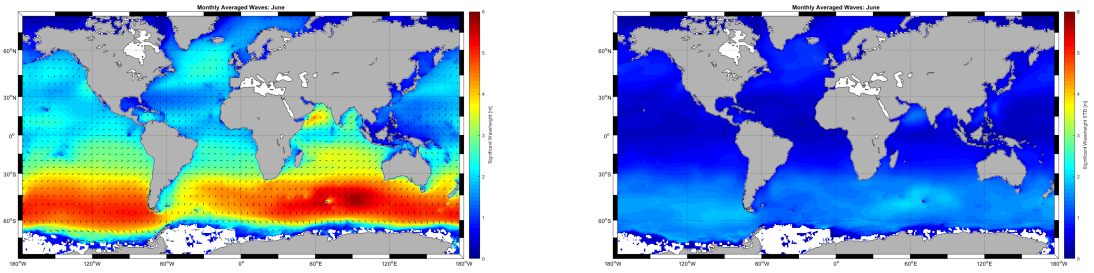

(a) Average significant waveheight (b) Standard deviation of significant waveheight

Figure 4.5: Monthly averaged wave characteristics

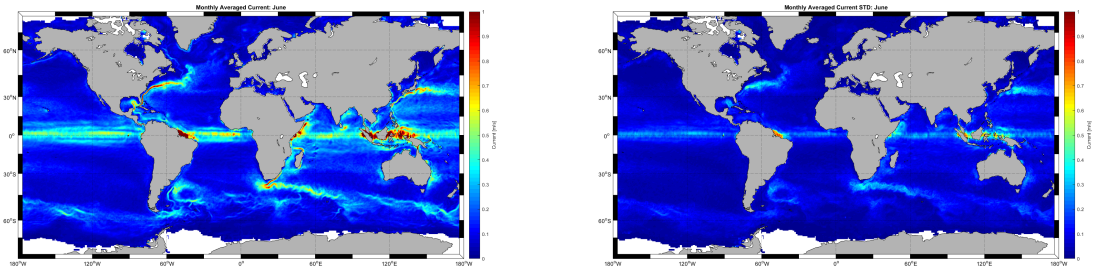

(a) Average current speed (b) Standard deviation of current speed

Figure 4.6: Monthly averaged current characteristics

From the figures of the monthly averages and standard deviations, it can be seen that the standard deviations are usually quite small compared to the averaged values, indicating that the usage of monthly averaged sailing conditions can result increase the performance of optimal route detection.

5

Main Conclusions of the Literature Review

In the previous chapters, the most important modules for a weather routing application have been discussed. In order to build the application and provide an answer to the research questions, a tool based on Dijkstra's Algorithm and a 3-D dynamic programming approach is selected. The ideal sailing condition performance will be determined by FPM [2].

To evaluate performance in real sailing conditions, the performance figures will be adjusted for the three main influences, namely the current, the waves and the wind. Current will be dealt with using a moving-block approach and the HYCOM forecasts provided by NOAA [62]. For the wind and waves, the Blendermann model [13] and modified Kreitner model [48] will be used, taking weather predictions from NOAA's WaveWatch III model [61].

To increase the selection of best routes and in an attempt to avoid detours that appear to be unnecessary due to wrong predictions of current and/or weather, monthly averaged conditions have been generated on a global level. The final decision on which route to sail will thus not only be based on weather predictions, but also on monthly averaged weather and potentially on shortest path sailed.

These conclusions have been included in the schematic representation of the weather route optimizer shown in figure 1.1, summarizing this part of the project in one figure.

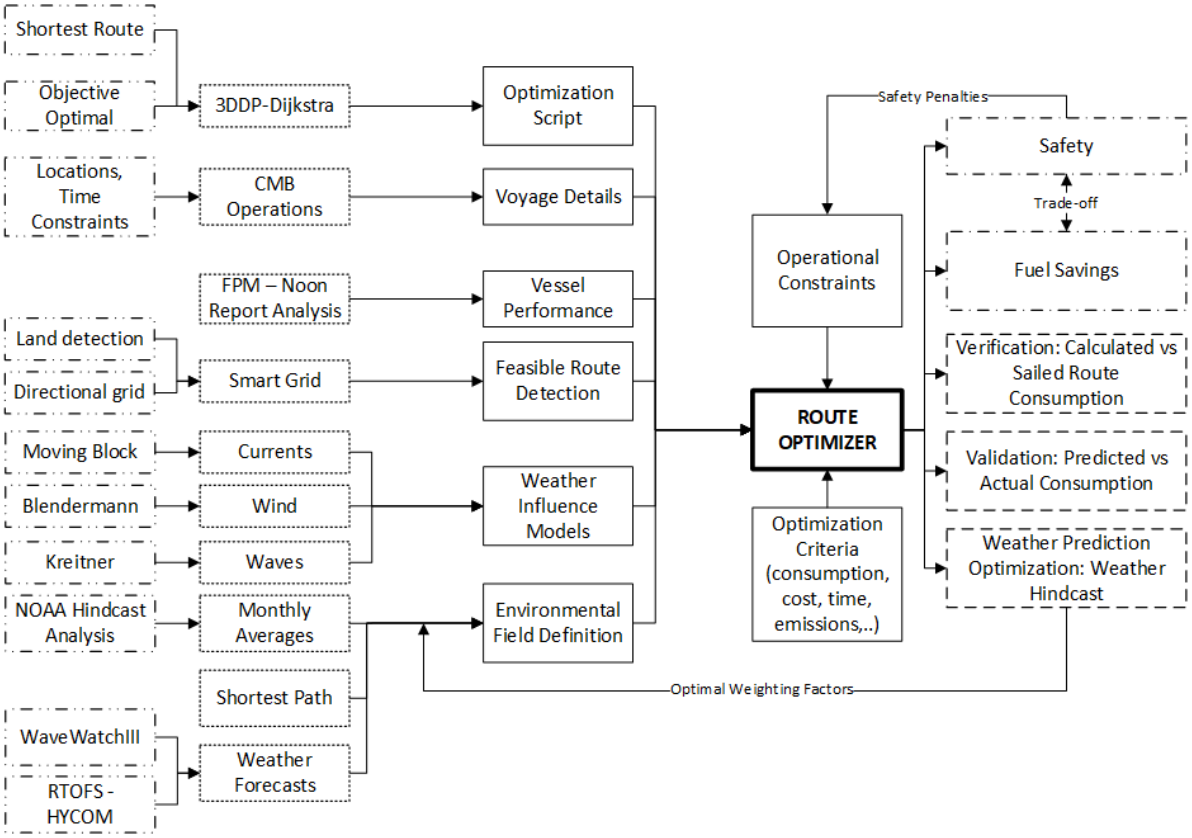

Figure 5.1: Enhanced schematic module representation of a weather routing optimization tool.

Part II
Weather Route Optimization Tool

Having a better view on the required algorithms, performance models for vessels and correction models for the environment, as well as detailed weather and current forecasts, a weather route optimization tool is developed. The tool will be discussed with a focus on fuel savings, but is built up in such a way that any objective with respect to route selection can be implemented by changing the objective function while keeping the rest of the source code untouched.

The code is split up in 5 parts, each discussed in one separate chapter. The main code is designed to pass on information from one module to another one, load forecasts, monthly averages, performance data of the different vessels, topological maps, etc. and is discussed in more detail in chapter 6. After filling in the required values in the user interface, a global approximation, around which a case dependent grid will be built, is looked for, as explained in chapter 7. The methods used to build this case dependent grid are discussed in chapter 8. This case dependent grid is then used as input for the actual solver (see chapter 9) and to end this part, the outputs of the optimization process are discussed in chapter 10.

A general flow diagram of the application is shown in figure 5.2. Note that, aiming at a practical tool for users without a programming or engineering background, all settings, inputs and outputs will be contained within a user interface and rolled out as stand-alone executable.

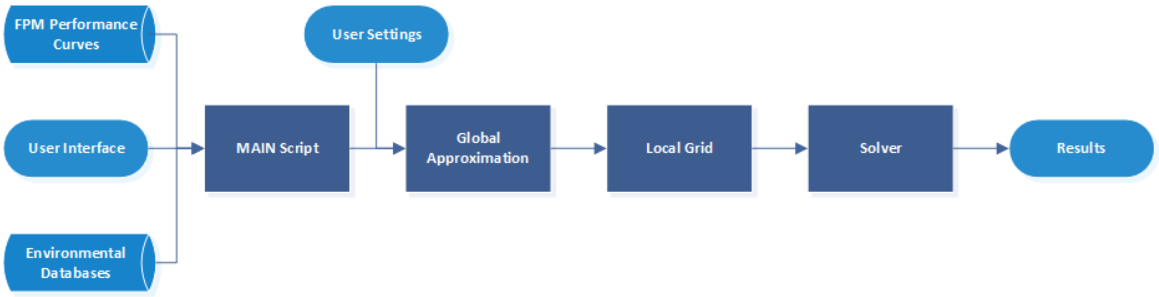

Figure 5.2: Schematic module representation of a weather route optimization tool.

6

MAIN

In the main part of the code, no calculations can be found. It is the glue that connects the other parts of the code and makes sure the different modules are correctly linked to each other. It also houses the user interface definition, which greatly increases the user friendliness of the tool. It mainly consists of required user input fields, settings and maps to represent the proposed route. A flow diagram, representing most of the functionalities within the MAIN script, is shown in figure 6.1.

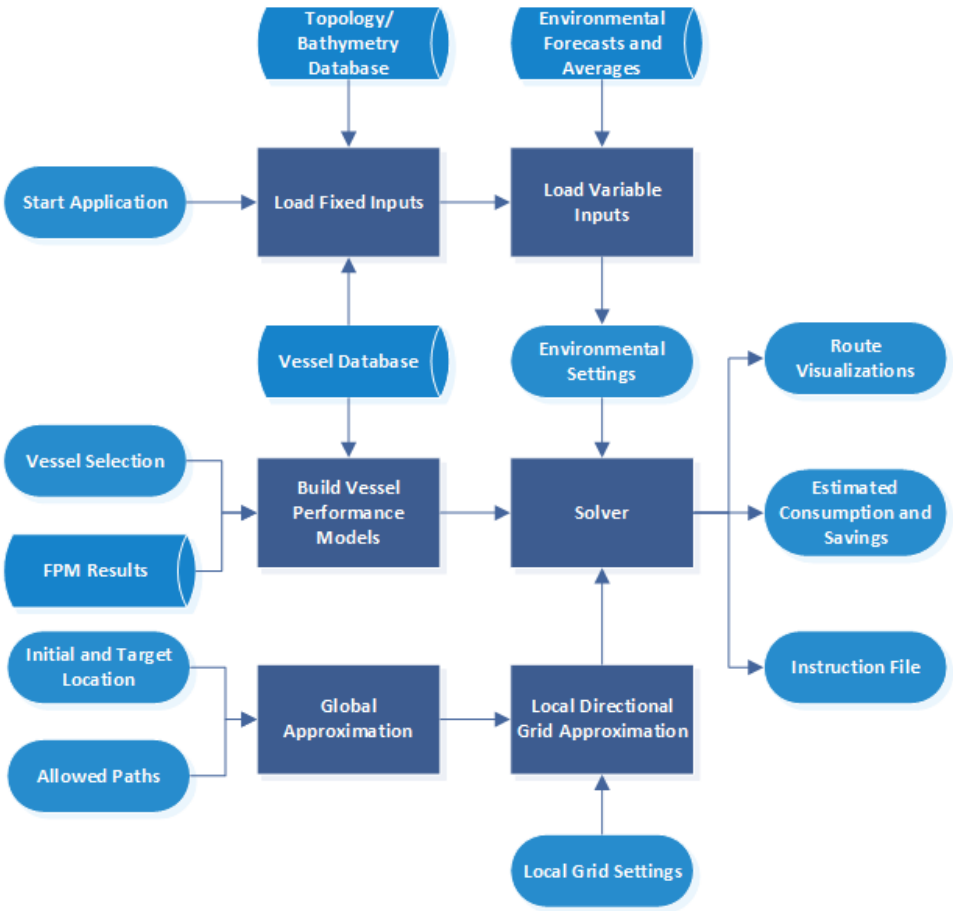

Figure 6.1: Flow diagram of the MAIN script. Rounded light blue rectangles are inputs or outputs, rectangles function executions and cylinders represent databases.

6.1. Fixed Inputs

Some inputs required to run the program are always the same and cannot be influenced by the users. In this section, each of these inputs is explained in more detail.

6.1.1. Fleet Overview

A list containing all the available ships is required to allow users to investigate the optimal route for the specific ship of interest. Therefore, a list of all vessels is generated, based on excel files found in a dedicated map. This map contains an excel file for each ship, containing a detailed description of the vessel's design and specifications. Including an additional vessel can be done by simply placing an excel file for the new vessel in the dedicated map, making it possible to add new vessels to the software without changing the code. As an example, the data contained in the excel file of the Maersk Niagara is given in appendix A.3.

The excel files are used as input for both FPM [2] and the weather route optimizer. For the route optimizer, the most relevant parameters are:

- Specific Fuel/Oil Consumption (SFOC), provided by the engine shop tests, describing the efficiency of the engine at different %MCR settings.
- Frontal and longitudinal projected area above the water line A_F and A_L, respectively.
- Waterline length (L_{WL}) defined as the longitudinal distance between the most forward and most backward location at the water line.
- Vessel even keel draft (T).
- Vessel breadth (B).
- Block coefficient (C_B).

The SFOC values are determined by means of linear interpolation (or extrapolation in case interpolation is not possible). The values for the Maersk Niagara are visualized in figure 6.2. In this case, the engine appears to be most efficient between 75 and 90 %MCR.

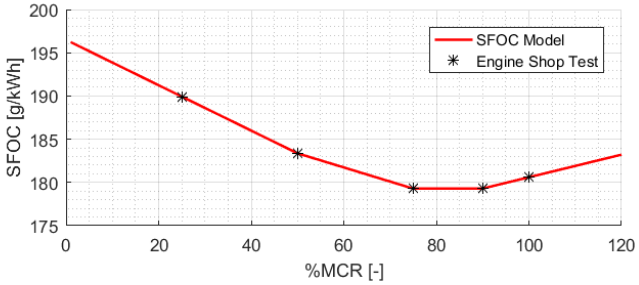

Figure 6.2: Specific fuel/oil consumption for the Maersk Niagara, assuming MGO with a lower heat value of 42.700 kJ/kg is used.

To speed up the calculations later on, a coefficient array for each direction of incoming wind, required to define the induced wind resistance, is computed while the user selects a vessel, using an accuracy of one degree. As will be explained in chapter 9, there will potentially be millions of calls to a wind resistance calculator, making this approach the fastest and hence the preferred one. For each wind direction, the Blendermann resistance coefficient in longitudinal direction [13] is defined as:

$$C_X = A_F \left[-C_{D_l} \cdot \frac{A_L}{A_F} \cdot \frac{cos(\epsilon)}{1 - \frac{\delta}{2} \cdot \left(1 - \frac{C_{D_l}}{C_{D_t}}\right) \cdot sin^2(2\epsilon)} \right] \tag{6.1}$$

Where values for longitudinal resistance coefficient C_{D_l}, lateral resistance coefficient C_{D_t} and the cross-force parameter δ can be found in table A.2. Note that the frontal projected area A_F is already multiplied with this resistance coefficient, making the C_X expression in the application in m^2 rather than dimensionless, as originally done by W. Blendermann [13]. The longitudinal resistance coefficient is plotted for every wind angle in

figure 6.3, using the relevant parameters of the Maersk Niagara.

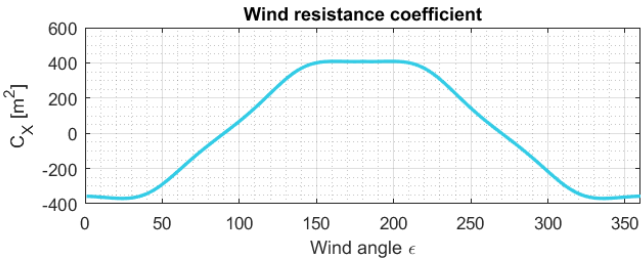

Figure 6.3: Blendermann's wind resistance coefficient for every wind angle with a precision of 1 degree, using the dimensions of Maersk Niagara

For the resistance coming from waves, a single number is stored once again to avoid calculating that same value for millions of times during the optimization process. The stored value, based on Kreitner's equation [48] is calculated using equation 6.2:

$$C_K = 0.64 B^2 C_B \frac{\rho_{sw}}{L_{WL}} g \tag{6.2}$$

Where C_K is called the Kreitner coefficient, B represents the ship breadth, the sea water density ρ_{sw} is assumed to be constant and equal to 1025 kg/m^3, L_{WL} is the waterline length and the gravitational constant is denoted as g and is assumed to be 9.81 m/s^2 everywhere on the globe.

6.1.2. Unstructured Global Grid

Dynamic Programming is used to find the optimal solution. This means that a grid will be used to simulate vessel movements, which asks for a grid definition. As can be seen the flow diagram in figure 6.1, an unstructured global grid and a structured local grid will be used. Starting from an approximation of the shortest path to sail from the initial to the final location, a local grid will be drawn and the real optimum will be looked at. The unstructured grid takes care of the approximated shortest path.

More details on this approximated shortest path can be found in chapter 7; what is important here is that the predefined, unstructured grid is precomputed and loaded at startup. The unstructured grid is defined using five arrays. The first two arrays contain the longitudinal and latitudinal position of a node, the third array contains the initial node number of a connection within the grid, the fourth one the target node number of the same connection and the final one the distance it takes to sail from the initial nodes in the third array to the final nodes in the fourth array.

The grid contains 2.07 million nodes and 5.79 million connections between these nodes, equivalent to a rectangular grid between -70 and 70 degrees latitude with a grid size of 10 by 10 arc minutes. At first, a structured grid was used, placing a node exactly each 10 arc minutes. However, the result was not satisfying, because it only allowed certain directions to move in, as can be seen in figure 6.4. A better approximation can be obtained when adding a random variation in the grid. The exact reasons why this is easier will be discussed in chapter 8. The variation is limited to half the grid size to make sure no overlapping or crossing connections between nodes exist. The location of the nodes is stored and reloaded when the application starts up.

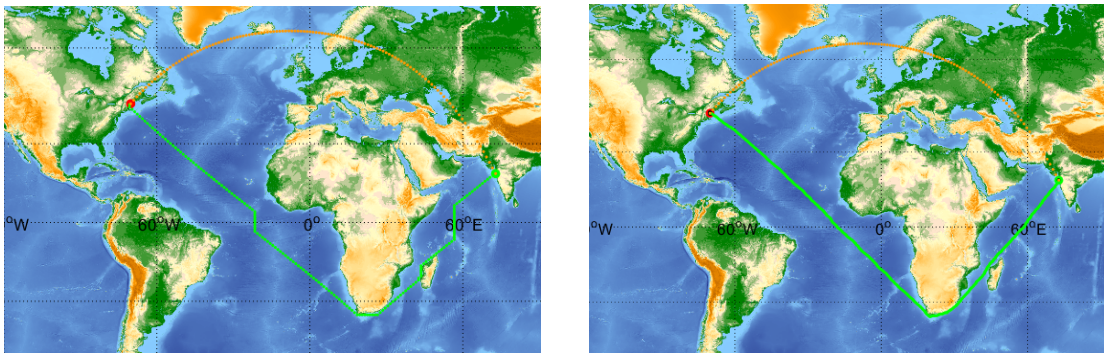

(a) Structured grid approach (b) Unstructured grid approach

Figure 6.4: Approximation of the shortest path between Bombay (India) and Portland (USA). Green line indicates the chosen path, orange line the great circle.

When all nodes are defined, the nodes that are placed on land or in too shallow waters must be removed. To achieve this, a function capable of detecting land, based on the topology map discussed in section 6.1.4, is used on each node, detecting whether or not a node or connection between two nodes is (crossing) land. On the computer used (specs in appendix A.9), the land detection for nodes executes at almost 2 MHz. The nodes located on land are removed from the sequence.

Then, for the remaining nodes, a connection to the points that would be exactly in the North, East, South or West without the random variations, is made for each node and stored in the initial and target node arrays. These connections define between which nodes the vessel can travel on the global grid. Using the same land detection algorithm at 50 equally distributed locations on each connection, the defined connections are checked on land crossing. When the connection is impossible, it is removed from the list of connections. Note again that the random variation within the global grid is used to allow sailing in any direction on a larger scale, avoiding block-like movements. This approach is valid since an approximated path is looked for at this stage of the optimization, not the ideal route.

Finally, the remaining connections are assigned a weight according to the distance between the two points. Generating this grid is rather time consuming; therefore, it was decided to generate this grid on a global level one time, then save it and loading the solution when the application is started.

6.1.3. Monthly Averaged Environment

The monthly averaged environment is considered to be unchanging and is loaded at startup of the program. Depending on the specified ratio between forecast, monthly averages and shortest path, a specific weight will be assigned to the monthly averaged data. More details can be found in section 9.3.

6.1.4. Topological Map

Being able to prevent routes from crossing land is key in the design of a routing tool for vessels. Instead of using a bitmap-based algorithm, as done by for example Szłapczynska et al. [81] or the coastline data used by G. Mannarini et al. [53], the two arc-minute bathymetry model ETOPO2v2 [15], provided by NOAA, is used. The strength of this database is that it contains a huge matrix describing the topology of the entire globe, hence using this map is preferred over a map of coastlines, since shallow waters can also be detected and, when needed, avoided. Visualizing this map using Aendekerk's land/sea colormap, available on the MATLAB file exchange [3], results in a very familiar view, shown in figure 6.5. The visualization suggests that the matrix provided by the ETOPO2v2 database is interpret correctly.

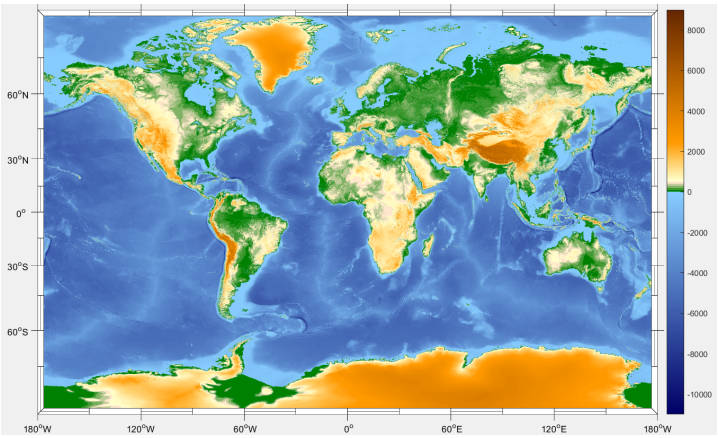

Figure 6.5: Visualization of the ETOPO2v2 topology file, using the land/sea colormap, which colors the topology data based on surface height, as shown in the legend.

6.2. Uncontrollable, Variable Inputs

Another group of inputs required, consists of continuously changing inputs the user cannot control. Two distinct groups are identified: the environmental forecasts and the real-time performance of all vessels in the fleet.

6.2.1. Environmental Forecasts

The monthly averaged sailing environment from section 6.1.3 is always the same, but the forecasts are updated automatically every night. As explained in section 4.3, MATLAB's application compiler and windows task scheduler take care of downloading and saving all the parameters required for the selected correction models.

The forecasts data used is limited to following parameters:

- Wind components in North and East direction.
- Significant waveheight, defined as the mean waveheight of the 1/3rd highest waves [9]. No distinction between wind generated waves and swell waves is made.
- Wave direction with zero degrees when waves come from the North, moving counterclockwise (waves from east are defined as 90 degrees).
- Current components in North and East direction.

The wind and wave models are coupled in the WaveWatchIII model [61] and contains more detailed information, like primary and secondary wave periods or peak wave height, allowing for a large variety of different environmental correction models. Less influential parameters, like sea water density, salinity level, air pressure, sea water temperature, etc. are also available, but are not used for the weather routing because (1) the influence appears to be marginal in comparison with the influences listed above [71] and (2), because they gradually change and would only affect consumption when very large detours are taken.

6.2.2. FPM Vessel Performance

The second uncontrollable but variable input is a description of the vessel's performance. The methods used to evaluate vessel performance are placed out of the scope of this project, but it is important to know that the performance figures are updated every day, producing a numerical summary for each vessel. The parameters below are taken from the FPM [2] performance results:

- Speed-Consumption relation according to equation 6.3 or equation 6.4, depending on the available data range. Example shown in figure 6.6a.

- Linear relation between %MCR and DFOC, as shown in figure 6.6b
- Third-power relation between %MCR and propeller revolutions per minute, visualized in figure 6.6c

Two different speed-consumption relations are used. The first one relates speed to consumption according to a power factor, as shown in equation 6.3 and can be applied as soon as three measurement points are available:

$$DFOC = A \cdot V^B \tag{6.3}$$

Where DFOC is the daily fuel oil consumption, V the speed in knots and B a factor between 2.5 and 3.2.

During the development of FPM (Fleet Performance Monitoring), another curve shape to describe the relation between consumption and speed was found, outperforming the power curves on wave front representation (at a certain speed and critical Froude number, the wave generated by the vessel's bow consumes most of the additional power supplied to the engine, creating an almost asymptotic speed-consumption relation at higher speeds) [1]. The curve takes the form of equation 6.4, showing the curve is not forced to go through the origin (no consumption when not moving). Because of this, speed measurements over a bigger speed range are required to use this form. To fully automate the performance curve generation, only vessels with speed variations of over 8 knots over the evaluated period are using this form, the others use the power curve approach of equation 6.3.

$$DFOC = A \cdot e^{B \cdot V^3} + C \tag{6.4}$$

Where DFOC is the daily fuel oil consumption, V the speed in knots and A, B and C best fitting real numbers.

The linear relation between consumption and %MCR is logical, since %MCR is defined as % of the maximum possible fuel supply to the engine. The relation between the %MCR and RPM is a third power, because the rotational speed of the propeller has a squared relation with resistance and conversion from resistance to power requires another multiplication with the rotational speed. Because the models are based on measurements, no knowledge about the propulsive efficiency is required for this relation.

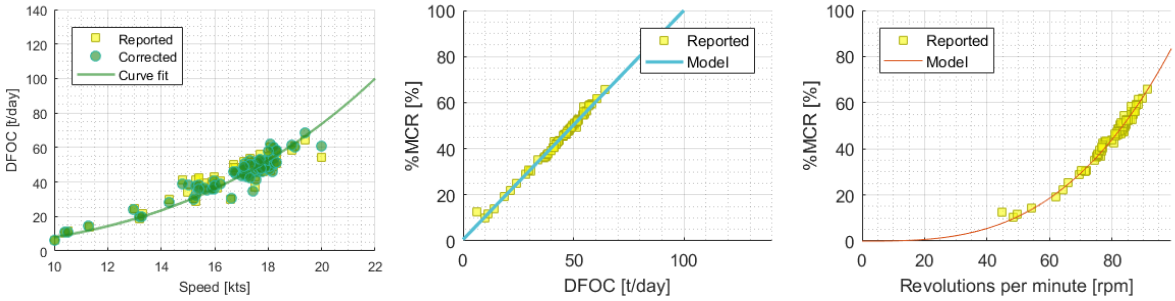

(a) Speed-DFOC relation (b) DFOC-%MCR relation (c) %MCR-RPM relation

Figure 6.6: Visualization of performance curves generated by FPM

6.3. User Inputs

Apart from all the inputs the user cannot influence, there are still many parameters left the user can (and should) modify. Apart from selecting a ship out of the list of available ships, the inputs discussed in the following sections, are available for the user.

6.3.1. Initial and Target Position

Without initial and target position, there cannot be a route to optimize. There are three methods to specify positions in the weather routing tool, namely:

1. Selecting a port from a dropdown list, based on the World Port Index [55], displayed in figure 6.7.
2. Providing coordinates.
3. Selecting a location on the map, making use of MATLAB's function `ginput` [83].

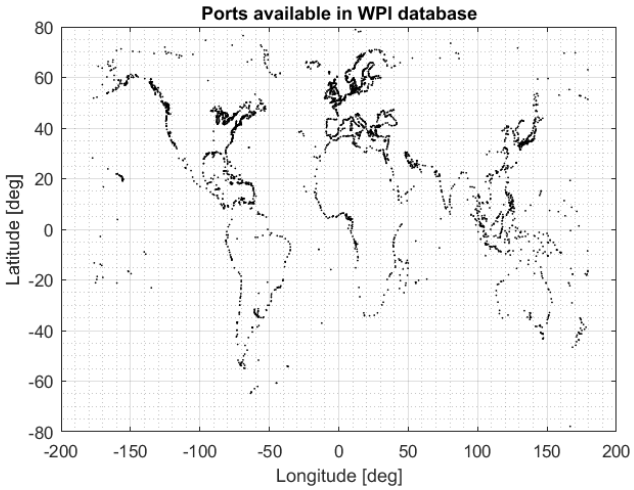

Figure 6.7: Visualization of ports found in the WPI database [55].

Each method results in a longitudinal value between -180 and 180 degrees and a latitudinal value between -90 and 90 degrees. Visualization is done by converting the longitudinal and latitudinal values to the proper (x,y) values, using the M_Mapping toolbox [68]. Figure 6.8 shows a part of the user interface indicating the selected initial and final point.

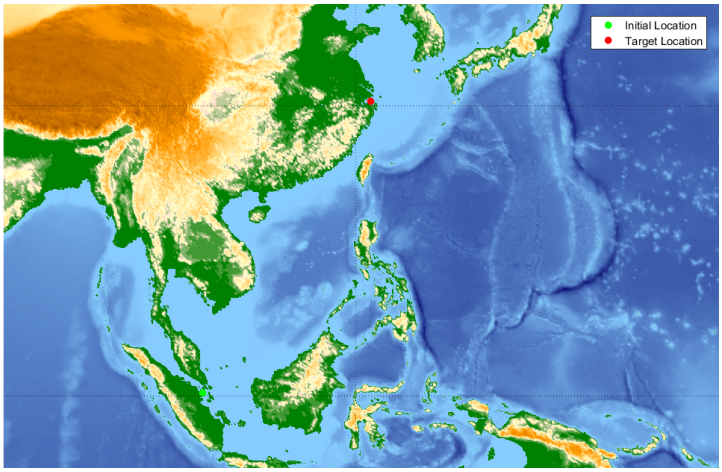

Figure 6.8: Initial and final location selection as shown in the UI, sailing from Singapore to Shanghai.

To increase the user friendliness of the application, the current and target position of the vessel selected, as documented on the SQL server of CMB, are automatically loaded in the departure and arrival panels shown in figure 6.9.

6.3.2. Time Frame selection

Apart from setting the required locations, the departure and arrival times are main drivers in finding the optimal route. Standard settings are the time of start-up as starting time and 15 days later as arrival time, but this has to be changed in almost any case. To keep things as clear as possible, the dates and times specified must

(a) Departure panel with coordinate inputs enabled

(b) Arrival panel with port selection enabled

Figure 6.9: Fields to be completed by the user, specifying the details of the voyage.

be given in Coordinated Universal Time (UTC), which matches the environmental forecast timescale. When a ship is specified by the user, the current location, target location and target arrival time will automatically be loaded.

6.3.3. Canals

Due to additional costs or maximum allowed vessel dimensions, three canals can be taken or avoided. A waiting time can also be specified for each of these canals, which can be up to three days at busy moments. Figure 6.10 shows the selection window from the UI.

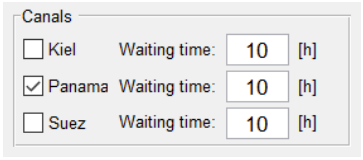

Figure 6.10: Canal options.

6.3.4. Optimization Weather Ratios

The ratios between forecast, monthly averages and shortest path, which will be discussed in more detail in chapter 12, are loaded at the best ratio found during this research, but the user is still able to manually modify the ratios. Changing these, however, is not recommended. The options available for the user can be seen in figure 6.11. The first two options describe at which point in time the monthly averaged weather and shortest path start influencing the optimization. The following two options describe the final influence of monthly averages and shortest path and the last parameter indicates at which moment in time these ratios should be set as fixed. When forecasts are not available anymore before the moment in time at which these final ratios should be used, the final ratios will be used before the final day.

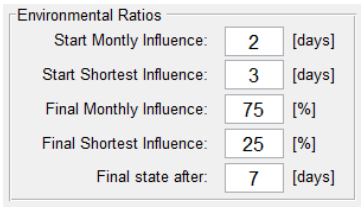

Figure 6.11: Environmental mixing options available to the user.

6.4. User Interface

The user interface consists of fields the user can control to find the desired route and visualizations of the route. The outputs are presented in chapter 10, the main settings available to the user are shown in figure B.4. Screen shots of each of the different tabs, can be found in appendix B.

6.5. Optimization Callback Functions

The final task taken care of by the MAIN script, is the correct initialization of callback functions and managing the inputs and outputs of these callback functions. Most callback functions are initiated using a push button from the user interface. In table 6.1, the most important callbacks, accompanied by their inputs and outputs, are presented.

Table 6.1: Most important callback functions of the weather optimization tool

Callback	**Inputs**	**Outputs**
shipcharacteristics	Ship specific excel file FPM Results	Voyage details Mathematical vessel model
globalGrid	Voyage details Predefined unstructured global grid	Approximated solution
localGrid	Approximated solution Grid settings	Local, structured grid
solver	Local, structured grid Voyage details Optimization settings	Proposed route as 3 arrays: longitude, latitude and time Fuel consumption (gains) Changes in environment encountered

Apart from these main callbacks, many small ones are available, for example functions that visually represent the resulting route as a GIF file, showing the route as function of current, waves or wind conditions, providing insight in the decisions made. More details on the post-processing functions are given in chapter 10.

7

Global Grid

As soon as the initial and target location are specified, an optimal solution has to be found. This is done in several steps, starting with an approximated solution, found on a globally ranging grid. Figure 7.1 shows the process of finding an approximated solution.

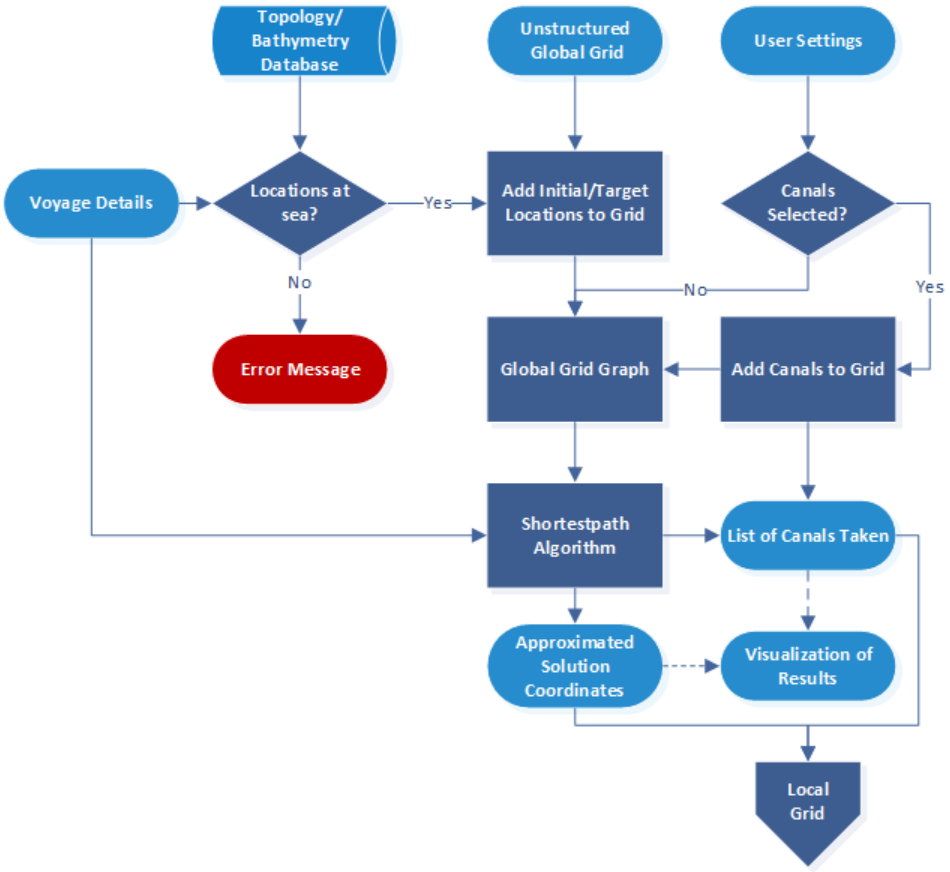

Figure 7.1: Schematic module representation of the global grid part of the weather route optimization tool.

As can be seen in the flowchart, the required inputs to approximate the best route are the global grid and the initial and target locations, together with the user decision on including canals in the route or not. The initial and target location are added to the unstructured grid and potential canal connections are also included in the global grid. After filtering out nodes and connections crossing land, outputs are generated and visualized. A part of the unstructured grid is visualized in figure 7.2 as mask over a Google maps image, using the

`plot_google_map` script provided by Z. Bar-Yehuda on the MATLAB file exchange [6].

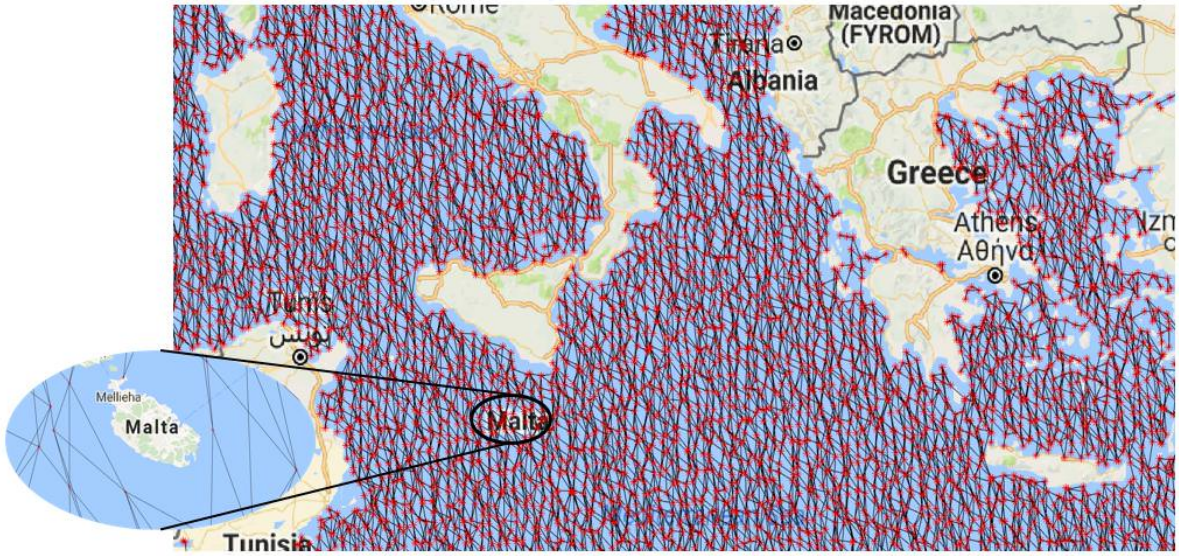

Figure 7.2: Visualization of a part of the global grid, including the sailable connections between the nodes. A zoomed-in view of Malta is given, showing the island is avoided by the unstructured grid.

7.1. Adding Initial and Target Location to the Unstructured Grid

When the initial and final voyage locations are given, they need to be checked for land and added to the grid. Following steps are taken for both the initial and target location to add them to the grid:

1. Verify that the location of interest is not placed on land. This can occur when, for example, an inland port (like Antwerp) is selected from the port list. If land is detected, an error message will appear.

2. If the point of interest is at sea, find the nodes from the unstructured grid that lay within 0.33 degrees longitude and latitude from the point to be added.

3. Define a connection between the new node and the nodes found in step 2.

4. For each connection created ensure no land is crossed. If land is crossed, remove the connection. If all connections are removed, an error message is prompted and a location closer at sea should be selected by the user.

5. For the remaining connections, use the great circle distance as weight to the weight array of the unstructured grid, adding it to new connections to the already existing predefined connections.

7.1.1. Land Detection Algorithm

A procedure that occurs multiple times during the different steps in the optimization process, is removing potential parts of a route when they are located on land. A specific function with only one purpose, namely detecting whether or not a node or a connection between nodes is interfering with land, is linked to the bathymetry matrix generated from the NetCDF ETOPO2v2 topology files [15]. The algorithm works as follows, taking longitude, latitude, topology, required depth and potentially number of intervals as input parameters:

1. Check number of arguments. If 5, a number of intervals is provided as input. This number of intervals is used to generate intermediate points between the two points specified in the input, using F. Beauducel's approach [7]. For each of these intermediate points, step 2 is applied. If there are 4 input arguments, only one node is specified, which is checked for land according to step 2.

2. Local depth is checked by calling the topology indices that correspond to the investigated location. If a certain depth is reached (e.g. 25 meters), the procedure accepts the point.

The topology is defined as a 10800x5400 matrix, containing longitudes starting at 179.9833W 89.9833S in [1,1] and ending in 179.9833E 89.9833N in [10800,5400]. To convert a longitudinal or latitudinal coordinate to a matrix position, equation 7.1 and equation 7.2 are used.

$$i = round(30 \cdot lon + 180) + 1 \tag{7.1}$$

$$j = round(30 \cdot lat + 90) + 1 \tag{7.2}$$

In the above equations, the topology matrix entry for location (lon,lat), is determined by identifying the relevant row i and column j.

F. Beauducel [7] provided a great circle function on the MATLAB file exchange. His code is mainly used for the great circle distance calculation between two nodes, generating equally spaced intervals on great cirlces and calculating the bearing between two points, assuming the earth has a constant radius of 6371 km. When checking a potential connection for land, the specified number of intervals will be generated and each generated point will be checked for land.

Visualization of the unstructured gridpoints in the Mediterranean in figure 7.3, which remain after removing locations with a depth less than 18 meters, shows the algorithm is capable of removing the unsailable nodes while keeping the feasible ones.

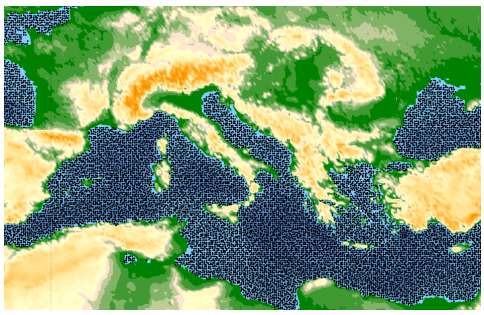

Figure 7.3: Remaining grid points in the Mediterranean after applying `landDetection` with 18 m depth requirement. Note the detection of Chott Melrhir in Algeria, where grid points remain, but any connection trying to move outside the lake will be broken.

7.2. Adding Canals and Narrow Streets to the Grid

As already stated before, the first optimization step will be approximating the solution on the unstructured grid. Logically, the approximation can depend on the choice of which canals are taken and which ones not. Depending on the input, additional connections are required to detect these canals or exclude them from the grid. The same principle is used to model certain narrow sea parts that gave problems when testing the algorithm, forcing additional connections. Following additional connections can be defined:

- Extended Bosporus
- Kiel Canal
- Panama Canal
- Strait of Gibraltar
- Strait of Hormuz
- Suez Canal

To add these narrow parts and canals to the global grid, their coordinates are defined as new nodes, and connections to them are added as discussed in section 7.1 while adding the initial and target location. The only difference is that the connections are only checked in a specific direction. for example, the eastern node of Gibraltar can only be connected to nodes to the east. The narrow streets are always included in the grid, but the canals are only initiated when the user selects them.

7.3. Approximated Solution

When all nodes are added to the network, an approximated solution can finally be determined. All nodes carry a number, which is linked to a location in longitude and latitude arrays, which have the same length as the number of nodes. Arrays s and t carry starting and target numbers, connecting the relevant nodes with each other. Their dimension is equal to each other, but much larger than the number of nodes because multiple connections between nodes exist. A final array w carries the distance of each of the defined connections and logically has the same number of elements as array s and array t. To calculate the weight array w, the great circle distance, calculated using the great circle script provided by F. Beauducel on the matlab file exchange [7].

As soon as array s, t and w are set up, the built-in function `graph` is used to create a graph with nodes, edges and weights. This is done to provide `shortestpath`, another built-in function, with the required inputs. Taking the graph that was set up, the initial and the final node as input, the algorithm searches for the route resulting in the lowest distance covered, based on the weights in w.

The output of `shortestpath` is an array containing a list of nodes to be taken. From this, the longitude and latitude of the nodes is recreated, allowing further processing of the shortest path found. Note that the execution of `shortestpath` does not directly require data contained in the longitude and latitude array, it only takes the specified weights into account.

Together with the initial and target node number, the numbers of the nodes containing narrow sea passages or canals are saved. If one of these numbers occurs in the shortest path found, it is stored to be used later on. The passages are also visually shown, alerting the user that such passage was taken, as displayed in figure 7.4. The exact location of the passed nodes is also visualized, making it easier to check if the route will be calculated as expected. Forgetting to select the proper canal, for example, will easily be seen, allowing the user to redefine the settings before executing the rest of the code.

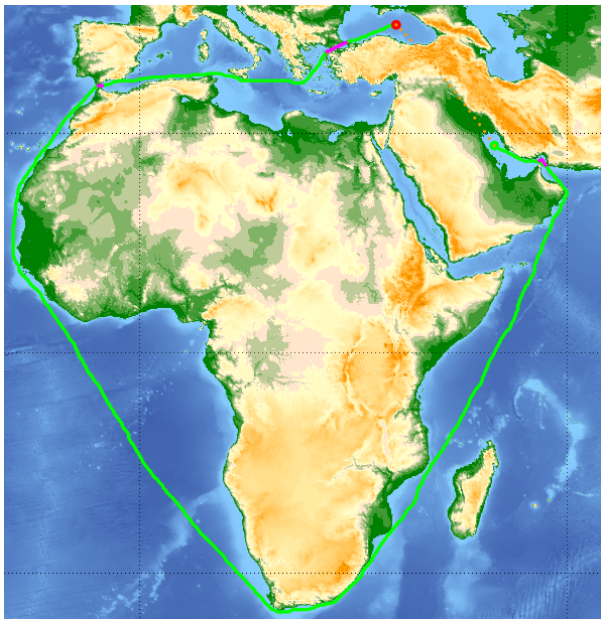

Figure 7.4: Example approximated solution between the Persian Gulf and the Black Sea, avoiding the usage of the Suez Canal. The strait of Hormuz, strait of Gibraltar and the Bosporus are passed and made visible to the user.

8

Local Grid

When an approximated voyage is simulated on the global, unstructured grid, a grid capable of simulating feasible vessel movements has to be drawn. A brief explanation of this process is given by the flowchart shown below.

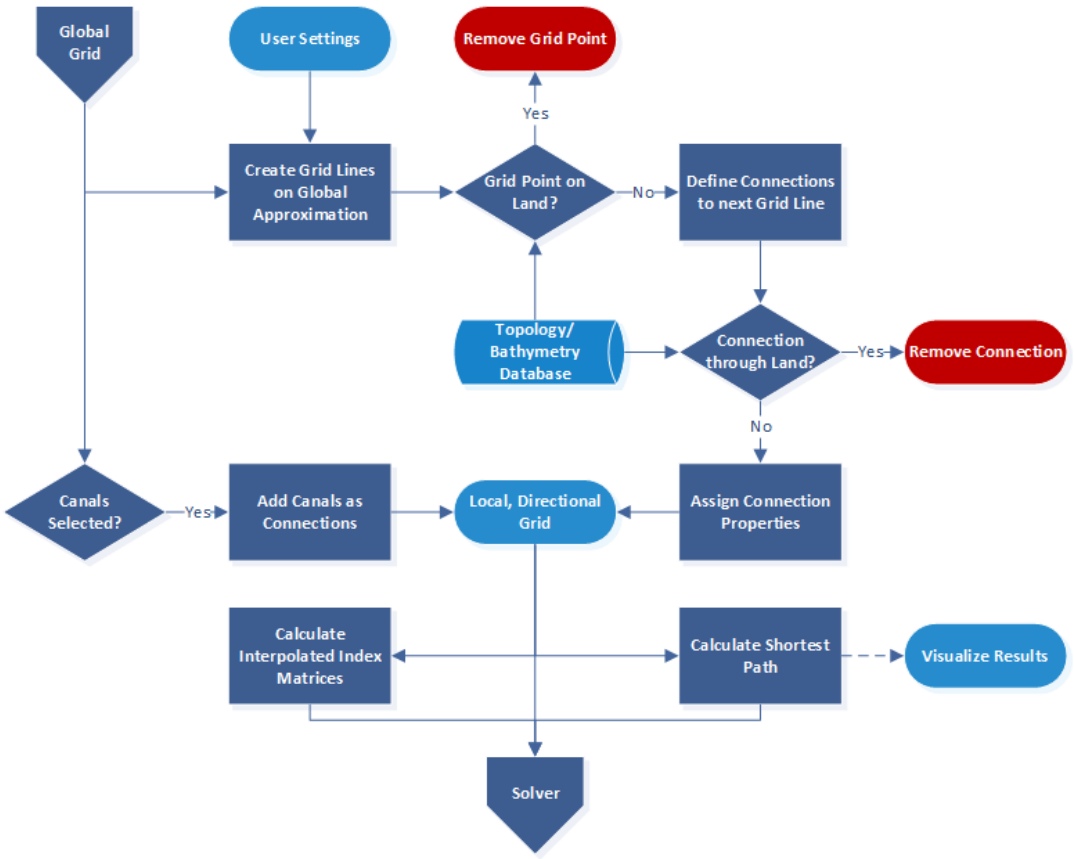

Figure 8.1: Flow diagram, describing the generation of a local, directional grid, required to find the optimal route.

From the global grid approximation, grid line definitions are constructed and covered with grid points (see figure 8.3 for more details). These grid points are then checked for land, drawing connections from the remaining grid points on line i to the remaining points on line i+1. For the connections not crossing land, properties such as their length, starting point, end point, ... are stored and the grid with its remaining connections is saved. Results are visualized and some matrix indices related to interpolations on the connections are computed within the local grid algorithm to speed up the total process. This will be explained in more

detail in chapter 9.

8.1. Grid Lines on a Directional Grid

To locally define a structured, directional grid, the global approximation found as discussed in chapter 7 is used as starting point. Using the canal passage list included in the approximated solution, the script treats each of the voyage parts between two narrow passages as separate trips, ending at the start of the canal or narrow strait. For simplicity, the starting point is treated as end-of-canal point, whereas the target point is modeled as the start of a canal. An example of a partitioned voyage as generated from the global grid is shown in figure 8.2.

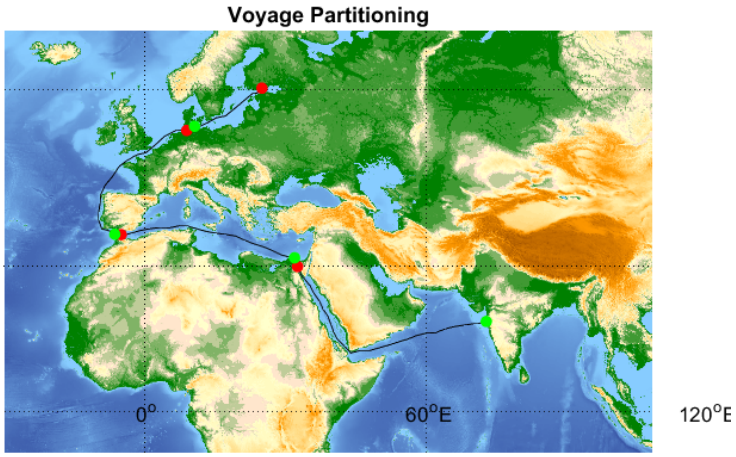

Figure 8.2: Voyage Partitioned in 4 parts, starting at the green dots and ending in the red ones. Note that the Suez Canal, the strait of Gibraltar and the Kiel Canal are the narrow passages, cutting the voyage in multiple parts.

For each part, locations to draw lines orthogonal to the sailing direction are determined using the global grid outcome and a user-specified line distance, which is defined as the number of global edges taken between the grid lines of the local grid. The number of edges between grid lines builds up gradually from start and end points of a part of a voyage, until the user-defined maximum value is reached, after which constant distances are used. When, for example, the maximum is defined as 12, the sequence starts as: 2, 6, 12, 18, 30, 42, ..., decaying when the target point is approached.

When the nodes to draw lines at are identified, each node is connected to the previous one and a line, orthogonal to the connected line, is defined through the node of interest, using equations 8.1 to 8.3:

$$R_i = -\frac{lon_i - lon_{i-1}}{lat_i - lat_{i-1}} \tag{8.1}$$

$$C_i = -R_i \cdot lon_i + lat_i \tag{8.2}$$

$$lat_i = R_i \cdot lon_i + C_i \tag{8.3}$$

Where R defines the gradient, C the constant and i the node through which a line has to be drawn.

After defining a function describing a relation between the longitude and latitude, points are defined on the calculated line that will function as grid points. Similar to the distance between the grid lines, the number of points generated on a line is gradually increased when further away from a start or end point. Points are defined by taking the steps below:

1. For each grid line, define number of grid points, based on closeness to the start/end of a voyage part. The number of grid points linearly scales up from 1 to the user specified maximum in 8 steps.
2. Determine the total number of grid points that will be defined on each grid line.
3. For each grid line origin (one of the global nodes taken), equally divide the number of nodes for that line on the perpendicular grid line specified by equations 8.1 to 8.3, using equal angular spacing. Store their locations as longitude and latitude according to equations 8.4 and 8.8.
4. As done on the global grid, remove nodes not matching the required ocean depth.

For each grid line, following equations are used to define node coordinates:

$$SN_i = 1 + \sum_{k=1}^{i-1} NGP_k \tag{8.4}$$

$$D_r = linspace(-maxDistance, maxDistance, max(NGP)) \tag{8.5}$$

$$NR_i = \frac{max(NGP)}{2} - \frac{NGP_i}{2} \tag{8.6}$$

$$lonNode(SN_i + j - 1) = lon_{gg,i} + D_r(Nr_i + j - 1) \cdot cos\left(tan^{-1}(R_i)\right) \tag{8.7}$$

$$latNode(SN_i + j - 1) = lat_{gg,i} + D_r(Nr_i + j - 1) \cdot sin\left(tan^{-1}(R_i)\right) \tag{8.8}$$

In the above equations, SN_i is the starting node number of grid line i, NGP_i is the number of grid points that have to be defined on grid line i, D_r is an array indicating the relative distance between the middle and the outside of a grid line, based on the maximum distance set equal to 6 degrees, NR_i defines the node range, indicating the range between the most outer grid points on a line and required when a reduced number of nodes is defined on a grid line. lonNode and latNode are used to store the coordinates of grid points, lon_{gg} and lat_{gg} represent the grid points from the global grid on which grid lines are defined and R_i is the gradient defined in equation 8.1. An example grid is shown in figure 8.3.

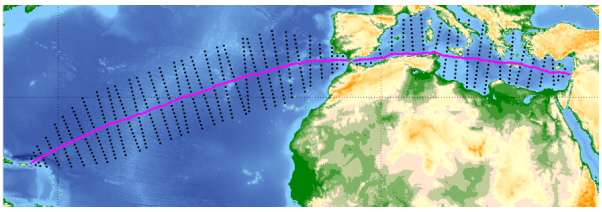

Figure 8.3: Directional grid points drawn between Lebanon and the British Virgin Islands. The magenta line is constructed using the result of the global grid and the local grid is built around it.

8.2. Advancing on the Directional Grid

Unlike the global unstructured grid, which is defined all around the globe, the directional grid, created as discussed in the previous section, is only defined locally, covering only the region in which the optimal route is expected to be. After defining the grid points, the next step is connecting the relevant points.

For each grid point, the line on which it is drawn is saved. When defining the possible connections, each grid point on grid line i, is connected to each grid point on grid line i+1. In a similar way as done for the global grid, the connections are checked for land and deleted if land is crossed. Checking for land is disabled for the connections modeled as canal, because the topology file is not detailed enough to detect the canals. In open sea conditions, defining all possible connections would result in NGP^2 connections per grid line, when NGP grid points are defined on a line. However, fewer connections are actually drawn, because:

- Often, the number of grid points or allowed connections is reduced due to land detection.
- When the grid lines between which a connection is drawn, are almost parallel to each other (maximum angle difference of 30 degrees), only relatively straight connections are defined. This does prevent connections taking an angle of more than 45 degrees and reduces the number of connections that need to be checked later on. This is visualized in figure 8.4.

- The number of grid points on a grid line is reduced close to initial point, final point and canals or narrow straits, if encountered.

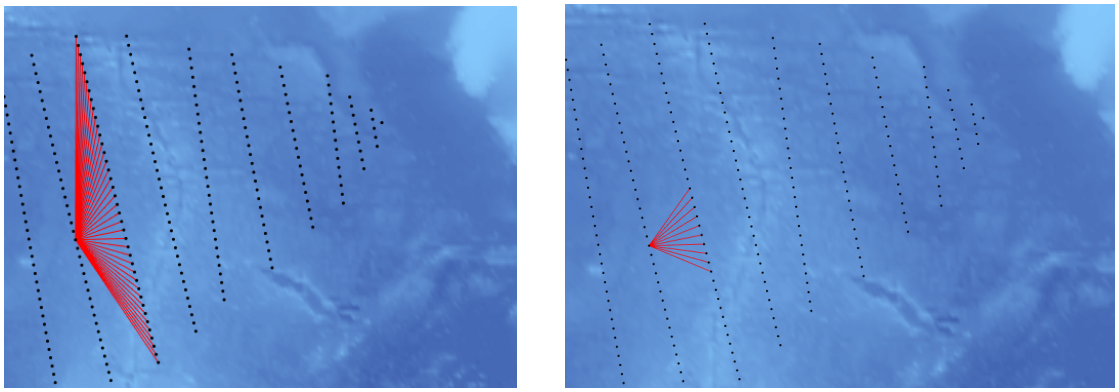

(a) All connections between two grid lines (b) Feasible connections between two grid lines

Figure 8.4: Removal of infeasible connections, containing an angle of more than 45 degrees, from the local, directional grid.

On a voyage from Veracruz (Mexico), to Burgas (Bulgaria), 2586 grid points remain and a total of 36215 connections are defined, which corresponds to an average of 14 possible connections per grid point. On another trip, from Mumbay (India), to Pepel (Sierra Leone), the average is 18.5. The difference can be explained by the strong reduction in connections in the Mediterranean.

The local connections on a grid containing up to 15 grid points on a single grid line is shown in figure 8.5. In reality, there are much more grid points, but the principle remains the same. The reduction in grid points was done to increase the visual understanding of the local grid movements available.

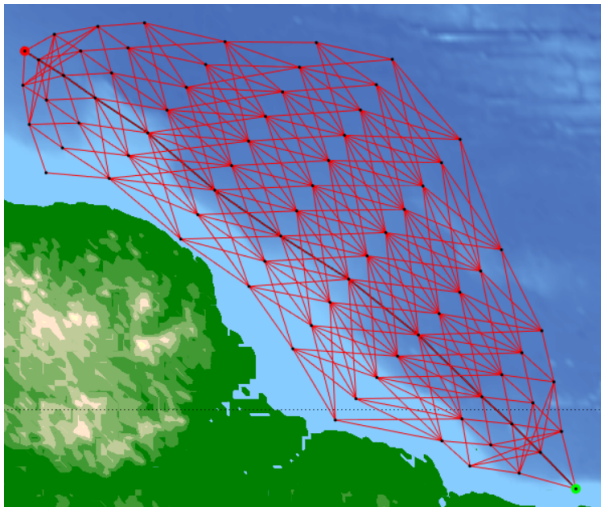

Figure 8.5: Visualization of local grid connections on a coarse grid.

8.3. Shortest Path Definition

When all grid points and connections are properly defined, the sequence of nodes to be taken to travel the least distance can be determined in a similar way as the global grid approximation of section 7.3. To make sure that the shortest path is actually found, several open sea parts are solved and compared with the calculated distance between those points. The results are summarized in table 8.1. With an average increase in distance of only 0.063 %, it can be seen that the methods used to build the local grid are functioning as expected.

Table 8.1: Comparison of shortest path found on the local grid with great circle distances.

Initial Point	Final Point	Grid Distance	Great Circle Distance	Absolute Difference	Relative Difference
Cape Town	New York	12563.93 km	12568.46 km	4.53 km	0.036 %
Natal	Coral Bay	15297.82 km	15289.32 km	4.53 km	0.056 %
Iquique	Choshi	16544.50 km	16535.78 km	8.72 km	0.053 %
Pepel	New York	6935.65 km	6931.91 km	3.73 km	0.054 %
50N 20W	50S 20W	11125.72 km	11119.49 km	6.23 km	0.056 %
50S 50W	50S 50E	6568.23 km	6560.21 km	8.02 km	0.122 %
					Average: 0.063 %

8.4. Preparations for the Execution of the Solver

While checking the possible connections to take, each connection between two nodes is checked, connection by connection. When a connection is allowed, it is not only added to the list of feasible paths, but some properties are already calculated in advance.

To start with, the connection is divided in an equal number of intervals, of which the coordinates are saved, reducing the calculation time the solver needs, as discussed in 9. Apart from the coordinates, two matrices, containing the relevant indices to quickly find the right value of weather at a specified location, are generated. The matrix containing indices for wind and waves is calculated in a straightforward manner, using equations 8.9 and 8.10, dealing with the 720x311 format the wind and wave data is downloaded.

$$i = round(2 \cdot lon + 1) \tag{8.9}$$

$$j = round(2 \cdot lat + 156) \tag{8.10}$$

Where the weather data on matrix position (i,j) gives the weather conditions at location (lon,lat).

The wind and wave format, as provided by NOAA, is relatively easy, because the longitude and latitude are evaluated in a linear way without influencing each other. Wind data at 10 degrees East will, for example, always be found in column 21. The current data is, on the other hand, formatted in a more complicated way. Up to 47 degrees North, a Mercator grid similar to the wind and waves one is used, but North of this 47 degrees line, the grid changes to a bi-polar format, as shown in figure 8.6. This is most likely done to reduce the grid on the main land of the US and in Russia, but retaining the required level of detail in the Atlantic and Pacific.

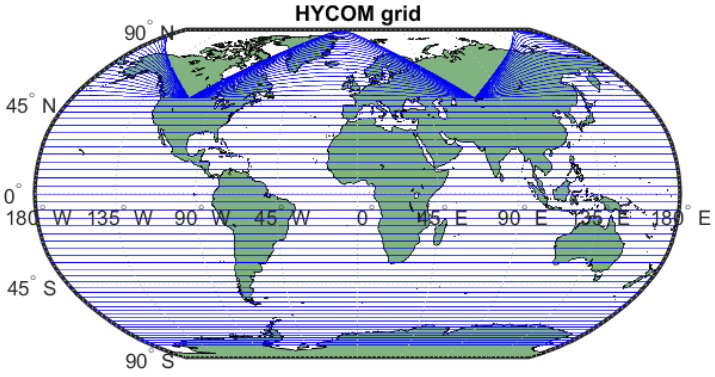

Figure 8.6: Representation of longitudes and latitudes found in the same matrix row, showing a bi-polar approach in the Northern part of the map.

Since no conversion function was found, no accurate conversion function could be determined by means of linear regression and computation time was drastically increased when applying a `find` routine within the weather routing application itself, a connecting matrix was set up, running a `find` algorithm over a linear Mercator grid once. The resulting matrix is loaded when the application starts up and links a combination of

longitude and latitude to the correct location of the requested current in the HYCOM matrix.

Whereas the different connections are stored in the form of an array, the indices that need to be checked for wind, waves and current data are stored in a 3 dimensional matrix, where each row corresponds to the indices related to that connection. Assuming there are N connections, which each require M wind iterations, the indices matrix has a NxMx2 dimension. The locations needed to determine the wind influence while evaluating node i can thus be found at locations (i,:,:) of this matrix.

The resulting grid, together with the shortest route found, is visualized for the user as shown in figure 8.7. Together with the visualization, the following variables, calculated for the local grid, are stored to be used later on:

- Nodes and their coordinates
- Connections, which nodes they connect and their length
- Interpolation matrices: (1) containing coordinates of the interpolated connection points, (2) carrying the HYCOM current indices corresponding to these coordinates and (3) carrying the corresponding WaveWatchIII wind and waves indices.
- Grid line description, including the node numbers for each line and the grid lines involving a canal involving a waiting time.

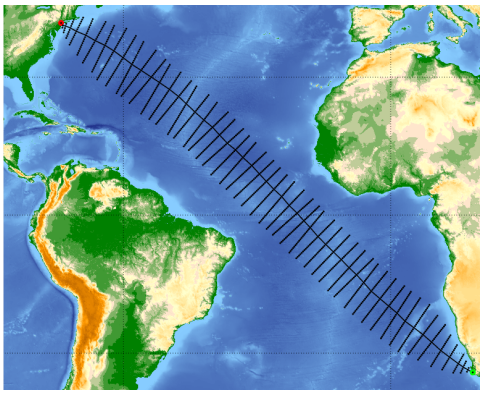

Figure 8.7: Local grid points and shortest path found between Cape Town (South Africa) and New York City (USA). Note that the grid points lay so close to each other that they appear as grid lines.

9 Solver

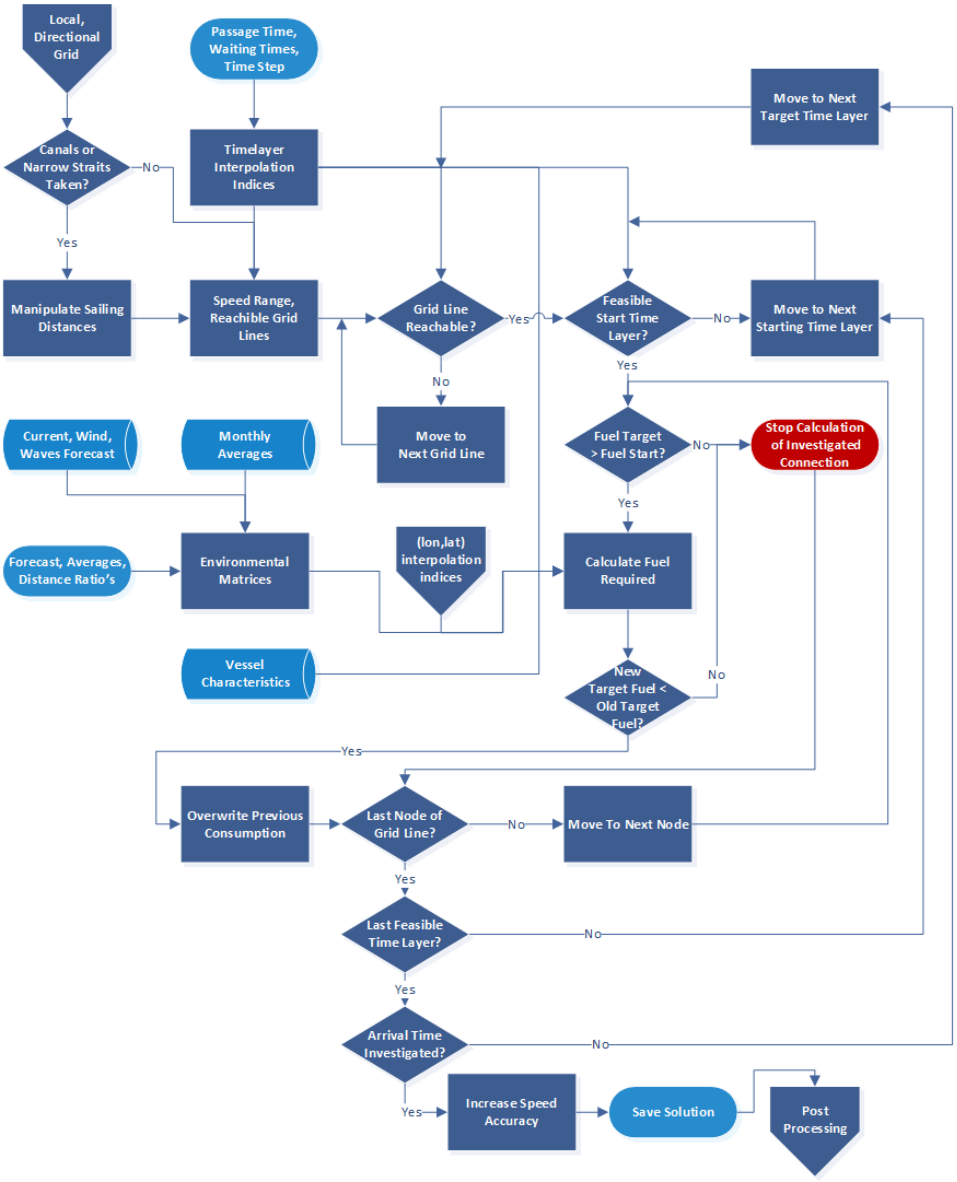

Figure 9.1: Flow Diagram of the Route Optimization Algorithm.

The flow diagram shown above, describes the working of the route optimization algorithm for fuel cost optimization. Before calculating fuel costs, certain measures need to be taken to speed up the calculation and include potential canals or narrow straits in the calculation, as discussed in section 9.1. When the preparations are done, an algorithm based on Dijkstra's algorithm [20] is executed. The steps described in section 9.2 will provide more details on the algorithm and will increase the understanding of the flow diagram. The function to calculate the fuel consumption, often called millions of times, is discussed in section 9.3 and incorporates the weather influence models, as well as the forecasted environment and monthly averages in the tool.

9.1. Preparation Measures

To avoid excessive execution time of the optimization script and to ensure the required variables are properly defined, several calculations are done before the real optimization part is initiated. Apart from programing requirements, like the unpacking of structures to speed up the succeeding calculations or loading certain grids, the feasibility of the route being investigated is checked.

To check the feasibility of the voyage, a simplified calculation of the route is performed, calculating the average sailing speed according to equation 9.1:

$$V_{mean} = \frac{D_{LG}}{t_f - t_s - \sum t_w} \tag{9.1}$$

The mean speed V_{mean} is expressed in kts, the shortest distance found on the local grid D_{LG} in nm; initial and final time are denoted as t_s and t_f respectively and, when canals are encountered, the sum of the expected waiting times of the canals passed is added to the equation. All times are expressed in hours.

Since the average speed is calculated under the assumption the shortest route is taken, the average speed found is the lowest average speed possible. When this speed is higher than the maximum attainable speed of the vessel, an error message is prompted and the real optimization is not initiated.

9.1.1. Sailing Distance Manipulation

When the route is marked feasible, the optimization script is initiated. The first thing to do, is incorporate the canal and narrow strait passages in the solution. Since the fuel consumption is different and uncontrollable during these passages, the fuel cost is treated differently for these parts of the voyage. As will be explained in more detail in section 9.2, the code checks only the locations that can be reached within a certain time frame for fuel consumption, avoiding to calculate paths that will never be part of the solution. The waiting times or increased passage times for the Bosporus and the strait of Hormuz need to be included in this process.

This is done by representing these passages as a longer distance than they actually are, assuming the mean speed is sailed in the canal and adding the distance that would be traveled during the waiting time to it. By doing so, the program is tricked into thinking there are no waiting times, making the optimization algorithm less complicated. This approach does not negatively influence the optimal solution found, since fuel costs of narrow passages are (1) hard to control due to dense traffic and (2) treated as constant predefined value within the optimization.

Assume someone wants to sail a route from A to B, passing the Panama canal. The distance from A to Panama is 1000 km, the Panama canal itself is 100 km and the remaining part of the voyage is another 1000 km. The waiting time to enter the canal is 6 hours. The passage from A to B must be done within 2 days (48 hours).

Assuming there was no waiting time for the canal, the voyage of 2100 km takes 48 hours and the average speed required to arrive on time will be 43.75 km/h. However, since 6 hours of the voyage are spent waiting to enter the panama canal, only 42 sailing hours are available, requiring a speed of 50 km/h to arrive on time. Rather than changing the time interval (which is unwanted since the weather is linked to the time), the distance that must be covered in the Panama canal is changed from 100 km to 400 km. The solution to be found now relates to passing 2400 km in 2 days, which results in the same average speed of 50 km/h. Forcing the realistic 100

km fuel consumption to replace the algorithms 400 km consumption, the total consumption remains realistic and the expected time to exit the Panama canal is realistic as well.

9.1.2. Time Interpolation Matrix

Reducing the execution time of the objective function, calculating the fuel consumed at a connection at a certain speed and time, speeds up the entire process. A significant reduction in execution time can be achieved by calculating values that will be required multiple times in a separate loop. This has already been done in section 8.4, transforming coordinates to weather and current data indices, but a similar approach can be used for the time index related to the different speeds.

Taking the user defined time step, initial time and final time into account, the number of time steps can be defined and added to the grid. Two simplified cases, where 10 time steps are used, are shown in figure 9.2. For a realistic transatlantic passage simulation, about 250 time steps are used.

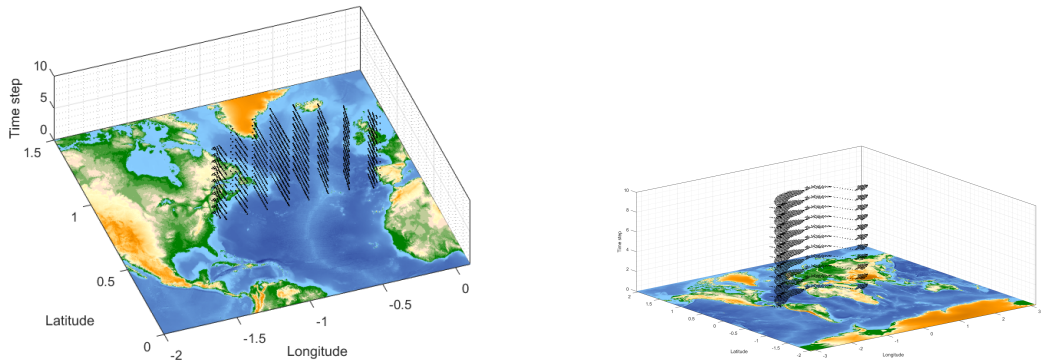

(a) Clear initial grid

(b) Clear time steps

Figure 9.2: Visualization of a simplified 3-D grid using 10 time steps between the initial and target location.

When the 3-D grid is defined, a 4 dimensional matrix can be defined. This matrix will contain information about the time steps of the current and weather forecast to be used when traveling over a connection between two specific time frames. The example below provides more insight in the exact purpose of this matrix.

The fuel consumption between two nodes, starting at the first node at time t_1 and arriving at the second node at time t_2, has to be calculated. While drawing the local grid, 10 intervals per connection have been defined. For each of these 10 intervals, the influence of the environment has to be known. Assuming a constant speed over the investigated connection, the time spent to travel from the first to the second point is divided in 10 equal intervals. These times are compared with the times contained in the forecasts, and a two time layers and the weight to linearly interpolate between these layers, are assigned to each of the 10 intervals.

Because each connection contains the same number of intervals, this process is only dependent on time and the number of the interval but not depending on the initial and final nodes. Together with the connection-specific coordinate matrices, containing the indices of the environmental matrices to be used, the time-indices and weights for the investigated time are now added in matrix form, after which cherry picking from the different matrices can be used to quickly gather the right information.

The 4-D matrix contains following information:

- Dimension 1: for each starting time layer
- Dimension 2: for each arriving time layer (only calculated for time layers later than the starting time layer)
- Dimension 3: for each interval (10, for the example)

- Dimension 4: Forecast time level 1, forecast time level 2, weight level 1, weight level 2.

The above description is true for the oceanic currents. For wind and waves, weather is not defined as locally as the currents and a layer is saved every three hours. Therefore, again to speed up the algorithm, the matrix for wind and waves is reduced from 4 to three dimensions, only containing one value in dimension 4, referring to the closest time level and not using the linear interpolation used for the current analysis.

A final matrix required before the optimization algorithm itself can start, is a matrix containing information with respect to the weighting factors of the available forecasts, the monthly averaged sailing conditions and the shortest path. This matrix is related to the time interpolation matrix, since it describes the weight factor based on the different time levels. Two weights are assigned to each time layer, namely a forecast weight and a monthly averages weight. The third factor, the shortest path, is only used in a passive way and does not require to be stored. In fact, the weather influence is simply disabled for the shortest path weight. Take, for example, a moment where the forecast is used for 50 % and the monthly average for 20 %. In this case, the power required to overcome the environmental conditions will be:

$$P_{req,env} = 0.5P_{forecast} + 0.2P_{monthly} + 0.3P_{shortest} = 0.5P_{forecast} + 0.2P_{monthly} \tag{9.2}$$

Since the power required to overcome the shortest path environment is equal to zero, it is left out of the equation. The power calculation method is explained in more detail in section 9.3.

9.2. Dijkstra Applied to Weather Routing

When the space and time index matrices are calculated,the optimization process can start. Two matrices are continuously being updated during the process, saving the best solution found so far. The first one, called the cost matrix, contains the fuel consumption required to reach a certain node at a specific time, the other one, used for backtracing at the end, is tracking the previous node passed to arrive at that exact solution.

The cost matrix is a NxM matrix, where N represents the number of nodes and M the number of time layers. In other words, Each point in space and time carries exactly one value, the lowest fuel consumption to reach that point. The backtracing matrix will ultimately lead back to the initial point at the first time level.

The optimization is executed in a similar way to the Dijkstra algorithm, which is discussed in section 2.3.1. The approach used for weather route optimization is given below:

1. Create an NxM cost matrix, where N is the number of grid nodes and M the number of time layers. Assign an infinite value to each of its entries, ensuring their value can be overwritten when a feasible solution is found. Create an NxMx2 backtracing matrix, which will be used to store from which node and time layer the number in the cost matrix is calculated.

2. Set the cost matrix for the initial node to zero and identify as fixed. No fuel is needed to reach the initial location.

3. Select the next time level as active time layer. On this time layer, perform steps 4 to 10.

4. Check which grid lines can potentially be reached at this time layer, according to section 9.2.1. For each grid line identified, repeat steps 5 to 9.

5. Determine the earliest and latest time layer to leave the previous grid line to arrive at the current grid line at the time layer from step 3. These layers will be used in step 8.

6. For each of the nodes on the investigated grid line, find the connections that end in that node and follow step 7 to 9.

7. For each time layer in between and including the time layers identified in step 5, follow steps 8 and 9.

8. If the fuel cost at the start of the investigated connection and start time layer is lower than the fuel cost at the arrival point and time level selected in step 3, proceed to step 9. Else, move on to the next starting time layer.

9. Calculate the fuel required to sail the investigated connection from the time level selected in step 7 to the time layer of step 3. If starting fuel cost plus the calculated connection cost is lower than the fuel cost found in the end point and time of the investigated connection, overwrite the value with the new, lower value and update the origin of that fuel cost by storing the starting node and time in the backtracing matrix. Else, move on to the next connection and/or time to be investigated. When a canal passage is detected, a fixed fuel consumption is used rather than a calculated one.
10. When all connections from all feasible time layers to all reachable nodes are checked for the time layer of step 3, set that time layer to fixed and move back to step 3.
11. When all time layers are labeled as fixed, Check the value at the final node and final time layer. This is the lowest fuel consumption to arrive in time.
12. Check the originating node and time layer that led to the lowest consumption in the final point. Follow steps 13 and 14 to find the entire optimal route.
13. In the backtracing matrix, check the origin of the previously identified origin. Store the node's location and time layer.
14. Repeat the previous step until the backtracing matrix refers to the initial node in the initial time layer.
15. Increase accuracy of the optimal path by re-evaluating the found passage on a more extensive time grid, as described in section 9.3.5.
16. At this point, all nodes taken and the corresponding passage times are known. The coordinates of the identified nodes can be read out and the required speed to match with the time layers can be calculated.

From the description above, it can be seen that the method used is closely related to Dijkstra's algorithm, but does not calculate all the weight of all possible connections.

9.2.1. Grid Line Selection

Step 4 of the procedure above includes the selection of grid lines that can be reached in a certain time layer. This is mainly determined by the minimum and maximum speed, which is calculated based on the average speed and the user-specified maximum speed deviation (standard setting: 2.5 kts). When these speeds are defined, the minimum and maximum distance traveled are defined from two fronts, one starting at the initial point, the other one at the final point.

Both approaches determine a minimal and maximum distance traveled. Based on the highest minimal distance and the lowest maximum distance, in combination with the distance at which the grid lines are located (based on shortest path), feasible grid lines are selected. A 10 % margin for the minimal distance is taken into account, allowing for detours covering up to 10 % increased distance traveled at minimum speed. For the maximum distance traveled, a 5% margin is taken, allowing for early arrivals in case this would be optimal.

For the time layer selection of step 5, a similar approach is used, checking which time layers are potentially covered during the investigated connection passage. The minimum and maximum speed, together with the connection length and a margin, are used to achieve this measure, which once again avoids calculating infeasible connections. When the results are unsatisfying, the speed margin can be increased, increasing the possibilities taken into account at the cost of computational time.

9.3. Fuel Consumption Calculation

The algorithm description above is heavily reliant on fuel consumption prediction, which is estimated in step 9. This prediction makes use of the vessel performance models discussed in chapter 3. As discussed before, the consumption at ideal sailing conditions will be based on the results generated by FPM [2] overnight, after which environmental influences for specific connections and times are added to the calculation. The inputs required to calculate the fuel consumption are:

- Initial and final coordinate of the investigated connection and the precomputed heading of the connection.

- Initial and final time.
- Current, waves and wind matrices.
- Vessel parameters: predetermined Blendermann wind resistance coefficient, Kreitner constant, power curves relating speed, consumption, propeller revolutions and %MCR and a specific fuel/oil consumption curve.
- Indices for the space and time interpolation for both the HYCOM and WaveWatchIII data.
- Monthly averaged current, waves and wind matrices, together with the indices required for space and time interpolation.
- Weighting matrix, describing the ratio between forecast environment, monthly averaged environment and shortest path for every interpolated moment in time.

From these parameters, the fuel consumption is calculated as follows:

1. Calculate the required speed over ground according to equation 9.3, which uses the Haversine function, included in [7].
2. Match this speed with a consumption and %MCR setting, using the speed-consumption and consumption-%MCR relations.
3. If the %MCR value does not exceed 120, continue to step 4, else, return infinite fuel consumption (impossible conditions are imposed) and terminate fuel calculation for that particular time and connection.
4. If current influence is selected, calculate the current influence on the speed through water according to section 9.3.1. Else, take speed over ground as speed through water.
5. Convert the speed through water and corresponding fuel consumption to power, using the inter- or extrapolated specific fuel/oil consumption that matches the %MCR.
6. If waves correction is selected, calculate additional power required due to waves as discussed in section 9.3.2. If not selected, assign a value of 0 kW to wave power.
7. If wind correction is selected, calculate additional power required due to wind as discussed in section 9.3.3. If not selected, assign a value of 0 kW to wind power.
8. Summarize the power required to maintain the speed through water, the wind and the wave power to find the total power required. Convert to fuel consumption using equation 9.4.

$$V_{req} = \frac{2r}{\Delta t} \cdot sin^{-1}\sqrt{sin(lat_2 - lat_1)^2 + cos(lat_1)\,cos(lat_2)\,sin(lon_2 - lon_1)^2} \tag{9.3}$$

Where V_{req} is the required speed, r the radius of the earth, assumed constant and 6371 km and Δt the time used to sail from the starting point (lon_1, lat_1) to the final point (lon_2, lat_2).

$$FC = \Delta t \cdot sfoc(P_{TW} + P_{waves} + P_{wind}) \tag{9.4}$$

Where FC is the fuel consumption, Δt the sailed time, $sfoc$ the specific fuel/oil consumption, P_{TW} the required power to sail the speed through water, P_{waves} the power to overcome the wave resistance and P_{wind} the power to overcome the wind resistance.

9.3.1. Current Influence

Changing from speed over ground to speed through water, is done by adding the parallel component of the local current to the speed over ground. For each interval on the connection, the longitude, latitude and time indices are read out and the corresponding u and v component of the current is composed by linear time interpolation.

When the heading of the vessel and the speed components of the current are known, the parallel current can be calculated. This is done for each interval, after which the current experienced over the connection is averaged. Non-numerical values are removed from the solution. When there is no numerical value, it is assumed there is no current. The usage of the average value is justified by the linear relation between speed over ground, speed through water and current, as shown in equation 9.5.

$$V_{TW} = V_{OG} + w_f V_{cur,f} cos(\theta_{cur,f}) + w_{ma} V_{cur,ma} cos(\theta_{cur,ma}) \tag{9.5}$$

Where V_{TW} is the speed through water, V_{OG} the speed over ground, V_{cur} the velocity of the current and θ_{cur} the relative angle of the current, where current coming from the stern is described as zero degrees. subscript f indicates forecast, whereas ma refers to the monthly averages. w is the weight of the forecast or monthly averaged value.

If current is taken into account during the optimization process, the above procedure is followed. If not, the speed through water is set equal to the speed over ground, and the other parts of the fuel cost are calculated. The power required to attain the speed through water calculated according to equation 9.5, is converted to power using the speed-%MCR relation provided by FPM.

9.3.2. Waves Influence

To calculate the power required to overcome the waves for a certain connection, the closest time layer, as well as the right longitudinal and latitudinal indices are read out. The course is again required, since the direction of the waves influences the amount of power required. From the wave data, the relative direction and the Kreitner coefficient, determined according to equation 6.2, the wave resistance is calculated. To convert the wave resistance to power, the speed through water is taken into account.

When C_K is the Kreitner coefficient, $H_s w$ the significant wave height, θ_{waves} the relative wave direction, this time using the bow as reference, and V_{TW} the speed through water, w the weighting factor for the forecast f and monthly averages ma, the power required to overcome the wave resistance is given by:

$$P_{waves} = \left[w_f \left(\frac{2}{3} + \frac{1}{3} cos(\theta_{waves,f}) \right) H_{sw,f}^2 + w_{ma} \left(\frac{2}{3} + \frac{1}{3} cos(\theta_{waves,ma}) \right) H_{sw,ma}^2 \right] C_K V_{TW} \tag{9.6}$$

Here, it becomes clear why the Kreitner coefficient has been precomputed. If this was not done, the same number would have been computed for each investigated connection. Similar to the current influence, the procedure above is repeated for each connection interval and then averaged. To make the averaging possible, it has been chosen to calculate the power required. Since each interval has the same length, averaging power is allowed while optimizing for fuel consumption, since consumption and power have a linear relation when assuming a constant specific fuel/oil consumption. Looking at figure 6.2 and knowing the %MCR will hardly change over the connection, this assumption seems valid.

9.3.3. Wind Influence

The wind influence is evaluated in a similar way as the influence of the waves, but is slightly more complicated. The speed and direction is not only relative to the heading of the ship, but also has a different influence depending on the sailed speed.

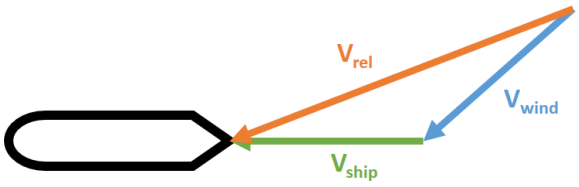

Figure 9.3: Relative and absolute wind acting on a ship.

As can be seen in figure 9.3, the relative influence of the wind is depended on both the speed of the ship and the speed and relative direction of the wind itself, but the influence of the wind generated by the ship is already included in the ideal condition consumption. Simply calculating the power required for the wind itself, ignoring the ship speed, is also not possible, because of the third power relation between wind speed and power required. Therefore, a different approach is used:

1. Calulate the relative wind speed and direction, as experienced on the vessel itself, according to equations 9.7 and 9.8.
2. Calculate the resistance due to this relative wind according to equation 9.9
3. Calculate the wind resistance due to the self-induced wind on the ship, using equation 9.10.
4. Calculate the total resistance due to wind by subtracting the wind resistance due to the ship movement from the total relative wind resistance (equation 9.11), singling out the wind influence.
5. Convert to power, using the speed over ground. As explained in the beginning of section 9.3, this power will be added to the other environmental influences and the ideal conditions power, allowing for the fuel cost calculation.

$$V_{rel} = \sqrt{V_{OG}^2 + V_{wind}^2 + 2V_{OG}V_{wind}cos(\theta_{wind})} \tag{9.7}$$

Where θ_{wind} is the direction of the absolute wind, relative to the sailing direction.

$$\theta_{wind,rel} = cos^{-1}\left(\frac{V_{wind}^2 - V_{rel}^2 - V_{OG}^2}{-2V_{OG}V_{rel}}\right) \tag{9.8}$$

To calculate the wind resistance according to Blendermann [13], following equation is used for both the total relative wind and the wind due to the ships movement:

$$R_{wind,rel} = \frac{1}{2}C_X(\theta wind, rel)\,\rho_{air}V_{rel}^2 \tag{9.9}$$

$$R_{wind,ship} = \frac{1}{2}C_X(0)\,\rho_{air}V_{rel}^2 \tag{9.10}$$

Recall that, during the ship selection procedure explained in section 6.1.1, the resistance coefficient C_X has been calculated for all wind angles. Making calls to this array is much faster than recomputing it within the wind power calculation for each connection investigated.

$$R_{wind} = R_{wind,rel} - R_{wind,ship} \tag{9.11}$$

$$P_{wind} = R_{wind}V_{OG} \tag{9.12}$$

As for the current and the waves, this is repeated for each interval on the investigated connection using both the wind forecast and monthly averaged wind, after which the average power required is taken to calculate the total consumption increase due to wind over the connection, as shown in equation 9.13.

$$P_{wind} = w_f P_{wind,f} + w_{ma}P_{wind,ma} \tag{9.13}$$

Where the influence based on the wind forecast and the weight w_f is summarized with the monthly averaged influence, weighted according to w_{ma}.

9.3.4. Fuel Consumption for Canals and Narrow Passages

The fuel consumption while passing a canal or narrow passage is calculated in a different way, not taking the environmental conditions into account. By doing this, some accuracy in the estimated total fuel consumption is lost, but this does not influence the optimization process, since no different routes can be taken for these parts and the speed sailed is depending more on the canal traffic than the captain's wishes.

Compared with the straight line distance and consumption, following modification have been made on canals and narrow passages:

- Gibraltar: No modification
- Panama and Suez canal: factor 1.1 increased sailing distance and time
- Bosporus and Kiel canal: factor 1.3 increased sailing distance and time
- Strait of Hormuz: factor 1.7 increased sailing distance and time

When a canal passage is detected, the original objective function is not called and the fuel consumption and time spent are implemented as fixed values. While verifying the code, these passages will not be taken into account, since it is not possible to optimize for the canal passages. After passing through a canal, it is recommended to redo the optimization process, using the real time that the end of the canal is reached rather than the originally expected time.

9.3.5. Increased Speed Accuracy

Something only briefly touched until now, is the biggest drawback of the optimization method discussed throughout this chapter, namely the fixed arrival times on a grid point. Because of the nature of the time layer grid, the possible arrival times at an intermediate grid point are fixed to a finite set of points in time, which most likely does not contain (yet approximates) the optimal arrival time at that place. Assume a 1 hour time interval is selected and the investigated grid point is located 100 nm away from the initial point and part of the first grid line. Arrival times exactly 1, 2, ... , 20 hours after the voyage start are investigated, but in reality, arriving 8 hours and 20 minutes after the start would result in the optimal solution. This possibility is not investigated using the current algorithm.

One could reason that the time interval could be reduced, including a time layer every minute or even every second, approximating the optimum closer and closer. While this is indeed correct, this approach is infeasible due to the nearly quadratic relation between calculation time and number of time layers. Therefore, a different approach is used to reduce the influence of the arrival time inaccuracy.

When the optimal route on the 3-D grid is found, the route found is set as fixed. However, the arrival times at the intermediate nodes are not fixed yet. A second optimization loop, similar to the loop described in section 9.2 is initiated over the fixed path, allowing time variations with a much small interval (5 minutes by default) ranging up to one original time interval away from the solution found by the main algorithm, covering the entire route with a 5 minutes precision.

The proposed method does not guarantee the optimal solution is found, but it does guarantee that the optimal solution on the selected grid is found (see chapter 11 for more details). Finding an even better solution can be done by increasing the number of grid lines, grid points and/or time layers at the cost of computational time.

9.3.6. Algorithm Modularity

The entire code, including the optimization algorithm discussed in this chapter, is build up in a highly modular way. The fuel consumption calculator, for example, calls three different functions to determine the influence of the current, the wind and the waves. This makes it easier to replace the models used, when better models become available, as long as the outputs (current speed and power required, in this case) remain the same.

Another advantage of the usages of many modules, is the option to include a different objective function in the algorithm. The main structure of the code can remain unchanged, the only required change to optimize for something different is the objective function. For example, changing the objective from fuel required to costs could be done when the zones requiring cleaner (but more expensive) fuels are included in the optimization function, checking the fuel price for each connection investigated, then multiplying this with the calculated consumption. Other possibilities could include emissions, distance sailed, lowest significant waveheight encountered, reduced rainfall (when connected to the proper databases), ...

10

Outputs

When the final route, including the optimal path, is found, the results are interpret, visualized and comprehensively documented for the operators and captains. The result visualizations shown within the application are discussed in section 10.1, the externally saved solutions in section 10.2 and the commands, sent to the vessels, are discussed in section 10.3. To wrap up the chapter, voyage safety will briefly be discussed.

In this chapter, the same transatlantic voyage is always used. To demonstrate the capabilities of the tool, a voyage with severe weather conditions has been selected, sailing from Dover (United Kingdom) towards Charleston (USA). The voyage is simulated using the Maersk Niagara, leaving on January 15, 2018 at 00:00 UTC and arriving on January 27 at 12:00 UTC. The voyage of over 3 500 nautical miles (nm) as the crow flies, passes through heavy weather in the north-east part of the Atlantic when not modifying the route taken.

10.1. Outcomes Contained in the Application

Within the application, there are five screens and the command window displaying the optimal solution found. Each of these is discussed in a separate section below. The graphs are found in the different tabs of the application and checking them to increase thrust in the result is advised.

10.1.1. Command Window

To start with, the calculated optimal path and corresponding current, waves, wind and consumption, are compared with the shortest route at constant speed, providing the user with the gains achieved by the optimization algorithm. An example of a passage where strong gains are made due to very heavy weather on the Atlantic, is shown in figure 10.1. In this figure, it can be seen that the optimal route is taking a detour of 118.29 nm, increasing favorable current by 0.17 knots on average (a counter current is still experienced) and reducing the average wind speed encountered from 10.34 m/s to 8.74 m/s. The significant waveheight is expected to be reduced by 0.71 m. With these changes, a total of approximately 55.29 tons of Marine Gas Oil (MGO) is saved by the optimization process, which corresponds to a consumption reduction 14.04 %. In this case, weather optimization seems to be extremely powerful, however, this is a very specific case, aiming at heavy weather conditions. In general, the savings will be much lower, as will be discussed in more detail in chapter 13.

```
%%%%%%%%%%%%%%%%%%%%%%%%%%%%%%%%%%%%%%%%%%%%%%%%%%%%%%%%%%%%%%%%%%%%%%%
%%                                RESULTS                                %%
%%%%%%%%%%%%%%%%%%%%%%%%%%%%%%%%%%%%%%%%%%%%%%%%%%%%%%%%%%%%%%%%%%%%%%%
                        Shortest Path Results
Distance Covered: 2988.72 nm.
Mean favorable current: -0.18426 knots.
Mean wind speed : 8.7546 m/s.
Mean significant waveheight : 4.1626 m.
Estimated Fuel Consumption: 346.1255 tons MGO.
=========================================================
                        Optimal Path Results
Distance Covered: 3083.0447 nm.
Mean favorable current: -0.032014 knots.
Mean wind speed : 6.7882 m/s.
Mean significant waveheight : 3.4432 m.
Estimated Fuel Consumption: 289.9485 tons MGO.
=========================================================
                           Differences
Distance sailed increased by 94.3248 nm.
Favorable current increased by 0.15225 knots.
Wind speed reduced by 1.9664 m/s.
Sighnificant waveheight reduced by 0.71938 m.
56.177 tons MGO saved. (16.2303 %)
%%%%%%%%%%%%%%%%%%%%%%%%%%%%%%%%%%%%%%%%%%%%%%%%%%%%%%%%%%%%%%%%%%%%%%%
```

Figure 10.1: Voyage optimization information through the command window of a transatlantic voyage.

10.1.2. Topological Map

The second visualization is found on the topological map, on which the grid, shortest path and proposed optimal solution are visualized. This helps to understand why certain routes are taken, possibly taking a detour while avoiding sailing through shallow waters. The result of the transatlantic voyage is shown in figure 10.2.

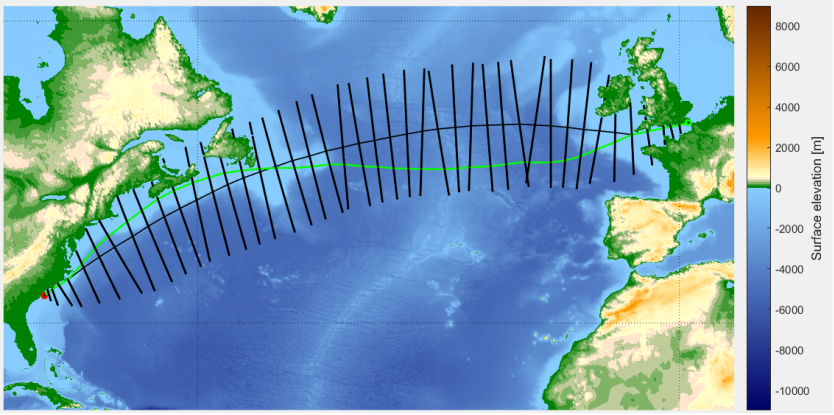

Figure 10.2: Voyage optimization information of a transatlantic voyage, visualized on the topological map.

It can be seen that the grid points furthest away from the shortest path, are nowhere taken while looking for the optimal route. If this is ever the case, the width of the local grid can be increased to make sure the fuel consumption is reduced as much as possible.

10.1.3. Current Map

Next, the route found is visualized on the monthly averaged current map, as shown in figure 10.3. This map is static, hence the background is fixed. Therefore, it was chosen to visualize the monthly averaged current, rather than the most recent current forecast. This map proves to be most useful when looking at the latter part of the voyage. To see the first part of the voyage, plotted on the current forecast, see appendix C.

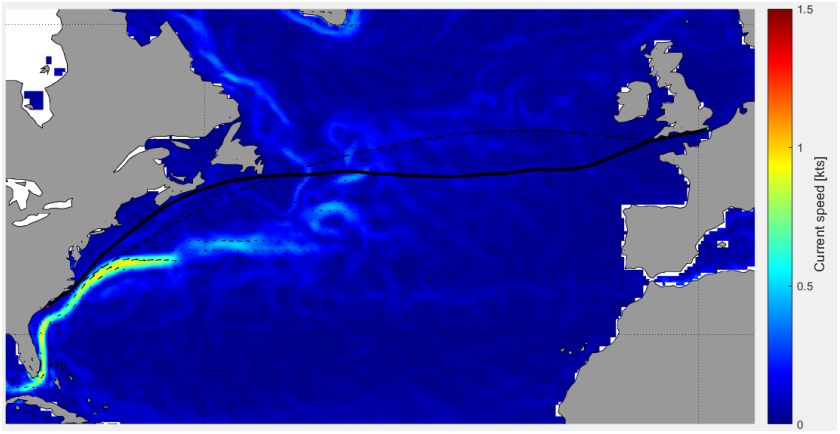

Figure 10.3: Voyage optimization information of a transatlantic voyage, visualized on the monthly averaged current map.

The influence of the monthly current can be seen at the final part of the voyage, where no forecast data is available anymore, and route selection is based on monthly averaged weather. To avoid the strong gulf stream counter current, the proposed optimal route sails very close to the USA coast, where the adverse current is expected to be weaker.

10.1.4. Waves Map

In the same way, the optimal path is shown on a waves chart, again using the monthly averaged values rather than the wave forecast data. To see the route plotted on a waves forecast chart, please refer to section 10.2 or appendix C.

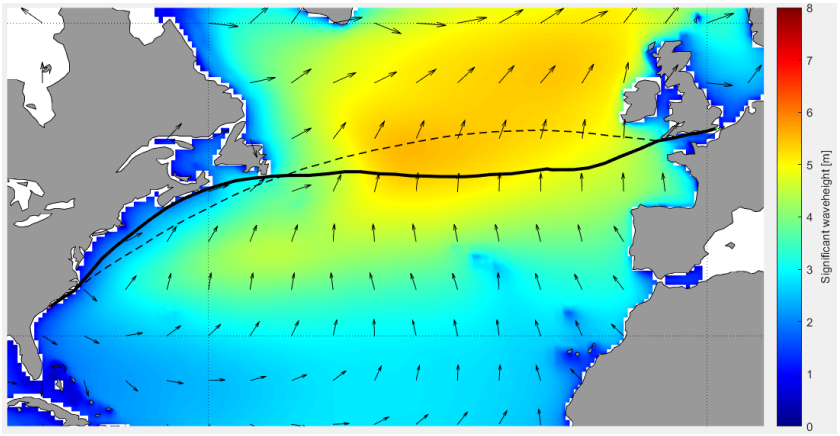

Figure 10.4: Voyage optimization information of a transatlantic voyage, visualized on the monthly averaged waves map.

Sailing closer to the coastline of the USA seems to not only benefit the encountered current, but also results in a reduction in significant waveheight in an average month January.

10.1.5. Wind Map

Following the monthly averaged chart approach, the optimal route found is plotted against a monthly averaged wind chart as well. To see the route plotted on a wind forecast chart, please refer to appendix C.

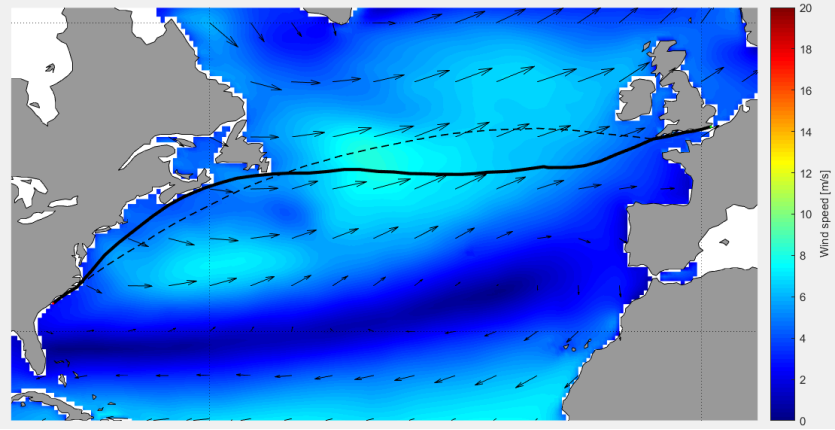

Figure 10.5: Voyage optimization information of a transatlantic voyage, visualized on the monthly averaged wind map.

A wind speed reduction, similar to the significant wave height reduction, is expected while sailing close to the coastline of the USA.

10.1.6. Instructions

A brief overview on the instructions to be sent to the captain, is given in the “Instructions” tab. It shows the required engine setting (%MCR) over time, together with the heading. As can be seen from figures 10.6 and 10.7, there is a print button next to the graphs, which can be used to generate a pdf file to send towards the captain of the investigated vessel. More details on this file can be found in section 10.3. The purpose of visualizing this, is providing a quick insight on the critical moments for the captain to either change course or change engine setting.

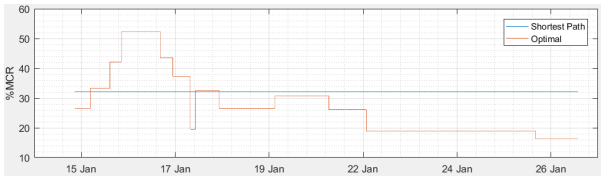

Figure 10.6: Engine setting over time, expressed in %MCR.

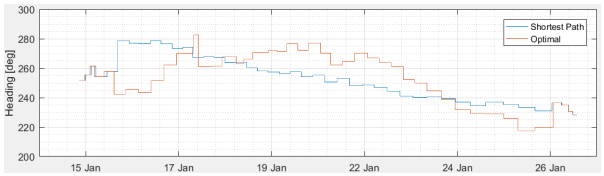

Figure 10.7: Required heading to sail the optimal route found.

Important to note is the blockwise %MCR representation. The optimization loop does not result in such a smooth engine setting evolution, but shows small variations for each connection between two grid points taken. Feedback from colleagues of the operational department of CMB [14], who are the main users of the tool, revealed that constant fiddling with the engine setting is something captains prefer to avoid. Therefore, if the engine settings are very close to each other, the engine setting is smoothed and divided in blocks. The default engine smoothing setting is 2 %MCR, averaging the engine setting for parts within the 2 %MCR margin.

The route optimizer suggests a higher power setting from January 16 till January 17. This does seem to make sense, because speeding up the first two days ensures the heaviest weather in the north-east part of the At-

lantic is avoided. This is clearly visible in figures 10.15 and 10.16, where the orange and red wave visualizations represent the heaviest weather conditions.

The heading is defined as 0 degrees while sailing north, then advancing clockwise (90 degrees heading means sailing east). The shortest path shows a relative constant change in heading during the open sea part of a voyage, including small variations due to the finite nature of the local grid. The optimal heading, however, indicates that there will be a steep turn towards the south in the beginning of the voyage, which will slowly be corrected for during the rest of the voyage. Sailing more to the south again helps to avoid too heavy weather.

10.2. Visual Voyage Simulations

Apart from visualizations and numerical values within the application, it is possible to generate GIF files, simulating the entire voyage using the weather forecast to draw current, waves or wind in the background. The first 12 frames, using wave visualizations as background, are shown in figures 10.8 till 10.19. The same figures for wind and current, can be found in appendix C.

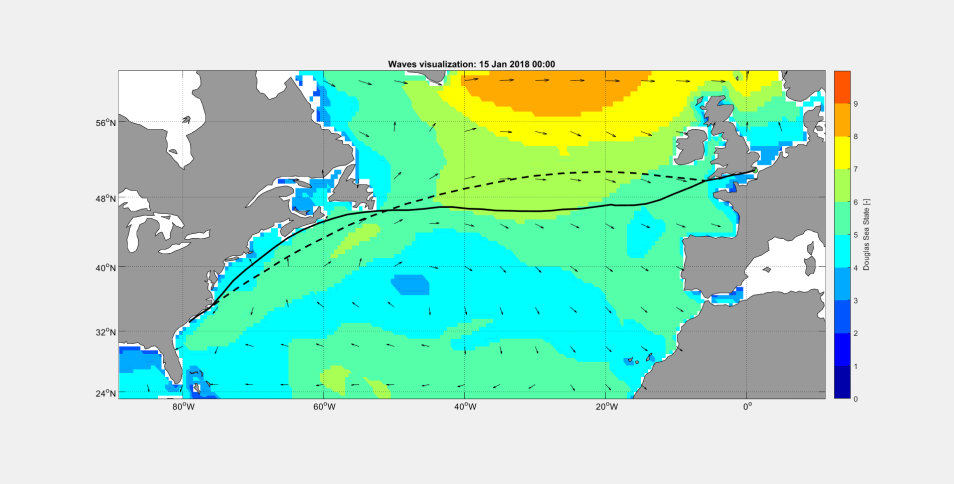

Figure 10.8: Voyage simulation: 15-Jan-2018 00:00

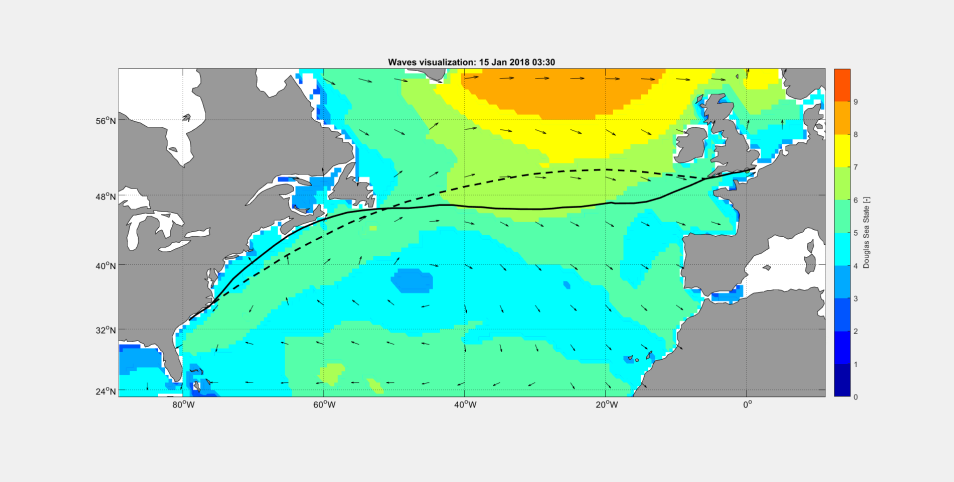

Figure 10.9: Voyage simulation: 15-Jan-2018 03:30

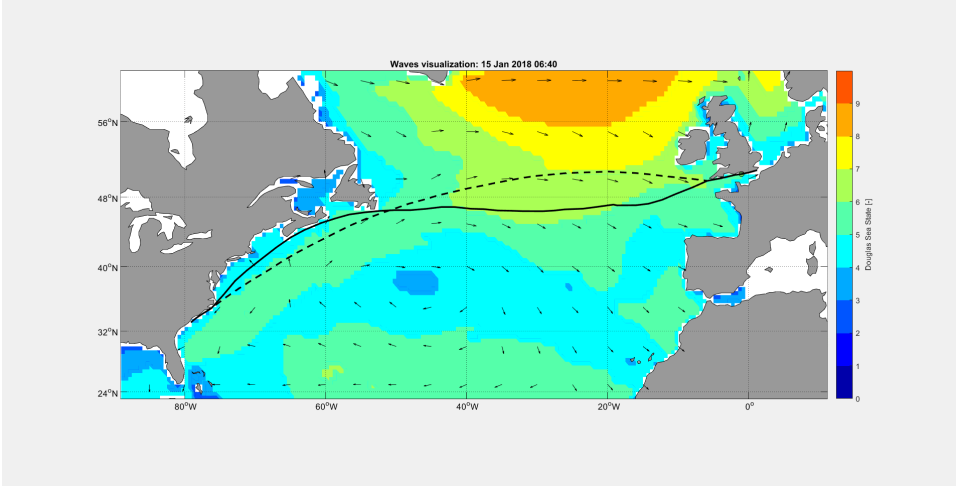

Figure 10.10: Voyage simulation: 15-Jan-2018 06:40

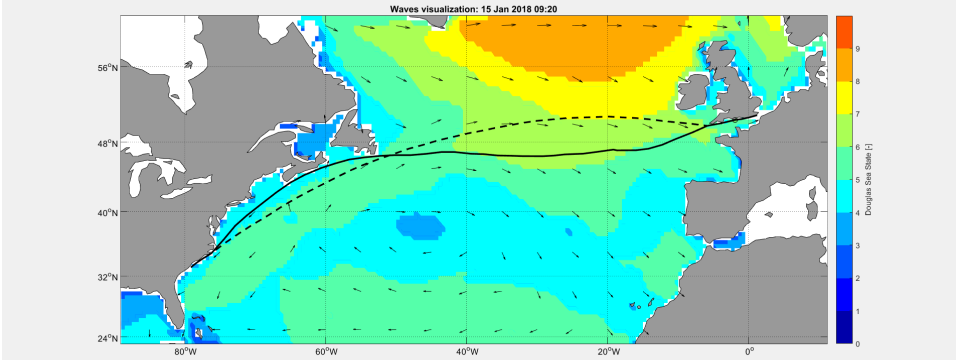

Figure 10.11: Voyage simulation: 15-Jan-2018 09:20

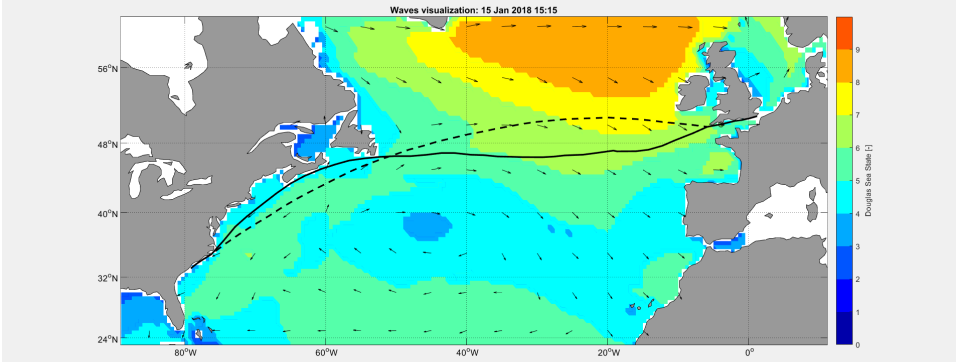

Figure 10.12: Voyage simulation: 15-Jan-2018 15:15

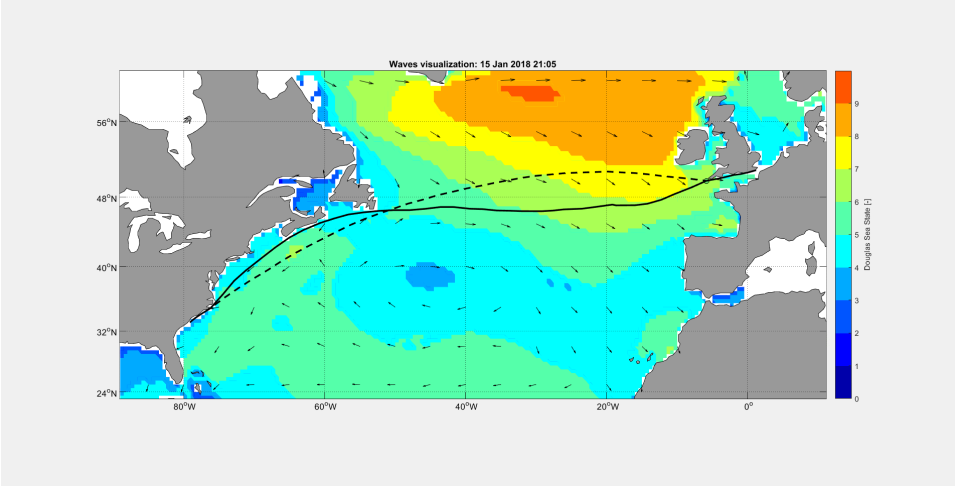

Figure 10.13: Voyage simulation: 15-Jan-2018 21:05

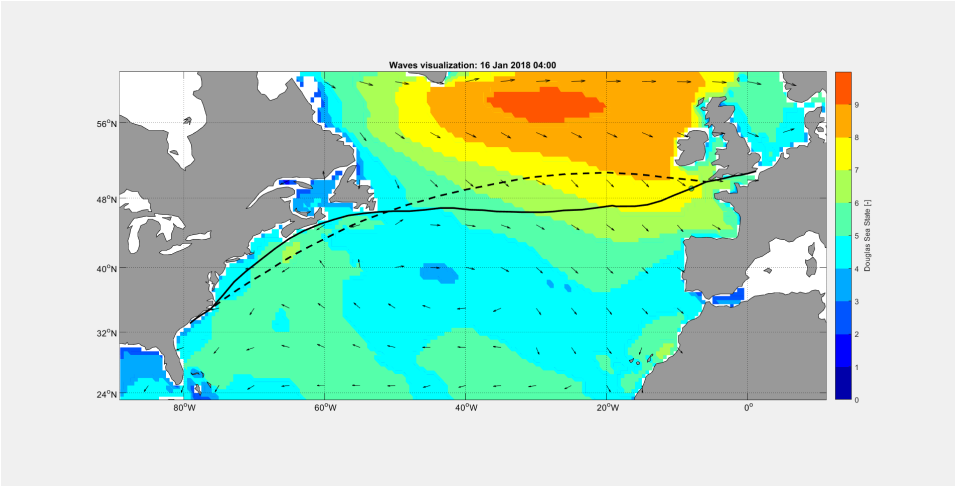

Figure 10.14: Voyage simulation: 16-Jan-2018 04:00

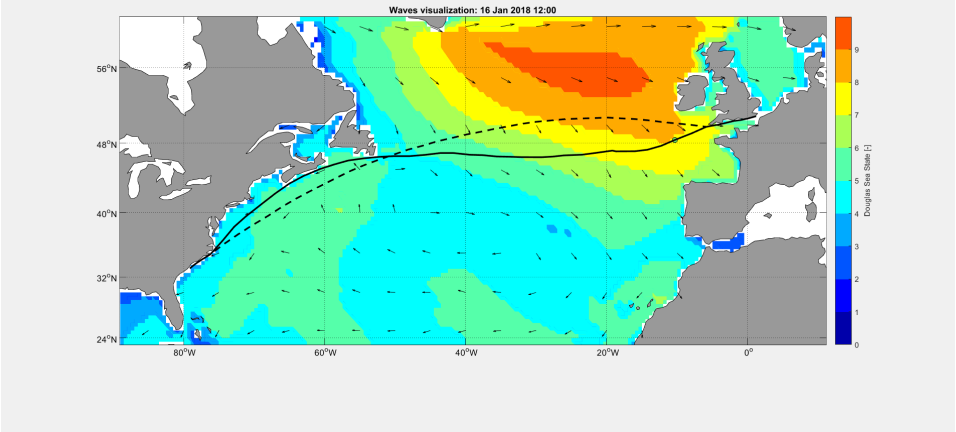

Figure 10.15: Voyage simulation: 16-Jan-2018 12:00

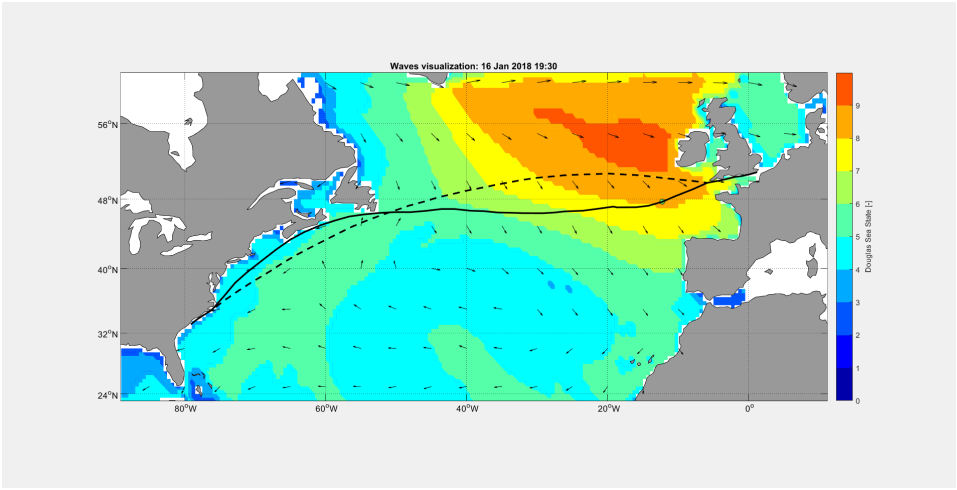

Figure 10.16: Voyage simulation: 16-Jan-2018 19:30

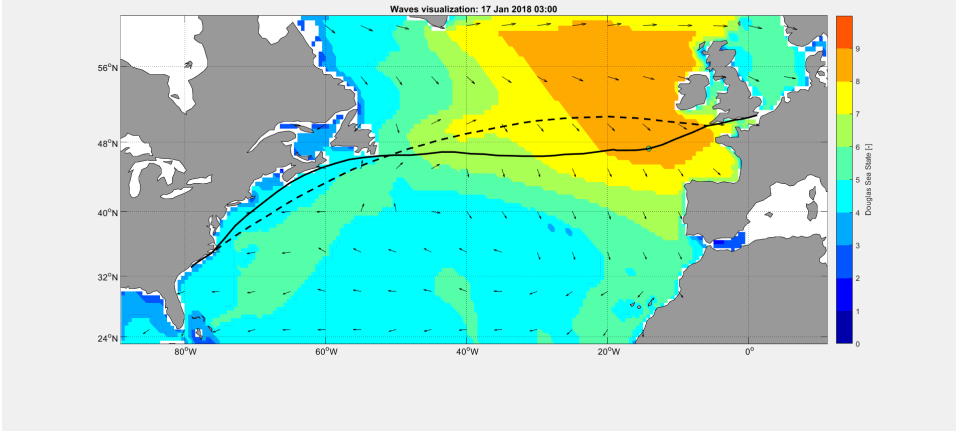

Figure 10.17: Voyage simulation: 17-Jan-2018 03:00

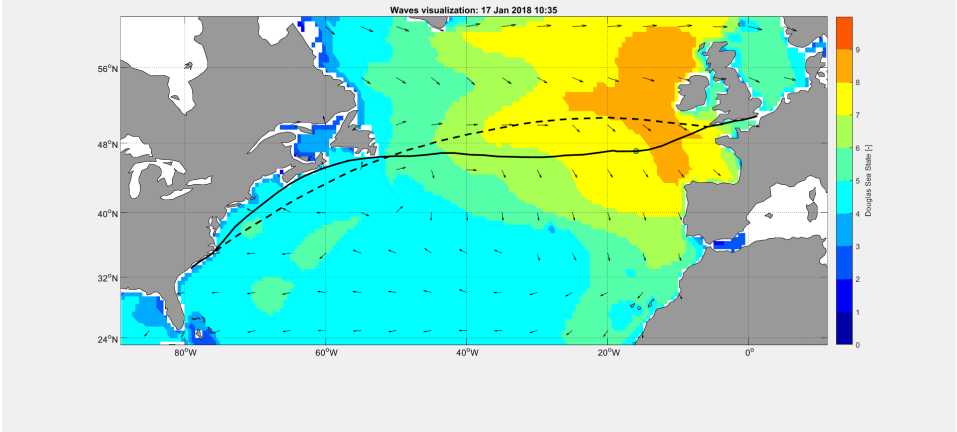

Figure 10.18: Voyage simulation: 17-Jan-2018 10:35

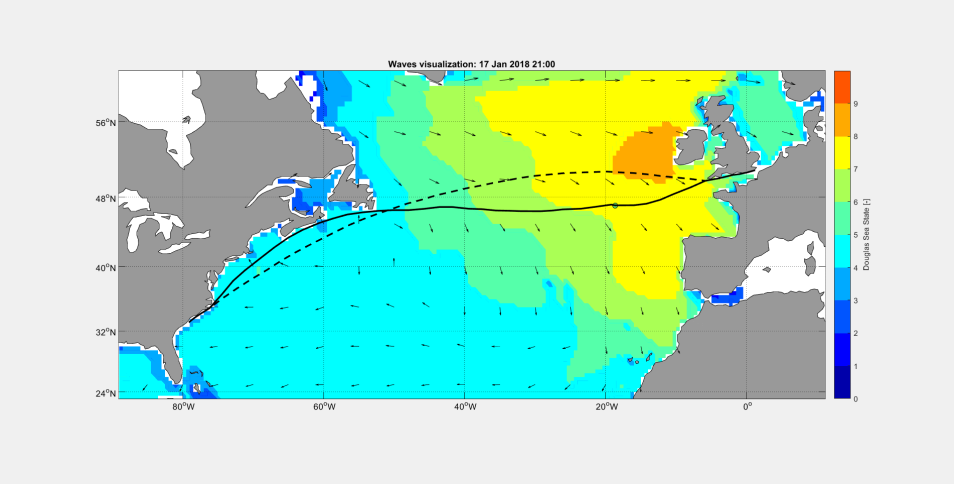

Figure 10.19: Voyage simulation: 17-Jan-2018 21:00

10.3. On-board Instructions

The captain of a ship is always responsible for the route taken. Therefore, only suggestions can be done from the shore, preferably limiting the amount of data required. To deal with this matter, a pdf file can be generated by the users, containing a time at which a certain position must be reached. The required speed over ground and course to reach the next point are given, and the expected engine setting required to reach the specified coordinate on time is provided as well. Apart from this table, which is shown in table 10.1, a map on which the proposed route is visualized, is given as well. The map of the route discussed in this chapter, is shown in figure 10.20.

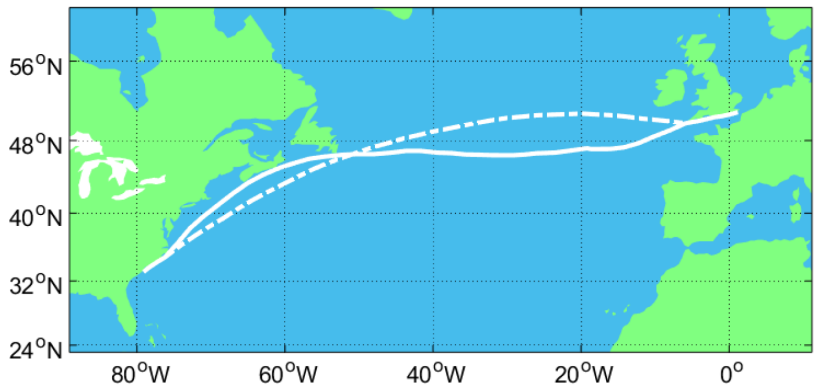

Figure 10.20: Visualization of the proposed route, sent to the captain. The full line represents the optimal route, the dashed line the shortest one.

Timestamp (UTC)	Coordinate	Speed over ground	%MCR	Course
15-Jan-2018 00:00	50^o56.88'N 1^o11.12'E	12.96 kts	26.54 %	251.62 ^{o}
15-Jan-2018 03:30	50^o42.52'N 0^o3.05'E	13.35 kts	26.54 %	255.58 ^{o}
15-Jan-2018 06:40	50^o31.94'N 1^o1.41'W	13.02 kts	26.54 %	261.38 ^{o}
15-Jan-2018 09:20	50^o26.7'N 1^o55.31'W	13.48 kts	33.26 %	254.21 ^{o}
15-Jan-2018 15:15	50^o4.8'N 3^o55.21'W	13.28 kts	33.26 %	257.79 ^{o}
15-Jan-2018 21:05	49^o48.22'N 5^o52.71'W	13.41 kts	42.11 %	242.35 ^{o}
16-Jan-2018 04:00	49^o4.97'N 7^o58.82'W	12.92 kts	52.39 %	245.36 ^{o}
16-Jan-2018 12:00	48^o21.64'N 10^o20.89'W	11.52 kts	52.39 %	243.40 ^{o}
16-Jan-2018 19:30	47^o42.79'N 12^o16.2'W	11.04 kts	52.39 %	251.71 ^{o}
17-Jan-2018 03:00	47^o16.61'N 14^o12.42'W	9.66 kts	43.52 %	262.08 ^{o}
17-Jan-2018 10:35	47^o6.36'N 15^o59.1'W	10.54 kts	37.25 %	269.78 ^{o}
17-Jan-2018 21:00	47^o5.56'N 18^o40.26'W	7.49 kts	19.53 %	282.76 ^{o}
18-Jan-2018 00:00	47^o10.51'N 19^o12.48'W	12.16 kts	32.54 %	261.04 ^{o}
18-Jan-2018 08:00	46^o55.08'N 21^o33.31'W	12.74 kts	32.54 %	261.56 ^{o}
18-Jan-2018 14:20	46^o43.05'N 23^o29.79'W	12.89 kts	26.47 %	267.61 ^{o}
18-Jan-2018 22:40	46^o38.22'N 26^o6.05'W	13.14 kts	26.47 %	262.83 ^{o}
19-Jan-2018 03:25	46^o30.31'N 27^o36.07'W	12.94 kts	26.47 %	266.39 ^{o}
19-Jan-2018 08:40	46^o25.9'N 29^o14.42'W	12.88 kts	26.47 %	270.53 ^{o}
19-Jan-2018 18:00	46^o26.58'N 32^o8.74'W	12.55 kts	26.47 %	272.30 ^{o}
19-Jan-2018 23:15	46^o29.09'N 33^o44.28'W	12.79 kts	30.63 %	271.40 ^{o}
20-Jan-2018 05:15	46^o30.78'N 35^o35.64'W	12.34 kts	30.63 %	276.63 ^{o}
20-Jan-2018 11:50	46^o39.95'N 37^o33.02'W	12.47 kts	30.63 %	272.21 ^{o}
20-Jan-2018 18:00	46^o42.74'N 39^o24.98'W	12.69 kts	30.63 %	277.15 ^{o}
21-Jan-2018 01:35	46^o54.43'N 41^o44.46'W	12.50 kts	30.63 %	270.15 ^{o}
21-Jan-2018 07:35	46^o54.44'N 43^o34.18'W	12.51 kts	26.09 %	262.30 ^{o}
21-Jan-2018 14:50	46^o42.05'N 45^o45.36'W	12.39 kts	26.09 %	264.65 ^{o}
21-Jan-2018 22:10	46^o33.34'N 47^o56.99'W	12.27 kts	26.09 %	270.09 ^{o}
22-Jan-2018 05:55	46^o33.21'N 50^o15.19'W	12.37 kts	18.98 %	266.89 ^{o}
22-Jan-2018 12:50	46^o28.35'N 52^o19.25'W	12.45 kts	18.98 %	263.65 ^{o}
22-Jan-2018 20:15	46^o17.89'N 54^o32.13'W	12.44 kts	18.98 %	260.93 ^{o}
23-Jan-2018 03:30	46^o3.44'N 56^o40.58'W	12.40 kts	18.98 %	252.22 ^{o}
23-Jan-2018 10:20	45^o37.4'N 58^o36.19'W	12.51 kts	18.98 %	249.93 ^{o}
23-Jan-2018 17:40	45^o5.72'N 60^o38.59'W	12.54 kts	18.98 %	244.64 ^{o}
24-Jan-2018 02:35	44^o17.59'N 63^o0.39'W	12.54 kts	18.98 %	238.65 ^{o}
24-Jan-2018 10:40	43^o24.68'N 65^o0.16'W	12.38 kts	18.98 %	231.90 ^{o}
24-Jan-2018 19:45	42^o15.14'N 67^o0.53'W	12.44 kts	18.98 %	229.23 ^{o}
25-Jan-2018 04:30	41^o3.93'N 68^o50.6'W	12.47 kts	18.98 %	229.14 ^{o}
25-Jan-2018 15:50	39^o31.26'N 71^o10.3'W	12.48 kts	18.98 %	225.82 ^{o}
26-Jan-2018 00:30	38^o15.79'N 72^o49.74'W	12.47 kts	18.98 %	217.59 ^{o}
26-Jan-2018 10:50	36^o33.63'N 74^o28.4'W	12.42 kts	16.20 %	219.84 ^{o}
26-Jan-2018 21:35	34^o51.03'N 76^o13.44'W	12.50 kts	16.20 %	236.42 ^{o}
27-Jan-2018 02:55	34^o14.12'N 77^o20.77'W	12.45 kts	16.20 %	235.14 ^{o}
27-Jan-2018 07:00	33^o45.05'N 78^o11.03'W	12.43 kts	16.20 %	230.58 ^{o}
27-Jan-2018 09:30	33^o25.32'N 78^o39.81'W	12.25 kts	16.20 %	228.31 ^{o}

Table 10.1: Table containing instructions, sent to the captain.

10.4. Voyage Safety Indication

A voyage is said to be safer, when the chances to lose a life or lose cargo are smaller. Logically, the better the weather, the lower the risks of losing someone or something. To indicate the user whether a route becomes safer or not, the mean average wave height and wind speed is prompted when the simulation is completed, as shown in figure 10.1.

Looking at the weather influence models, it can be expected that optimizing the route reduces the weather encountered, however, there are some cases where this is not always true, especially while following a strong

oceanic current that takes the ship through heavier weather. In chapter 13, where several routes and environmental ratio's are investigated, more details on safety will be provided.

11

Verification and Validation

Aiming at a reliable and usable tool, the correctness of the code has to be shown. The most important part of the code, the modified Dijkstra algorithm, will be verified in section 11.1. To validate the environmental and performance models used in the weather route optimization tool, the accuracy of the expected fuel consumption will be tested as discussed in section 11.2. Finally, the correct implementation of the forecast models and seasonal averages will be discussed in section 11.3.

11.1. The Optimization Loop

The optimization loop is based on Dijkstra's Algorithm, which has been proven to result in the lowest cost for directional graphs containing only nonzero and nonnegative entries (for example by K. Subramani [80]), however, proving Dijkstra does not guarantee the algorithm is implemented correctly.

To prove a correct implementation, the optimization process is temporary executed using empty environmental matrices, only containing zero's. If the optimization tool returns the same path as found by MATLAB's build-in function `shortestpath`, the algorithm was implemented correctly. Executing for exactly the same voyages from table 8.1, the optimizer returns exactly the same solution for every case. This indicates that the implementation of the algorithm itself happened correctly, but does not yet verify the corrections for local weather, nor the estimated fuel consumption.

11.2. Fuel Consumption and Environmental Influence

To check the quality of the fuel consumption and environmental models, a modification of the wind, waves and current matrices is used once again. This time, however, rather than using zero's, hindcast models, are used to calculate the total fuel cost. Due to the modularity of the code, it is possible to use the fuel consumption function of the optimizer on past voyages, as long as the path of the vessel in space and time is correctly defined.

Originally, it was planned to use NOAA's monthly updated hindcast data provided in [60] and [59]. However, the data is currently not updated for the past 4 months, when forecasts were saved. Therefore, the forecast data from [61] and [62], which has been locally saved to determine optimal ratios between forecasted weather, averaged weather and shortest path, is used to generate an approximated hindcast. To generate the hindcast, it is assumed that the forecast model of a certain day is completely correct until the next forecast is available. In other words, the first 24 hours of a forecast are assumed to be correct.

To validate the models used, the fuel consumption calculation model from the route optimizer is used in combination with CMB's noon report data and the hindcast models. From the noon reports, following numbers are extracted:

- Location, reporting time and time zone
- Average speed over ground

- Fuel and fuel type consumed, including specific heat value

- Displacement

The location, reporting time and time zone are used to initiate the consumption simulation, assuming the sailed speed was constant and the great circle (shortest distance) was sailed between those points. Following the approach of section 9.3, the fuel consumption is simulated.

This simulated consumption is then compared to the real consumption, which is first subjected two normalization processes, ensuring the same conditions apply on both the real consumption and the simulated one. The first correction applied is a fuel type correction, converting the actual fuel used to reference Marine Gas Oil (MGO) with a lower caloric heat value of 42.700 kJ/kg, which is the fuel type used for the optimization process. This conversion is done according to equation 11.1.

$$FC_{MGO} = \frac{LCV_{NR}}{LCV_{MGO}} \cdot FC_{NR} \tag{11.1}$$

Where FC stands for fuel consumption, LCV for lower calorific heat value, MGO for marine gas oil and NR for noon report (reports from the captain).

The other correction required, converts the measured displacement to the reference displacement used in the optimizer. A vessel obviously consumes more when it is deeper in the water, making an up- or downscaling essential while comparing results. The correction is done under the assumption that the Admiralty coefficient is constant and following the approach discussed by N. Bialystocki et al. in [10], shown in equation 11.2.

$$FC_{real} = FC_{MGO}\left(\frac{\nabla_{ref}}{\nabla_{NR}}\right)^{\frac{2}{3}} \tag{11.2}$$

Where C_{real} is the real consumption, FC_{MGO} the noon report consumption converted to MGO, ∇_{NR} the displacement found in the noon report and ∇_{ref} the displacement at reference conditions, which is used in the optimizer.

The results of the noon reports and the simulation for the transatlantic part of the route shown in figure 11.1 are summarized in table 11.1. Important to note is the detour taken on November 7, which was done to avoid tropical storm Rina. This movement disturbed the originally planned path and led to severely increased consumption on November 8, when the captain tried to make up for the time lost by increasing speed.

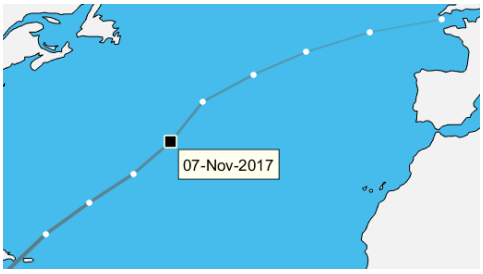

Figure 11.1: Analyzed part of a transatlantic voyage of the Maersk Niagara. It can be seen that a detour was taken, in order to avoid tropical storm Rina. Image generated by FPM [2]

Table 11.1: Comparison between simulated fuel consumption and the consumption reported by the captain of the Maersk Niagara.

Date	**Rep. FC**	**Sim. FC**	**Rep. Speed**	**Sim. Speed**	**Rep. Distance**	**Sim. Distance**
[dd-mm-yyyy]	[ton]	[ton]	[kts]	[kts]	[nm]	[nm]
03-11-2017	41.59	42.60	17.20	17.15	430.0	428.8
04-11-2017	43.26	42.03	16.52	16.47	411.0	411.9
05-11-2017	41.13	41.08	15.67	15.62	376.0	375.0
06-11-2017	39.94	38.41	15.72	15.70	393.0	392.5
07-11-2017	39.46	38.43	16.13	16.05	387.0	385.2
08-11-2017	45.83	35.89	15.76	15.12	394.0	378.0
09-11-2017	44.64	44.76	17.50	17.50	420.0	420.0
10-11-2017	46.94	46.80	17.60	17.61	440.0	440.2
11-11-2017	45.85	46.74	17.72	17.55	443.0	438.9
Sum/Average	**388.64**	**376.74**	**14.98**	**14.88**	**3694.0**	**3671.1**

From the table, a total difference in fuel consumption of 3.16 % is seen, where the real consumption is higher than the simulated one. However, removing November 8 of the data set, this difference over the entire voyage in only 0.58 %. Day-to-Day comparison results in an average offset of 2.04 %. The same can be said for the simulated and reported speed and distance, with again an exception on November 8. So what happened on that day?

As stated before, a detour had to be taken to avoid tropical storm Rina. This means that a greater distance than originally expected had to be sailed, hence some time had to be made up for. From the existing weather routing solutions, discussed in chapter 2. Right the moment the detour was initiated, lower speeds were sailed. To make up for this, the ship sailed at full throttle for some time, which is extremely bad for the fuel consumption, knowing there is a third power relation between speed and power required.

Not taking this particular day into account, Differences of only 2 % and a final value of half a percent off, figures are well within an acceptable range of 5 %. A slightly lower consumption in the simulated journey was also expected, since the shortest path at constant engine settings is simulated. Changes in real speed are unnoticed in the noon reports, but often result in worse performance. For example, sailing at 10 knots for 12 hours, then sailing at 20 knots for the remaining 12 hours, will be reported at a speed of 15 knots, but the consumption will be much higher than a day where the speed of the vessel was 15 knots all day. Plans currently exist to stop sending noon reports, but sent a report whenever the sailing conditions significantly change (speed chances, course changes, extreme weather, ..)

Another cause of the deviation could be the exact time that the captain fills in the report. Even though it is reported to be filled in at noon, it could be ten minutes earlier or half an hour late. Checking the exact moment is hard, since reports are sent as soon as a decent internet connection is available, which usually is not exactly at the time the report is filled in. A last, obvious cause for deviations, is the quality of the correction models, which is being checked here, but looking at the differences, all of the above mentioned causes only have a small impact, validating the weather models used.

To gain more trust in the models used, appendix A.4 contains additional tables, comparing simulated and reported fuel consumption. All models show similar results, containing small deviations on each report, but matching very closely over a longer period of time.

11.3. Environmental Field Verification

The validation of the current, waves and wind data is placed outside of the scope of this project, but the implementation of these models into the weather route optimizer is checked in two ways. First, the interpretation of the incoming data is shown by means of database visualizations. Then, the functionality of picking the right data within the fuel cost calculation will be demonstrated by exaggerating the effects of the environment.

11.3.1. Environmental Field Visualization

Most fields have already been visualized in chapter 4, but several less modified fields are shown to increase insights in the data format.

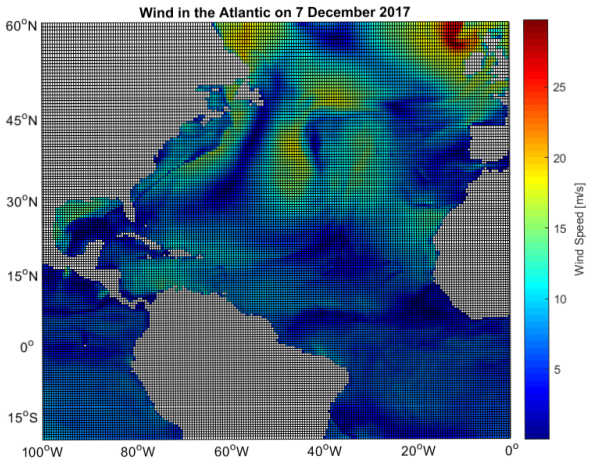

(a) Wind speed

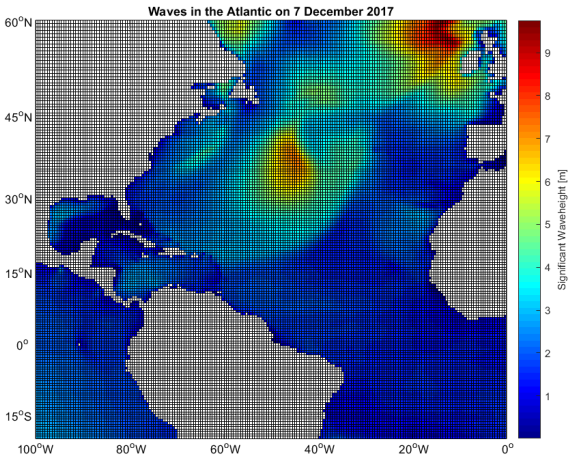

(b) Significant waveheight

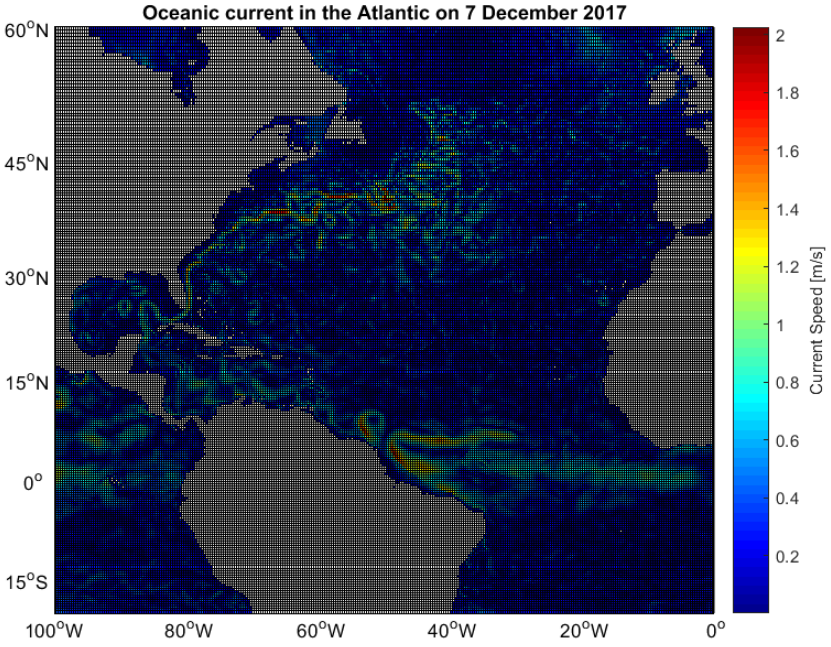

(c) Current speed

Figure 11.2: Faceted visualization of incoming Environmental data for the Atlantic on December 7, 2017.

While not actively drawing the world map, the incoming NaN values, returning a white field in the grids above, clearly represent the globe. Note that the oceanic current grid is finer than the wind and waves grid.

11.3.2. Environmental Field and Fuel Consumption Integration

To ensure both the environmental fields are interpret in the correct way and that the effects are properly modeled, the option to single out either the current, the wind or the waves is used (see appendix B figure B.4, Environmental Influences panel). To start with, a route passing the gulf stream is simulated on a static current field with a constant current description. It is expected that the route optimizer suggests a route following the

gulf stream. As can be seen in figure 11.3, the suggested route indeed follows the gulf current up to about 40 degrees North.

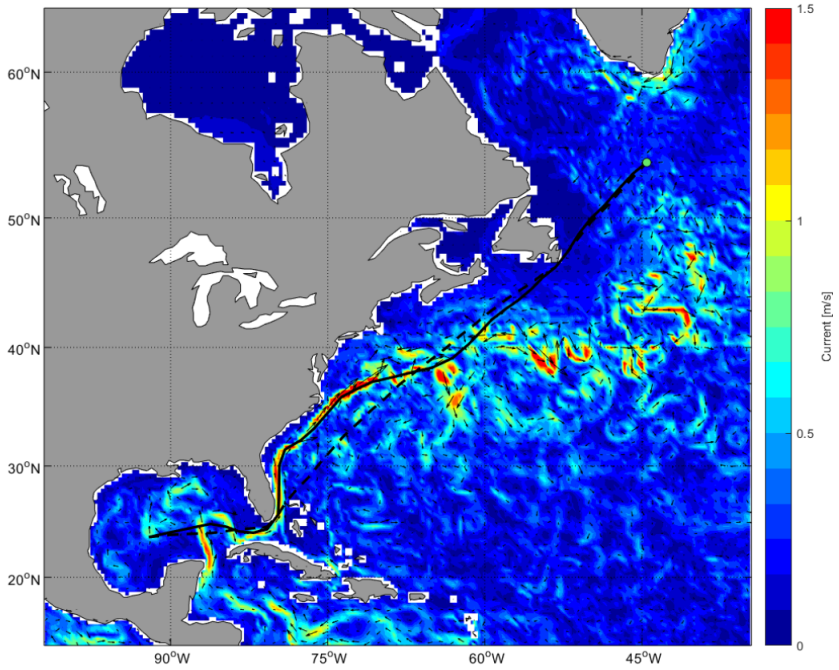

Figure 11.3: Proposed route when only taking current into account. The dashed line represents the shortest path, the black line the suggested path taken. The green dot represents the target location.

A similar approach is used on wind data, selecting a route from the South of Australia to South of South-Africa, where strong adverse winds are present. Figure 11.4 shows the weather optimization tool avoids the strongest winds while searching the optimal route. During this simulation, the effect of the wind is multiplied by 5 to make sure a significantly different route could be visualized. Note how suggested route, going more North than the shortest one, avoids the heavy winds around 40 degrees South and 40 degrees East.

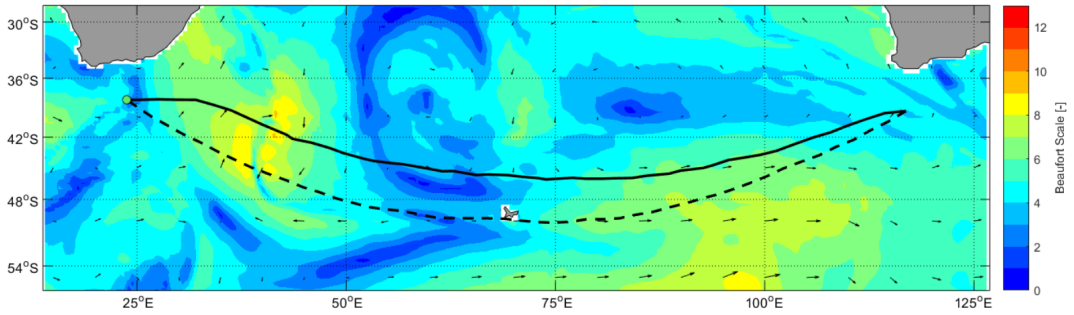

Figure 11.4: Proposed route when only taking wind into account. The dashed line represents the shortest path, the black line the suggested path taken. The green dot represents the target location.

To end this chapter, the same principle is applied on a route where only waves are considered. This time, waves as high as 11 meters are found in the Atlantic. Modeling to go from the East of these waves to the West, reveals the tool manages to properly deal with waves as well. As shown in figure 11.5, a big detour is suggested to avoid these high waves in the Atlantic.

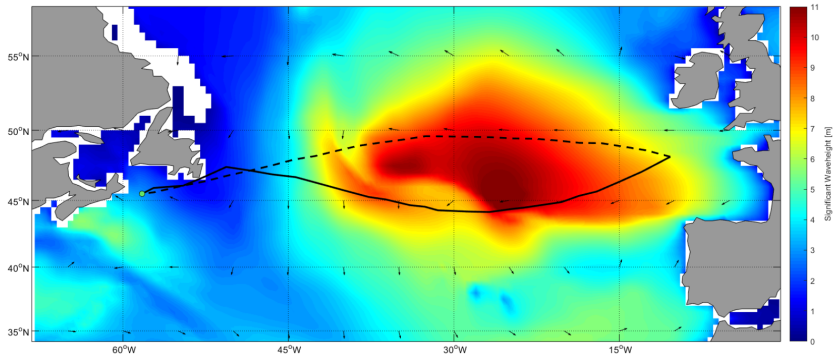

Figure 11.5: Proposed route when only taking waves into account. The dashed line represents the shortest path, the black line the suggested path taken. The green dot represents the target location.

Part III
Outcomes of the Project

Armed with a functional weather routing application, producing reliable fuel consumption estimations, the effect of using weather route optimization can be investigated. Showing that the simulated values of fuel consumption approximate the on-board measurements in chapter 11, methods to answer the research questions posed in the introduction can be looked at. Due to the nature of the constantly varying sailing conditions in both space and time, it is chosen to perform a lot of simulations to acquire sufficient data to draw reliable conclusions.

From this point in the report, it will be assumed that, in case the real sailing conditions (current, waves and wind) are known, the fuel consumption estimation used in the weather routing tool is exact. This assumption makes it possible to move away from actual measurements and generate much more data within an acceptable time frame. Apart from the amount of data, it also becomes possible to simulate different decisions made, which is needed to compare wide range of proposed routes to each other, which is impossible using real vessels, since vessels cannot sail two paths at the same time.

Before determining the actual gains op weather route optimization, the optimal ratio between environmental forecasts, monthly averages and shortest path taken. Chapter 12 is dedicated to finding this optimum. When the optimal mixture is found, the gains while using optimal settings, can be discussed in more detail. The discussion of the potential gains can be found in chapter 13.

12

Optimal Environmental Influence Ratios

There is currently no weather routing service available that incorporates monthly averaged environment in the optimization process, making it unclear whether or not it can be beneficial to use an averaged environment to optimize for fuel. However, it can be expected that applying monthly averages to the weather routing case, will, in some cases, result in lower total consumption.

Blindly trusting in the environmental forecasts available does not always seem to be a good idea. Suppose a detour is taken because bad weather is expected at a certain location on the shortest route. After several days, it becomes clear that the location of the bad weather is actually predicted inaccurately and a detour was not necessary, however, it was already decided to move away from the original route. In the end, an unnecessary detour was taken, resulting in increased fuel consumption due to the usage of a weather route optimizer. This should be avoided at any time, and optimization of the parameters discussed below, will help to prevent such events.

As can be seen in figure 6.11, a total of 5 parameters are to be optimized. The parameters of figure 6.11 are used to show the mixing ratio between 0 and 10 days, visualized in figure 12.1. The five parameters to optimize for, are indicated with four stars (*) and a dotted line. Note that only linear increases in shortest path and monthly average influence are considered.

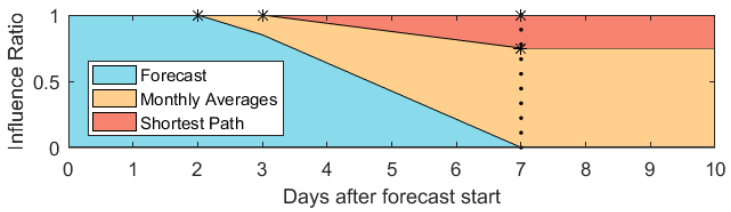

Figure 12.1: Visualization of weather influence ratios and values to optimize for.

The parameters to optimize are the following:

- Moment in time after which the monthly averages start influencing the fuel consumption prediction.
- Moment in time after which the shortest path starts influencing the fuel consumption prediction.
- Final monthly averages ratio.
- Final shortest path ratio.
- Moment in time after which these final ratios must be used reached.

When the optimal parameters are used, the total savings will be the highest in general. This does not mean that every route taken is optimized. It is perfectly possible that the forecast could be trusted for the entire

available period for a certain voyage, which would have resulted in the lowest fuel consumption possible, but this cannot be sure in advance. Therefore, the ratios at which the least fuel is consumed on infinite voyages is looked at.

The optimization of the environmental ratios, is broken down in several steps. The first step is finding the final ratio of monthly averages and shortest paths. The procedure to find these numbers, is discussed in more detail in section 12.1. The ratio found, serves as starting point for the next optimization process and so on, until a final optimum is reached..

12.1. Final Environmental Ratios

To find the best final environmental ratio, it is assumed that no weather forecasts are available. In other words, only the monthly averages and shortest path are available to find the optimal route. To evaluate the effect of using different ratios, a total of 100 voyages is simulated for different settings. The following sections discuss this procedure in more detail.

12.1.1. Set-up of the Optimal Environmental Solution

To determine the optimal ratio, 100 voyages are simulated eleven times each, changing the environmental ratios from 0 % to 100 %, taking steps of 10 %. The 100 voyages are randomly chosen, based on random coordinate picking. When the coordinates are found to be at sea, the global and local grid are searched for a solution. Choosing a random vessel and selecting a random (yet realistic) speed, a random departure time is filled in. An arrival time, matching the random speed selected, is chosen and the optimization process is executed, saving the route to be taken.

When all eleven environmental ratios and their corresponding routes have been saved, the available hindcast data, which has already been discussed in chapter 11, is used to calculate the actual fuel consumed while following each of the proposed routes. The analyzed voyages are shown in figure 12.2.

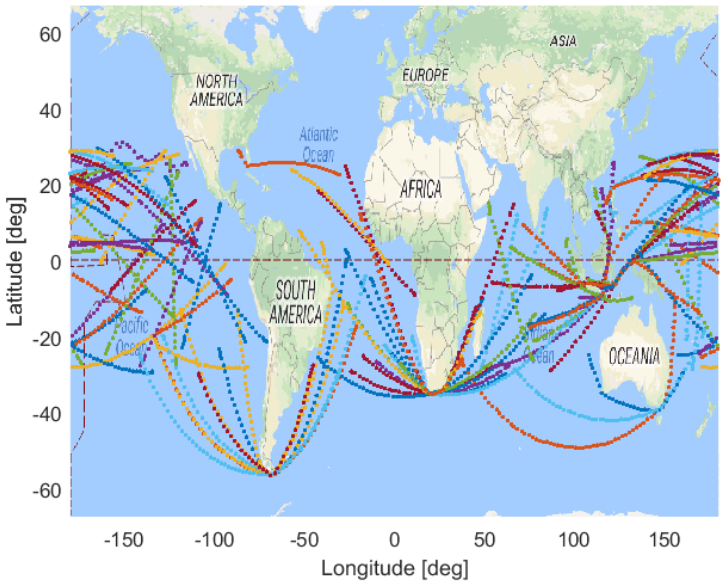

Figure 12.2: Voyages used to analyze the final environmental influence ratio.

12.1.2. Execution

The voyages shown in figure 12.2 are analyzed for the different settings of environmental ratios. As expected, changing the environmental influence settings has an effect on the exact route selected. One of the random voyages, for example, proposes the routes shown in figure 12.3, depending on the monthly average (M.A.) used. The randomly selected ship was the Hermes Arrow, a 2500 TEU container vessel.

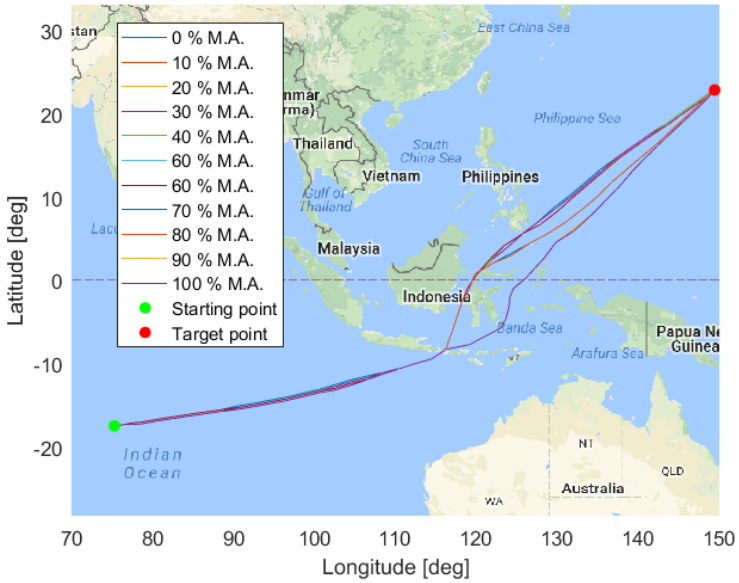

Figure 12.3: Different routes proposed for one of the randomly selected routes.

These different routes are the ones found by the route optimizer discussed in part II corresponding to each monthly average ratio investigated. For the shortest path (0 % monthly averages), it turns out to be most efficient to head north right after passing Bali (Indonesia), passing through the Makassar Strait and the Celebes Sea, continuing South of the Philippines. On the other hand, when ignoring the shortest route and fully relying on the monthly averages, the Flores Sea is taken after passing Bali, passing through the Molucca Sea to finaly reach the South of the Philippines.

After determining the different routes, they are loaded in a hindcast module, checking how much fuel would actually have been required to sail the proposed path, based on the actual weather conditions that occurred over the sailing period. The resulting consumption for the routes shown above, is visualized in figure 12.4a. Clearly, the best solution would be taking the route using 100 % monthly averaged sailing conditions and not looking at the shortest path, together with using 90 % monthly averages and 10 % shortest path, which actually resulted in the same route.

Apart from the absolute fuel consumption, the fuel consumption relative to the optimal mixing ratio (100-0 in this case) is plotted in figure 12.4b. In this case, the worst result is found by taking 10 % monthly averaged sailing conditions and 90 % shortest path, which would have resulted in 2 % additional fuel consumption (4.03 tons). The speed regime selected on the 100-0 route is slightly better than the one of the 90-10 solution, saving a total of 0.016 ton.

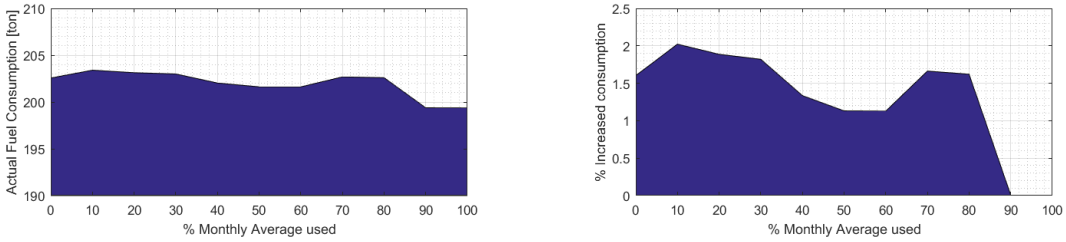

(a) Actual fuel consumption for each evaluated setting

(b) Relative % increased consumption

Figure 12.4: Actual fuel consumption comparison between different ratios of monthly averaged environment and shortest path.

The procedure discussed above, is repeated for one of the other random voyages, this time using the Mineral Ningbo (Deadweight of 178 120 metric tons), producing the same graphs as shown in figure 12.4. Adding the second set of values to the absolute and relative consumption graph, produces the results shown in figure 12.5.

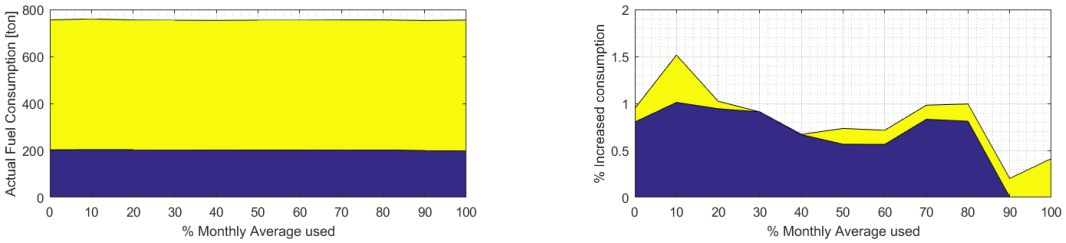

(a) Actual fuel consumption for each evaluated setting (b) Relative % increased consumption

Figure 12.5: Fuel consumption comparison of two random voyages.

Whereas the absolute fuel consumption graph is less clear due to the differently scaled y-axis, it varies between 760 tons and 752.75 tons of fuel. The grap in figure 12.5b provides more insight, indicating that the second investigated voyage performed best at 30 and 40 % monthly averaged weather and 60 and 70 % shortest path. In total for the two cases discussed, choosing a 90 % monthly average and 10 % shortest path would have been best.

12.1.3. Large Scale Results

Looking at the graphs in figure 12.5, it becomes clear that there is no ratio that always results in the lowest consumption. Therefore, the settings that, on the long run, will result in the least fuel consumption, are looked at. The procedure above is repeated for all of the 100 voyages, evaluating a total of 1100 different routes. The results, shown in figure 12.6 speak for themselves; fully using the monthly averaged environmental conditions when no weather forecast is available will in total reduce the fuel consumed the most.

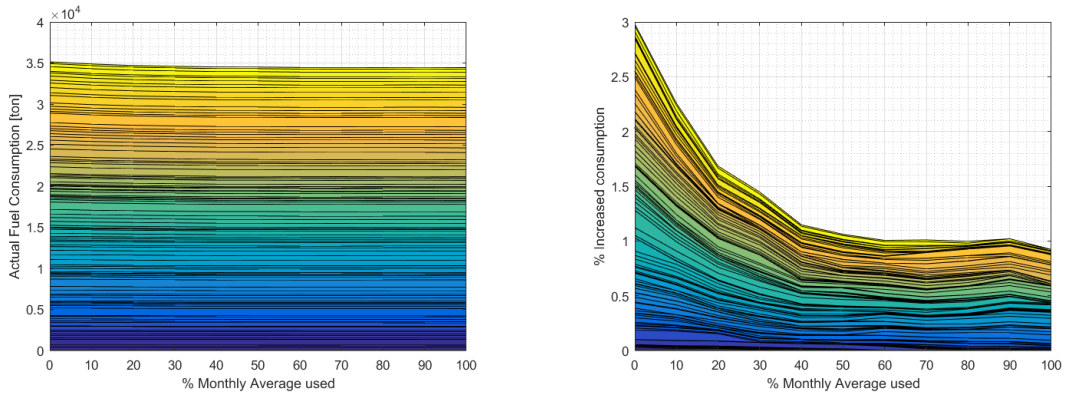

(a) Actual fuel consumption for each evaluated setting (b) Relative % increased consumption

Figure 12.6: Fuel consumption comparison of all 100 random voyages.

For the 100 random voyages evaluated, the total fuel consumption, shown in figure 12.6a, reduces from 35 140 tons to 34 438 tons, a reduction of 702 tons or 2.04 %. This corresponds to the difference visible in the second graph, where the average increase in fuel consumption with respect to the “would have been the best” setting changes from 2.98 % at the shortest path to 0.92 % when fully using monthly averages. Note that the calculated gain in the second case is 2.06 % rather than the 2.04 % found before. This is due to the fact the percentage increased consumption weights each voyage equally, whereas the total consumption is not weighted and total consumption is influenced by voyage length, average speed sailed and ship selected. All numbers

are tabulated in appendix A.5

The obtained results simplify the remaining part of the optimization process, which intended to look for shortest path incorporation in the weather routing application as well. Since monthly averaged conditions outperform the shortest path in the long run, the shortest path can completely be left out of the calculations and at this point, the weather influence ratios look like the plot shown in figure 12.7.

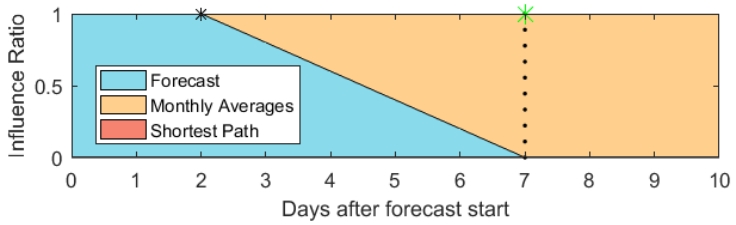

Figure 12.7: Visualization of weather influence ratios and values to optimize for. The green star indicates an optimal setting has been found; black indicators represent values that still require optimization.

12.2. Available Forecast Time Reduction

Looking back at figure 12.1, the final ratio between monthly averages and shortest path has been determined when forecast is not available anymore. As it turns out the shortest path is not required to find, in general, the best solution, there are only two parameters left to optimize. The first one deals with the point in time after which the final ratio should be used, which will be discussed in the remaining of this section.

Despite the fact the forecasts presented by NOAA are probabilistic descriptions, based on multiple runs with small variations in unpredictable and inaccurate parameters [61], the forecasts are not always correct. Logically, since the forecast of time i is based on the conditions at time i-1, forecasts describing the weather in 7 days are less reliable than the forecasts of tomorrow.

To determine when the environmental ratios should move to their final state, a time inverse approach will be used, starting to evaluate the usage at the last day available (8 days) and moving forward. When using the forecast results in higher consumption than using the final ratio, the final ratio will be used earlier and later forecasts will be discarded.

12.2.1. Setup of Reduced Forecast Reliability Determination

Setting up the simulations looking at the moment in time at which transitioning to the final ratios is optimal (the dotted line in figure 12.1) is done very similar to the final ratio setup discussed in section 12.1. Proposed routes found using a one day reduction of forecast time available, are tested against full forecast times used. If, again in the long run, the full forecast results in a better actual consumption, using at least a fraction of the forecast available will ultimately lead to reduced fuel consumption. If reducing the forecast duration by one day results in better consumption, a reduction of two days will be tested. If that still appears to be beneficial, three days will be left out and so on....

12.2.2. One Day Forecast Reduction

Running the simulations at different settings is done similar to the process used to test the final ratios required, however, only two cases per voyage in stead of the eleven cases from section 12.1 have to be simulated. The randomly selected routes are visualized in figure 12.8. The routes slightly vary, depending on the duration of the forecast used. A total of 100 different voyages are evaluated, assuming that, if a clear difference exists, the amount of different simulations is sufficient to draw a conclusion concerning the forecast reliability.

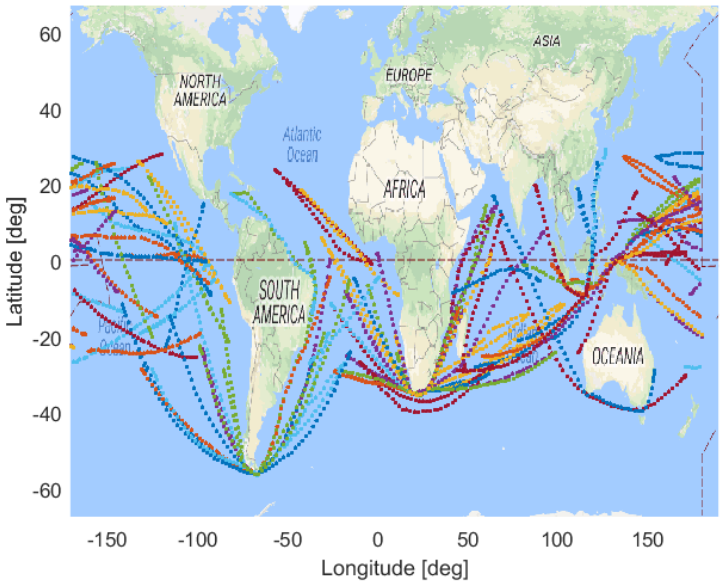

Figure 12.8: Different routes proposed for one of the randomly selected routes.

12.2.3. One Day Forecast Reduction Results

The generated data is processed as described in section 12.1.3. Summation of the total consumption using 6.5 days of forecast compared to the 7.5 days available, shows that a one day reduction from 32 104 to 32 058 tons of fuel is achieved, which corresponds to a fuel consumption reduction of 0.144 %. Looking at the percentage increased consumption wrt. the best option, a difference of 0.135 % in favor of the full forecast is found. Figure 12.9 shows the obtained results.

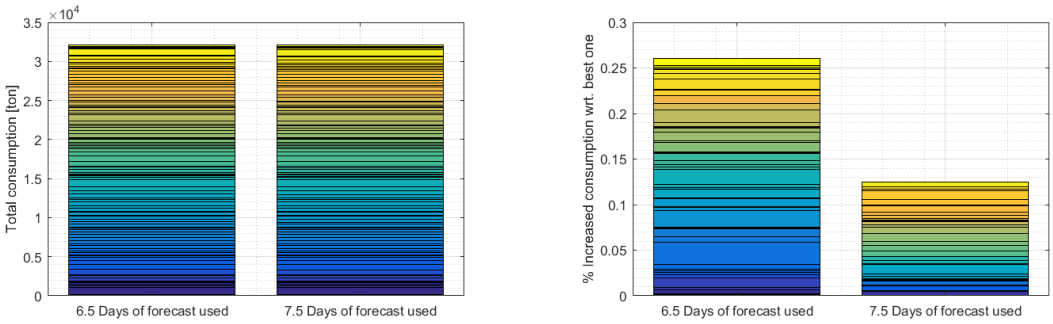

(a) Actual fuel consumption for each evaluated setting

(b) Relative % increased consumption

Figure 12.9: Fuel consumption comparison of all 100 random voyages for the final ratio determination.

The consumption values, tabulated in appendix A.6 table A.8 show that 39 out of 100 simulations favor the 6.5 days forecast usage, whereas 61 of the simulations result in lower consumption when the full forecast is used. This, together with the consumption figures found, indicates that using the last day of the forecast reduces the total consumption in the long run, however, the gains are rather small. The small difference was to be expected due to reduced forecast reliability and the fact a single day in voyages that can last up to two months has limited impact. An additional reason for the small differences, is that detours are often initiated to avoid bad weather after 6.5 days, which is still present after 7.5 days.

No statements concerning the forecast reliability could be found, but it is reasonable to believe that forecast data is only provided up to 7.5 days in the future because after that period, the forecasts are simply not reliable enough anymore. The decreased reliability of the weather forecast is already sensed by the weather route optimizer, seeing that in 4 out of 10 cases, the monthly averaged weather is actually more reliable than the

forecast.

Under the assumption that weather forecast reliability reduces further away from the current day and that using 7.5 days of forecast is usually better than using 6.5 days only, it can be concluded that results will reduce further when using less than 6.5 days of forecast. In other words, another parameter is optimized, namely the moment in time at which transition towards monthly averages should happen, which is only when forecasts are not available anymore. The optimization progress is shown in figure 12.10.

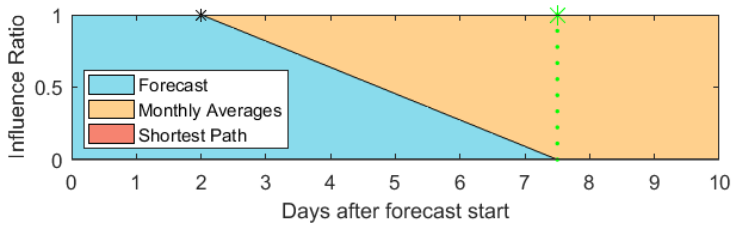

Figure 12.10: Visualization of weather influence ratios and values to optimize for. The green indicators represent optimal setting setting found; black indicators values that still require optimization.

12.3. Monthly Averages Starting Time

With known final ratios and time at which these ratios must be used, together with the fact that sailing according to monthly averaged environment is more reliable than simply taking the shortest path, results in only one more parameter that requires optimization, the starting point of using monthly averages.

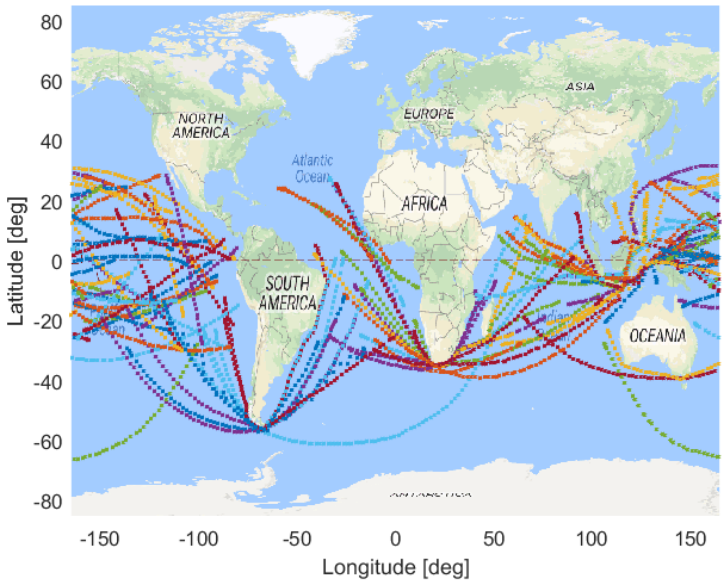

Figure 12.11: Routes used to determinet the moment after which monthly averages should start influencing the optimization.

As done for the previous parameters, the 100 voyages shown in figure 12.11 are simulated using different settings and compared to each other. This time, the difference in settings is found in starting moment of the influence of the monthly averages. Varying the settings from 0 to 8 days (settings at 8 days results in using as forecast wherever possible), each voyage is simulated 9 times. Values are tabulated in appendix A.7 tableA.10 and visualized in figure 12.12.

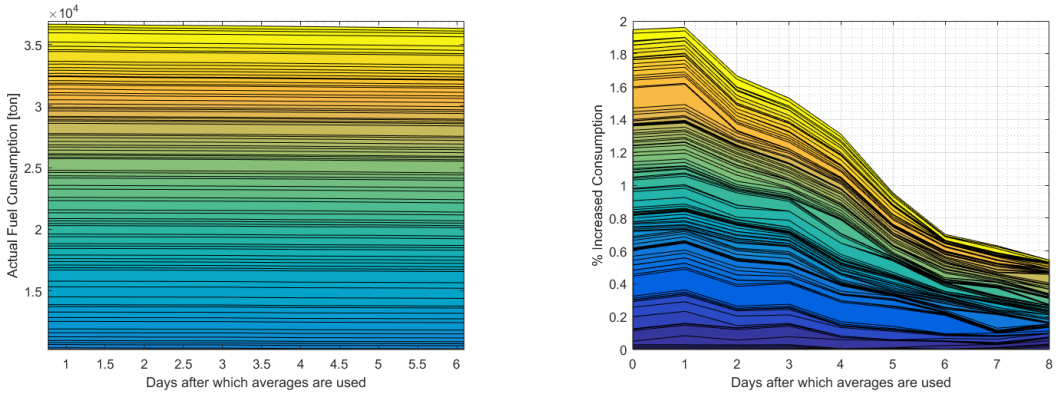

(a) Actual fuel consumption for each evaluated setting

(b) Relative % increased consumption

Figure 12.12: Fuel consumption comparison of all 100 random voyages for the final ratio determination.

Apart from initiating the monthly average after one or two days, a significant change in fuel savings can be seen. The later the monthly averages start to play a role, the better the consumption gets. In other words, as long as forecasts are available, they should be fully used. In some cases, it would have been better to transition faster, which explains the 0.58 % relative increased consumption with respect to the "would have been best" option.

To be more exact, a total consumption of 33 400 tons is calculated for cases where the monthly averages start playing at day one (starting at 0 % on day zero, increasing with 13.3 % each day), which reduces to 33 028 tons when fully relying on forecasts when they are available, ignoring monthly averages till that moment in time. This is a fuel consumption reduction of 1.13 % and thus strongly favors the forecast usage.

Despite the gains discussed, the trend in fuel gains when delaying the usage of monthly averages cannot be found between monthly average initialization at day zero and day one. Even worse, day one results in slightly higher consumption than starting at day zero. This effect can be explained by two factors;

- The latest forecast available will be used, which means that the forecast is always slightly lagging behind. Assume for example a voyage starting on 23-Nov-2017 22:00. This voyage is evaluated using the forecast generated at 23-Nov-2017 00:00 and will the earliest forecast used is already 22 hours old (and thus almost hitting day one). They day zero and day one setting are thus less different than for example the day five and day six settings.

- Due to the smaller difference between the first 24 hours, a chance factor might cause the irregularity between the day zero and day one setting.

Apart from these two settings, the trend is clear. The total result makes sense: fully rely on the forecast data when available and when there is no more forecast available, switch to 100 % monthly average influence in favor of the shortest available path. All of the parameters to optimize for are now fixed, so within the defined spectrum of possibilities, the optimal ratios are found as visualized in figure 12.13.

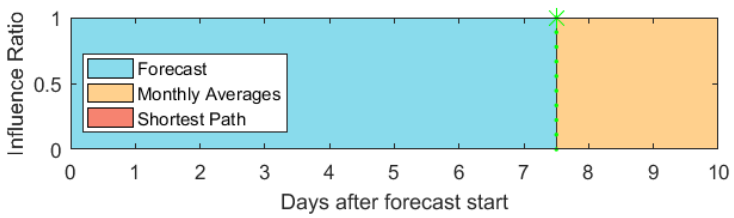

Figure 12.13: Visualization of optimal settings to be used to achieve the lowest fuel consumption in the long run.

12.4. Conclusion on Influence Ratios

With five parameters to be optimized, the optimization process has been logically broken down in subproblems. First of all, optimal settings in case of unavailable forecasts are looked at, reducing the remaining number of parameters to be optimized from five to three. The results coming from a total of 1100 simulations, indicated that shortest path usage was actually an irrelevant parameter, removing the starting point of shortest path from the parameters to be optimized and removing the unknown parameters to two.

One of these parameters, the moment in time at which the final conditions must be met, is investigated under the assumption that weather forecast reliability reduces over time. The obtained data showed that reducing the usage of forecast increases consumption, hence at least a fraction of the available forecast should be used. The moment in time at which monthly average start playing, is the final parameter to optimize for. It could clearly be seen that using monthly averages when forecast data is available, increases fuel consumption and should thus be avoided.

The first research question, dealing with the ratio between environmental forecasts, monthly averages and shortest routes, has been answered throughout this chapter. It became clear that *forecasts are, in the long run, favorable over monthly averages and monthly averages are, in general, favored over the shortest path*. Despite some cases, where the above statement is not true, using these ratios will eventually save more fuel than it will cost.

13

Potential Savings

With the optimal settings concerning forecasts, monthly averages and shortest path found, the potential gains of using weather routing can be investigated. As done in chapter 12, simulations are carried out on large scale. The theoretically better option would be sailing a route without optimization first, then sailing the same route under the same weather conditions with optimization applied, but this is obviously not possible. In chapter 11, it has been shown that the simulations approximate reality, making the conclusions from this chapter more reliable.

Since forecasts are the most reliable environmental representation, they should be used as much as possible, so it makes sense to recalculate routes when new forecasts become available. In chapter 10, where the outputs of the optimizer are discussed, figure 10.1 shows an expression for savings, both as percentage and absolute value. These values approximate the expected gains for a certain voyage based on the forecasts and monthly averages used to plan the route. This is, however, only an approximation of reality, since the forecasts and monthly averages do not represent the actual sailing conditions.

13.1. Simulation Setup

Similar to the previous large-scale simulations, random voyages are selected and assigned an appropriate sailing speed and time frame to complete the voyage. This time, however, the focus shifts from finding optimal settings to performing daily reruns to map out the routes to be taken when using weather routing in a realistic way. A strongly varying rerun-based solution is shown in figure 13.1.

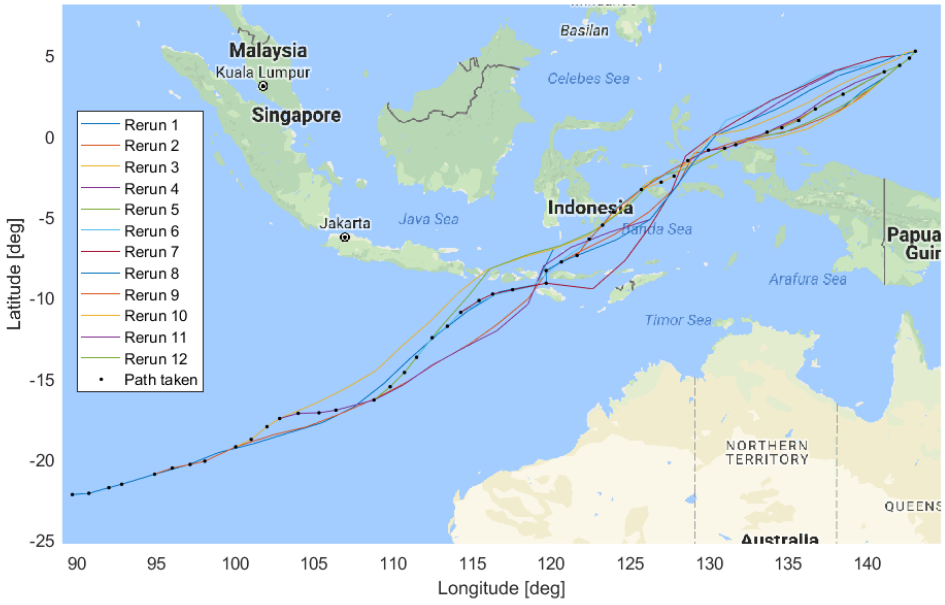

Figure 13.1: Changes in route suggestion over time, based on forecasts and monthly averages

The variation in route suggestions for the selected voyage, which starts in the Indian Ocean and ends in the Pacific, south of Guam, is stronger than the usual variations and does not represent a normal rerun pattern. It is good to show the effect of reruns though, suggesting a different route each time a rerun is performed.

The dots represent the actual path that would have been sailed, before new weather routing suggestions became available. As soon as a new rerun is performed, the dotted line moves away from the old line and continues on the last line suggested. Note that a new line always starts at a point located on the old line. This principle is shown in more detail in figure 13.2, showing the interaction between the first four runs.

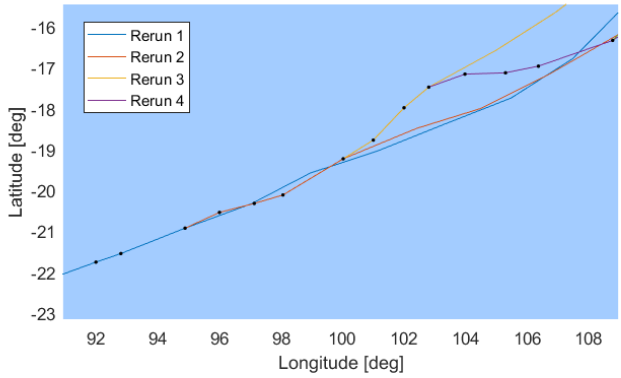

Figure 13.2: Changes in route suggestion over time.

For each of the random voyages, three major route suggestions are saved:

1. The shortest path route, ignoring forecasts or monthly averages. This route does not require reruns and can be set at the beginning of a voyage.
2. Route based on optimal ratios identified in chapter 12. Reruns are required as soon as new data becomes available.
3. Route based on forecast, then shortest path. This is done in order to quantify the gains that can be attributed to the monthly averages used. For this analysis, daily reruns are required as well.

13.2. Execution of the Reruns

As stated before, several reruns are required for the forecast-based options. In order to do so, the first run is performed based on random feasible routes. When the simulation is predicting a position on a new day, this means a new forecast set is available until the target location is reached. To demonstrate the process in more detail, appendix A.8 shows a daily updated view of the weather encountered. For this voyage, starting in the Pacific and ending close to Arequipa (Peru), three entirely different routes are taken for the three investigated cases.

For the three cases considered, the black line represents the shortest path without weather routing optimization, the red one the shortest path when no forecasts are available and the green line the optimal combination of forecasts and monthly averages found. The voyage based on shortest path when forecasts become unavailable, remains North of the equator for the first part of the voyage, whereas the voyage using monthly averages moves more to the South. Looking at the monthly averaged current, wind and waves of December D.4, moving south seems to be the right choice. Not only is the weather calmer to the south, there is also a strong counter current expected around the equator, which is not taken into account without the usage of the monthly averages.

Moving forward to day 6 of the voyage (December 10), it becomes clear why such deviation from the shortest path was necessary; a strong counter current right where the shortest path voyage passes, is present, as shown in figure 13.3. The two cases taking forecast into account, notice this in time and both initiate a detour starting right when the voyage starts.

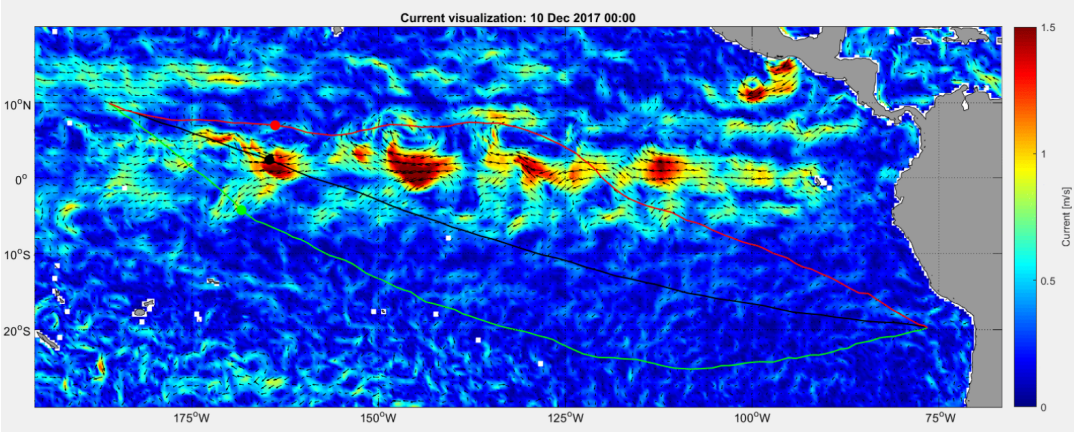

Figure 13.3: Visualization of the strong counter current encountered when not using weather routing optimization.

The next notable event occurs on December 21. The red option unknowingly is stuck North of the strong current present around the equator (in contrast to the monthly averages-based route). When it becomes clear that this current has to be passed at a certain point, the optimizer decides to make this move when the counter current is as weak as possible as shown in figure 13.4, avoiding counter currents stronger than 0.5 knots.

Finally, while looking at the the average waveheight, it becomes clear that the usage of monthly averages again turned out to be the right choice. The better monthly expected conditions, shown in figures D.1 to D.3, turn out to be a good representation of the actual state of the sea, which is visualized in figure 13.5, whereas the waveheight encountered by the red route is significantly higher than both the no weather routing and monthly average cases.

In the end, following results are achieved for the three different routes:

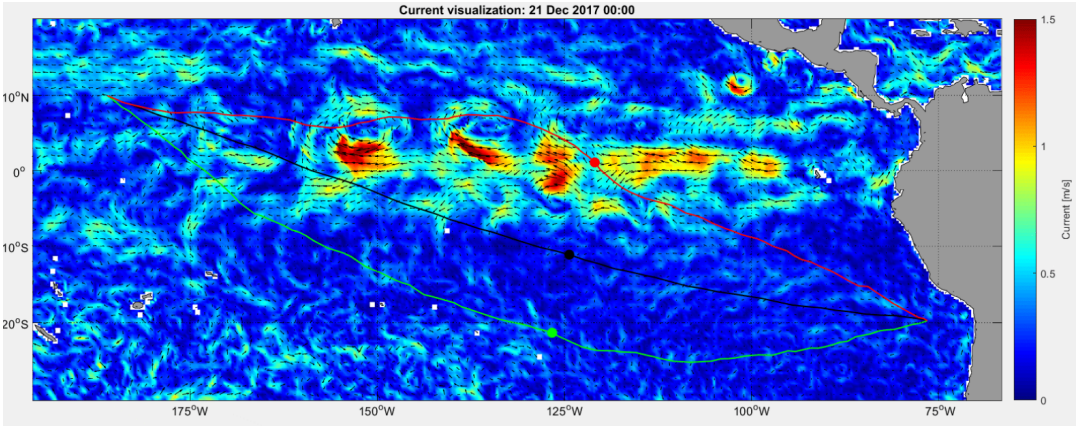

Figure 13.4: Counter current avoidance by forecast-shortest path optimization settings.

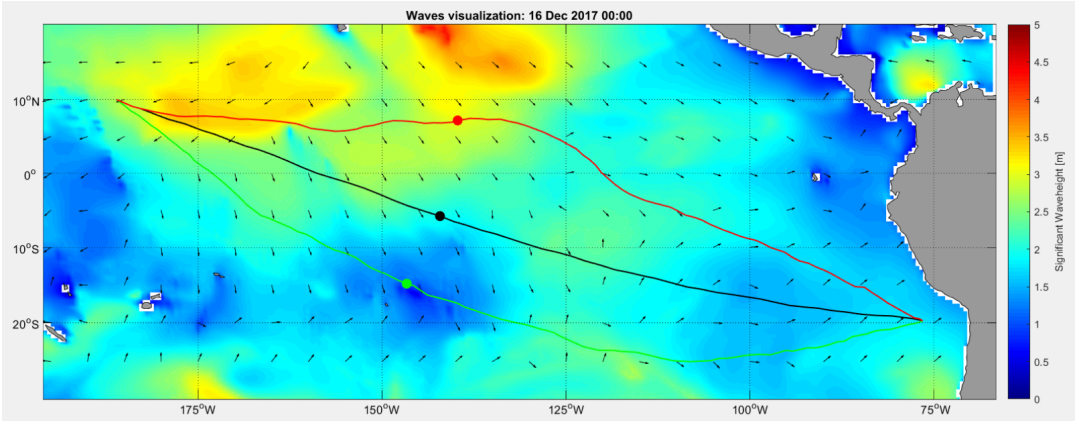

Figure 13.5: Higher significant wave height encountered North of the equator.

Table 13.1: Results for the rerun case study. Note that this corresponds to the 13^{th} case in appendix A.8.

	Consumption [tons]	**Distance [nm]**	**Current [m/s]**	**Wind [m/s]**	**Waves [m]**
No WRO	284.71	6708.73	0.47	6.95	2.09
WRO-Shortest	288.32	6980.91	0.007	6.81	2.14
WRO-Averages	253.43	6869.84	0.017	6.04	1.75

From table 13.1, several conclusions can be drawn. First of all, it appears that using no weather route optimization (No WRO) turned out to be better than using weather routing based on forecasts and shortest path. This can be explained by the detour of no less than 272 nautical miles taken to avoid the strong adverse current around the equator, which was not available in the forecasts during the first days of the voyage. Apart from this, more severe weather was encountered in the second part of the voyage, whereas the southern route was relatively calm. In the end, the adverse current is avoided, resulting in an average counter current of 0.007 knots, which is negligible.

The forecast and monthly average route, however, significantly outperforms the other two in this case. Looking at the monthly averages of December in appendix D.1, it becomes clear that both the adverse current around the equator and the more severe weather to the North, are predicted by the monthly averaged environment. Based on this, the forecasted counter current on December 10 is avoided by moving to the South. Taking a detour of 161 nm results in 11 % less fuel consumed with respect to the no weather routing case and reduces the counter current to almost zero. The average wind speeds and waveheight encountered also drops significantly in comparison with the other options (see table 13.1).

13.3. Total Results

The voyage in the Pacific, used as example above, strongly favors the usage of monthly averages. This is not always the case though. In total, 54 voyages are simulated with daily reruns and different settings, resulting in a total of 2038 reruns and three suggested routes per voyage, as discussed in the previous section. In 13 cases, using no weather routing at all appeared to be the best route; 15 cases favored the usage of forecast, then shortest path and the remaining 26 cases were in favor of using the forecasts available, then relying on the monthly averages. Table 13.2 covers the most important parameters of the simulated voyages. The voyages and different routes suggested are shown in figure 13.6.

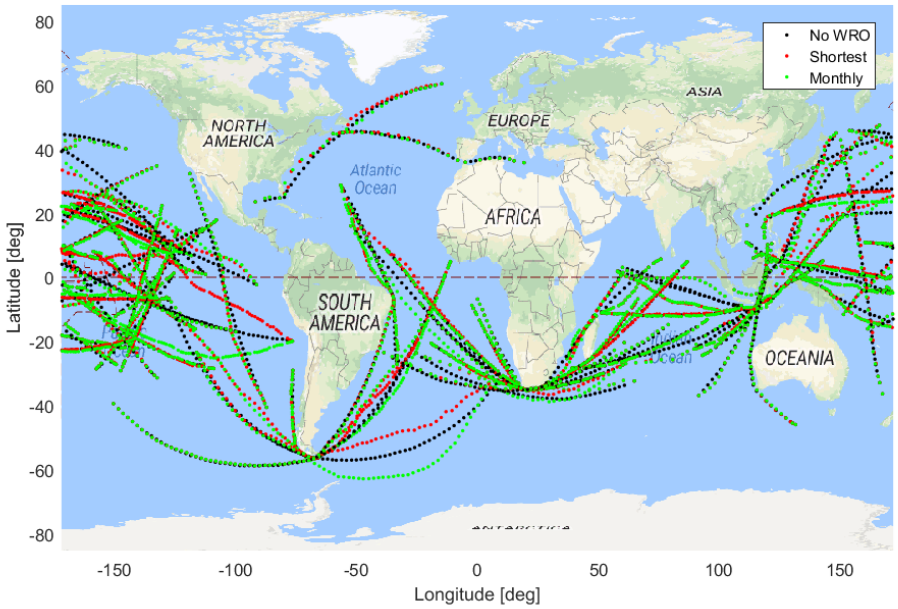

Figure 13.6: Routes used to determine the expected fuel savings by using weather route optimization. No WRO is the shortest route, whereas the route denoted as Shortest (red) is the route based on forecasts, then shortest route. The green dots represent the routes based on forecast and monthly averages.

Table 13.2: Summary of the simulated voyages. Consumption and distance are totals, whereas the environmental conditions are averaged.

	Consumption [tons]	**Distance [nm]**	**Current [m/s]**	**Wind [m/s]**	**Waves [m]**
No WRO	17 956	255 537	-0.0246	6.77	2.27
WRO-Shortest	17 520	258 666	-0.1811	6.71	2.13
WRO-Averages	17 398	258 873	-0.2063	6.67	2.11

13.3.1. Analysis of the Results

In general, the average sailing conditions between the two cases where weather routing is used, are similar, where the monthly averages result in slightly better fuel consumption. All currents are negative, meaning that on average, favorable current was encountered. The 0.0246 knots from the no weather routing case, can be seen as coincidence, however, the weather routing cases clearly show a gain in favorable current.

A slight reduction in wind speeds encountered, as well as a reduction in significant waveheight are achieved. Looking back at equation 6.2, it can be seen that there is a quadratic relation between wave resistance and significant waveheight, in other words, the reduction of average waves encountered from 2.27 m to 2.11 m, means a wave resistance reduction of 13.6 %. Note that for wind and waves, the direction also influences the resistance. The models account for this, but the values found are not tabulated.

The fuel savings are visualized in figure 13.7, showing the total gains and percentage gains according to the procedure discussed in 12.1.2.

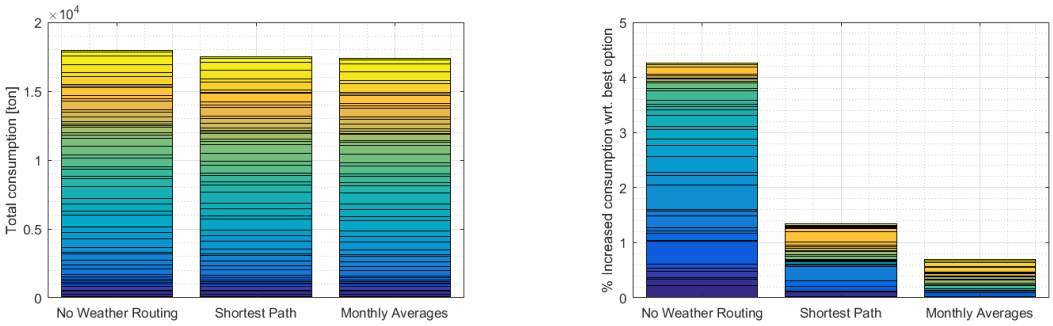

(a) Actual fuel consumption for each evaluated setting

(b) Relative % increased consumption.

Figure 13.7: Actual fuel consumption comparison between no weather routing optimization, forecast then shortest path optimization and forecast then monthly averages optimization.

Together, figure 13.7 and table 13.2 provide a lot of insights concerning weather route optimization for oceanic vessels. To start with, figure 13.7a shows that considerably more fuel is required for the no weather routing case in comparison with the forecast, then shortest path case, even though both options were considered the best option a similar number of times. This indicates that weather routing with shortest path either has little to no effect (not changing the route would have been best) or has a strong influence when the forecast, then shortest path is the favorable one. For the 26 cases where the usage of monthly averages turns out to be most beneficial, the no weather routing case is better than the forecast and shortest path case in only 5 cases, against 21 cases putting the weather routing with shortest path afterwards on the second place.

From figure 13.7b, it can be seen that, while using monthly averages, there hardly are surprises and losses are minimal in case one of the other options turned out to perform better. The forecasts first, then shortest path case does indicate some surprises occur. The example case discussed in the previous section, is one of these cases, represented by the big blue bar in figure 13.7b on the shortest path bar in the middle. When not using routing, many cases show strongly increased consumption.

13.3.2. Expected Fuel Savings

Figure 13.7b shows the increased consumption with respect to the “would have been best” option, however, the number to be found is the fuel that can be saved, taking the no weather routing case as reference. Table 13.3 shows the realized savings in more detail. To calculate the 95 % confidence interval, an inversely exponential distribution is assumed, based on the histogram provided in figure 13.8.

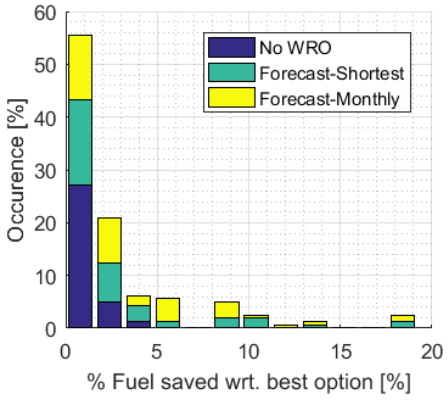

Figure 13.8: Distribution of the achieved fuel savings.

Table 13.3: Statistical data for the three investigated cases.

Parameter	Unit	No WRO	WRO-Shortest	WRO-Averages
Total consumption	[ton]	17 956	17 520	17 398
Fuel savings	[%]	0.000	2.428	3.108
Weighted fuel savings	[%]	0.000	2.587	3.175
Standard Deviation	[%]	1.139	4.456	4.505
Lower confidence boundary	[%]	-0.111	2.050	2.541
Upper confidence boundary	[%]	0.148	3.301	4.018

Looking at the histogram, the first 1.5 % fuel savings bar is clearly the biggest one for all three cases considered. This indicates that, in nearly half of the investigated cases, weather route optimization does not provide significant different results. This can be interpret as follows: weather route optimization often indicates that simply sailing the shortest route is the best option, since taking detours increases the distance sailed, which requires a higher velocity and will only be profitable in certain cases. It also shows that the maximum fuel losses by mistakingly relying on weather routing, are very limited (4.42 % in one case, number 47 in appendix A.8.), but still is not eliminated due to both forecast and monthly averages uncertainties.

When weather routing actually suggest taking a different route, the gains become significant. Because about half the routes do not suggest a different route, the average savings while a significantly different route is suggested, are twice as big as the total values found in table 13.3. In other words, savings of 5-6 % are achieved on average, when the weather route optimization software suggests a detour.

13.3.3. Hypothesis Testing

Looking at the figures provided in table 13.3, it is clear that weather routing has a positive effect on the fuel consumption, however; the confidence interval of the mean savings of using weather routing and shortest route, or weather routing and monthly average, overlaps. In order to determine whether the statement that monthly averages significantly reduce the fuel consumption is valid, the statement will be tested using statistics.

Fisher's ANOVA method (ANalysis Of VAriation) [23] can be used to analyze the chance of two independent set to originate from a single data set. However, as discussed in [23], the results are only valid when:

1. All data sets follow a normal distribution.
2. All data sets have a similar variance.
3. The samples are random and independent of each other.

Using the Kolmogorov-Smirnov test [56], which is a build-in function in MATLAB on each of the sets, shows the chance of the two sets coming from a normal distribution, is equal to less than 1e-20. Therefore, the first ANOVA condition is not met.

An alternative testing method is the Kruskal-Wallis method, which is a rank-based method [50]. As stated on page 585 in [50], the method is advantageous to use when conditions for parametric analysis are not met. For the Kruskal-Wallis method, following assumptions must be valid:

1. Observations must be independent.
2. Each sample contains data from a single population.
3. The different populations have a similar form.

Points 1 and two are met, but to make use of this method, the similarity between the two populations must be demonstrated. While trying to reject the third requirement, a two-sample Kolmogorov-Smirnov test [56] is conducted, using the build-in MATLAB function `kstest2`. With a p-value of 0.4939, the null hypothesis that

both data sets come from populations with the same distribution is accepted. While assuming the distributions are similar, the third condition is met if it can be shown that the variance of both sets is similar.

In order to do so, the Barlett's test [4] is used, which is also included in the statistical toolbox of MATLAB. With the null hypothesis that the variance between the two populations is equal, the function `vartestn` returns a p-value of 0.91, indicating there is no reason to reject the null hypothesis. This result of the Barlett's test, the two sample Kolmogorov-Smirnov test and the graph shown in figure 13.8, indicate the third assumption to use the Kruskal-Wallis method is met, allowing it's usage concerning the weather route optimization problem.

Once again using the statistical toolbox of MATLAB, the probability that the weather routing savings based on forecasts, then shortest path data comes from the same population as the weather routing savings while also applying the monthly averages, can be calculated using function `kruskalwallis`. The test returns a value of 0.1593, which means that there is a chance of 15.93 % that the advantages the monthly averages offer, are based on luck.

Despite not reaching a 95 % confidence in the hypothesis that the usage of monthly averages is beneficial (the confidence in the hypothesis is slightly over 84 %), the results suggest that weather route optimization using monthly averages results in larger savings than weather route optimization without it, which is in line with the expected results.

Since the method used for statistical analysis for random distributions is rather vague, a second method from Kean University [18] is used for hypothesis testing. The null hypothesis tests the difference between two population means for two samples from populations that are not normally distributed and calculates the z-score according to equation 13.1:

$$z = \frac{(\bar{x}_1 - \bar{x}_2) - (\mu_1 - mu_2)_0}{\sqrt{\frac{\sigma_1^2}{n_1} + \frac{\sigma_2^2}{n_2}}} \tag{13.1}$$

Where $\bar{x}$ is the average of a sample size, μ is the true mean, which is unknown for both samples and thus ignored as done in [18], n the number of data points in a sample and σ the standard deviation.

With this equation, the null hypothesis that the savings of the monthly averages case are the same or greater than the savings using forecasts without monthly averages is tested. The resulting z-score is 0.5838, which corresponds to a p-value of 0.7203, hence the null hypothesis is not rejected. The result of this test indicates less certainty of the conclusion than the Kruskal-Wallis test, but favors the same conclusion that has been expected throughout the entire project.

Matching the achieved results with the consumption of the CMB fleet and the global 20 ports average fuel prices of today (HFO: 376.5 USD/mt, MGO: 626 USD/mt),[76]), the achieved savings would result in:

Table 13.4: Savings due to weather routing under the assumption that the savings are equally distributed over the different fuel types used.

Parameter	**Unit**	**No WRO**	**WRO-Shortest**	**WRO-Averages**
HFO consumption	[mt/year]	676 334	658 838	654 861
MGO consumption	[mt/year]	63 862	62 210	61 834
HFO saved	[mt/year]	0	17 497	21 474
MGO saved	[mt/year]	0	1 652	2 028
Total cost reduction	[USD/year]	0	7.620 M	9.354 M
CO_2 emission reduction [64]	[mt/year]	0	60 549	79 537

To quantify the reduction in CO_2 emission, the emission data of the world bank [84] is consulted. Using the latest data for Belgium (2014), the savings achieved by applying weather routing with monthly averages correspond to the total CO_2 emission of 9 550 average Belgian citizens.

The calculated results are not truly matching with reality. First of all, the party that pays the fuel is depending on the contract type. Therefore, the bunker costs saved does not benefit CMB alone. Apart from this,

clients might use some sort of weather route optimization, but whether or not this is used by third parties and what the effects of it is, remains unclear. Again, a reduction in actual gains is expected due to this, since some routes are already (partially) optimized. A third contributing factor is the method used to calculate the potential gains. By selecting random locations as initial and final point, the routes taken are usually corresponding to open-sea routes. While maneuvering to the quay in ports or when leaving a port, the route cannot be optimized, hence total savings will be slightly lower.

Despite these saving reductions, which are hard to quantify, there is a lot of confidence that the developed weather route optimization tool can still significantly reduce both costs and greenhouse gas emissions for the CMB fleet. In an extremely pessimistic case, where only 10 % of the theoretical savings could be achieved, the savings are still worth the effort.

13.3.4. Note on Voyage Safety

A voyage is said to be safer, when less severe weather conditions are encountered. To gain more insight in this, tables A.17 and A.18 are created, containing the maximum wind and maximum waves found while sailing the simulated routes. Table 13.5 summarizes the most significant findings:

Table 13.5: Summary of the simulated voyages with respect to safety.

Parameter	**Unit**	**No WRO**	**WRO-Shortest**	**WRO-Averages**
Average counter current	[m/s]	-0.0246	-0.1811	-0.2063
Average wind speed	[m/s]	6.77	6.71	6.67
Average significant waveheight	[m]	2.27	2.13	2.11
Average maximum counter current	[m/s]	1.1072	0.8711	0.7676
Average maximum wind speed	[m/s]	12.11	11.98	12.04
Average maximum significant waveheight	[m]	3.82	3.76	3.74
Median of maximum counter current	[m/s]	1.0367	0.8390	0.7461
Median of maximum wind speed	[m/s]	10.93	10.74	10.71
Median of maximum significant waveheight	[m]	3.52	3.38	3.43
Maximum counter current	[m/s]	2.3856	1.7882	1.6171
Maximum wind speed	[m/s]	24.60	23.77	23.77
Maximum significant waveheight	[m]	10.98	11.28	11.28

As discussed before, the averages go down while using weather routing, with slightly better results when monthly averages are involved. While looking at the average of the worst sailing conditions encountered during a voyage, this pattern remains, with exception of the wind speed, which slightly goes up while involving monthly averages. The biggest change is found in the average maximum counter current, which indicates that strong counter currents are likely to be avoided, especially while using monthly averages. This makes sense, knowing that several strong currents are present on the globe (see figure 4.6a).

The median of the worst conditions encountered during the voyages, is systematically lower than the average. This means that the average is pulled up by a relative small number of voyages extremely bad conditions, which are thus unavoidable by weather routing. On the other hand, severe weather is entirely avoided in most cases. For the wind, 76 % of the optimized voyages do not encounter a maximum Beaufort number higher than 6 and for 50 % of the optimized voyages does not even surpass a Beaufort number of 5 at any time (in comparison with 70 % and 42 % when no routing is used).

The last tabulated parameters, the absolute maximum encountered during one of the 54 voyages, again indicates that the usage of monthly averages is especially reducing the counter currents encountered. The extreme counter currents are always avoided, resulting in an extremal drop of no less than 0.77 m/s. The maximum encountered, however, is not saying everything, since there is a certain amount of (bad) luck involved in this single number.

Another story is the maximum significant waveheight encountered, which increases for both weather route

optimization cases. The two cases indicate the exact same maximum was encountered. Visualization of the particular voyage, of which the relevant moment is given in figure 13.9, shows an extremely large bad weather zone, which requires a detour hundreds of nautical miles to avoid. The zone moves from west to east, not allowing for a local speed-up or slow down.

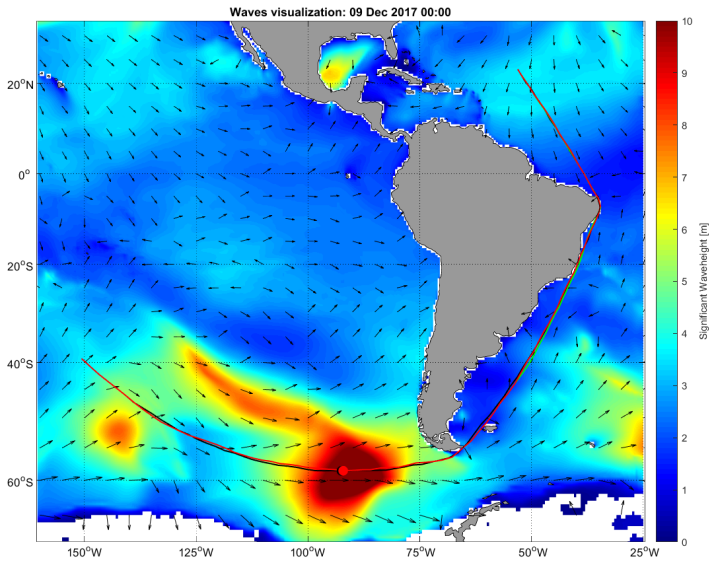

Figure 13.9: Visualization of the highest significant waveheight encountered over all simulations combined.

Ignoring this particular voyage, the maximum significant waveheight reduces to 7.28 m for the case without optimization, 6.75 m for the forecast, then shortest path case and 7.06 m for the monthly averages case.

In general, a reduction in weather severity is realized by applying weather routing. Looking at the small differences due to the usage of monthly averages, it is safe to say that the forecasts are the main factor in determining voyage safety. When weather conditions as severe as the ones shown in figure 13.9 occur, the operators or captain should be warned about this and a potential delay in departure or arrival should be considered. Container vessels are more sensitive to severe weather because the loss of containers significantly increases.

14

Conclusions and Recommendations

In an attempt to reduce the fuel consumption and greenhouse gas emission by the vessels owned by CMB, research regarding the usage weather route optimization for oceanic vessels, incorporating monthly averaged sailing conditions, based hindcast data analyses, has been conducted. From the research, the conclusions discussed in section 14.1 can be drawn. Investigating the research questions gave rise to new and unanswered questions and possible improvements, which are documented in section 14.2.

14.1. Conclusions

To investigate the effect of weather routing, a MATLAB-based software model to find optimal routes has been developed. This model, based on the 3D Dynamic programming model [87] and Dijkstra's algorithm [20], in combination with self-developed automatic smart grid generation, made it possible to analyze the effect of weather route optimization, as well as the effect of monthly averaged weather usage.

While varying the ratios determining the environmental fields (current, wind and waves) in time, it became clear that:

- When no weather data is available, using monthly averaged environmental conditions in stead of the shortest path results, on average, in lower fuel costs.
- Using forecasts up to 7.5 days is, on average, slightly better than using the monthly averaged conditions in stead of the last available day of forecast. This is the full duration of the forecasts available but at the limit, the difference between forecasts and monthly averages is relatively small, indicating significant uncertainties in the forecasts.
- When forecasts are available, omitting the shortest path and monthly averaged conditions results in the least fuel consumption. In other words, any available forecast should, in general, be fully relied on, since it results in better routes.

The items above can be summarized as: *In general, using any forecast available results in the lowest fuel consumption. When no forecast data is available, using monthly averages to determine the effect of the environment on the consumption is preferred over taking the shortest route.*

With this conclusion, the achievable savings of using weather route optimization could be tested. From the conducted tests, which used stored forecast data and matching hindcast data to evaluate the effect of decisions taken based on the data available during the planning of the route, it can be seen that, in general:

- Weather routing using forecasts, then the shortest route, results in savings of 2.43 %(2.05 % - 3.3 %) with respect to the no weather routing case.
- Weather routing using forecasts, then monthly averages, results in savings of 3.11 % (2.54 % - 4.02 %) with respect to the no weather routing case.

If these theoretical savings are achieved, a total of up to 9.35 million US Dollar and 79 537 metric tonnes of CO_2 emission reductions are realized, which corresponds to the total CO_2 emission of almost 10 000 average Belgian citizen. However, due to the open-sea simulations used during the saving analysis and because the fact some vessels already use weather route optimization software was not taken into account, realistic savings are expected to be slightly lower.

The simulation data strongly suggests that using monthly averages improves fuel consumption, which was expected. However, the 95 % confidence intervals between brackets above, indicate there is a small overlap and the conclusion cannot be said with 95 % certainty.

Regarding crew and cargo safety, it can be be seen that the severity of the weather encountered is generally reduced. Both the average and median of the encountered wind, waves and counter current when weather route optimization is applied. Apart from one outlier in the significant waveheight, the same can be said about the most extreme weather condition encountered during all realistic voyage simulations. Since fuel consumption increases while more severe weather is encountered, this conclusion is in line with the expectations.

14.2. Recommendations

From the conclusions above, it becomes clear that weather routing and the usage of monthly averaged sailing conditions is beneficial in terms of fuel savings. There are still many improvements possible though. Following parts should still be implemented in the tool to use more of its potential:

- Fuel consumption of the auxiliary engines and the boiler, especially focusing on the low engine settings at which an auxiliary blower is needed to run the main engine.
- Fuel zones, containing the zones in which different types of fuel can be used. Avoiding low sulfur zones can reduce the total bunker costs even further.
- Heavy weather avoidance: As became clear while investigating the worst weather conditions encountered, a method to avoid such severe conditions should be developed.
- Piracy zones: There are several areas where piracy is still a problem. Avoiding these zones when needed should be possible.
- Accessing in-land ports should be possible without the need to manually select the right location at sea to enter the port, allowing for further automation of the process.

Apart from modifications to the tool itself, several procedures are recommended to further improve this research and to gain more thrust in the outcomes:

- An increased number of simulations should be performed, aiming at a higher confidence level of the results.
- More realistic voyages, including port arrivals and departures, could increase the accuracy of the potential savings.
- The current project includes data from October till January. Extending this on a yearly basis could lead to knowledge about the most critical zones to apply weather routing depending on the season.
- Weather routing on different types of vessels is expected to give different results.
- Moving from simulations to experiments on real ships could give a better view on realistic savings.
- Collecting data from other weather providers than NOAA could lead to improvements.
- During this project, the reliability of the current, wind and waves data has been treated together. It is, however, possible that changes in the influence ratio for the separate environmental contributors could turn out beneficial.

- Automatic interaction between the autopilot and the weather route optimization software could reduce the human workload involved.
- Not only looking at CO_2 emissions, but including other types of emission like SO_X or NO_x could increase the environmental gains of weather route optimization.

The effects on the operations of the CMB fleet when applying weather routing is placed outside the scope of this project. It is possible that in reality the fuel savings will be converted to increased operating speed which increases the cargo transported by the fleet. The effect of weather route optimization would remain significant in terms of revenue for CMB, but due to the possible higher sailing speeds, the positive effect on emissions could be entirely different.

Part IV
Appendices

A

Numbers and Tables

A.1. Hollenbach Regression Coefficients

The table below shows all regression coefficients derived by K.U. Hollenbach. The bottom describes feasible range of vessel parameters for this model [35].

Table A.1: Hollenbach coefficients

	Mean			Minimum	
	Single-screw			Single-screw	
	Design draught	Ballast draught	Twin-screw	Design draught	Twin-screw
$a1$	−0.3382	−0.7139	−0.2748	−0.3382	−0.2748
$a2$	0.8086	0.2558	0.5747	0.8086	0.5747
$a3$	−6.0258	1.1606	−6.7610	−6.0258	−6.7610
$a4$	−3.5632	0.4534	−4.3834	−3.5632	−4.3834
$a5$	9.4405	11.222	8.8158	0	0
$a6$	0.0146	0.4524	−0.1418	0	0
$a7$	0	0	−0.1258	0	0
$a8$	0	0	0.0481	0	0
$a9$	0	0	0.1699	0	0
$a10$	0	0	0.0728	0	0
b_{11}	−0.57424	−1.50162	−5.34750	−0.91424	3.27279
b_{12}	13.3893	12.9678	55.6532	13.38930	−44.1138
b_{13}	90.5960	−36.7985	−114.905	90.59600	171.692
b_{21}	4.6614	5.55536	19.2714	4.6614	−11.5012
b_{22}	−39.721	−45.8815	−192.388	−39.7210	166.559
b_{23}	−351.483	121.820	388.333	−351.483	−644.456
b_{31}	−1.14215	−4.33571	−14.35710	−1.14215	12.4626
b_{32}	−12.3296	36.0782	142.73800	−12.3296	−179.505
b_{33}	459.254	−85.3741	−254.76200	459.25400	680.921
c_1	$Fr/Fr{\cdot}krit$	$10C_B(Fr/Fr{\cdot}krit-1)$	$Fr/Fr{\cdot}krit$	–	–
d_1	0.854	0.032	0.8970	–	–
d_2	−1.228	0.803	−1.4570	–	–
d_3	0.497	−0.739	0.7670	–	–
e_1	2.1701	1.9994	1.8319	–	–
e_2	−0.1602	−0.1446	−0.1237	–	–
f_1	0.17	0.15	0.16	0.17	0.14
f_2	0.20	0.10	0.24	0.20	0
f_3	0.60	0.50	0.60	0.60	0
g_1	0.642	0.42	0.50	0.614	0.952
g_2	−0.635	−0.20	0.66	−0.717	−1.406
g_3	0.150	0	0.50	0.261	0.643
h_1	1.204	1.194	1.206	–	–
Ship length $L(m)$	42.0–205.0	50.2–224.8	30.6–206.8	42.0–205.0	30.6–206.8
$L/\nabla^{1/3}$	4.49–6.01	5.45–7.05	4.41–7.27	4.49–6.01	4.41–7.27
C_B	0.60–0.83	0.56–0.79	0.51–0.78	0.60–0.83	0.51–0.78
L/B	4.71–7.11	4.95–6.62	3.96–7.13	4.71–7.11	3.96–7.13
B/T	1.99–4.00	2.97–6.12	2.31–6.11	1.99–4.00	2.31–6.11
L_{OS}/L_{WL}	1.00–1.05	1.00–1.05	1.00–1.05	1.00–1.05	1.00–1.05
L_{WL}/L	1.00–1.06	0.95–1.00	1.0–1.07	1.00–1.06	1.00–1.07
D_P/T	0.43–0.84	0.66–1.05	0.50–0.86	0.43–0.84	0.50–0.86

A.2. Blendermann Wind Coefficients

The table below describes the values needed to calculate wind resistance according to Blendermann's approach [13].

Table A.2: Blendermann coefficients

Vessel type	C_{D_t}	$C_{D_{l,\epsilon=0}}$	$C_{D_{l,\epsilon=\pi}}$	δ	κ
Car Carrier	0.95	0.55	0.60	0.80	1.2
Cargo vessel, loaded/container on deck	0.85	0.65/0.55	0.55/0.50	0.40	1.4
Loaded container vessel	0.90	0.55	0.55	0.65	1.1
Destroyer	0.85	0.60	0.65	0.65	1.1
Diving support vessel	0.90	0.60	0.80	0.55	0.7
Drilling vessel	1.00	0.70	0.75	0.1	1.7
Ferry	0.90	0.45	0.50	0.80	1.1
Fishing vessel	0.95	0.70	0.70	0.40	1.1
LNG Tanker	0.70	0.60	0.65	0.50	1.1
Offshore supply vessel	0.90	0.55	0.80	0.55	1.2
Passenger liner	0.90	0.40	0.40	0.80	1.2
Research vessel	0.85	0.55	0.65	0.60	1.4
Speed boat	0.90	0.55	0.60	0.60	1.1
Tanker, loaded/ballast	0.70	0.90/0.75	0.55	0.40	3.1/2.2
Tender	0.85	0.55	0.55	0.65	1.1
Mean of data set	0.86	0.62	0.59		
Standard deviation	0.09	0.13	0.12		

A.3. Vessel Specific Excel Files

An example of the excel file that must be filled in for every operational vessel, is shown for the Maersk Niagara in the screenshots in this section.

General

Vessel type	Container	<-- use dropdown
IMO number	9434905	
Maximum operational speed [kts]	21,1	
Overall Length (L_{OA}) [m]	210,09	
Length between perpendiculars (L_{PP}) [m]	199	
Breadth (B) [m]	30,2	
Design sea margin [%]		
PBCF installed (Y/N)	No	<-- use dropdown
Mewis duct (Y/N)	No	<-- use dropdown
Trim optimization onboard (Y/N)	Yes	<-- use dropdown

Cargo specific

	Ballast	Design	Scantling	Comments
Waterline length (L_{WL}) [m]	195,87	199	199	
Transverse frontal area above water (A_F) [m^2]	844,6	680	680	
Longitudinal projected area above water (A_L) [m^2]	4060	4984,9	4984,9	
Displacement (∇) [m^3]	21618	45668	45668	
Even keel draft (T) [m]	6,24	11,50	11,50	
Wetted surface (S) [m^2]	5403,4	8020,7	8020,7	
Longitudinal center of buoyancy wrt. midship (LCB) [m]	-0,379	-2,553	-2,553	Negative for behind midship
Block coefficient (C_B) [-]	0,560	0,643	0,643	
Prismatic coefficient (C_P) [-]	0,587	0,659	0,659	
Optimal trim [m]	-3,50	-0,70	-0,70	

Figure A.1: General and dimensional specifications of the Maersk Niagara

Propeller

Diameter [m]	7,2
Number of blades [-]	5
Direction of rotation [CW] or [CCW]	Clockwise
A_e/A_0 ratio [-]	
Pitch at 0.6R [m]	7,3944
Pitch at 0.25R [m]	6,8501
Hub/diameter ratio [-]	0,19444

Rudder

Rudder type	HOR	<-- use dropdown and consult drawing on the left -->
Aspect ratio Λ [-]	1,622	
Total projected rudder area [m^2]	37,11	Area, not wetted surface
Non rotating area [m^2]	9,411	
Movable area [m^2]	27,7	
Flap area (BEC only) [m^2]		

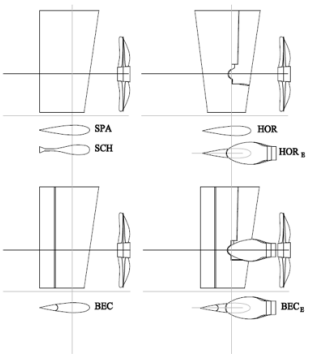

Figure A.2: Propeller and rudder specifications of the Maersk Niagara

M/E

MCR [kW]	21560
SMCR [kW]	
NMCR [kW]	19166
DFOC at MCR [t/day]	87
Kick in point of auxiliary blower %MCR [%]	25%
Maximum RPM [rpm]	99

A/E

ME Load	Consumption [t/24h]
10%	4,3
Below kick in point AUX blower	4,7
Above kick in point AUX blower	4,6
100%	5,5
Base Load consumption Target in Port	3,5
Base Load consumption Target while Idle	5,1

Boiler

Upper Load Limit [%MCR]	18%
Consumption below load limit [t/24h]	2,4

Figure A.3: Main engine, auxiliary engine and boiler specifications of the Maersk Niagara

Specific Fuel Oil Consumption M/E

%MCR	SFOC [gr/kWh]	As documented in sho
25	184,397	
50	178,028	
75	174,066	
90	174,072	
100	175,341	

Figure A.4: SFOC values, as found in the engine shop test of the Maersk Niagara

Tank Towing Test

Draft conditions
Fore:4.20
Aft: 7.90

Speed [kts]	Power [kW]
19	10360
19,5	11513
20	12756
20,5	14117
21	15621
21,5	17280
22	19141
22,5	21189

Draft conditions
Fore:11.50
Aft: 11.50

Speed [kts]	Power [kW]
18	10697
18,5	11783
19	12995
19,5	14331
20	15753
20,5	17267
21	18921
21,5	20985

Draft conditions
Fore:11.50
Aft: 11.50

Speed [kts]	Power [kW]
18	10697
18,5	11783
19	12995
19,5	14331
20	15753
20,5	17267
21	18921
21,5	20985

Figure A.5: Tank Towing Test details of the Maersk Niagara

Event List

Event type	Date
Last Dry Dock	24/05/2013
Last UW cleaning	11/05/2013
Last Propeller cleaning	21/11/2016

Use dd-mm-yyyy format

Anti-fouling paint (maker & type)	International Organotin free self polishing

Event type (use drop-down)	Date
Entering service	25/11/2008
Dry-docking: spot blast	23/05/2013
Propeller polish	21/11/2016
Inspection	21/11/2016

Use dd-mm-yyyy format

Figure A.6: Event list of the Maersk Niagara

A.4. Hindcast Based Validation

The tables below are meant to support the model validation discussed in section 11.2, comparing simulations with the actual measurements. There are many possible explanations of why the numbers do not exactly match, but reported and simulated numbers are close to each other, indicating correct usage of the models.

Figure A.7: Route taken by the Mineral Ningbo from December 15 till December 30.

Table A.3: Comparison between simulated fuel consumption and the consumption reported by the captain of the Mineral Ningbo (Bulk Carrier - deadweight tonnage: 178 120 ton).

Date [dd-mm-yyyy]	**Rep. FC** [ton]	**Sim. FC** [ton]	**Rep. Speed** [kts]	**Sim. Speed** [kts]	**Rep. Distance** [nm]	**Sim. Distance** [nm]
15-12-2017	29.63	28.45	9.76	9.34	234.2	233.62
16-12-2017	30.47	31.35	9.67	9.65	241.7	241.35
17-12-2017	29.26	30.16	9.61	9.62	230.7	230.88
18-12-2017	30.01	32.17	9.69	10.13	242.2	242.43
19-12-2017	29.48	27.23	9.83	9.39	235.9	234.75
20-12-2017	30.22	31.90	9.82	9.81	245.4	245.25
21-12-2017	29.20	27.98	9.63	9.61	231.2	230.74
22-12-2017	29.10	28.65	9.69	9.68	232.5	232.43
23-12-2017	29.66	29.45	9.82	9.84	235.6	236.19
24-12-2017	30.50	31.96	9.91	9.90	247.7	247.56
25-12-2017	29.48	29.39	9.55	9.56	229.3	229.65
26-12-2017	29.48	28.31	9.65	9.89	237.4	237.45
27-12-2017	29.94	30.56	9.83	9.849	235.1	236.38
28-12-2017	31.05	33.30	9.43	9.46	235.8	236.72
29-12-2017	29.85	27.00	9.56	9.32	229.5	223.85
30-12-2017	30.40	33.38	10.33	10.56	247.9	253.66
31-12-2017	29.80	25.08	10.59	10.55	254.1	253.43
Sum/Average	**507.6**	**506.4**	**9.78**	**9.78**	**4046.2**	**4046.4**

Note that in table A.3, the captain incorrectly reported the time zone on December 18, which results in different speeds sailed on December 18 and 19. The daily reports are not completely matching, but the total consumption for both the simulation and the actual route are only 0.25 % apart from each other. The increased real consumption on December 31 can be explained by the end of sea passage, where additional fuel to maneuver in port is used.

Figure A.8: Route taken by the CMB Giulia from November 7 till November 21.

Table A.4: Comparison between simulated fuel consumption and the consumption reported by the captain of the CMB Giulia (Bulk Carrier - deadweight tonnage: 34 297 ton).

Date [dd-mm-yyyy]	**Rep. FC** [ton]	**Sim. FC** [ton]	**Rep. Speed** [kts]	**Sim. Speed** [kts]	**Rep. Distance** [nm]	**Sim. Distance** [nm]
07-11-2017	12.18	11.50	10.61	10.51	254.6	252.26
08-11-2017	13.61	12.27	11.00	10.90	264.0	261.77
09-11-2017	14.02	13.39	11.13	11.21	267.0	269.16
10-11-2017	13.99	13.63	11.38	11.35	273.0	272.52
11-11-2017	14.15	14.90	11.83	11.80	284.0	283.38
12-11-2017	14.23	16.83	12.37	12.31	297.0	295.55
13-11-2017	14.46	13.02	11.33	11.12	272.0	266.89
14-11-2017	14.50	14.45	11.63	11.65	279.0	279.70
15-11-2017	14.57	13.23	11.38	11.23	273.0	269.53
16-11-2017	14.64	14.16	11.42	11.42	274.0	274.23
17-11-2017	14.72	15.47	11.67	11.70	280.0	280.94
18-11-2017	14.72	15.26	11.42	11.27	274.0	270.54
19-11-2017	14.58	14.82	11.17	11.36	268.0	272.66
20-11-2017	14.42	14.13	11.58	11.42	278.0	274.27
21-11-2017	14.93	15.73	11.54	11.54	277.0	277.06
Sum/Average	**213.8**	**212.9**	**11.43**	**11.39**	**4114.6**	**4100.5**

A same pattern can be seen once again, likely due to the exact moment of reporting and the variation in speed to maintain the eta as good as possible.

A.5. Final Ratio Determination

The table below contains information about the randomly generated voyages, used to determine the optimal ratio between monthly averaged weather and shortest path when no weather forecasts are available (anymore).

Table A.5: Random Voyage Descriptions - Final Ratios

#	Vessel	Initial Location	Target Location	Initial Time	Final Time
1	Mineral Subic	24^o20.96'S 1^o18.24'W	9^o48.17'S 48^o56.52'E	13-Dec-2017 15:29	28-Dec-2017 17:49
2	Cuckoo Hunter	19^o38.37'S 133^o36.18'W	17^o7.63'S 21^o10.72'W	28-Nov-2017 04:02	27-Dec-2017 01:46
3	Mineral Energy	12^o40.06'S 118^o57.85'W	11^o26.65'S 28^o15.43'W	20-Nov-2017 12:51	18-Dec-2017 23:14
4	Bochem Oslo	19^o6.86'N 115^o26.14'E	14^o49.93'S 89^o3.52'E	28-Nov-2017 23:58	12-Dec-2017 11:16
5	Mineral Noble	27^o4.97'N 124^o23.04'W	27^o36.28'S 121^o29.01'W	23-Nov-2017 16:47	07-Dec-2017 16:09
6	Delphis Finland	13^o44.6'N 84^o44.31'E	22^o9.04'S 5^o3.03'W	19-Nov-2017 18:22	15-Dec-2017 05:10
7	CMB Virginie	23^o0.69'N 171^o38.75'W	28^o54.31'S 86^o43.8'E	18-Nov-2017 19:32	18-Dec-2017 20:08
8	Bochem Ghent	7^o28.29'S 137^o42.52'W	24^o43.4'S 158^o1.51'E	01-Dec-2017 03:11	16-Dec-2017 00:53
9	CMB Ariane	9^o25.86'S 156^o0.09'E	25^o57.46'S 36^o37.5'E	19-Nov-2017 04:49	17-Dec-2017 18:50
10	Bochem Brussels	22^o40.14'S 129^o1.71'W	27^o50.97'S 81^o31.69'W	05-Dec-2017 09:51	16-Dec-2017 09:24
11	Maersk Nimes	7^o18.33'N 148^o21.71'E	25^o15.17'N 115^o36.58'W	09-Dec-2017 20:28	31-Dec-2017 16:33
12	CMB Partner	27^o16.67'S 173^o37.79'W	9^o50.1'N 144^o55.22'E	27-Nov-2017 11:21	11-Dec-2017 16:51
13	Nadine Venture	20^o32.59'S 162^o42.66'E	27^o25.79'N 164^o42.45'E	14-Dec-2017 04:06	26-Dec-2017 05:18
14	CMB Ariane	24^o56.64'N 27^o23.01'W	27^o51.43'S 54^o30.55'E	07-Dec-2017 09:45	01-Jan-2018 06:36
15	Maersk Nijmegen	22^o51.6'S 118^o5.15'W	15^o4.56'N 96^o39.94'W	03-Dec-2017 01:55	14-Dec-2017 09:25
16	Mineral Belgium	27^o33.45'N 136^o48.96'E	14^o32.97'S 122^o44.82'W	19-Nov-2017 14:22	14-Dec-2017 15:32
17	Barcelona Express	11^o19.62'S 102^o59.97'E	20^o3.66'S 9^o59.19'E	20-Nov-2017 05:28	13-Dec-2017 17:48
18	Maersk Nijmegen	14^o53.34'N 66^o13.5'E	24^o58.24'S 17^o18.62'W	05-Dec-2017 10:20	31-Dec-2017 20:55
19	CMB Mae	21^o16.06'S 82^o40.13'W	22^o9.44'N 127^o22.56'W	02-Dec-2017 16:26	17-Dec-2017 21:14
20	CMB Kristine	18^o57.92'S 131^o50.3'W	4^o57.84'S 91^o0.99'W	18-Dec-2017 17:38	30-Dec-2017 03:34
21	Mongoose Hunter	0^o38.69'S 3^o11.85'W	24^o0.19'N 56^o47.89'W	17-Nov-2017 00:51	01-Dec-2017 17:54
22	CMB Ariane	27^o22.08'N 154^o43.06'E	8^o48.62'S 92^o49.61'W	13-Nov-2017 08:50	10-Dec-2017 10:31
23	Cuckoo Hunter	25^o45.79'N 146^o36.35'W	0^o47.55'S 96^o29.96'E	22-Nov-2017 01:07	22-Dec-2017 19:09
24	Maersk Nienburg	18^o41.68'N 42^o29.2'W	8^o57.38'S 11^o29.34'E	15-Dec-2017 10:03	29-Dec-2017 09:48
25	Mineral Hope	7^o56.49'N 144^o40.88'E	13^o17.4'S 140^o51.65'W	13-Dec-2017 12:58	01-Jan-2018 15:28
26	Nadine Venture	28^o14.13'N 119^o50.12'W	0^o52.64'S 160^o0.5'E	17-Nov-2017 11:17	06-Dec-2017 23:05
27	Mineral Belgium	27^o33.45'N 136^o48.96'E	14^o32.97'S 122^o44.82'W	19-Nov-2017 14:22	14-Dec-2017 15:32
28	Barcelona Express	11^o19.62'S 102^o59.97'E	20^o3.66'S 9^o59.19'E	20-Nov-2017 05:28	13-Dec-2017 17:48
29	Maersk Nijmegen	14^o53.34'N 66^o13.5'E	24^o58.24'S 17^o18.62'W	05-Dec-2017 10:20	31-Dec-2017 20:55
30	CMB Mae	21^o16.06'S 82^o40.13'W	22^o9.44'N 127^o22.56'W	02-Dec-2017 16:26	17-Dec-2017 21:14

Table A.5: Random Voyage Descriptions - Final Ratios

#	Vessel	Initial Location	Target Location	Initial Time	Final Time
31	CMB Kristine	18^o57.92'S 131^o50.3'W	4^o57.84'S 91^o0.99'W	18-Dec-2017 17:38	30-Dec-2017 03:34
32	Mongoose Hunter	0^o38.69'S 3^o11.85'W	24^o0.19'N 56^o47.89'W	17-Nov-2017 00:51	01-Dec-2017 17:54
33	CMB Ariane	27^o22.08'N 154^o43.06'E	8^o48.62'S 92^o49.61'W	13-Nov-2017 08:50	10-Dec-2017 10:31
34	Cuckoo Hunter	25^o45.79'N 146^o36.35'W	0^o47.55'S 96^o29.96'E	22-Nov-2017 01:07	22-Dec-2017 19:09
35	Maersk Nienburg	18^o41.68'N 42^o29.2'W	8^o57.38'S 11^o29.34'E	15-Dec-2017 10:03	29-Dec-2017 09:48
36	Mineral Charlie	22^o57.29'S 97^o23.31'W	0^o28.29'N 26^o32.49'W	18-Nov-2017 22:13	17-Dec-2017 08:23
37	Mineral Hokusai	25^o43.87'N 164^o46.37'W	0^o41'S 80^o36.94'E	18-Nov-2017 01:35	17-Dec-2017 17:08
38	Nadine Venture	0^o39.96'S 93^o56.51'W	27^o44.14'S 170^o47.62'E	09-Dec-2017 07:29	31-Dec-2017 12:02
39	Harmonious	26^o25.37'S 10^o7.14'W	27^o27.24'S 63^o41.41'E	30-Nov-2017 11:12	17-Dec-2017 23:34
40	Bochem Mumbai	19^o3.16'N 111^o21.12'E	21^o0.48'S 77^o51.23'E	30-Nov-2017 17:19	17-Dec-2017 13:10
41	Robin Hunter	4^o3.38'S 16^o10.24'W	19^o35.8'S 128^o23.4'W	29-Nov-2017 03:56	30-Dec-2017 17:19
42	Maersk Nijmegen	12^o28.85'S 44^o47.44'E	29^o4.24'S 23^o55.32'W	18-Nov-2017 19:27	05-Dec-2017 01:12
43	Bochem Chennai	13^o51.16'S 83^o15.01'E	2^o52.33'N 27^o0.45'W	22-Nov-2017 18:42	20-Dec-2017 08:50
44	CMB Chardonnay	3^o40.32'N 163^o35.38'W	10^o9.02'N 133^o39.19'E	25-Nov-2017 17:21	12-Dec-2017 05:37
45	CMB Julliette	4^o58.75'N 40^o22.99'W	12^o34.41'S 86^o52.07'W	18-Nov-2017 23:35	17-Dec-2017 10:19
46	Mineral Kyoto	13^o48.89'N 168^o55.93'E	24^o22.7'N 137^o16.84'W	14-Dec-2017 18:31	26-Dec-2017 22:04
47	CMB Mae	28^o38.95'S 33^o1.48'E	11^o14.21'S 26^o9.55'W	19-Nov-2017 05:06	05-Dec-2017 11:01
48	Bochem Mumbai	11^o59.59'N 68^o34.93'E	27^o59.02'S 48^o29.14'E	25-Nov-2017 11:11	07-Dec-2017 11:03
49	Hermes Arrow	5^o32.56'S 54^o3.35'E	13^o6.08'N 111^o59.6'E	29-Nov-2017 13:05	19-Dec-2017 09:44
50	Mineral Faith	29^o35.82'S 61^o21.97'E	4^o32.34'S 13^o8.56'W	07-Dec-2017 01:42	26-Dec-2017 19:35
51	Mineral Hope	7^o56.49'N 144^o40.88'E	13^o17.4'S 140^o51.65'W	13-Dec-2017 12:58	01-Jan-2018 15:28
52	Nadine Venture	28^o14.13'N 119^o50.12'W	0^o52.64'S 160^o0.5'E	17-Nov-2017 11:17	06-Dec-2017 23:05
53	Mineral Utamaro	27^o51.43'S 54^o30.55'E	26^o2.37'N 122^o11.71'E	03-Dec-2017 19:46	27-Dec-2017 08:12
54	Mineral Belgium	27^o33.45'N 136^o48.96'E	14^o32.97'S 122^o44.82'W	19-Nov-2017 14:22	14-Dec-2017 15:32
55	Barcelona Express	11^o19.62'S 102^o59.97'E	20^o3.66'S 9^o59.19'E	20-Nov-2017 05:28	13-Dec-2017 17:48
56	Maersk Nijmegen	14^o53.34'N 66^o13.5'E	24^o58.24'S 17^o18.62'W	05-Dec-2017 10:20	31-Dec-2017 20:55
57	CMB Mae	21^o16.06'S 82^o40.13'W	22^o9.44'N 127^o22.56'W	02-Dec-2017 16:26	17-Dec-2017 21:14
58	CMB Kristine	18^o57.92'S 131^o50.3'W	4^o57.84'S 91^o0.99'W	18-Dec-2017 17:38	30-Dec-2017 03:34
59	Mongoose Hunter	0^o38.69'S 3^o11.85'W	24^o0.19'N 56^o47.89'W	17-Nov-2017 00:51	01-Dec-2017 17:54
60	CMB Ariane	27^o22.08'N 154^o43.06'E	8^o48.62'S 92^o49.61'W	13-Nov-2017 08:50	10-Dec-2017 10:31
61	Cuckoo Hunter	25^o45.79'N 146^o36.35'W	0^o47.55'S 96^o29.96'E	22-Nov-2017 01:07	22-Dec-2017 19:09
62	Delphis Bothnia	15^o40.63'N 170^o24.76'E	28^o21.77'S 165^o43.85'E	10-Dec-2017 07:22	21-Dec-2017 12:46
63	Mineral New York	27^o2.91'N 158^o19.06'E	13^o40.27'N 158^o48.76'W	20-Dec-2017 15:59	31-Dec-2017 15:36
64	A La Marine	24^o46.77'S 107^o58'E	29^o20.46'S 160^o16.92'E	03-Dec-2017 05:58	16-Dec-2017 21:58

Table A.5: Random Voyage Descriptions - Final Ratios

#	Vessel	Initial Location	Target Location	Initial Time	Final Time
65	Hawk Hunter	22^o39.85'N 30^o21.07'W	28^o59.79'N 86^o45.78'W	21-Nov-2017 05:28	04-Dec-2017 02:28
66	CMB Giulia	20^o8.35'S 133^o35.13'W	29^o48.4'S 46^o21.02'W	26-Nov-2017 12:11	18-Dec-2017 00:25
67	CMB Coralie	9^o40.37'S 103^o18.16'E	24^o6.31'N 141^o4.12'W	05-Dec-2017 14:53	02-Jan-2018 21:10
68	CMB Kristine	3^o37.23'N 64^o39.62'E	9^o43.26'S 132^o13.41'E	06-Dec-2017 18:33	25-Dec-2017 07:34
69	Delphis Riga	16^o7.94'N 171^o24.39'W	16^o56.97'S 96^o39.51'E	04-Dec-2017 01:55	27-Dec-2017 23:24
70	Bochem Singapura	7^o50.4'S 90^o47.12'E	15^o6.14'N 168^o39.57'E	11-Dec-2017 09:08	02-Jan-2018 14:57
71	Mineral Faith	25^o22.53'S 42^o18.12'W	3^o38.99'S 76^o19.97'E	26-Nov-2017 05:51	22-Dec-2017 23:19
72	Mineral Beijing	11^o2.74'N 107^o11.32'W	25^o24.79'S 170^o45.93'E	14-Nov-2017 21:25	06-Dec-2017 18:52
73	Maersk Niteroi	8^o8.86'N 52^o54.28'W	13^o26.3'S 47^o58.01'E	23-Nov-2017 16:04	23-Dec-2017 14:18
74	Bochem Mumbai	9^o43.03'N 128^o17.9'W	24^o14.34'S 169^o30.95'E	28-Nov-2017 00:07	14-Dec-2017 17:42
75	CMB Pomerol	26^o46.89'S 3^o14.61'E	14^o1.13'S 78^o7.97'E	29-Nov-2017 02:57	16-Dec-2017 22:15
76	Mineral Ningbo	14^o57.8'N 126^o5.83'W	12^o47.04'N 123^o4.25'E	19-Nov-2017 19:12	20-Dec-2017 18:42
77	Mineral Ningbo	14^o33.7'N 148^o24.27'W	22^o30.79'N 137^o58.91'E	08-Dec-2017 05:45	25-Dec-2017 12:29
78	MINERAL HOKKAIDO	2^o1.94'N 136^o15.37'E	29^o11.27'S 134^o20.86'W	07-Dec-2017 17:15	30-Dec-2017 14:11
79	Mineral Noble	16^o19.13'N 156^o57.45'W	15^o15.69'N 118^o1.66'E	19-Nov-2017 01:24	09-Dec-2017 22:15
80	Mineral Hokusai	1^o34.61'N 134^o4.28'W	8^o3.46'N 154^o44.23'E	26-Nov-2017 13:50	13-Dec-2017 10:33
81	CMB Weihai	3^o25.93'S 125^o48.6'E	4^o59.03'N 110^o39.08'W	20-Nov-2017 17:15	21-Dec-2017 22:07
82	Harrier Hunter	5^o51.15'N 95^o53.5'E	2^o49.12'N 166^o56.51'W	27-Nov-2017 01:20	22-Dec-2017 18:41
83	CMB Kristine	23^o36.6'N 134^o52.87'W	6^o3.34'N 128^o23.53'E	02-Dec-2017 15:38	25-Dec-2017 01:05
84	Mineral Ningbo	7^o29'S 157^o4.66'W	15^o59.96'N 110^o44.52'W	12-Dec-2017 15:54	26-Dec-2017 16:47
85	Mineral Dragon	29^o35.32'N 165^o4.7'W	21^o18.2'S 70^o54.07'W	26-Nov-2017 11:39	20-Dec-2017 14:22
86	Mongoose Hunter	9^o34.66'N 71^o23.65'E	13^o37.77'S 169^o15.19'E	26-Nov-2017 18:32	25-Dec-2017 01:47
87	Mineral Subic	29^o13.36'N 127^o3.75'W	0^o27.09'S 163^o25.36'W	23-Nov-2017 14:36	05-Dec-2017 14:17
88	Mineral Hope	27^o32.68'S 141^o20.91'W	10^o22.27'N 107^o35.04'W	02-Dec-2017 14:17	14-Dec-2017 21:25
89	Mineral Cloudbreak	15^o5.28'N 52^o15.25'E	26^o0.67'S 76^o58.43'E	21-Nov-2017 23:58	03-Dec-2017 02:49
90	Mineral Charlie	29^o10.2'S 30^o30.01'W	24^o50.86'S 141^o29.7'W	29-Nov-2017 16:22	23-Dec-2017 06:04
91	Barcelona Express	27^o31.76'S 45^o17.47'W	29^o35.77'S 108^o44.71'W	16-Dec-2017 00:06	02-Jan-2018 02:16
92	Mineral Kyoto	16^o51.49'S 74^o35.22'E	19^o27.38'N 163^o24.94'E	27-Nov-2017 03:12	22-Dec-2017 04:20
93	Mineral Ningbo	25^o46.69'S 37^o41.49'E	12^o31.85'N 19^o2.82'W	08-Dec-2017 02:43	28-Dec-2017 22:06
94	Mineral Hokusai	22^o6.92'N 139^o8.65'E	27^o37.51'N 156^o12.61'W	23-Nov-2017 08:57	07-Dec-2017 23:26
95	Mineral Dragon	3^o2.9'N 134^o48.45'W	4^o16.16'N 154^o6.32'E	24-Nov-2017 21:01	12-Dec-2017 17:06
96	Mineral Edo	24^o17.74'S 160^o24.9'W	23^o27.01'N 119^o53.25'W	23-Nov-2017 21:38	09-Dec-2017 09:18
97	Maersk Niteroi	28^o36.03'S 66^o58.37'E	18^o3.39'S 172^o27.68'E	16-Nov-2017 21:04	12-Dec-2017 01:11
98	Mineral Utamaro	3^o59.57'N 109^o51.35'W	25^o22.77'N 141^o5.77'E	01-Dec-2017 04:50	29-Dec-2017 13:03

Table A.5: Random Voyage Descriptions - Final Ratios

#	Vessel	Initial Location	Target Location	Initial Time	Final Time
99	Barcelona Express	21^o19.98'N 141^o0.34'E	5^o36.07'S 111^o52.9'W	15-Nov-2017 01:25	14-Dec-2017 05:24
100	Hermes Arrow	17^o24.42'S 75^o17.26'E	22^o56.54'N 149^o26.24'E	08-Dec-2017 02:10	29-Dec-2017 08:05

Table A.6: Hindcast-based consumption in tons for different Monthly Average (M.A.) Ratio

#	0% M.A.	10% M.A.	20% M.A.	30% M.A.	40% M.A.	50% M.A.	60% M.A.	70% M.A.	80% M.A.	90% M.A.	100% M.A.
1	433.29	427.77	427.76	424.53	424.04	421.70	420.90	421.56	421.59	421.46	420.74
2	235.32	235.32	234.41	233.28	233.02	232.97	232.94	233.58	233.57	232.95	232.94
3	698.32	698.23	698.67	700.34	700.31	700.19	696.71	695.45	695.44	694.69	694.68
4	159.42	159.77	160.00	159.99	158.83	158.83	158.85	158.85	158.91	159.52	159.54
5	323.46	323.46	323.46	323.46	323.46	323.46	321.81	321.81	321.84	322.38	322.38
6	172.54	172.84	172.18	171.62	171.61	171.54	170.89	166.52	165.43	165.04	165.01
7	276.62	277.02	277.24	277.24	277.20	277.11	278.14	278.79	278.56	278.38	278.56
8	177.66	177.66	177.66	177.66	178.98	178.98	178.98	178.88	178.27	178.03	178.03
9	449.74	448.12	440.41	415.08	413.00	413.03	416.54	416.55	417.00	417.38	415.37
10	69.73	69.74	69.74	69.74	69.74	69.74	69.73	69.79	69.77	69.79	69.79
11	427.39	425.10	423.55	425.48	424.35	420.53	421.92	425.36	425.46	424.80	424.57
12	162.43	162.35	162.32	162.32	162.31	159.79	159.78	159.80	159.30	159.32	159.33
13	255.08	255.08	253.82	254.79	254.79	259.52	259.51	259.50	259.53	259.54	256.63
14	322.98	322.99	319.67	318.91	319.24	319.20	319.13	319.13	319.38	320.09	320.13
15	105.40	104.46	104.58	103.95	103.95	103.97	104.13	104.16	104.17	104.08	104.11
16	887.30	886.61	886.65	887.48	885.15	890.69	890.74	891.15	895.88	895.88	894.01
17	307.71	306.94	301.18	300.94	295.97	296.08	297.34	297.37	297.15	297.49	297.48
18	187.56	186.18	182.97	187.00	188.54	189.97	188.98	188.61	188.32	188.29	188.44
19	163.00	162.98	162.97	161.49	161.38	161.55	160.63	160.64	160.62	160.61	160.60
20	105.78	105.78	105.78	105.78	105.53	105.53	105.53	105.53	105.34	105.34	105.34
21	152.31	152.31	151.64	151.89	150.10	149.05	154.33	154.33	156.49	156.47	156.42
22	407.49	398.89	410.33	412.94	412.31	410.89	410.42	409.60	409.86	409.60	409.64
23	260.49	260.72	253.99	251.97	251.80	251.17	249.50	248.93	248.08	254.51	254.77
24	161.51	161.30	161.58	160.77	161.25	161.26	160.99	160.59	160.68	160.68	160.71
25	472.95	467.08	459.72	458.76	455.39	455.09	455.16	454.01	452.13	452.56	452.49
26	431.33	430.01	428.71	421.35	421.31	424.16	416.82	416.80	417.22	415.46	416.09
27	887.30	886.61	886.65	887.48	885.15	890.69	890.74	891.15	895.88	895.88	894.01
28	307.71	306.94	301.18	300.94	295.97	296.08	297.34	297.37	297.15	297.49	297.48

Table A.6: Hindcast-based consumption in tons for different Monthly Average (M.A.) Ratio

#	0% M.A.	10% M.A.	20% M.A.	30% M.A.	40% M.A.	50% M.A.	60% M.A.	70% M.A.	80% M.A.	90% M.A.	100% M.A.
29	187.56	186.18	182.97	187.00	188.54	189.97	188.98	188.60	188.33	188.29	188.43
30	163.00	162.98	162.97	161.49	161.38	161.55	160.63	160.64	160.62	160.61	160.60
31	105.78	105.78	105.78	105.78	105.53	105.53	105.53	105.53	105.34	105.34	105.34
32	152.31	152.31	151.64	151.89	150.10	149.05	154.33	154.33	156.49	156.47	156.42
33	407.49	398.89	410.33	412.94	412.31	410.89	410.42	409.60	409.86	409.60	409.64
34	260.49	260.72	253.99	251.97	251.80	251.17	249.50	248.93	248.08	254.51	254.77
35	161.51	161.30	161.58	160.77	161.25	161.26	160.99	160.59	160.68	160.68	160.71
36	633.72	631.61	631.56	631.56	632.57	632.27	633.15	633.43	635.62	635.47	635.53
37	607.68	609.75	607.87	607.88	608.27	608.52	608.30	610.71	610.99	611.49	611.63
38	522.23	522.23	522.06	522.01	521.84	521.84	516.19	516.19	518.33	518.02	518.02
39	445.78	448.52	448.99	444.86	444.92	444.86	434.33	431.36	431.22	431.23	431.57
40	196.35	196.33	196.31	195.92	195.56	194.66	194.99	195.26	194.92	195.46	195.45
41	439.63	435.16	432.93	433.25	433.35	431.19	432.28	432.92	432.61	432.59	432.70
42	173.10	172.51	167.87	165.37	166.98	166.96	168.08	169.75	172.05	172.36	172.26
43	233.98	233.27	233.11	232.63	231.65	231.40	230.59	230.94	226.86	226.74	226.36
44	210.05	209.50	209.22	205.20	204.01	203.30	202.21	202.19	202.58	202.57	203.51
45	389.16	357.47	356.50	356.51	349.46	349.41	349.50	347.82	347.35	347.85	347.79
46	466.29	467.85	467.83	467.83	466.76	466.82	466.85	466.88	466.87	466.80	466.87
47	138.79	138.79	136.33	136.32	136.12	135.63	135.65	136.66	136.77	136.78	136.82
48	112.97	112.54	111.94	111.93	111.78	111.77	111.77	110.87	110.87	110.37	105.56
49	232.80	217.80	211.81	211.80	207.48	205.70	202.57	202.34	203.18	200.93	200.90
50	484.41	484.75	484.11	474.60	471.93	472.51	470.81	469.70	469.73	469.74	469.78
51	472.95	467.08	459.72	458.76	455.39	455.09	455.16	454.01	452.13	452.56	452.49
52	431.33	430.01	428.71	421.35	421.31	424.16	416.82	416.80	417.22	415.46	416.09
53	555.74	540.72	539.67	540.83	540.73	540.42	540.48	540.53	541.41	541.72	541.72
54	887.30	886.61	886.65	887.48	885.15	890.69	890.74	891.15	895.88	895.88	894.01
55	307.71	306.94	301.18	300.94	295.97	296.08	297.34	297.37	297.15	297.49	297.48
56	187.56	186.18	182.98	187.02	188.54	189.97	188.98	188.61	188.31	188.29	188.41
57	163.00	162.98	162.97	161.49	161.38	161.55	160.63	160.64	160.62	160.61	160.60
58	105.78	105.78	105.78	105.78	105.53	105.53	105.53	105.53	105.34	105.34	105.34
59	152.31	152.31	151.64	151.89	150.10	149.05	154.33	154.33	156.49	156.47	156.42
60	407.49	398.89	410.33	413.01	412.32	410.89	410.42	409.61	409.87	409.84	409.77
61	260.49	260.72	253.99	251.97	251.80	251.17	249.50	248.93	248.08	254.51	254.77
62	85.16	85.16	85.16	85.16	79.53	79.21	79.23	79.35	79.56	79.59	79.30

Table A.6: Hindcast-based consumption in tons for different Monthly Average (M.A.) Ratio

#	0% M.A.	10% M.A.	20% M.A.	30% M.A.	40% M.A.	50% M.A.	60% M.A.	70% M.A.	80% M.A.	90% M.A.	100% M.A.
63	293.12	293.55	293.59	293.64	294.18	295.00	295.58	293.87	293.80	293.92	293.92
64	91.17	91.17	91.17	90.66	90.66	90.65	90.65	90.90	90.52	90.50	90.49
65	138.34	138.35	138.79	138.79	138.79	137.90	137.90	137.30	137.30	137.30	137.30
66	283.57	284.26	283.68	283.02	283.00	279.23	278.90	278.96	278.99	279.14	279.47
67	501.15	495.20	482.58	482.16	482.36	483.40	483.51	484.14	484.10	485.01	471.47
68	146.08	145.26	144.34	144.88	142.93	142.69	142.70	142.81	142.51	139.44	139.37
69	188.45	185.93	184.24	183.18	183.11	179.54	179.63	179.25	179.81	179.66	179.47
70	153.28	151.04	147.08	147.10	145.82	145.21	145.61	146.39	146.56	146.88	147.02
71	827.07	829.27	831.84	830.23	824.72	823.77	824.06	822.37	821.97	821.93	804.70
72	498.01	497.62	497.63	494.53	494.28	491.51	491.61	489.68	489.74	488.16	488.06
73	265.05	261.00	258.62	257.05	256.06	253.61	254.12	252.99	252.41	251.92	252.25
74	176.61	175.67	175.67	175.99	176.70	176.57	176.75	177.19	177.30	177.48	178.98
75	314.38	314.35	314.98	314.98	316.21	310.27	308.28	308.33	308.67	308.92	308.89
76	922.63	922.33	900.89	897.48	901.15	900.21	890.95	891.00	884.64	879.74	879.71
77	579.01	575.88	576.07	572.06	574.04	574.00	575.81	578.69	578.97	573.30	574.15
78	490.55	467.47	463.93	464.58	461.05	461.05	470.17	470.16	473.75	474.36	486.77
79	442.24	445.94	446.36	446.35	448.97	448.97	448.88	448.66	448.66	454.19	454.25
80	342.95	329.79	329.11	319.62	319.50	330.29	326.94	326.83	326.17	326.55	325.27
81	366.16	349.12	336.86	343.03	344.68	344.09	340.99	352.86	352.00	352.31	352.37
82	255.10	250.93	245.83	245.45	244.87	245.21	244.72	244.73	245.21	245.23	245.21
83	299.79	291.51	285.03	284.10	280.56	279.10	278.89	278.58	277.65	270.35	270.05
84	433.46	434.91	433.91	426.76	426.68	423.83	428.12	431.28	431.41	430.79	429.99
85	1150.73	1137.60	1133.65	1132.72	1129.72	1128.72	1115.72	1116.54	1116.29	1132.08	1131.87
86	219.69	219.28	219.94	219.90	222.83	222.85	223.27	230.65	232.35	233.02	233.03
87	284.06	284.10	284.11	285.48	285.38	285.43	285.54	285.49	285.41	285.53	285.37
88	331.60	332.38	332.40	332.40	332.40	332.09	330.66	330.67	330.97	330.99	330.97
89	411.17	407.69	405.17	405.16	405.23	406.00	402.33	392.58	392.54	392.60	392.62
90	913.05	897.94	882.26	878.01	877.68	879.22	879.02	867.94	869.15	871.32	873.30
91	321.25	312.00	307.73	308.81	308.94	307.58	306.18	306.18	306.24	304.23	303.84
92	626.30	625.94	625.71	629.62	627.60	630.60	630.54	640.54	631.47	637.82	636.30
93	552.79	556.74	552.07	551.19	551.22	553.04	552.85	552.84	553.21	553.36	555.74
94	346.07	346.07	344.40	344.40	344.40	344.40	344.30	344.34	344.36	344.45	344.46
95	506.07	476.64	473.34	471.04	456.31	455.49	455.49	455.76	450.82	448.00	447.69
96	381.40	381.41	381.40	381.03	380.91	379.84	377.62	377.64	377.63	377.67	377.67

Table A.6: Hindcast-based consumption in tons for different Monthly Average (M.A.) Ratio

#	0% M.A.	10% M.A.	20% M.A.	30% M.A.	40% M.A.	50% M.A.	60% M.A.	70% M.A.	80% M.A.	90% M.A.	100% M.A.
97	197.32	198.21	198.21	197.36	197.39	197.37	198.71	196.37	194.84	196.96	196.98
98	574.16	577.60	559.60	556.61	556.06	553.75	552.59	551.22	551.18	551.23	551.17
99	370.35	369.98	371.29	367.96	364.27	364.31	363.76	363.91	358.75	358.63	352.03
100	202.56	203.40	203.13	203.00	202.03	201.62	201.62	202.68	202.60	199.38	199.37

A.6. Final Day Determination

Table A.7: Random Voyage Descriptions - Final Ratios

#	Vessel	Initial Location	Target Location	Initial Time	Final Time
1	Maersk Nijmegen	22^o51.6'S 118^o5.15'W	15^o4.56'N 96^o39.94'W	03-Dec-2017 01:55	14-Dec-2017 09:25
2	Mineral Belgium	27^o33.45'N 136^o48.96'E	14^o32.97'S 122^o44.82'W	19-Nov-2017 14:22	14-Dec-2017 15:32
3	Barcelona Express	11^o19.62'S 102^o59.97'E	20^o3.66'S 9^o59.19'E	20-Nov-2017 05:28	13-Dec-2017 17:48
4	Maersk Nijmegen	14^o53.34'N 66^o13.5'E	24^o58.24'S 17^o18.62'W	05-Dec-2017 10:20	31-Dec-2017 20:55
5	CMB Mae	21^o16.06'S 82^o40.13'W	22^o9.44'N 127^o22.56'W	02-Dec-2017 16:26	17-Dec-2017 21:14
6	CMB Kristine	18^o57.92'S 131^o50.3'W	4^o57.84'S 91^o0.99'W	18-Dec-2017 17:38	30-Dec-2017 03:34
7	Mongoose Hunter	0^o38.69'S 3^o11.85'W	24^o0.19'N 56^o47.89'W	17-Nov-2017 00:51	01-Dec-2017 17:54
8	CMB Ariane	27^o22.08'N 154^o43.06'E	8^o48.62'S 92^o49.61'W	13-Nov-2017 08:50	10-Dec-2017 10:31
9	Cuckoo Hunter	25^o45.79'N 146^o36.35'W	0^o47.55'S 96^o29.96'E	22-Nov-2017 01:07	22-Dec-2017 19:09
10	Maersk Nienburg	18^o41.68'N 42^o29.2'W	8^o57.38'S 11^o29.34'E	15-Dec-2017 10:03	29-Dec-2017 09:48
11	Mineral Charlie	22^o57.29'S 97^o23.31'W	0^o28.29'N 26^o32.49'W	18-Nov-2017 22:13	17-Dec-2017 08:23
12	Mineral Hokusai	25^o43.87'N 164^o46.37'W	0^o41'S 80^o36.94'E	18-Nov-2017 01:35	17-Dec-2017 17:08
13	Nadine Venture	0^o39.96'S 93^o56.51'W	27^o44.14'S 170^o47.62'E	09-Dec-2017 07:29	31-Dec-2017 12:02
14	Harmonious	26^o25.37'S 10^o7.14'W	27^o27.24'S 63^o41.41'E	30-Nov-2017 11:12	17-Dec-2017 23:34
15	Bochem Mumbai	19^o3.16'N 111^o21.12'E	21^o0.48'S 77^o51.23'E	30-Nov-2017 17:19	17-Dec-2017 13:10
16	Maersk Nijmegen	12^o28.85'S 44^o47.44'E	29^o4.24'S 23^o55.32'W	18-Nov-2017 19:27	05-Dec-2017 01:12
17	Bochem Chennai	13^o51.16'S 83^o15.01'E	2^o52.33'N 27^o0.45'W	22-Nov-2017 18:42	20-Dec-2017 08:50
18	CMB Chardonnay	3^o40.32'N 163^o35.38'W	10^o9.02'N 133^o39.19'E	25-Nov-2017 17:21	12-Dec-2017 05:37
19	CMB Julliette	4^o58.75'N 40^o22.99'W	12^o34.41'S 86^o52.07'W	18-Nov-2017 23:35	17-Dec-2017 10:19
20	Mineral Kyoto	13^o48.89'N 168^o55.93'E	24^o22.7'N 137^o16.84'W	14-Dec-2017 18:31	26-Dec-2017 22:04
21	CMB Mae	28^o38.95'S 33^o1.48'E	11^o14.21'S 26^o9.55'W	19-Nov-2017 05:06	05-Dec-2017 11:01
22	Mineral Faith	29^o35.82'S 61^o21.97'E	4^o32.34'S 13^o8.56'W	07-Dec-2017 01:42	26-Dec-2017 19:35
23	CMB Pomerol	1^o43.11'S 99^o39.52'E	19^o26.85'S 162^o28.98'W	25-Nov-2017 03:34	20-Dec-2017 11:46
24	Lake Dolphin	10^o54.93'S 82^o19.63'W	26^o23.38'N 133^o16.49'W	30-Nov-2017 04:38	15-Dec-2017 08:00

Table A.7: Random Voyage Descriptions - Final Ratios

#	Vessel	Initial Location	Target Location	Initial Time	Final Time
25	Delphis Gdansk	8^o3.06'S 18^o4.17'W	7^o40.42'N 92^o13.59'E	02-Dec-2017 19:59	01-Jan-2018 13:44
26	Hawk Hunter	6^o23.55'S 5^o18.07'W	14^o28.53'N 60^o0.05'E	22-Nov-2017 00:11	17-Dec-2017 02:26
27	CMB Boris	15^o17.75'N 159^o26.46'W	3^o27.35'S 90^o1.5'W	25-Nov-2017 02:44	12-Dec-2017 09:22
28	Delphis Finland	12^o14.56'N 64^o11.73'E	28^o49.51'S 20^o11.58'W	23-Nov-2017 21:13	19-Dec-2017 05:34
29	Mineral Kyoto	19^o57.88'S 94^o5.94'E	29^o23.53'N 126^o41.59'E	13-Dec-2017 21:58	29-Dec-2017 22:54
30	Hermes Arrow	0^o6.86'S 95^o15.29'W	4^o28.78'N 140^o17.9'E	28-Nov-2017 22:20	28-Dec-2017 08:42
31	CMB Liliane	24^o59.45'S 58^o14.74'E	16^o8.5'N 168^o48.36'E	03-Dec-2017 21:33	01-Jan-2018 09:16
32	Lake Dolphin	22^o44.9'S 169^o3.36'W	0^o56.53'S 126^o56.92'E	20-Nov-2017 08:21	06-Dec-2017 06:10
33	Bochem Brussels	13^o5.27'S 47^o19.15'E	2^o8.88'N 0^o18.56'W	16-Nov-2017 22:46	06-Dec-2017 02:03
34	CMB Weihai	26^o44.73'S 18^o53.44'W	9^o46.1'N 113^o0.74'W	30-Nov-2017 16:36	01-Jan-2018 00:01
35	Bochem Singapura	2^o23.93'N 170^o56.77'E	23^o59.2'S 111^o22.28'E	24-Nov-2017 14:43	13-Dec-2017 07:42
36	Barcelona Express	11^o33.47'S 142^o19.21'W	23^o53.98'S 15^o22.78'W	20-Nov-2017 14:34	18-Dec-2017 16:47
37	Mineral Edo	16^o38.06'N 146^o41.89'W	2^o1.57'N 141^o47.83'E	09-Dec-2017 06:15	28-Dec-2017 11:03
38	Mineral Hokusai	11^o1.37'N 155^o3.16'E	13^o21.81'N 128^o46.25'W	16-Nov-2017 15:48	06-Dec-2017 12:28
39	CMB Boris	23^o57.81'S 98^o40.57'E	24^o30.6'S 10^o48.31'E	16-Nov-2017 04:27	06-Dec-2017 19:15
40	CMB Coralie	17^o52.18'N 81^o50.24'W	13^o37.42'S 36^o23.85'W	06-Dec-2017 07:31	22-Dec-2017 16:29
41	Mineral Hope	7^o56.49'N 144^o40.88'E	13^o17.4'S 140^o51.65'W	13-Dec-2017 12:58	01-Jan-2018 15:28
42	Nadine Venture	28^o14.13'N 119^o50.12'W	0^o52.64'S 160^o0.5'E	17-Nov-2017 11:17	06-Dec-2017 23:05
43	Mineral Utamaro	27^o51.43'S 54^o30.55'E	26^o2.37'N 122^o11.71'E	03-Dec-2017 19:46	27-Dec-2017 08:12
44	Mineral Belgium	27^o33.45'N 136^o48.96'E	14^o32.97'S 122^o44.82'W	19-Nov-2017 14:22	14-Dec-2017 15:32
45	Barcelona Express	11^o19.62'S 102^o59.97'E	20^o3.66'S 9^o59.19'E	20-Nov-2017 05:28	13-Dec-2017 17:48
46	Maersk Nijmegen	14^o53.34'N 66^o13.5'E	24^o58.24'S 17^o18.62'W	05-Dec-2017 10:20	31-Dec-2017 20:55
47	CMB Mae	21^o16.06'S 82^o40.13'W	22^o9.44'N 127^o22.56'W	02-Dec-2017 16:26	17-Dec-2017 21:14
48	CMB Kristine	18^o57.92'S 131^o50.3'W	4^o57.84'S 91^o0.99'W	18-Dec-2017 17:38	30-Dec-2017 03:34
49	Mongoose Hunter	0^o38.69'S 3^o11.85'W	24^o0.19'N 56^o47.89'W	17-Nov-2017 00:51	01-Dec-2017 17:54
50	CMB Ariane	27^o22.08'N 154^o43.06'E	8^o48.62'S 92^o49.61'W	13-Nov-2017 08:50	10-Dec-2017 10:31
51	Cuckoo Hunter	25^o45.79'N 146^o36.35'W	0^o47.55'S 96^o29.96'E	22-Nov-2017 01:07	22-Dec-2017 19:09
52	Maersk Nienburg	18^o41.68'N 42^o29.2'W	8^o57.38'S 11^o29.34'E	15-Dec-2017 10:03	29-Dec-2017 09:48
53	Mineral Charlie	22^o57.29'S 97^o23.31'W	0^o28.29'N 26^o32.49'W	18-Nov-2017 22:13	17-Dec-2017 08:23
54	Mineral Hokusai	25^o43.87'N 164^o46.37'W	0^o41'S 80^o36.94'E	18-Nov-2017 01:35	17-Dec-2017 17:08
55	Nadine Venture	0^o39.96'S 93^o56.51'W	27^o44.14'S 170^o47.62'E	09-Dec-2017 07:29	31-Dec-2017 12:02
56	Harmonious	26^o25.37'S 10^o7.14'W	27^o27.24'S 63^o41.41'E	30-Nov-2017 11:12	17-Dec-2017 23:34
57	Bochem Mumbai	19^o3.16'N 111^o21.12'E	21^o0.48'S 77^o51.23'E	30-Nov-2017 17:19	17-Dec-2017 13:10
58	Maersk Nijmegen	12^o28.85'S 44^o47.44'E	29^o4.24'S 23^o55.32'W	18-Nov-2017 19:27	05-Dec-2017 01:12

Table A.7: Random Voyage Descriptions - Final Ratios

#	Vessel	Initial Location	Target Location	Initial Time	Final Time
59	Bochem Chennai	13^o51.16'S 83^o15.01'E	2^o52.33'N 27^o0.45'W	22-Nov-2017 18:42	20-Dec-2017 08:50
60	CMB Chardonnay	3^o40.32'N 163^o35.38'W	10^o9.02'N 133^o39.19'E	25-Nov-2017 17:21	12-Dec-2017 05:37
61	CMB Julliette	4^o58.75'N 40^o22.99'W	12^o34.41'S 86^o52.07'W	18-Nov-2017 23:35	17-Dec-2017 10:19
62	CMB Mae	28^o38.95'S 33^o1.48'E	11^o14.21'S 26^o9.55'W	19-Nov-2017 05:06	05-Dec-2017 11:01
63	Bochem Mumbai	11^o59.59'N 68^o34.93'E	27^o59.02'S 48^o29.14'E	25-Nov-2017 11:11	07-Dec-2017 11:03
64	Mineral Faith	29^o35.82'S 61^o21.97'E	4^o32.34'S 13^o8.56'W	07-Dec-2017 01:42	26-Dec-2017 19:35
65	CMB Pomerol	1^o43.11'S 99^o39.52'E	19^o26.85'S 162^o28.98'W	25-Nov-2017 03:34	20-Dec-2017 11:46
66	Lake Dolphin	10^o54.93'S 82^o19.63'W	26^o23.38'N 133^o16.49'W	30-Nov-2017 04:38	15-Dec-2017 08:00
67	Delphis Gdansk	8^o3.06'S 18^o4.17'W	7^o40.42'N 92^o13.59'E	02-Dec-2017 19:59	01-Jan-2018 13:44
68	Delphis Finland	12^o14.56'N 64^o11.73'E	28^o49.51'S 20^o11.58'W	23-Nov-2017 21:13	19-Dec-2017 05:34
69	Mineral Kyoto	19^o57.88'S 94^o5.94'E	29^o23.53'N 126^o41.59'E	13-Dec-2017 21:58	29-Dec-2017 22:54
70	Mineral New York	4^o58.05'N 68^o50.01'E	29^o58.12'S 171^o7.14'E	28-Nov-2017 20:35	23-Dec-2017 23:17
71	Hermes Arrow	0^o6.86'S 95^o15.29'W	4^o28.78'N 140^o17.9'E	28-Nov-2017 22:20	28-Dec-2017 08:42
72	CMB Liliane	24^o59.45'S 58^o14.74'E	16^o8.5'N 168^o48.36'E	03-Dec-2017 21:33	01-Jan-2018 09:16
73	Lake Dolphin	22^o44.9'S 169^o3.36'W	0^o56.53'S 126^o56.92'E	20-Nov-2017 08:21	06-Dec-2017 06:10
74	Bochem Brussels	13^o5.27'S 47^o19.15'E	2^o8.88'N 0^o18.56'W	16-Nov-2017 22:46	06-Dec-2017 02:03
75	Bochem Oslo	20^o0.74'S 125^o17.13'W	25^o52.32'N 156^o46.36'W	10-Dec-2017 19:40	24-Dec-2017 02:46
76	CMB Weihai	26^o44.73'S 18^o53.44'W	9^o46.1'N 113^o0.74'W	30-Nov-2017 16:36	01-Jan-2018 00:01
77	Bochem Singapura	2^o23.93'N 170^o56.77'E	23^o59.2'S 111^o22.28'E	24-Nov-2017 14:43	13-Dec-2017 07:42
78	Barcelona Express	11^o33.47'S 142^o19.21'W	23^o53.98'S 15^o22.78'W	20-Nov-2017 14:34	18-Dec-2017 16:47
79	Mineral Edo	16^o38.06'N 146^o41.89'W	2^o1.57'N 141^o47.83'E	09-Dec-2017 06:15	28-Dec-2017 11:03
80	Mineral Hokusai	11^o1.37'N 155^o3.16'E	13^o21.81'N 128^o46.25'W	16-Nov-2017 15:48	06-Dec-2017 12:28
81	Mineral Cloudbreak	22^o0.94'N 164^o42.56'E	8^o0.82'S 144^o49.07'W	07-Dec-2017 19:03	22-Dec-2017 14:23
82	CMB Boris	23^o57.81'S 98^o40.57'E	24^o30.6'S 10^o48.31'E	16-Nov-2017 04:27	06-Dec-2017 19:15
83	CMB Coralie	17^o52.18'N 81^o50.24'W	13^o37.42'S 36^o23.85'W	06-Dec-2017 07:31	22-Dec-2017 16:29
84	CMB Charlotte	25^o21.55'S 100^o47.35'W	12^o24.17'N 144^o49.8'E	19-Nov-2017 21:10	18-Dec-2017 22:10
85	CMB Chardonnay	14^o31.95'S 115^o20.92'W	25^o33.61'S 36^o7.21'W	24-Nov-2017 09:33	17-Dec-2017 01:43
86	CMB Yasmine	4^o14.32'S 26^o28.96'W	28^o32.03'S 131^o17.66'W	19-Nov-2017 20:10	19-Dec-2017 07:06
87	CMB Chardonnay	9^o57.55'N 117^o45.03'W	0^o59.6'N 138^o2.17'E	16-Nov-2017 23:20	12-Dec-2017 02:35
88	Maersk Niteroi	18^o33.13'N 162^o12.17'W	22^o47.32'S 87^o0.99'E	20-Nov-2017 03:06	19-Dec-2017 05:58
89	Delphis Gdansk	19^o9.34'S 29^o43.03'W	28^o46.07'S 85^o36.87'W	04-Dec-2017 12:01	22-Dec-2017 14:38
90	Delphis Finland	28^o29.51'S 125^o14.06'W	18^o57.24'S 27^o36.64'W	23-Nov-2017 06:18	16-Dec-2017 13:16
91	Delphis Bothnia	28^o42.06'S 44^o34.27'E	18^o2.01'N 143^o41.97'E	03-Dec-2017 04:28	29-Dec-2017 08:38
92	Bochem London	28^o54.55'S 153^o47.36'E	17^o1.45'N 64^o20.61'E	04-Dec-2017 05:09	31-Dec-2017 06:04

Table A.7: Random Voyage Descriptions - Final Ratios

#	Vessel	Initial Location	Target Location	Initial Time	Final Time
93	Mineral Subic	19^o4.29'S 98^o46.16'W	23^o35.01'S 160^o21.77'W	17-Dec-2017 17:42	31-Dec-2017 18:27
94	CMB Partner	1^o40.24'N 63^o3.74'E	6^o9.49'N 30^o56.53'W	26-Nov-2017 04:16	24-Dec-2017 14:16
95	Harrier Hunter	13^o10.45'N 146^o5.55'W	8^o43.67'S 173^o39.27'E	27-Nov-2017 00:06	07-Dec-2017 13:57
96	Mineral Stonehenge	5^o11.66'S 15^o51.4'W	22^o27.64'S 98^o47.62'W	30-Nov-2017 02:19	27-Dec-2017 13:13
97	CMB Giulia	26^o43.37'S 38^o12.04'W	4^o5.8'S 0^o26.94'E	16-Dec-2017 06:32	26-Dec-2017 06:38
98	Maersk Nienburg	6^o6.18'S 116^o36.19'E	20^o6.79'N 87^o26.26'E	04-Dec-2017 13:24	16-Dec-2017 12:31
99	Santa Regula	8^o21.7'S 41^o48.89'E	5^o9.96'S 89^o46.69'E	10-Dec-2017 02:58	22-Dec-2017 01:58
100	Bochem Luxembourg	9^o4.85'N 166^o10.83'E	5^o47.42'S 94^o4'W	19-Nov-2017 11:35	16-Dec-2017 07:57

Table A.8: Hindcast-based consumption - Final Day

#	6.5 Days	7.5 Days
1	104.64	104.66
2	913.56	912.28
3	295.97	295.63
4	177.49	176.74
5	160.44	161.13
6	107.03	107.11
7	150.40	150.01
8	400.48	396.38
9	247.91	247.85
10	159.20	159.25
11	632.88	631.17
12	652.29	650.58
13	516.03	515.07
14	389.74	391.70
15	193.88	193.87
16	167.94	167.68
17	228.43	228.62
18	193.65	192.49
19	345.40	345.40
20	450.48	452.69
21	138.36	135.07
22	475.88	472.97

Table A.8: Hindcast-based consumption - Final Day

#	6.5 Days	7.5 Days
23	389.40	389.40
24	389.18	386.08
25	269.00	269.14
26	311.43	311.37
27	228.40	228.15
28	134.39	134.35
29	402.09	402.34
30	220.45	220.42
31	321.49	315.60
32	421.59	420.37
33	102.98	102.81
34	393.13	393.62
35	120.14	119.19
36	446.45	445.74
37	312.64	313.42
38	501.54	502.87
39	259.61	262.31
40	223.69	221.71
41	455.05	454.90
42	415.32	414.73
43	541.96	540.00
44	909.43	894.29
45	297.33	297.32
46	184.78	185.00
47	161.06	161.56
48	107.40	107.92
49	153.42	153.09
50	415.31	414.27
51	252.48	251.29
52	161.55	160.30
53	637.35	636.91
54	653.66	653.64
55	516.01	515.52
56	441.12	443.70

Table A.8: Hindcast-based consumption - Final Day

#	6.5 Days	7.5 Days
57	196.06	196.09
58	175.92	176.90
59	234.26	234.37
60	198.67	199.54
61	371.16	371.15
62	138.17	136.83
63	106.35	106.13
64	471.24	475.33
65	394.22	390.34
66	393.55	392.08
67	270.29	269.91
68	139.88	140.86
69	419.74	420.49
70	812.09	811.89
71	222.60	221.46
72	324.84	320.42
73	420.86	420.95
74	106.84	107.26
75	182.64	182.75
76	414.09	411.45
77	121.94	121.98
78	446.15	446.29
79	315.63	316.34
80	500.64	502.36
81	514.32	509.59
82	261.16	262.08
83	229.42	230.85
84	329.42	329.39
85	406.43	406.91
86	434.48	437.05
87	396.97	400.88
88	222.38	222.73
89	197.23	196.13
90	196.68	196.52

Table A.8: Hindcast-based consumption - Final Day

#	6.5 Days	7.5 Days
91	229.31	226.79
92	188.89	189.40
93	425.99	423.37
94	380.61	378.74
95	104.67	104.64
96	818.36	822.59
97	137.42	137.42
98	99.17	98.95
99	118.46	118.28
100	182.37	181.00

A.7. Monthly Averages Initiation

Description of the final runs to determine the optimal environmental settings.

Table A.9: Random Voyage Descriptions - Monthly averages initiation

#	Vessel	Initial Location	Target Location	Initial Time	Final Time
1	Mineral Hope	7^o56.49'N 144^o40.88'E	13^o17.4'S 140^o51.65'W	13-Dec-2017 12:58	01-Jan-2018 15:28
2	Nadine Venture	28^o14.13'N 119^o50.12'W	0^o52.64'S 160^o0.5'E	17-Nov-2017 11:17	06-Dec-2017 23:05
3	Mineral Utamaro	27^o51.43'S 54^o30.55'E	26^o2.37'N 122^o11.71'E	03-Dec-2017 19:46	27-Dec-2017 08:12
4	Mineral Belgium	27^o33.45'N 136^o48.96'E	14^o32.97'S 122^o44.82'W	19-Nov-2017 14:22	14-Dec-2017 15:32
5	Barcelona Express	11^o19.62'S 102^o59.97'E	20^o3.66'S 9^o59.19'E	20-Nov-2017 05:28	13-Dec-2017 17:48
6	Maersk Nijmegen	14^o53.34'N 66^o13.5'E	24^o58.24'S 17^o18.62'W	05-Dec-2017 10:20	31-Dec-2017 20:55
7	CMB Mae	21^o16.06'S 82^o40.13'W	22^o9.44'N 127^o22.56'W	02-Dec-2017 16:26	17-Dec-2017 21:14
8	CMB Kristine	18^o57.92'S 131^o50.3'W	4^o57.84'S 91^o0.99'W	18-Dec-2017 17:38	30-Dec-2017 03:34
9	Mongoose Hunter	0^o38.69'S 3^o11.85'W	24^o0.19'N 56^o47.89'W	17-Nov-2017 00:51	01-Dec-2017 17:54
10	CMB Ariane	27^o22.08'N 154^o43.06'E	8^o48.62'S 92^o49.61'W	13-Nov-2017 08:50	10-Dec-2017 10:31
11	Cuckoo Hunter	25^o45.79'N 146^o36.35'W	0^o47.55'S 96^o29.96'E	22-Nov-2017 01:07	22-Dec-2017 19:09
12	Maersk Nienburg	18^o41.68'N 42^o29.2'W	8^o57.38'S 11^o29.34'E	15-Dec-2017 10:03	29-Dec-2017 09:48
13	Mineral Charlie	22^o57.29'S 97^o23.31'W	0^o28.29'N 26^o32.49'W	18-Nov-2017 22:13	17-Dec-2017 08:23
14	Mineral Hokusai	25^o43.87'N 164^o46.37'W	0^o41'S 80^o36.94'E	18-Nov-2017 01:35	17-Dec-2017 17:08
15	Nadine Venture	0^o39.96'S 93^o56.51'W	27^o44.14'S 170^o47.62'E	09-Dec-2017 07:29	31-Dec-2017 12:02
16	Harmonious	26^o25.37'S 10^o7.14'W	27^o27.24'S 63^o41.41'E	30-Nov-2017 11:12	17-Dec-2017 23:34
17	Bochem Mumbai	19^o3.16'N 111^o21.12'E	21^o0.48'S 77^o51.23'E	30-Nov-2017 17:19	17-Dec-2017 13:10

Table A.9: Random Voyage Descriptions - Monthly averages initiation

#	Vessel	Initial Location	Target Location	Initial Time	Final Time
18	Maersk Nijmegen	12^o28.85'S 44^o47.44'E	29^o4.24'S 23^o55.32'W	18-Nov-2017 19:27	05-Dec-2017 01:12
19	Bochem Chennai	13^o51.16'S 83^o15.01'E	2^o52.33'N 27^o0.45'W	22-Nov-2017 18:42	20-Dec-2017 08:50
20	CMB Chardonnay	3^o40.32'N 163^o35.38'W	10^o9.02'N 133^o39.19'E	25-Nov-2017 17:21	12-Dec-2017 05:37
21	CMB Julliette	4^o58.75'N 40^o22.99'W	12^o34.41'S 86^o52.07'W	18-Nov-2017 23:35	17-Dec-2017 10:19
22	Mineral Kyoto	13^o48.89'N 168^o55.93'E	24^o22.7'N 137^o16.84'W	14-Dec-2017 18:31	26-Dec-2017 22:04
23	CMB Mae	28^o38.95'S 33^o1.48'E	11^o14.21'S 26^o9.55'W	19-Nov-2017 05:06	05-Dec-2017 11:01
24	Bochem Mumbai	11^o59.59'N 68^o34.93'E	27^o59.02'S 48^o29.14'E	25-Nov-2017 11:11	07-Dec-2017 11:03
25	Mineral China	25^o4.83'N 31^o18.56'W	7^o0.31'S 50^o41.96'E	16-Nov-2017 11:25	16-Dec-2017 17:07
26	Lake Dolphin	6^o27.31'N 66^o57.52'E	15^o26.62'N 156^o15.14'E	28-Nov-2017 12:24	24-Dec-2017 04:53
27	Mineral Faith	15^o1.91'S 80^o11.72'W	21^o0.15'S 152^o24.9'E	24-Nov-2017 13:19	25-Dec-2017 06:22
28	Mongoose Hunter	12^o44.72'S 113^o45.66'E	23^o49.28'S 9^o33.44'E	20-Nov-2017 18:09	16-Dec-2017 01:33
29	CMB Weihai	8^o40.51'N 167^o55.59'W	20^o29.12'S 106^o38.47'E	26-Nov-2017 23:23	19-Dec-2017 07:14
30	Maersk Niagara	9^o11.32'N 57^o8.95'E	6^o25.75'N 146^o53.34'E	23-Nov-2017 11:30	19-Dec-2017 05:52
31	Delphis Gdansk	22^o29.5'N 128^o4.45'E	10^o44.26'N 66^o23.94'E	17-Nov-2017 00:05	07-Dec-2017 08:19
32	CMB Chardonnay	8^o54.54'S 70^o35.73'E	2^o40.14'S 157^o52.78'E	17-Nov-2017 09:31	10-Dec-2017 12:42
33	Mineral Honshu	9^o59.32'S 96^o40.36'W	20^o1.89'S 157^o25.39'W	15-Dec-2017 01:32	30-Dec-2017 03:56
34	Mineral Utamaro	14^o43.55'S 4^o7.78'E	27^o32.99'N 33^o24.08'W	11-Dec-2017 18:23	25-Dec-2017 08:58
35	Mineral Beijing	19^o2.04'S 65^o40.02'E	28^o17.97'S 170^o43.12'W	01-Dec-2017 14:02	30-Dec-2017 12:57
36	Bochem Mumbai	29^o2.48'S 136^o20.5'W	11^o58.25'S 26^o6.32'W	27-Nov-2017 19:39	26-Dec-2017 05:16
37	Mineral Edo	1^o15.55'S 143^o41.42'E	14^o23.56'N 60^o56.79'E	01-Dec-2017 14:26	24-Dec-2017 08:54
38	CMB Boris	22^o12.59'N 150^o15.48'E	0^o32.58'N 82^o2.62'W	13-Nov-2017 19:47	14-Dec-2017 23:16
39	Delphis Gdansk	9^o9.98'N 122^o19.53'E	25^o39.67'N 146^o33.88'W	18-Nov-2017 17:21	14-Dec-2017 10:55
40	Harmonious	14^o52.24'S 125^o12.05'W	2^o15.72'N 142^o51.16'E	28-Nov-2017 06:10	20-Dec-2017 02:21
41	Mineral New York	23^o3.04'S 91^o33.5'W	23^o32.76'S 51^o30.5'E	14-Nov-2017 20:59	16-Dec-2017 19:45
42	Grouse Hunter	14^o35.52'S 102^o8.9'E	2^o28.45'S 170^o15.92'W	08-Dec-2017 02:11	30-Dec-2017 12:37
43	Mineral Stonehenge	3^o41.42'S 145^o47.84'E	6^o32.92'N 95^o7.9'W	27-Nov-2017 16:37	25-Dec-2017 13:50
44	Bochem Chennai	12^o15.77'S 172^o15.75'E	6^o50.87'S 90^o58.08'W	18-Nov-2017 21:18	13-Dec-2017 16:26
45	Cuckoo Hunter	16^o5.23'N 113^o59.56'W	23^o53.01'N 141^o30.58'E	14-Nov-2017 21:11	09-Dec-2017 05:25
46	Hermes Arrow	16^o35.64'S 136^o0.07'W	19^o49.52'S 20^o37.4'W	13-Nov-2017 16:35	10-Dec-2017 15:28
47	CMB Yasmine	14^o6.76'N 127^o28.8'E	0^o13.98'S 54^o36.05'E	20-Nov-2017 06:27	13-Dec-2017 14:54
48	Harrier Hunter	0^o47.46'N 30^o12.78'W	15^o27.49'S 120^o7.21'W	26-Nov-2017 06:49	28-Dec-2017 07:21
49	Mineral Faith	28^o13.51'S 38^o23.85'E	25^o28.46'N 30^o6.69'W	09-Dec-2017 09:34	02-Jan-2018 02:52
50	CMB Coralie	6^o48.63'S 95^o6.37'E	2^o25.33'N 156^o54.58'E	23-Nov-2017 09:27	09-Dec-2017 09:01
51	CMB Ariane	27^o56.99'N 157^o28.55'W	6^o46.46'S 95^o4.48'W	01-Dec-2017 21:51	20-Dec-2017 08:59

Table A.9: Random Voyage Descriptions - Monthly averages initiation

#	Vessel	Initial Location	Target Location	Initial Time	Final Time
52	Mineral Tianjin	13^o54.92'N 62^o4.9'E	26^o1.55'N 139^o31.35'E	21-Nov-2017 19:21	17-Dec-2017 17:25
53	CMB Boris	25^o28.09'S 32^o49.41'W	10^o3.22'S 40^o30.16'E	05-Dec-2017 04:54	26-Dec-2017 15:27
54	Mineral Maureen	8^o4.33'N 52^o43.06'E	12^o4.68'N 167^o43.65'E	27-Nov-2017 14:03	28-Dec-2017 21:11
55	Maersk Nienburg	28^o11.13'S 42^o45.2'E	7^o6.07'N 95^o22.33'E	30-Nov-2017 23:55	15-Dec-2017 09:49
56	Maersk Niagara	6^o3.09'N 110^o50.8'E	26^o25.79'S 156^o1.25'W	01-Dec-2017 04:24	25-Dec-2017 17:18
57	Maersk Niteroi	23^o17.02'S 114^o26.1'W	4^o36.6'S 169^o44.53'E	07-Dec-2017 13:56	25-Dec-2017 14:22
58	MINERAL HOKKAIDO	4^o35.03'N 91^o40.86'W	8^o52.51'N 169^o55.55'E	16-Nov-2017 00:39	10-Dec-2017 21:31
59	Hawk Hunter	16^o41.8'S 162^o34.96'W	23^o21.5'S 107^o51.44'E	02-Dec-2017 11:35	24-Dec-2017 16:24
60	MINERAL HOKKAIDO	19^o4.06'S 148^o57.62'W	19^o56.01'S 30^o35.24'W	04-Dec-2017 18:55	31-Dec-2017 20:34
61	Mineral Honshu	16^o30.33'N 37^o6.13'W	6^o20.67'S 2^o42.78'E	17-Dec-2017 18:52	29-Dec-2017 09:50
62	Mineral Belgium	25^o25.46'S 98^o31.48'W	6^o56.94'S 13^o45.56'W	01-Dec-2017 07:49	28-Dec-2017 05:26
63	Nadine Venture	16^o47.3'N 141^o46.57'W	29^o25.84'S 108^o58.59'W	18-Nov-2017 04:42	02-Dec-2017 10:16
64	Grouse Hunter	10^o0.06'S 124^o27.99'W	29^o29.79'S 15^o45.16'W	17-Nov-2017 10:31	14-Dec-2017 20:14
65	CMB Paule	13^o17.45'N 148^o55.83'E	1^o18.93'N 80^o36.88'E	06-Dec-2017 22:03	25-Dec-2017 10:05
66	Mineral Noble	18^o19.62'S 107^o41.09'W	21^o18.73'N 122^o37.49'W	15-Dec-2017 01:30	24-Dec-2017 22:24
67	Maersk Nienburg	14^o35.97'S 88^o12.59'E	6^o19.85'N 157^o31.41'E	23-Nov-2017 15:16	10-Dec-2017 21:08
68	Mineral Hokusai	28^o4.61'S 100^o52.37'W	27^o38.49'S 106^o12.2'E	20-Nov-2017 14:57	19-Dec-2017 03:45
69	Maersk Niagara	12^o2.48'N 155^o42.03'W	13^o33.69'N 137^o32.3'E	16-Dec-2017 07:24	01-Jan-2018 07:52
70	A La Marine	15^o49.66'N 92^o8.26'E	22^o34.5'S 169^o30.8'W	14-Nov-2017 12:02	16-Dec-2017 06:26
71	Delphis Riga	2^o28.09'N 172^o53.37'W	7^o17.68'S 132^o57.83'E	18-Nov-2017 10:58	03-Dec-2017 17:27
72	CMB Charlotte	18^o49.45'S 136^o7.5'W	6^o54.61'N 132^o7.62'E	28-Nov-2017 12:20	21-Dec-2017 01:02
73	CMB Coralie	19^o39.88'S 91^o13.44'E	19^o53.47'N 126^o32.74'E	09-Dec-2017 15:04	23-Dec-2017 16:57
74	Hawk Hunter	13^o8.78'S 144^o16.46'E	8^o44.04'S 136^o14.51'W	01-Dec-2017 06:55	22-Dec-2017 02:32
75	CMB Yasmine	3^o26.02'N 77^o18.04'E	9^o16.1'S 17^o40.21'W	22-Nov-2017 13:08	22-Dec-2017 01:06
76	CMB Julliette	29^o45.85'S 83^o39.57'W	22^o23.59'N 162^o30.84'E	16-Nov-2017 03:05	16-Dec-2017 17:08
77	Bochem Luxembourg	24^o50.12'S 0^o19.3'E	19^o37.09'S 86^o48.13'W	04-Dec-2017 12:27	30-Dec-2017 23:13
78	Maersk Niteroi	15^o33.92'N 164^o54.85'W	3^o35.56'N 113^o36.17'W	24-Nov-2017 13:54	07-Dec-2017 11:45
79	Mineral Belgium	2^o41.2'N 158^o13.45'E	28^o44.08'S 84^o19.17'W	13-Nov-2017 04:24	10-Dec-2017 20:12
80	Hermes Arrow	0^o25.84'N 125^o51.51'E	4^o0.27'S 135^o0.13'W	04-Dec-2017 18:22	30-Dec-2017 16:57
81	Bochem London	4^o12.46'N 80^o36.82'W	21^o54.09'S 128^o44.17'W	25-Nov-2017 21:35	08-Dec-2017 11:11
82	CMB Coralie	24^o42.4'N 149^o56.93'W	8^o26.44'S 159^o55.77'E	14-Dec-2017 09:59	30-Dec-2017 06:09
83	Delphis Bothnia	8^o30.78'N 119^o39.25'W	25^o59.34'S 161^o33.42'W	17-Dec-2017 15:28	30-Dec-2017 21:58
84	Mineral New York	6^o53.64'N 87^o30.9'W	23^o13.93'S 157^o59.15'W	27-Nov-2017 23:20	17-Dec-2017 05:56
85	Bochem Antwerp	0^o3.67'N 143^o6.26'W	15^o8.58'S 146^o23.3'E	15-Nov-2017 04:36	02-Dec-2017 13:51

Table A.9: Random Voyage Descriptions - Monthly averages initiation

#	Vessel	Initial Location	Target Location	Initial Time	Final Time
86	Cuckoo Hunter	24^o13.62'N 59^o34.7'W	0^o29.52'N 11^o51.55'W	18-Nov-2017 05:12	30-Nov-2017 14:25
87	CMB Edouard	29^o53.19'S 108^o26.29'W	20^o25.74'N 171^o57.62'W	10-Dec-2017 11:13	29-Dec-2017 10:08
88	CMB Pomerol	18^o56.77'S 75^o52.2'E	8^o7.73'S 20^o53.11'W	26-Nov-2017 12:19	22-Dec-2017 04:27
89	Mineral Kyoto	6^o55.12'N 174^o10.9'W	0^o43.24'N 138^o42.64'E	07-Dec-2017 07:20	18-Dec-2017 07:41
90	Maersk Nimes	3^o4.72'S 147^o30.54'E	13^o26.12'S 111^o41.69'W	26-Nov-2017 13:59	22-Dec-2017 20:00
91	CMB Charlotte	1^o15.13'N 165^o5.3'W	0^o29.57'N 84^o18.46'W	09-Dec-2017 09:26	28-Dec-2017 03:16
92	CMB Edouard	13^o52.5'S 117^o47.55'W	27^o20.06'S 39^o24.79'W	28-Nov-2017 11:57	19-Dec-2017 20:47
93	Delphis Gdansk	11^o0.64'S 157^o34.33'W	25^o53.06'N 129^o55.61'E	09-Dec-2017 17:21	29-Dec-2017 20:53
94	Harrier Hunter	24^o33.32'S 59^o16.45'E	2^o1.99'N 41^o21.29'W	18-Nov-2017 17:55	14-Dec-2017 23:29
95	Mineral Utamaro	28^o19.06'N 116^o25.92'W	27^o42.3'S 98^o8.25'W	08-Dec-2017 04:52	23-Dec-2017 14:14
96	Delphis Finland	12^o28.15'S 158^o49.71'W	15^o39.49'N 158^o48.72'E	14-Nov-2017 01:29	27-Nov-2017 16:56
97	Cuckoo Hunter	11^o25.97'S 40^o56.88'E	10^o43.81'N 135^o48.8'E	17-Nov-2017 20:29	14-Dec-2017 04:24
98	Harrier Hunter	29^o41'S 10^o51.3'W	0^o49.26'N 90^o9.62'E	07-Dec-2017 20:42	02-Jan-2018 08:21
99	CMB Weihai	1^o17.06'S 105^o48.3'W	3^o35.37'N 136^o6.75'E	18-Nov-2017 08:06	19-Dec-2017 04:35
100	Maersk Nienburg	29^o13.75'S 5^o29.04'E	7^o35.52'N 115^o0.47'E	27-Nov-2017 14:49	27-Dec-2017 21:54

Table A.10: Hindcast-based consumption - Monthly averages initiation

#	Day 0	Day 1	Day 2	Day 3	Day 4	Day 5	Day 6	Day 7	Day 8
1	452.50	452.54	452.36	452.23	449.14	448.55	448.36	449.73	456.10
2	413.51	413.49	412.98	413.18	409.21	411.50	410.53	411.80	413.60
3	542.86	542.86	542.66	542.89	539.51	540.21	537.92	538.97	540.50
4	893.99	893.99	894.59	895.53	894.44	894.10	913.06	910.77	912.25
5	297.55	307.25	299.84	305.25	307.13	303.98	298.13	291.26	295.64
6	188.01	188.01	187.99	188.09	179.13	177.32	177.13	177.57	176.68
7	161.69	161.69	161.70	161.81	161.54	160.34	160.50	161.28	161.32
8	107.24	107.24	107.18	107.09	106.94	107.03	107.03	107.07	107.11
9	158.37	158.28	149.48	148.40	147.63	147.53	149.74	150.62	150.53
10	417.08	417.55	417.36	415.05	414.78	414.81	400.62	400.28	394.43
11	256.39	257.36	255.52	255.90	249.95	249.51	249.14	248.05	247.73
12	160.54	160.57	160.33	160.61	159.54	159.40	159.80	159.20	159.58
13	631.74	631.74	631.70	632.08	632.27	632.26	630.76	630.60	631.18
14	654.75	654.50	653.13	652.96	653.95	652.14	649.89	651.93	648.24
15	514.86	514.86	514.86	514.86	514.89	515.06	508.35	515.66	514.84

Table A.10: Hindcast-based consumption - Monthly averages initiation

#	Day 0	Day 1	Day 2	Day 3	Day 4	Day 5	Day 6	Day 7	Day 8
16	431.53	433.58	431.33	433.60	430.93	427.92	428.10	384.86	393.43
17	195.45	195.50	195.55	194.86	194.87	194.85	194.09	193.88	193.32
18	171.87	171.87	171.97	168.83	167.77	168.26	168.59	168.30	168.68
19	228.48	228.48	228.81	228.36	228.31	228.62	229.03	229.20	228.63
20	198.56	198.63	198.26	198.17	199.28	199.07	192.90	193.14	192.51
21	344.31	344.31	344.30	343.93	344.93	345.42	345.22	345.38	345.91
22	463.20	463.20	461.90	457.13	452.68	453.42	451.95	450.45	453.64
23	137.76	136.92	137.47	137.23	136.52	136.54	135.69	136.19	134.46
24	105.56	106.24	105.56	104.99	105.30	101.91	102.66	110.32	102.26
25	735.87	735.87	737.91	737.99	736.03	737.90	737.98	737.90	737.90
26	525.29	525.29	524.06	524.00	522.71	524.15	526.40	524.23	525.43
27	692.19	692.39	693.11	691.57	691.51	692.53	690.39	688.95	688.94
28	281.63	281.63	281.84	281.48	281.43	280.95	285.94	281.43	280.30
29	255.03	255.03	255.06	256.49	250.49	250.14	249.48	250.29	249.24
30	161.10	160.60	161.05	160.98	158.14	157.49	158.89	158.43	159.98
31	172.44	172.19	171.58	171.60	171.29	171.24	171.52	170.03	170.00
32	300.60	300.57	299.80	300.98	301.08	299.63	299.49	298.75	297.87
33	342.94	334.09	342.91	342.62	342.29	333.26	333.73	332.60	333.17
34	303.37	303.37	303.63	303.30	301.93	304.58	304.05	303.93	304.48
35	614.98	615.50	615.59	611.02	613.67	614.76	610.88	609.53	609.33
36	307.74	307.74	307.60	307.97	305.62	308.56	304.86	304.88	304.80
37	447.32	447.29	447.12	446.63	445.94	445.92	445.88	445.58	445.67
38	433.61	433.61	433.66	432.86	433.33	431.09	429.05	426.80	426.68
39	162.53	162.53	162.45	162.38	162.51	161.73	161.89	161.39	164.32
40	626.15	632.34	632.48	631.13	628.57	626.91	628.36	628.84	621.64
41	819.12	819.12	819.12	819.21	819.05	817.59	817.54	818.41	817.64
42	457.70	457.70	457.70	454.14	453.41	457.01	448.45	458.38	451.16
43	916.48	916.61	916.34	909.17	908.01	907.53	902.30	901.74	903.18
44	176.81	176.81	176.80	176.76	177.04	176.50	176.19	175.99	176.35
45	214.28	214.28	214.28	214.33	214.61	214.66	213.43	213.85	214.99
46	277.45	277.45	277.24	278.25	280.67	278.60	278.53	278.59	278.94
47	251.07	250.62	250.60	250.25	250.18	249.69	249.47	249.59	249.27
48	287.63	287.57	287.91	288.89	288.02	286.31	286.04	287.10	287.66
49	534.47	534.47	534.37	534.40	534.33	530.67	532.07	531.03	527.45

Table A.10: Hindcast-based consumption - Monthly averages initiation

#	Day 0	Day 1	Day 2	Day 3	Day 4	Day 5	Day 6	Day 7	Day 8
50	203.14	202.80	200.86	200.72	200.48	200.45	200.58	201.75	202.20
51	189.75	189.75	184.94	189.83	184.80	184.66	182.54	182.33	183.58
52	560.13	560.13	559.70	559.74	567.09	567.05	547.38	532.31	530.53
53	217.44	217.44	218.11	214.39	214.34	215.63	214.89	215.41	214.93
54	684.04	685.89	681.59	680.83	680.62	682.97	685.32	685.73	686.02
55	166.69	166.69	170.33	168.17	165.42	158.83	159.73	159.14	158.61
56	210.81	211.47	210.75	210.82	211.33	210.53	208.69	209.10	209.15
57	190.91	190.90	191.08	191.09	190.09	190.20	190.54	190.20	189.56
58	473.29	473.34	473.28	473.68	473.32	473.40	473.94	495.21	474.09
59	234.95	234.13	229.28	229.27	247.80	229.52	229.05	229.85	228.86
60	751.03	751.03	751.97	750.50	749.66	746.78	750.25	749.54	750.06
61	265.42	265.42	264.88	265.08	263.53	262.27	262.78	262.90	271.90
62	674.90	670.92	670.51	669.55	669.67	669.78	669.36	670.76	669.50
63	296.71	297.01	294.58	294.29	294.04	294.04	293.24	291.22	291.04
64	599.51	599.51	599.37	599.37	599.35	599.35	602.32	602.97	602.00
65	177.30	177.30	177.22	177.82	175.10	174.91	173.65	173.68	174.51
66	270.19	270.19	270.51	262.38	264.40	260.91	263.28	264.66	262.75
67	172.89	172.72	172.61	170.36	172.10	170.46	169.14	169.94	170.23
68	947.96	947.96	947.12	949.88	940.51	944.64	948.04	923.04	924.30
69	119.05	119.46	119.00	119.00	118.91	119.14	118.40	118.56	117.51
70	174.56	174.62	174.49	174.55	174.55	174.46	174.19	174.22	174.04
71	104.85	104.89	105.28	102.98	103.14	102.99	104.34	103.62	103.40
72	299.74	299.61	299.63	299.63	299.23	296.85	296.82	297.21	305.02
73	246.31	246.31	246.31	246.31	246.31	242.86	243.13	241.73	242.00
74	171.58	171.37	171.27	171.27	171.40	171.83	170.84	170.83	168.65
75	283.43	283.43	283.38	283.29	286.15	283.58	282.70	280.60	283.63
76	304.20	304.20	303.83	303.74	299.05	302.48	302.57	301.78	302.69
77	208.36	208.13	205.47	204.96	205.21	206.72	204.34	203.08	203.88
78	126.44	126.53	126.92	128.13	128.06	126.42	126.63	126.40	125.89
79	831.87	832.73	831.79	830.89	830.15	837.95	837.73	835.02	838.61
80	187.37	187.37	187.38	187.39	187.31	186.67	188.64	187.93	196.38
81	103.42	103.42	103.42	103.25	103.26	103.00	103.17	103.29	103.68
82	175.64	176.47	176.15	178.03	177.74	173.50	174.15	175.32	172.99
83	92.84	92.84	92.67	92.75	93.35	94.30	92.72	92.95	93.16

Table A.10: Hindcast-based consumption - Monthly averages initiation

#	Day 0	Day 1	Day 2	Day 3	Day 4	Day 5	Day 6	Day 7	Day 8
84	451.55	451.55	451.52	451.63	452.23	455.72	454.13	455.28	448.29
85	166.54	166.53	166.53	166.52	166.52	167.23	166.95	167.66	167.28
86	133.24	132.84	130.06	131.98	129.94	129.24	129.62	129.33	129.84
87	261.13	261.13	261.92	259.84	259.68	257.41	259.02	259.00	256.99
88	336.66	336.66	336.03	329.78	330.59	330.49	330.24	329.16	332.24
89	380.24	380.27	341.95	342.71	340.30	339.89	340.14	340.19	338.51
90	197.00	196.93	196.95	195.97	195.74	196.17	195.98	196.05	196.24
91	299.03	299.03	299.59	299.25	297.29	295.32	294.18	292.23	287.55
92	341.79	341.79	340.41	341.53	339.72	339.73	338.92	339.20	337.24
93	124.13	124.21	124.13	124.06	123.93	123.55	124.23	124.26	122.34
94	214.51	214.51	213.17	211.31	211.36	208.58	208.88	208.43	208.40
95	319.23	319.24	319.25	319.28	313.73	316.39	312.84	312.92	312.88
96	62.57	62.56	62.55	62.86	62.80	62.81	62.59	62.86	63.31
97	206.62	206.62	206.57	207.03	208.17	207.21	202.34	202.10	202.55
98	250.79	250.79	250.79	250.78	251.27	250.98	245.46	245.02	248.20
99	220.75	220.84	220.73	220.63	220.55	220.20	220.74	220.73	221.61
100	282.93	283.58	282.50	282.15	281.73	281.37	281.93	281.38	280.11

A.8. Rerun-Based Fuel Savings

Table A.11: Random Voyage Descriptions - Rerun Cases

#	Vessel	Initial Location	Target Location	Initial Time	Final Time
1	Delphis Riga	5^o48.78'N 76^o0.18'E	25^o8.84'S 37^o3.71'E	04-Dec-2017 20:40	17-Dec-2017 21:01
2	Robin Hunter	8^o12.62'N 158^o59.67'W	15^o54.84'S 116^o45.79'W	15-Nov-2017 01:14	27-Nov-2017 18:04
3	CMB Mae	21^o56.65'S 140^o48.95'W	1^o48.4'S 128^o0.87'E	05-Dec-2017 02:54	27-Dec-2017 17:35
4	Delphis Finland	1^o25.58'N 125^o38.94'W	28^o21.8'S 157^o43.18'W	19-Nov-2017 16:05	30-Nov-2017 10:26
5	Mineral New York	1^o3.91'N 112^o29.38'W	25^o34.51'N 153^o36.62'W	15-Dec-2017 00:37	26-Dec-2017 23:17
6	CMB Yasmine	12^o0.71'S 149^o48.62'W	18^o1.85'N 108^o3.96'W	21-Dec-2017 01:19	02-Jan-2018 09:22
7	Maersk Nijmegen	8^o37.36'S 109^o18.63'E	2^o1.44'N 58^o1.01'E	08-Dec-2017 02:10	22-Dec-2017 02:10
8	Bochem Singapura	6^o9.82'N 114^o15.89'E	4^o21.57'S 170^o19.12'E	08-Dec-2017 09:07	23-Dec-2017 11:52
9	Barcelona Express	2^o51.25'S 169^o31.34'E	27^o0.64'S 149^o30.42'W	18-Dec-2017 02:13	29-Dec-2017 07:06
10	CMB Edouard	22^o54.77'N 168^o5.92'W	6^o56.01'N 118^o21.53'W	09-Dec-2017 19:14	21-Dec-2017 21:52
11	Delphis Bothnia	26^o56.23'S 33^o15.86'W	28^o51.66'N 56^o34'W	13-Nov-2017 19:42	28-Nov-2017 03:40

Table A.11: Random Voyage Descriptions - Rerun Cases

#	Vessel	Initial Location	Target Location	Initial Time	Final Time
12	Mineral Faith	22^o10.97'S 89^o41.01'E	5^o15.22'N 143^o1.46'E	18-Dec-2017 01:45	31-Dec-2017 19:07
13	Maersk Nijmegen	9^o57.89'N 173^o56.73'E	19^o44.29'S 76^o31.9'W	04-Dec-2017 09:58	01-Jan-2018 12:33
14	CMB Boris	28^o51.06'S 76^o22.98'W	5^o3.27'N 11^o7.11'W	05-Dec-2017 04:49	30-Dec-2017 06:52
15	CMB Pomerol	16^o24.05'N 111^o38.4'E	40^o12'N 145^o33.77'W	07-Dec-2017 15:56	28-Dec-2017 00:11
16	Delphis Gdansk	32^o9.37'S 65^o1.35'E	23^o28.91'S 25^o19.2'W	01-Dec-2017 04:55	22-Dec-2017 02:44
17	Mineral Yarden	23^o39.89'N 91^o57'W	60^o27.47'N 14^o46.92'W	14-Nov-2017 19:40	01-Dec-2017 13:07
18	Mongoose Hunter	25^o42.82'S 55^o3.55'E	41^o3.85'N 166^o26.48'W	14-Nov-2017 20:31	16-Dec-2017 15:11
19	Santa Regula	3^o14.12'N 60^o6'E	47^o32.44'N 166^o28.63'E	20-Nov-2017 23:47	19-Dec-2017 07:13
20	Maersk Nimes	17^o54.44'N 143^o6.75'E	2^o7.86'S 91^o24.35'W	24-Nov-2017 16:23	22-Dec-2017 12:22
21	Mineral Stonehenge	16^o8.89'N 52^o24.62'W	27^o10.24'S 60^o14.59'E	27-Nov-2017 16:08	29-Dec-2017 05:53
22	Santa Regula	14^o35.02'S 79^o2.41'E	8^o0.68'S 23^o36.04'W	26-Nov-2017 09:22	23-Dec-2017 09:19
23	Mineral Honshu	32^o27.82'N 119^o2.59'W	40^o22.53'S 87^o16.65'W	28-Nov-2017 04:03	16-Dec-2017 20:27
24	CMB Giulia	30^o56.81'S 9^o37.96'E	6^o1.34'S 128^o45.69'W	17-Nov-2017 07:33	23-Dec-2017 03:58
25	Mineral Stonehenge	1^o46.61'N 120^o30.64'W	45^o51.83'N 154^o6.1'E	13-Dec-2017 15:58	01-Jan-2018 07:59
26	Mineral Energy	16^o49.39'S 99^o59.84'W	10^o20.39'N 168^o21.97'E	29-Nov-2017 06:23	23-Dec-2017 05:37
27	CMB Kristine	27^o23.24'N 172^o15.72'E	31^o9.3'S 132^o35.1'W	17-Nov-2017 08:29	09-Dec-2017 20:18
28	Mineral Yarden	6^o40.18'S 0^o6.27'E	1^o37.27'N 60^o15.59'E	26-Nov-2017 11:38	17-Dec-2017 14:33
29	Hermes Arrow	36^o41.46'S 91^o39.64'E	45^o7.37'N 148^o31.93'E	29-Nov-2017 12:47	26-Dec-2017 20:32
30	CMB Pomerol	14^o39.2'S 23^o8.19'W	23^o15.38'S 116^o13.28'W	08-Dec-2017 22:57	31-Dec-2017 13:53
31	Barcelona Express	15^o53.92'S 161^o39.92'E	15^o18.42'N 113^o48.29'W	06-Dec-2017 17:57	30-Dec-2017 14:11
32	Mineral Edo	8^o36.41'S 2^o16.46'W	5^o1.48'N 86^o51.25'E	03-Dec-2017 15:05	01-Jan-2018 04:02
33	Mineral New York	3^o10.54'S 162^o35'W	11^o2.35'N 111^o24.62'E	08-Dec-2017 12:03	29-Dec-2017 02:33
34	Mineral Stonehenge	6^o5.56'N 157^o16.93'W	11^o1.14'N 160^o31.69'E	13-Nov-2017 01:09	24-Nov-2017 06:44
35	Barcelona Express	28^o56.2'S 147^o37.86'W	14^o52.69'N 124^o12.96'W	16-Dec-2017 21:33	30-Dec-2017 06:23
36	Harmonious	3^o51.49'S 171^o4.25'W	28^o16.78'S 109^o7.59'W	03-Dec-2017 18:28	19-Dec-2017 11:59
37	Cuckoo Hunter	22^o35.22'S 173^o2.17'E	18^o47.33'S 141^o31.44'W	23-Dec-2017 04:27	02-Jan-2018 09:44
38	Grouse Hunter	7^o36.52'N 127^o12.05'W	23^o29.07'N 173^o38.06'E	07-Dec-2017 18:27	23-Dec-2017 17:13
39	Bochem Ghent	28^o5.91'S 39^o15.03'E	13^o2.23'S 95^o9.4'E	17-Nov-2017 15:51	30-Nov-2017 12:10
40	MINERAL SHIKOKU	24^o48.97'N 160^o37.78'W	7^o30.85'S 131^o44.26'W	30-Nov-2017 21:48	11-Dec-2017 06:19
41	CMB Edouard	23^o45.96'N 156^o26.43'E	10^o53.21'S 51^o34.28'E	02-Dec-2017 17:13	30-Dec-2017 19:28
42	Robin Hunter	6^o29.7'S 127^o38.56'W	3^o52.28'S 163^o29.69'E	13-Nov-2017 18:29	30-Nov-2017 01:31
43	Harmonious	29^o49.88'S 52^o5.59'E	8^o44.63'N 37^o29.09'W	05-Dec-2017 15:36	28-Dec-2017 23:40
44	Maersk Nijmegen	6^o36.3'S 66^o27.28'E	20^o24.57'S 19^o2.49'W	07-Dec-2017 23:02	31-Dec-2017 00:56
45	CMB Coralie	15^o35.65'N 119^o8.44'E	24^o10.59'S 93^o12.48'E	18-Nov-2017 20:17	01-Dec-2017 02:04

Table A.11: Random Voyage Descriptions - Rerun Cases

#	Vessel	Initial Location	Target Location	Initial Time	Final Time
46	Mineral Kyoto	20^o55.82'N 149^o31.54'W	15^o42.99'N 118^o11.2'E	07-Dec-2017 22:49	29-Dec-2017 19:14
47	Maersk Niteroi	17^o46.6'N 147^o28.48'W	0^o19.12'S 169^o5.16'E	20-Dec-2017 12:45	01-Jan-2018 07:14
48	Barcelona Express	22^o27.92'N 130^o34.09'W	18^o3.79'S 145^o11.31'W	04-Dec-2017 07:07	14-Dec-2017 11:03
49	MINERAL HOKKAIDO	35^o52.26'N 19^o18.77'E	44^o55.99'N 59^o44.76'W	05-Dec-2017 12:12	23-Dec-2017 03:56
50	Maersk Nijmegen	20^o11.97'S 60^o48.17'E	23^o18.06'S 38^o41.03'W	06-Dec-2017 10:46	26-Dec-2017 22:47
51	Mineral Stonehenge	36^o9.67'S 167^o44.83'E	42^o55.72'N 150^o24.69'E	03-Dec-2017 04:49	22-Dec-2017 00:02
52	Santa Regula	39^o13.54'S 150^o39.22'W	22^o57.64'N 53^o5.19'W	29-Nov-2017 21:26	31-Dec-2017 22:50
53	CMB Boris	34^o51.37'N 132^o43.84'W	11^o24.85'S 151^o35.83'E	21-Nov-2017 19:43	10-Dec-2017 17:59
54	Maersk Nienburg	10^o37.06'N 121^o51.12'E	45^o44.89'S 131^o45.67'E	10-Dec-2017 23:03	28-Dec-2017 03:08

Table A.12: Hindcast-based consumption - fuel consumption in tons

#	No WRO	WRO - Shortest Path	WRO - Monthly Averages
1	104.31	93.75	92.97
2	148.60	147.76	140.25
3	234.66	230.73	231.37
4	64.58	61.10	60.78
5	291.73	283.72	285.17
6	179.82	173.34	173.33
7	116.86	95.30	95.07
8	89.30	93.08	92.97
9	137.14	135.77	135.77
10	180.79	178.59	169.36
11	132.17	130.19	129.67
12	410.75	398.59	398.99
13	284.71	288.32	253.43
14	370.87	361.90	357.00
15	419.05	411.70	411.33
16	148.06	119.62	121.72
17	344.60	316.44	314.22
18	596.65	580.44	585.01
19	496.35	429.51	428.26
20	417.99	377.24	377.90
21	822.81	786.76	773.20
22	274.64	251.03	251.08
23	522.76	511.43	510.53
24	444.11	398.12	402.32
25	863.40	826.09	820.22
26	539.67	529.74	525.99
27	211.09	206.23	207.26
28	508.55	489.97	489.60
29	172.71	156.98	161.86
30	593.08	588.38	583.06
31	255.70	242.78	241.92
32	622.84	621.88	623.95
33	590.98	606.69	599.78
34	241.91	243.10	238.70
35	128.70	132.17	132.80
36	429.14	431.03	431.79
37	100.76	100.92	100.39
38	133.01	133.27	135.99
39	183.21	180.13	180.17
40	331.32	338.84	335.31
41	352.17	349.30	355.98
42	171.83	170.44	167.63
43	627.28	636.93	633.69
44	176.06	181.21	177.64
45	189.70	186.85	187.05
46	619.36	634.67	577.80
47	79.30	81.75	82.97
48	143.76	145.38	144.28
49	593.07	582.21	606.73
50	249.35	246.16	245.18
51	610.81	615.06	611.55
52	588.02	588.69	585.23
53	292.19	292.92	295.27

Table A.12: Hindcast-based consumption - fuel consumption in tons

#	No WRO	WRO - Shortest Path	WRO - Monthly Averages
54	123.69	125.85	126.36

Table A.13: Hindcast-based consumption - Voyage distance in nm

#	No WRO	WRO - Shortest Path	WRO - Monthly Averages
1	2989.88	3067.30	3115.34
2	2902.19	2915.26	2942.88
3	5525.21	5624.26	5618.74
4	2572.92	2602.65	2603.13
5	2798.88	2869.53	2865.72
6	3063.93	3112.30	3111.94
7	3141.18	3222.69	3227.52
8	3449.33	3593.22	3591.69
9	2765.18	2801.38	2803.21
10	3029.13	3058.56	3117.83
11	3708.08	3782.76	3776.06
12	3566.48	3650.25	3649.67
13	6708.73	6980.91	6869.84
14	6380.08	6467.65	6471.38
15	5348.32	5472.11	5469.92
16	4692.71	4776.03	4776.02
17	4059.55	4089.30	4089.20
18	8856.79	8917.53	8978.46
19	7820.90	7800.03	7764.13
20	7470.04	7603.64	7615.23
21	7248.00	7406.57	7468.33
22	6288.35	6370.37	6369.25
23	4719.69	4760.13	4755.35
24	7640.43	8018.67	8126.91
25	5140.40	5242.21	5178.58
26	5682.21	5793.42	5733.89
27	4729.37	4771.07	4784.09
28	5240.88	5300.23	5301.30
29	5872.00	6002.92	6050.91
30	6123.75	6263.32	6205.08
31	5353.25	5456.26	5468.31
32	6484.21	6503.84	6507.74
33	5259.07	5288.95	5276.53
34	2524.06	2534.81	2545.52
35	2965.49	2977.05	2979.31
36	3821.30	3831.33	3833.57
37	2556.99	2561.59	2563.94
38	3532.19	3550.88	3550.65
39	3246.97	3260.74	3261.85
40	2577.12	2590.92	2588.45
41	6931.18	6943.80	6958.23
42	4123.83	4140.14	4153.65
43	5836.87	5844.59	5842.16
44	5337.20	5364.34	5360.10
45	3152.42	3122.27	3128.56
46	5241.37	5269.38	5303.77
47	2788.39	2795.42	2799.69
48	2584.13	2595.61	2596.42

Table A.13: Hindcast-based consumption - Voyage distance in nm

#	No WRO	WRO - Shortest Path	WRO - Monthly Averages
49	3706.48	3719.32	3699.97
50	5445.50	5442.24	5451.65
51	4848.39	4843.48	4859.04
52	8748.37	8757.00	8749.18
53	5117.44	5124.45	5149.65
54	3820.53	3810.93	3813.19

Table A.14: Hindcast-based consumption - Mean countercurrent encountered

#	No WRO	WRO - Shortest Path	WRO - Monthly Averages
1	0.21	-0.19	-0.36
2	0.51	0.49	0.24
3	0.10	-0.12	-0.10
4	-0.60	-0.68	-0.70
5	-0.47	-0.69	-0.66
6	0.31	0.04	0.04
7	0.65	-0.25	-0.28
8	-0.56	-0.79	-0.79
9	-0.15	-0.29	-0.30
10	0.24	0.09	-0.24
11	-0.05	-0.28	-0.29
12	-0.03	-0.39	-0.39
13	0.47	0.00	0.02
14	-0.04	-0.17	-0.19
15	-0.49	-0.63	-0.66
16	0.11	-0.41	-0.38
17	-0.13	-0.32	-0.43
18	-0.07	-0.30	-0.30
19	-0.35	-0.69	-0.67
20	0.39	-0.04	-0.05
21	0.25	-0.06	-0.25
22	-0.24	-0.59	-0.59
23	0.13	-0.04	-0.04
24	0.30	0.07	0.11
25	-0.06	-0.31	-0.29
26	-0.53	-0.78	-0.68
27	0.18	0.07	0.05
28	0.18	-0.05	-0.06
29	-0.13	-0.50	-0.46
30	0.08	-0.01	-0.00
31	0.20	-0.10	-0.12
32	0.36	0.32	0.32
33	-0.22	-0.18	-0.21
34	-0.13	-0.12	-0.23
35	0.06	0.13	0.12
36	0.06	0.02	0.03
37	-0.04	-0.13	-0.15
38	-0.25	-0.31	-0.24
39	0.34	0.23	0.23
40	0.22	0.27	0.26
41	-0.10	-0.14	-0.10
42	-0.50	-0.57	-0.64
43	-0.37	-0.36	-0.37

Table A.14: Hindcast-based consumption - Mean countercurrent encountered

#	No WRO	WRO - Shortest Path	WRO - Monthly Averages
44	-0.22	-0.18	-0.24
45	-0.27	-0.23	-0.25
46	0.00	0.02	-0.27
47	-0.45	-0.39	-0.35
48	0.02	0.03	0.00
49	0.37	0.29	0.33
50	-0.06	-0.09	-0.11
51	-0.08	-0.08	-0.10
52	-0.22	-0.22	-0.24
53	-0.19	-0.19	-0.16
54	-0.05	0.04	0.05

Table A.15: Hindcast-based consumption - Mean wind in m/s

#	No WRO	WRO - Shortest Path	WRO - Monthly Averages
1	5.03	5.00	5.01
2	7.38	7.36	7.23
3	4.29	4.25	4.19
4	7.14	7.12	7.10
5	6.68	6.31	6.29
6	5.60	5.74	5.74
7	2.92	4.35	4.19
8	6.27	6.49	6.49
9	4.86	4.87	5.02
10	6.37	6.41	4.95
11	5.87	5.91	5.96
12	5.39	4.98	4.98
13	6.95	6.81	6.04
14	8.34	8.20	8.24
15	10.88	10.88	10.80
16	6.39	7.24	6.99
17	9.08	9.32	8.97
18	6.67	6.62	6.79
19	6.78	7.21	7.20
20	7.96	6.89	6.98
21	7.23	6.90	6.30
22	7.32	7.52	7.54
23	5.69	5.65	5.64
24	9.39	7.54	8.62
25	8.86	8.87	8.61
26	7.61	7.86	7.50
27	7.28	7.11	7.21
28	6.08	6.12	6.10
29	8.39	8.33	8.04
30	9.75	8.97	9.01
31	5.03	4.66	4.60
32	7.43	7.59	7.32
33	5.37	5.29	5.16
34	5.52	5.64	5.82
35	5.02	4.96	4.93
36	5.90	5.73	5.88
37	6.33	6.18	6.35
38	6.26	6.53	6.53

Table A.15: Hindcast-based consumption - Mean wind in m/s

#	No WRO	WRO - Shortest Path	WRO - Monthly Averages
39	7.47	7.09	7.09
40	6.70	6.43	6.60
41	5.74	5.58	5.62
42	6.02	6.13	6.27
43	7.52	7.45	7.46
44	5.70	5.84	5.93
45	5.33	5.27	5.27
46	7.00	6.99	7.03
47	6.43	6.29	6.37
48	5.05	4.94	5.06
49	8.93	9.07	9.15
50	6.41	6.29	6.32
51	6.16	6.24	6.20
52	10.96	10.89	10.87
53	7.83	7.73	7.83
54	6.98	6.94	6.79

Table A.16: Hindcast-based consumption - Mean significant waveheight in m

#	No WRO	WRO - Shortest Path	WRO - Monthly Averages
1	1.70	1.58	1.58
2	2.01	1.98	1.97
3	1.47	1.37	1.38
4	2.13	1.92	1.93
5	2.43	2.26	2.26
6	1.56	1.56	1.56
7	1.44	1.48	1.47
8	1.86	1.56	1.56
9	1.87	1.74	1.75
10	2.57	2.68	2.40
11	2.06	1.83	1.83
12	1.62	1.43	1.43
13	2.09	2.14	1.75
14	2.76	2.43	2.40
15	3.45	3.59	3.57
16	2.26	2.17	2.17
17	2.46	2.17	2.11
18	2.25	2.28	2.30
19	2.40	2.08	2.11
20	2.79	2.60	2.63
21	2.20	2.16	2.16
22	2.30	2.14	2.14
23	2.49	2.28	2.28
24	3.72	2.81	2.75
25	3.70	3.25	3.22
26	2.50	2.38	2.30
27	2.37	2.26	2.27
28	1.84	1.75	1.75
29	2.31	2.16	2.11
30	3.22	2.84	2.83
31	1.69	1.64	1.63
32	2.31	2.29	2.27
33	1.58	1.55	1.55

Table A.16: Hindcast-based consumption - Mean significant waveheight in m

#	No WRO	WRO - Shortest Path	WRO - Monthly Averages
34	1.77	1.78	1.82
35	1.77	1.59	1.59
36	2.09	1.89	1.90
37	1.93	1.86	1.90
38	2.79	2.61	2.56
39	2.41	2.35	2.35
40	2.51	2.36	2.37
41	1.78	1.68	1.69
42	1.78	1.67	1.69
43	2.31	2.12	2.12
44	2.07	2.06	2.06
45	1.24	1.17	1.18
46	2.69	2.58	2.53
47	2.06	1.90	1.88
48	2.00	1.88	1.88
49	3.41	3.20	3.20
50	2.19	2.09	2.08
51	2.03	1.93	1.93
52	4.01	3.75	3.74
53	2.53	2.46	2.49
54	1.82	1.77	1.71

Table A.17: Hindcast-based maximum wind velocities encountered

#	No WRO	WRO - Shortest Path	WRO - Monthly Averages
1	10.78	11.13	10.59
2	9.48	9.53	9.52
3	8.20	8.34	8.46
4	8.61	8.76	8.49
5	10.96	9.20	9.19
6	7.85	8.67	8.67
7	6.47	7.59	7.57
8	13.33	10.90	10.90
9	8.65	9.81	9.81
10	10.32	13.61	10.45
11	8.90	9.20	9.04
12	8.56	8.68	8.68
13	12.02	12.22	10.97
14	17.08	17.73	20.85
15	17.55	17.77	17.76
16	14.68	14.30	12.34
17	16.60	14.28	16.77
18	15.76	15.01	16.97
19	15.86	15.96	16.09
20	12.84	12.51	12.62
21	12.49	10.47	10.81
22	13.67	15.22	15.25
23	8.77	9.05	8.83
24	16.39	15.90	17.53
25	17.60	17.64	18.00
26	10.73	10.49	10.48
27	10.48	10.60	10.29
28	9.98	9.97	9.43

Table A.17: Hindcast-based maximum wind velocities encountered

#	No WRO	WRO - Shortest Path	WRO - Monthly Averages
29	22.24	22.31	20.61
30	15.83	15.98	15.57
31	8.33	8.58	9.31
32	16.32	16.25	16.08
33	10.27	10.27	10.27
34	8.88	8.68	9.66
35	8.46	8.42	8.42
36	9.04	9.02	9.03
37	12.73	12.74	13.06
38	11.24	11.72	11.39
39	9.64	9.63	9.63
40	10.25	10.09	10.19
41	10.53	10.52	10.52
42	7.74	7.91	7.98
43	13.32	12.96	13.05
44	9.03	10.28	10.20
45	10.32	10.50	10.61
46	11.66	11.90	12.14
47	8.73	8.83	8.64
48	10.89	10.88	10.89
49	16.98	12.80	14.16
50	15.64	12.79	12.68
51	11.52	10.51	11.00
52	24.60	23.77	23.77
53	12.55	12.57	12.66
54	12.57	12.56	12.30

Table A.18: Hindcast-based maximum significant waveheight encountered

#	No WRO	WRO - Shortest Path	WRO - Monthly Averages
1	3.17	3.47	3.42
2	2.33	2.34	2.34
3	2.22	2.22	2.23
4	2.77	2.79	2.84
5	3.11	3.08	3.08
6	1.93	2.01	2.01
7	1.75	1.89	1.91
8	3.59	2.67	2.67
9	2.07	2.16	2.15
10	4.12	4.28	4.03
11	3.39	3.30	3.30
12	2.55	2.60	2.60
13	3.63	3.71	3.18
14	6.19	5.40	7.07
15	5.62	6.04	6.02
16	4.16	3.16	3.17
17	4.96	3.95	4.32
18	5.05	5.09	5.01
19	5.55	5.52	5.63
20	3.56	4.25	4.50
21	3.34	3.22	3.59
22	3.59	3.47	3.48
23	3.61	3.68	3.68

Table A.18: Hindcast-based maximum significant waveheight encountered

#	No WRO	WRO - Shortest Path	WRO - Monthly Averages
24	5.90	5.15	5.92
25	7.03	6.75	6.66
26	2.91	2.98	2.93
27	3.13	3.08	3.15
28	2.90	2.99	3.04
29	7.28	6.47	5.42
30	5.43	5.08	4.94
31	2.33	2.21	2.27
32	4.35	4.62	4.53
33	2.46	2.46	2.46
34	2.53	2.54	2.58
35	2.37	2.37	2.37
36	2.74	2.74	2.74
37	3.23	3.28	3.46
38	3.96	3.91	3.48
39	3.67	3.67	3.67
40	3.49	3.50	3.50
41	3.02	3.01	3.02
42	1.95	1.95	1.95
43	3.54	3.71	3.71
44	3.59	3.69	3.70
45	2.36	2.39	2.39
46	5.77	6.40	4.95
47	2.52	2.52	2.51
48	2.73	2.72	2.72
49	5.52	5.37	5.10
50	4.34	3.94	3.99
51	3.30	3.01	2.98
52	10.98	11.28	11.28
53	4.46	4.42	4.44
54	4.31	4.30	4.28

A.9. Computer Specifications

Specifications of computer and MATLAB version used to execute all scripts. Increased/decreased performance might significantly speed-up or slow-down code execution. Note that running the code with less than 4 GB free RAM might result in parameters stored on disk, which should be avoided at all times.

- Model: Dell Latitude E5570
- Hard disk: SK hynix SC308 SATA (SSD)
- Processor: Intel(R) Core(TM) i5-6300U CPU @ 2.40GHz 2.50 GHz (3 MB cache)
- RAM: 8 GB DDR4
- Operating system: Windows 10 Pro version 1709 build 16299.64 (64-bit)
- MATLAB R2016b

B

User Interface

Screenshots of the user interface can be found in this appendix.

B.1. General Tab

B.1.1. Global Grid Executed

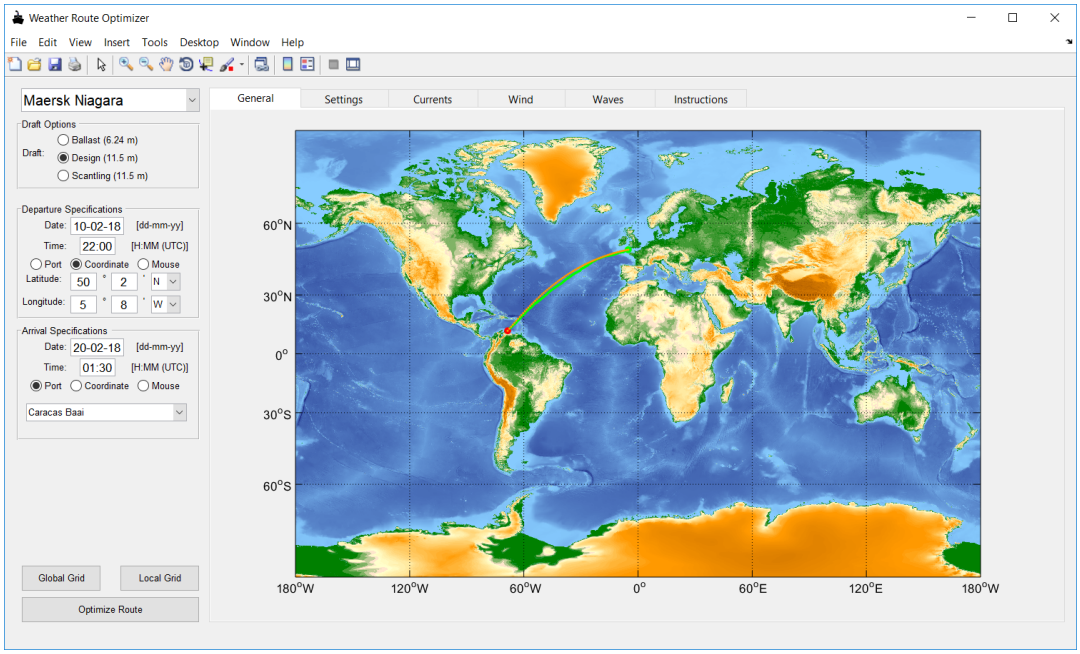

Figure B.1: General tab after executing the global grid callback

B.1.2. Local Grid Executed

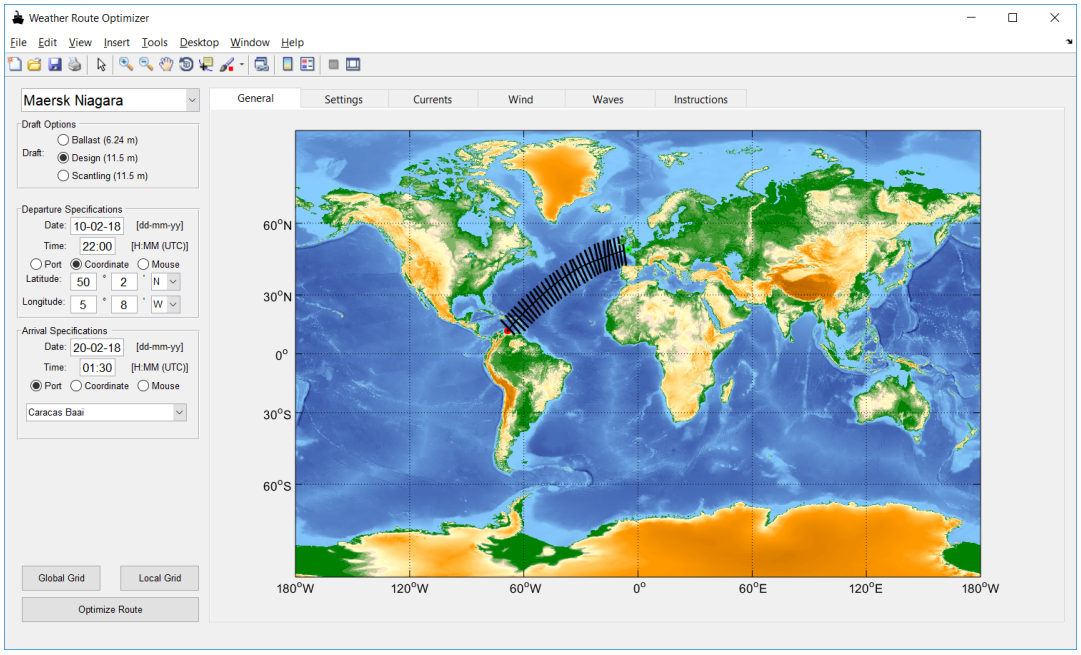

Figure B.2: General tab after executing the local grid callback

B.1.3. Optimization Executed

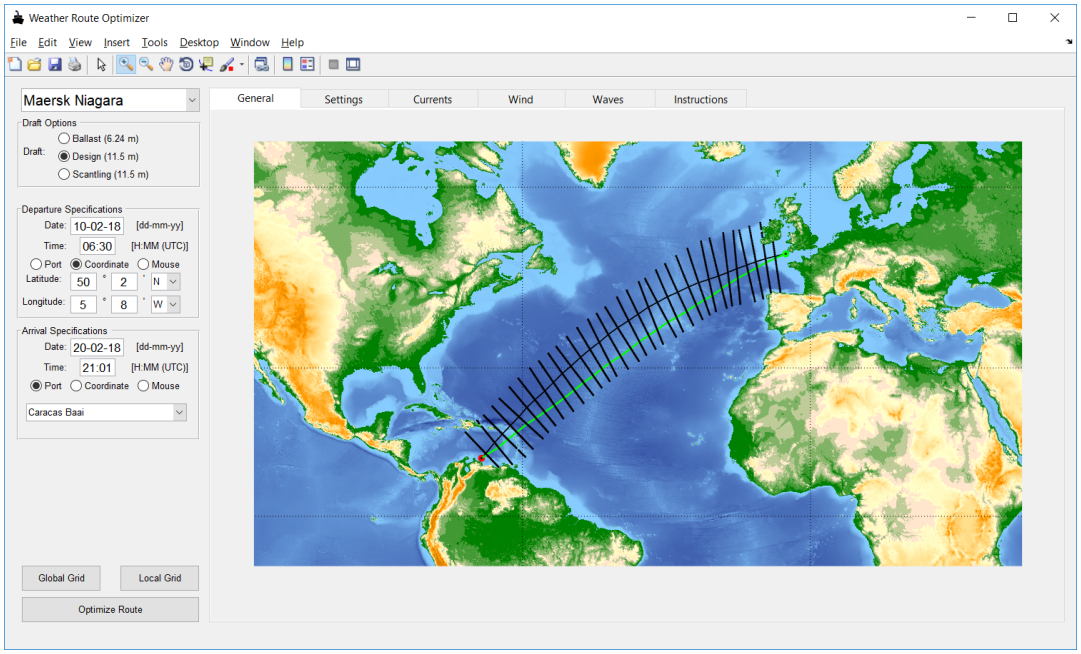

Figure B.3: General tab after executing the optimization callback

B.2. Settings Tab

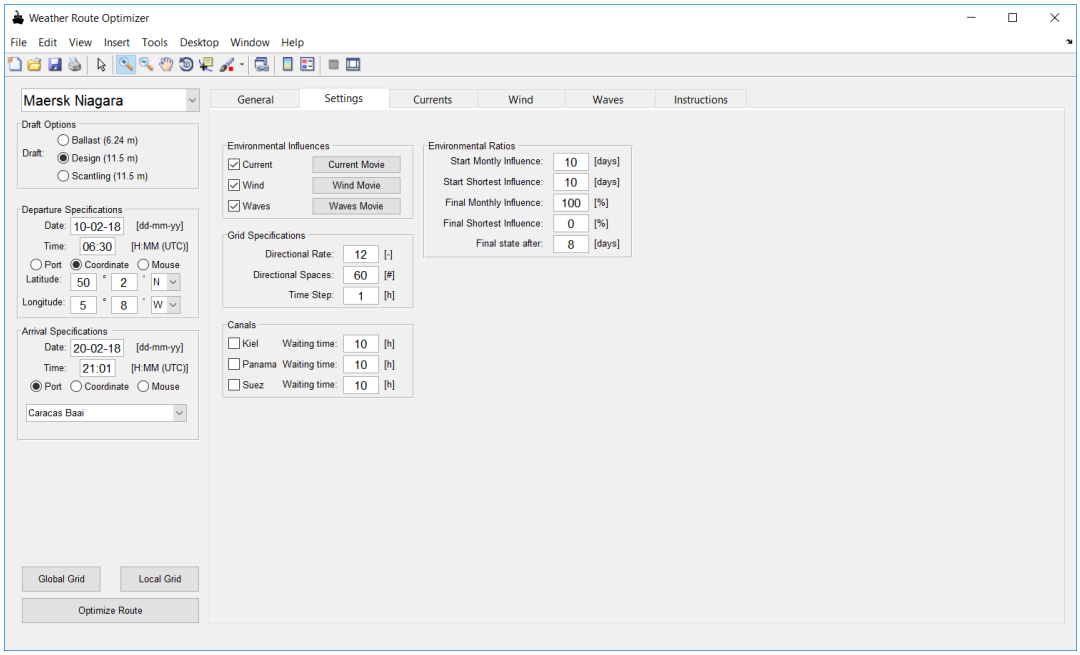

Figure B.4: Settings tab, containing the optimization options for the user

B.3. Current Tab

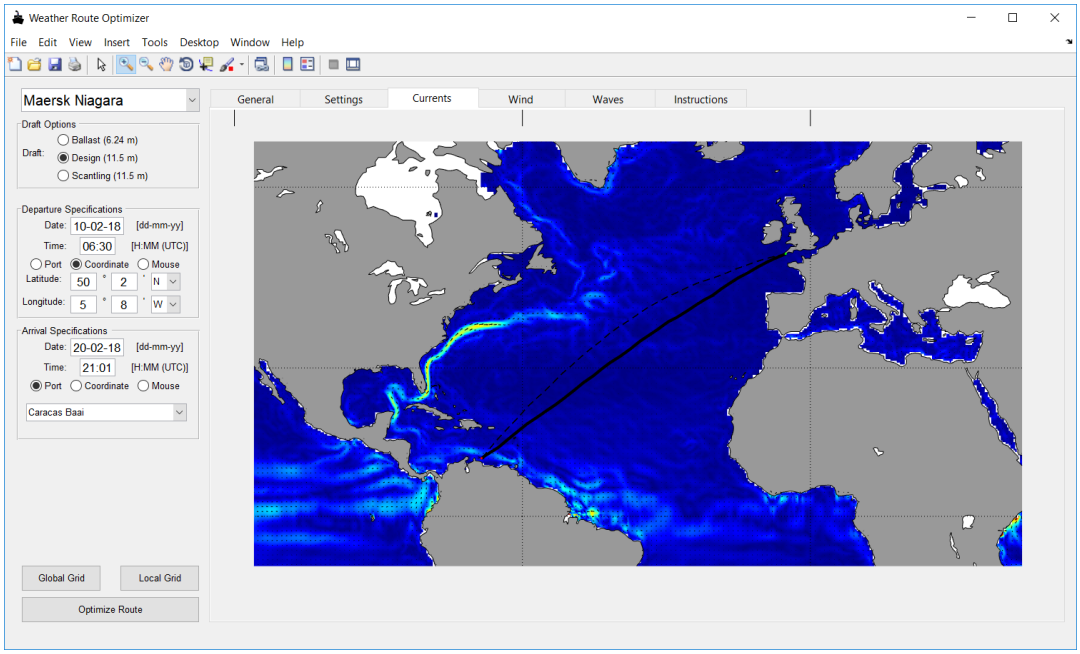

Figure B.5: Current tab, displaying the dominant month's average current

B.4. Wind Tab

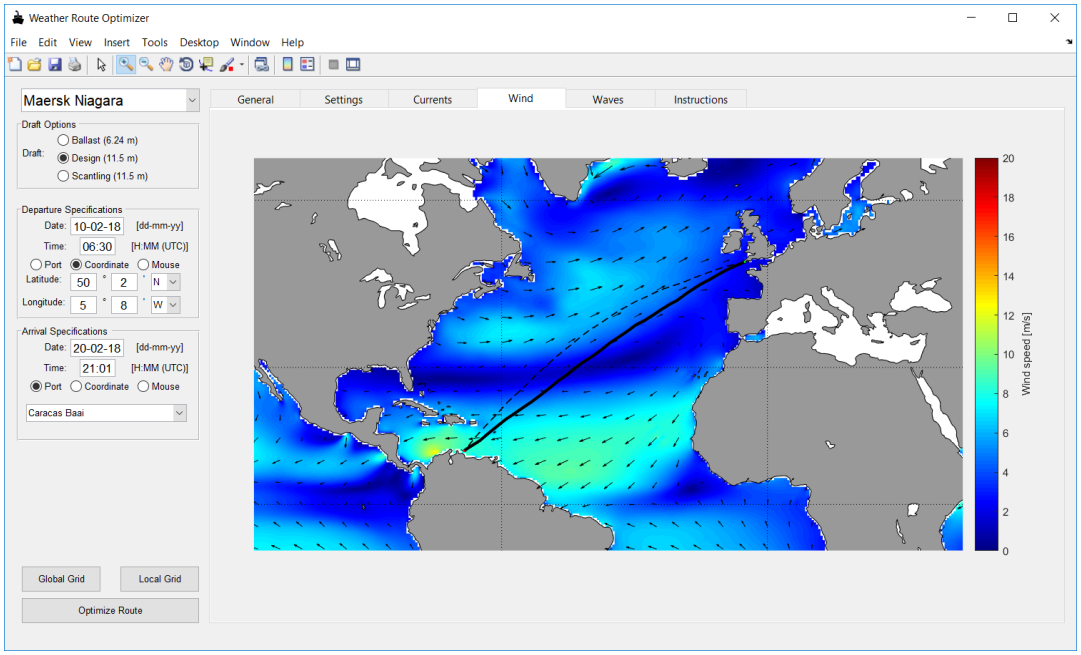

Figure B.6: Wind tab, displaying the dominant month's average wind

B.5. Waves Tab

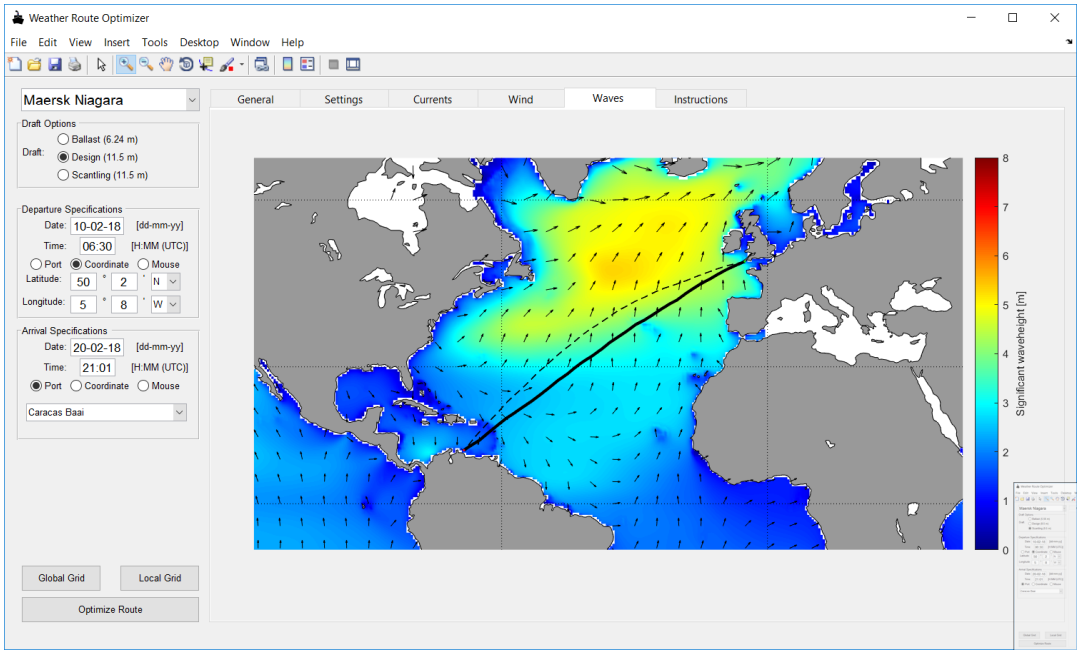

Figure B.7: Waves tab, displaying the dominant month's average waves

B.6. Instructions Tab

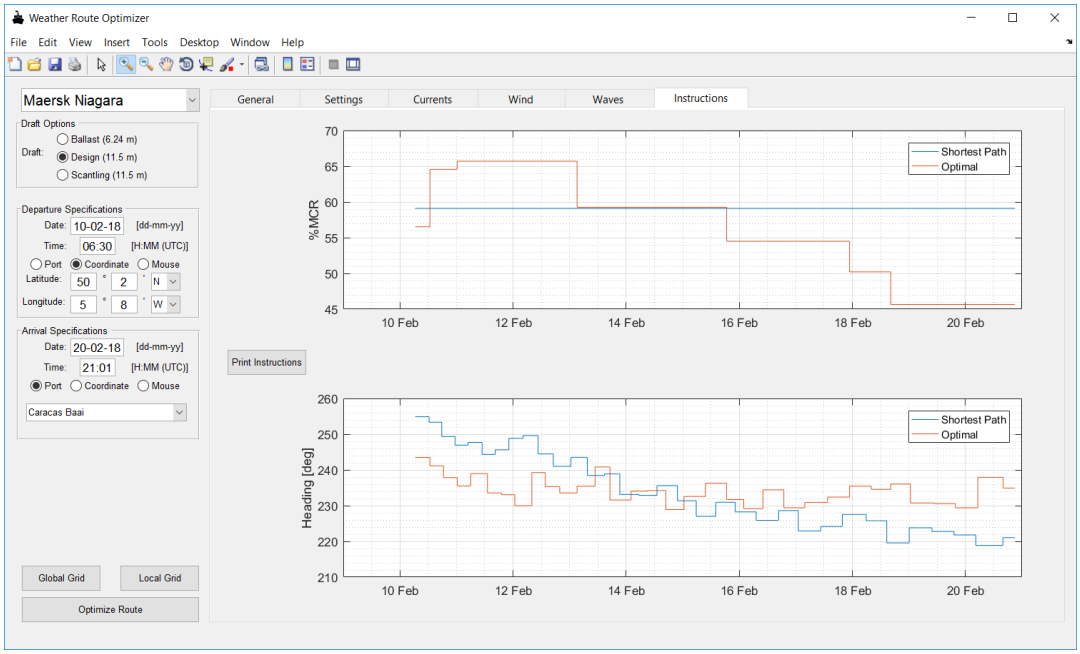

Figure B.8: Instructions tab, indicating engine setting and heading

C

Voyage Simulation

GIF extracts of the first days of the transatlantic route, discussed in section 10.2, can be found here.

C.1. Current Forecast

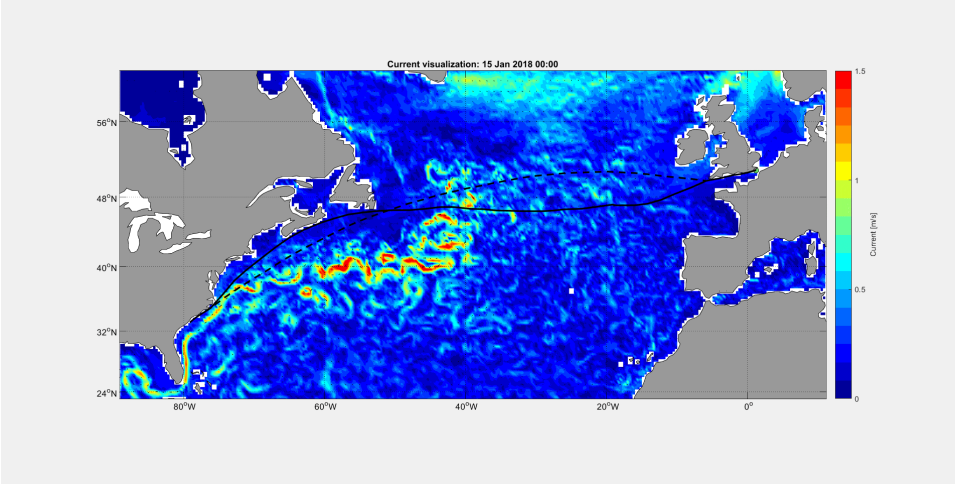

Figure C.1: Voyage simulation: 15-Jan-2018 00:00

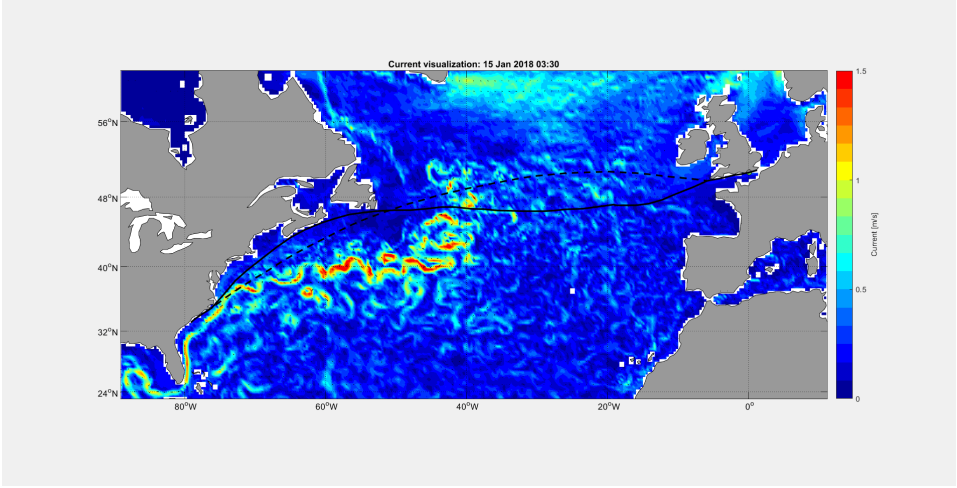

Figure C.2: Voyage simulation: 15-Jan-2018 03:30

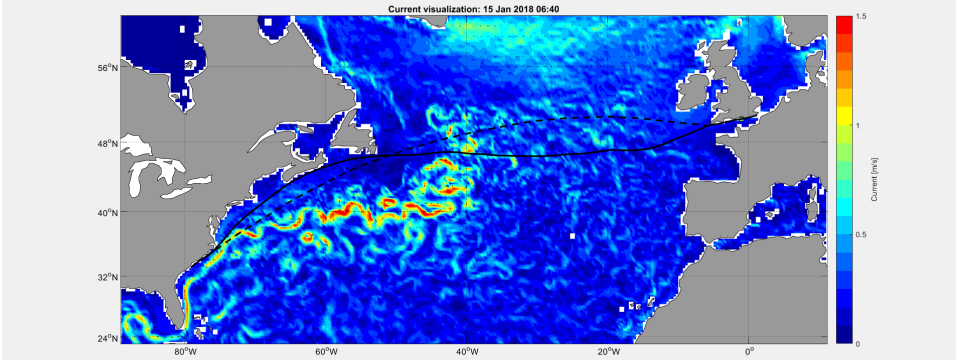

Figure C.3: Voyage simulation: 15-Jan-2018 06:40

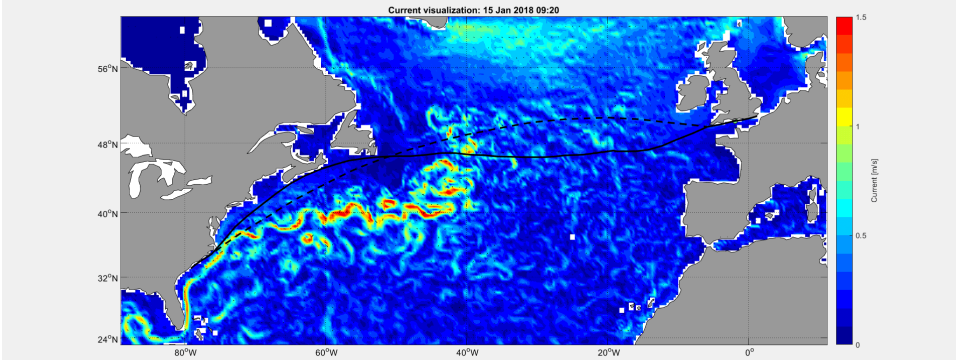

Figure C.4: Voyage simulation: 15-Jan-2018 09:20

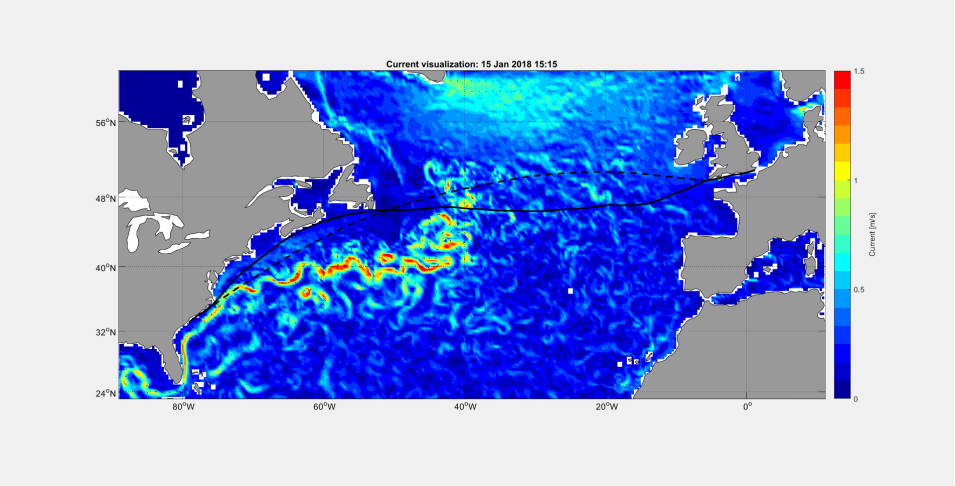

Figure C.5: Voyage simulation: 15-Jan-2018 15:15

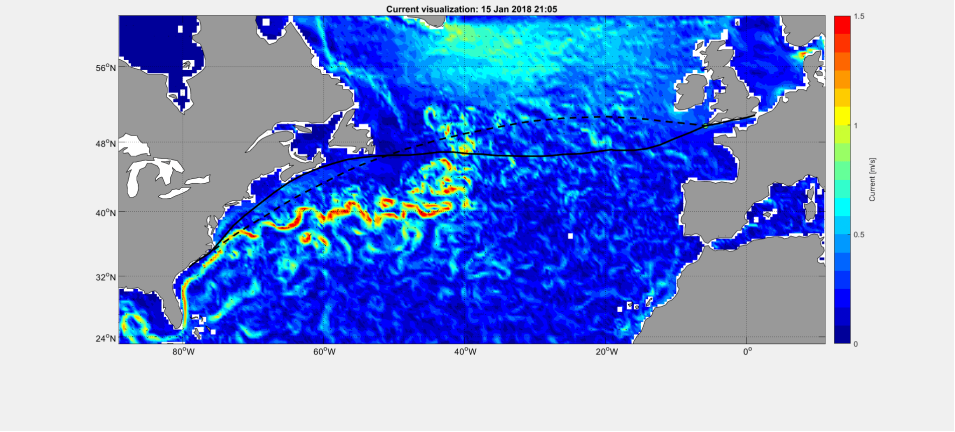

Figure C.6: Voyage simulation: 15-Jan-2018 21:05

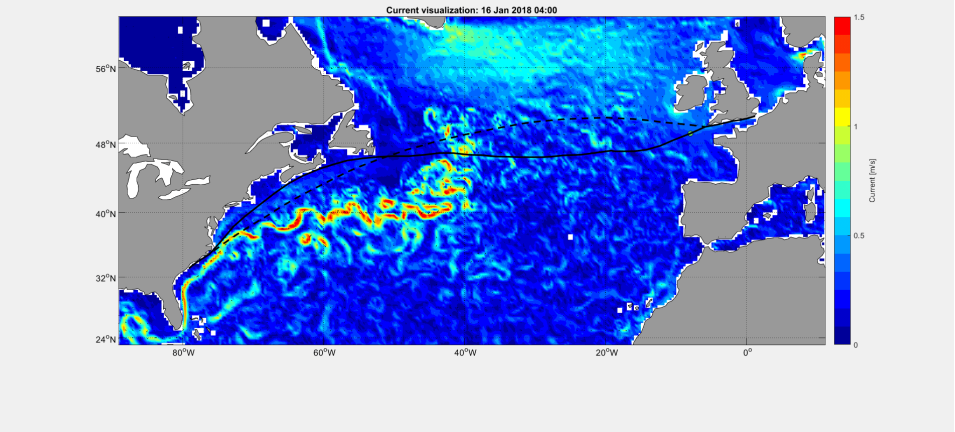

Figure C.7: Voyage simulation: 16-Jan-2018 04:00

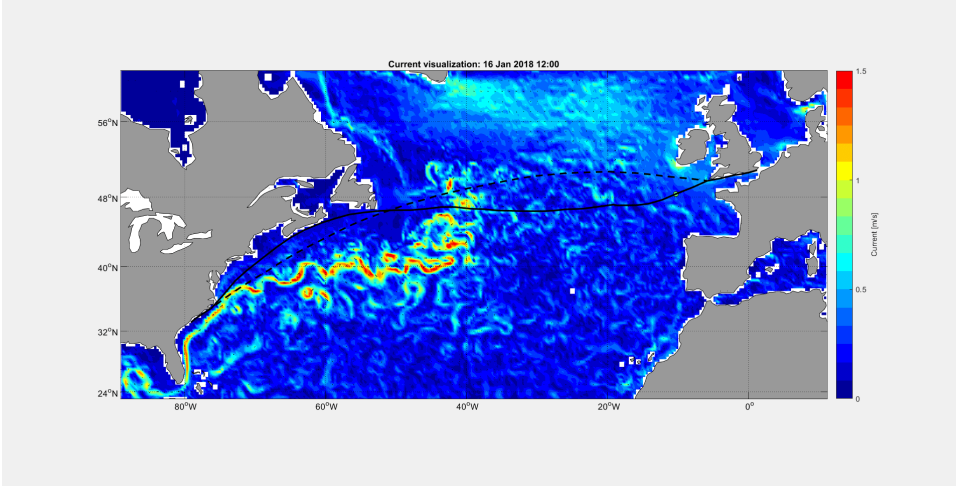

Figure C.8: Voyage simulation: 16-Jan-2018 12:00

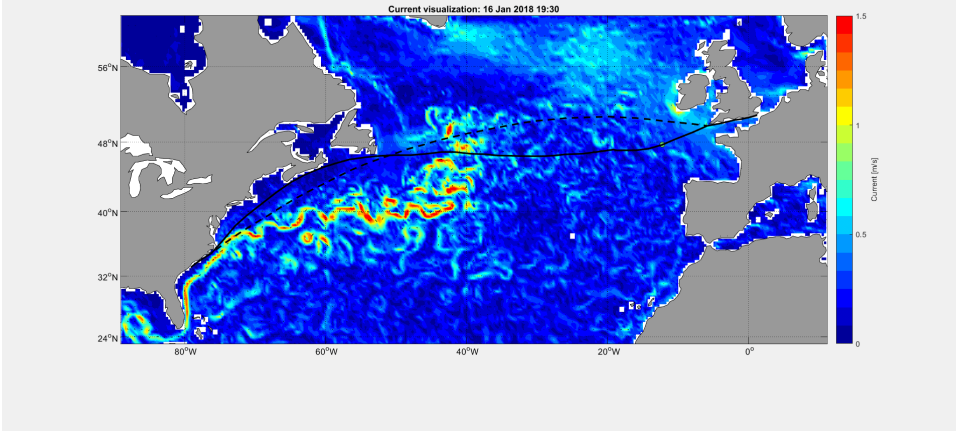

Figure C.9: Voyage simulation: 16-Jan-2018 19:30

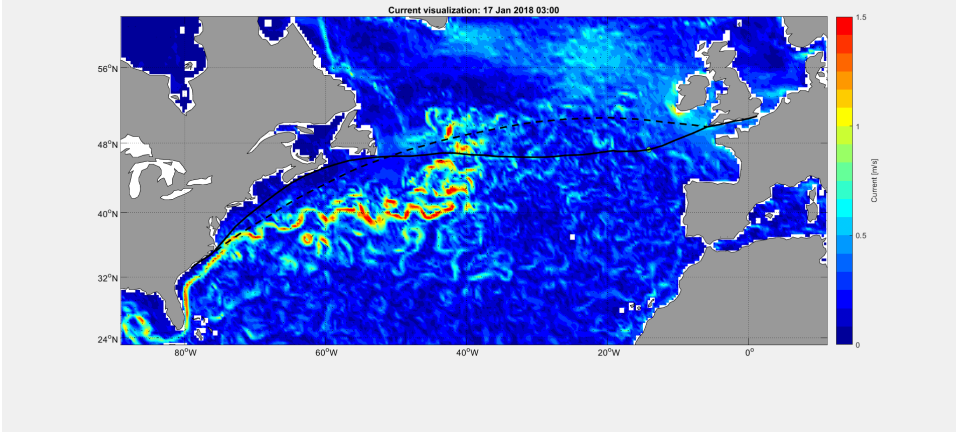

Figure C.10: Voyage simulation: 17-Jan-2018 03:00

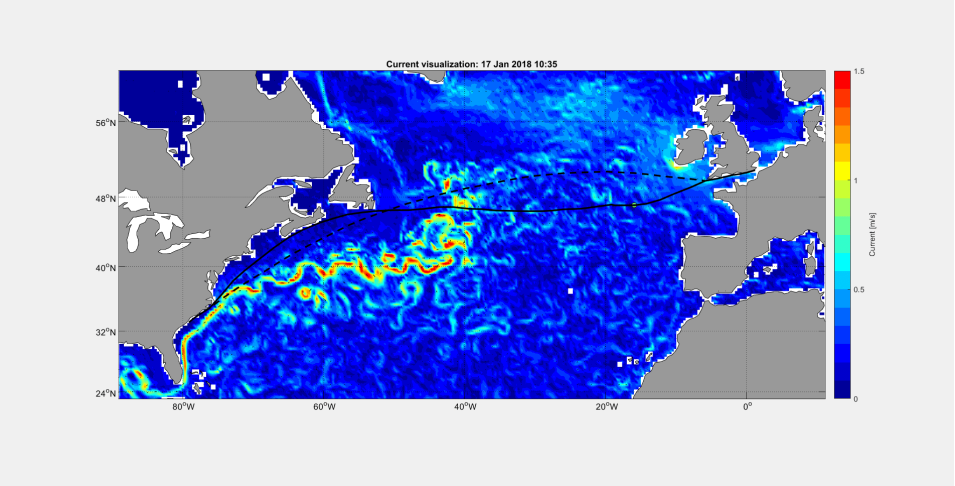

Figure C.11: Voyage simulation: 17-Jan-2018 10:35

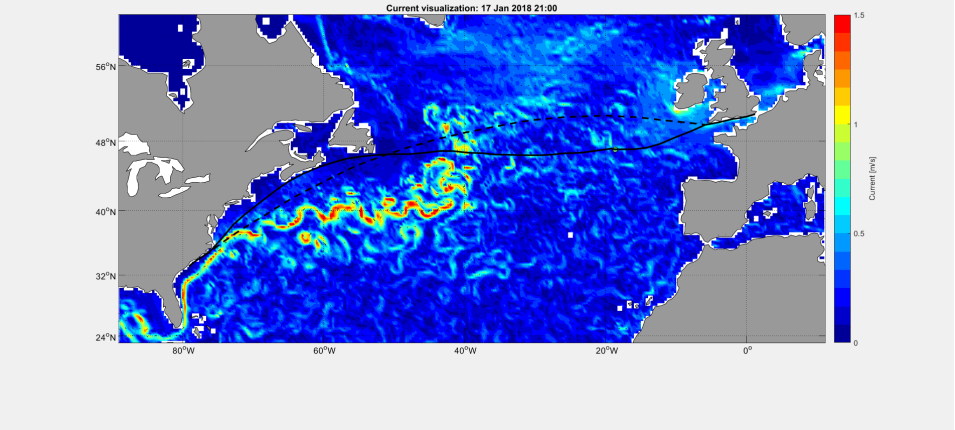

Figure C.12: Voyage simulation: 17-Jan-2018 21:00

C.2. Wind Forecast

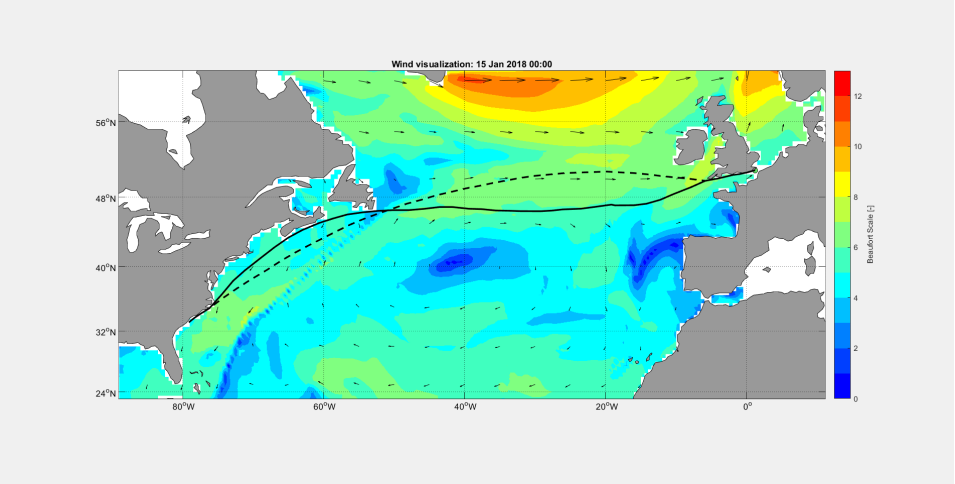

Figure C.13: Voyage simulation: 15-Jan-2018 00:00

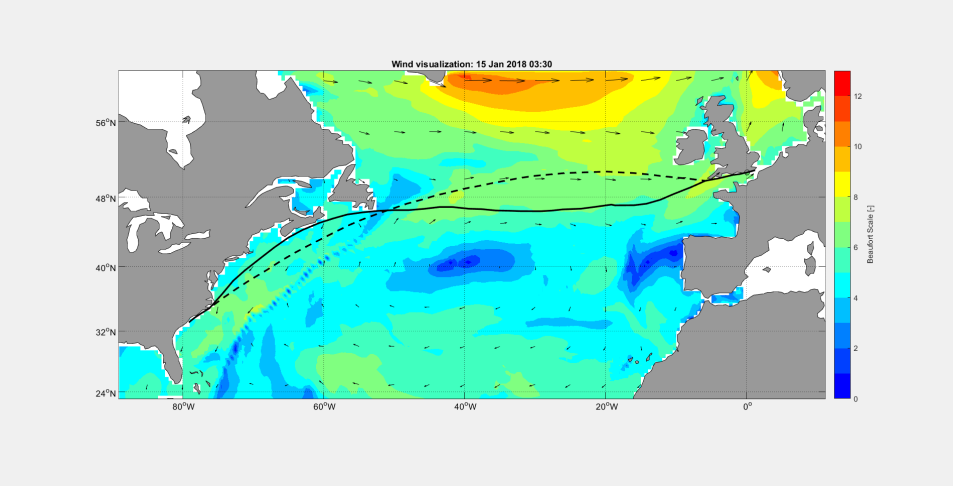

Figure C.14: Voyage simulation: 15-Jan-2018 03:30

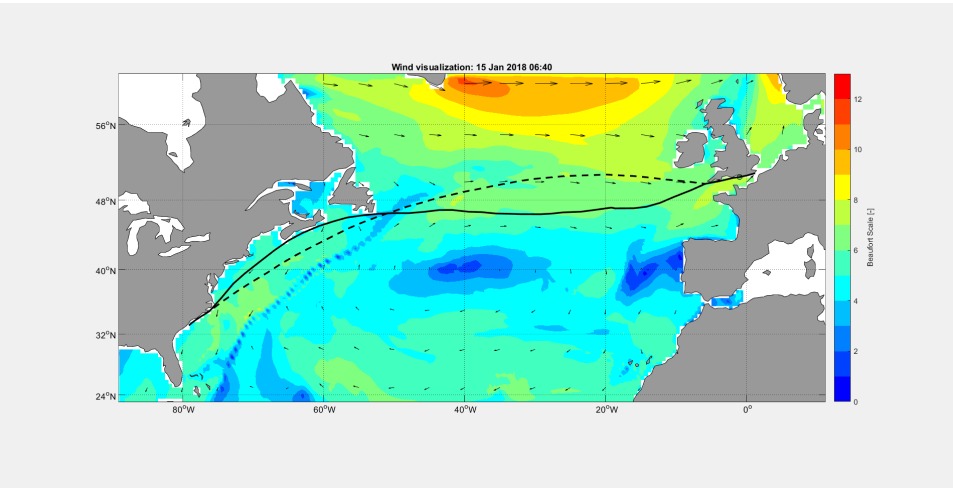

Figure C.15: Voyage simulation: 15-Jan-2018 06:40

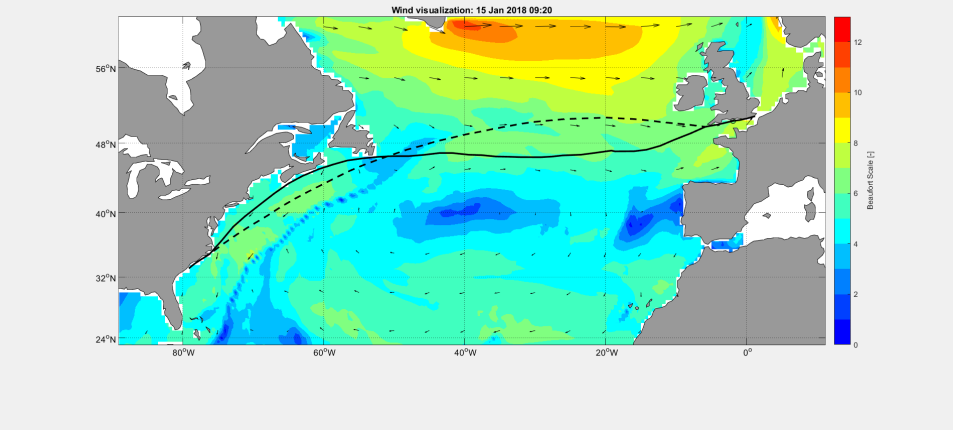

Figure C.16: Voyage simulation: 15-Jan-2018 09:20

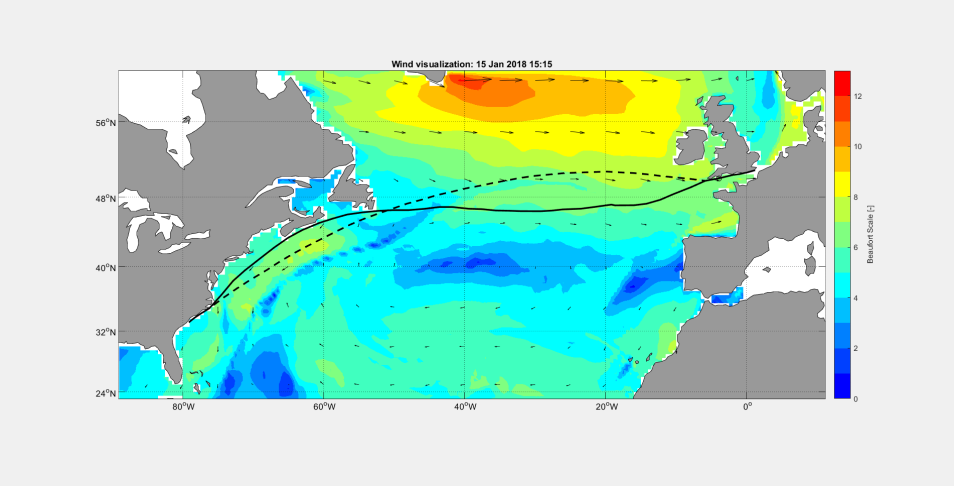

Figure C.17: Voyage simulation: 15-Jan-2018 15:15

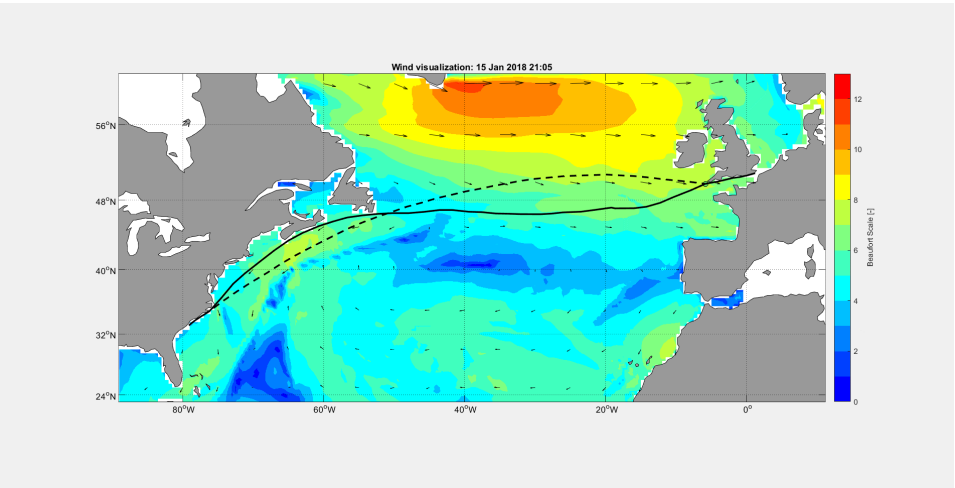

Figure C.18: Voyage simulation: 15-Jan-2018 21:05

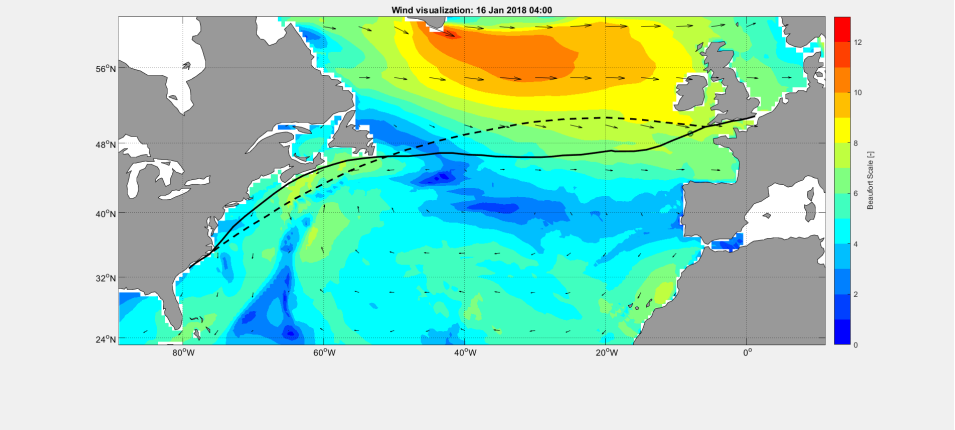

Figure C.19: Voyage simulation: 16-Jan-2018 04:00

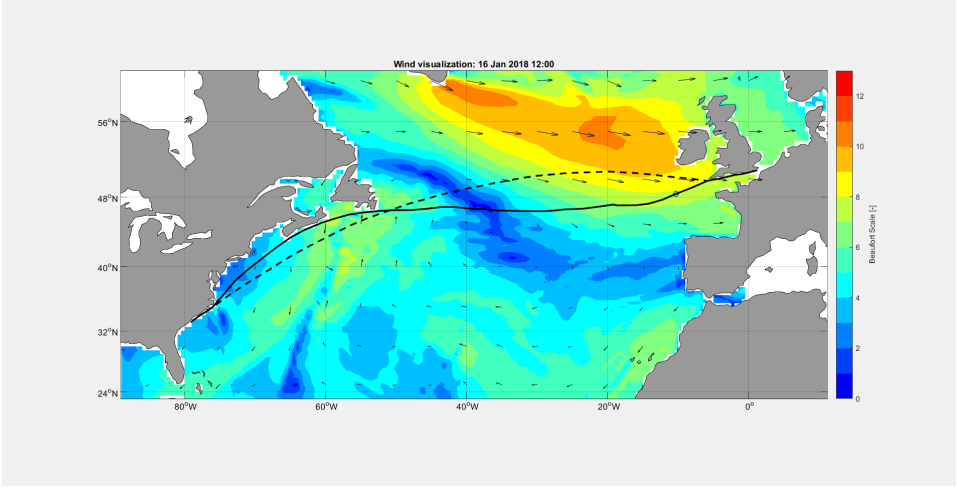

Figure C.20: Voyage simulation: 16-Jan-2018 12:00

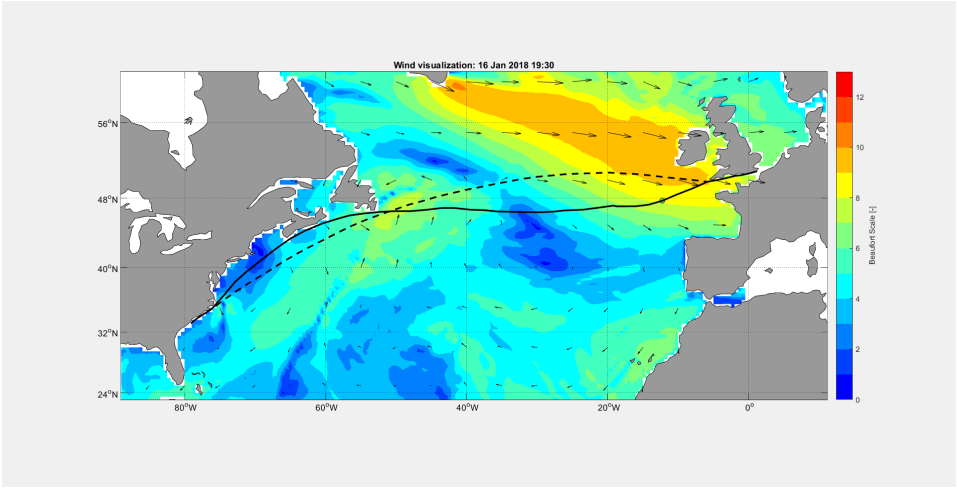

Figure C.21: Voyage simulation: 16-Jan-2018 19:30

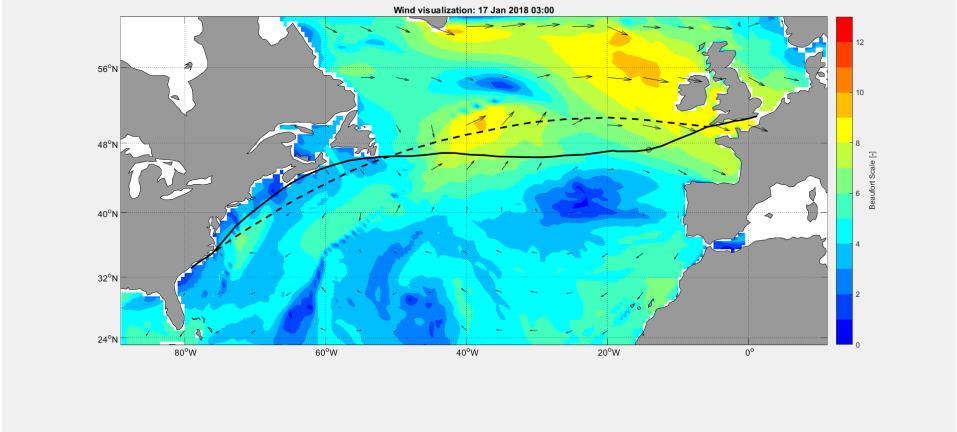

Figure C.22: Voyage simulation: 17-Jan-2018 03:00

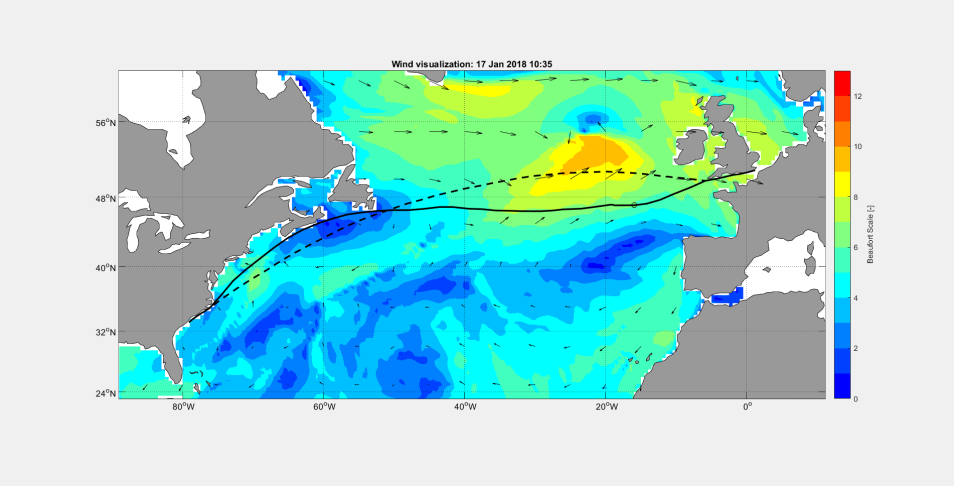

Figure C.23: Voyage simulation: 17-Jan-2018 10:35

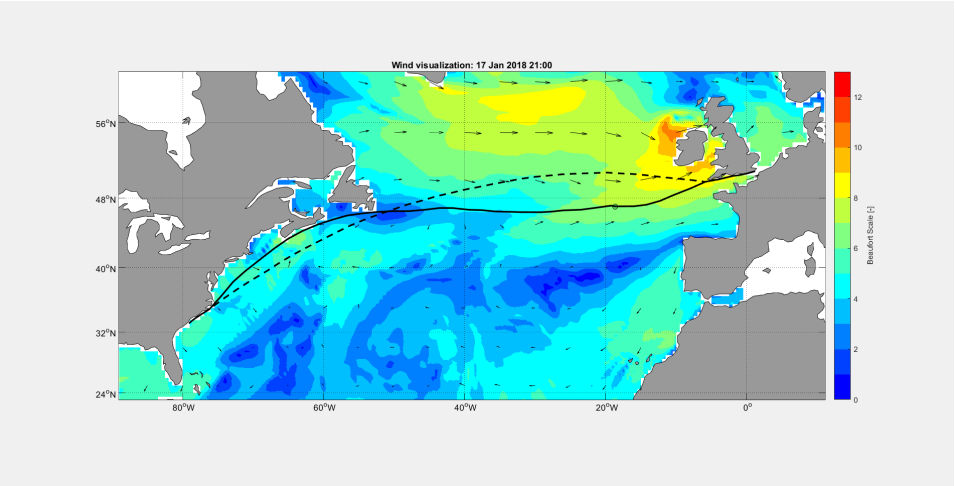

Figure C.24: Voyage simulation: 17-Jan-2018 21:00

D

Daily Visualization of the Example Rerun Case

Visualization of the example rerun case, featuring three completely distinct routes, can be found in this appendix. Black route is based on no weather route optimization at all, the red one on forecasts then shortest path, the green one on forecasts then monthly averages.

D.1. Monthly Averages

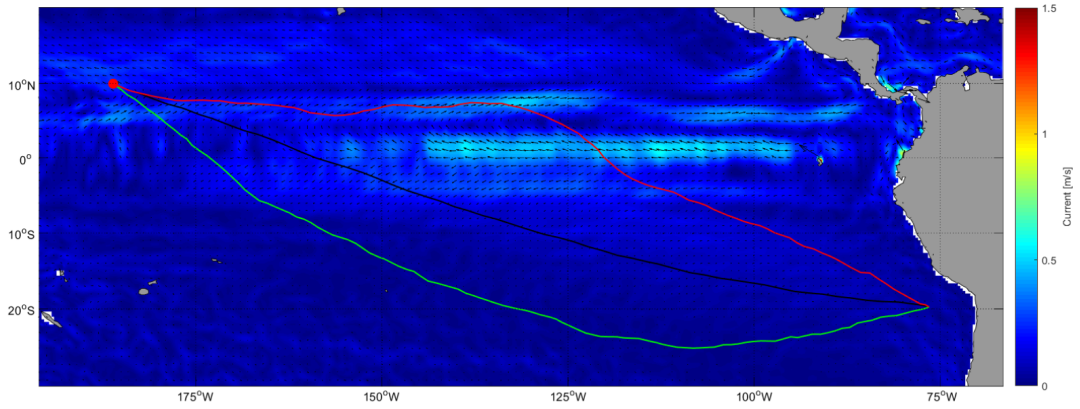

Figure D.1: Monthly averaged current: December

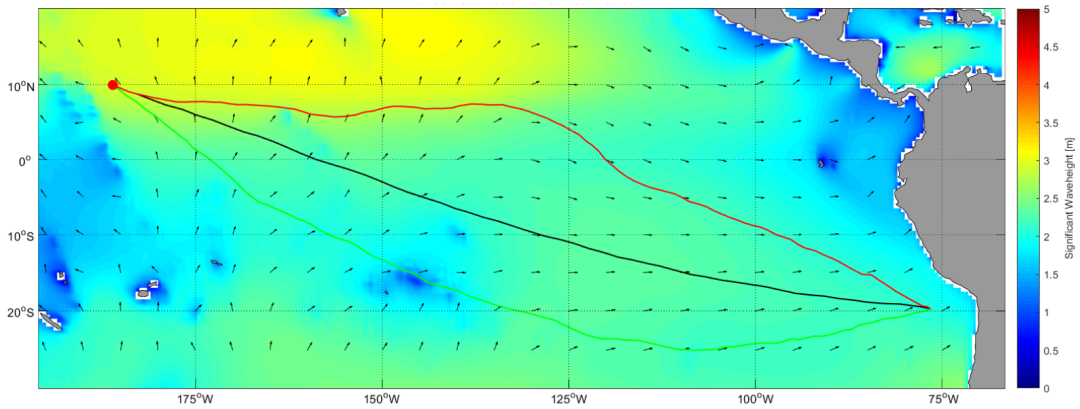

Figure D.2: Monthly averaged waves: December

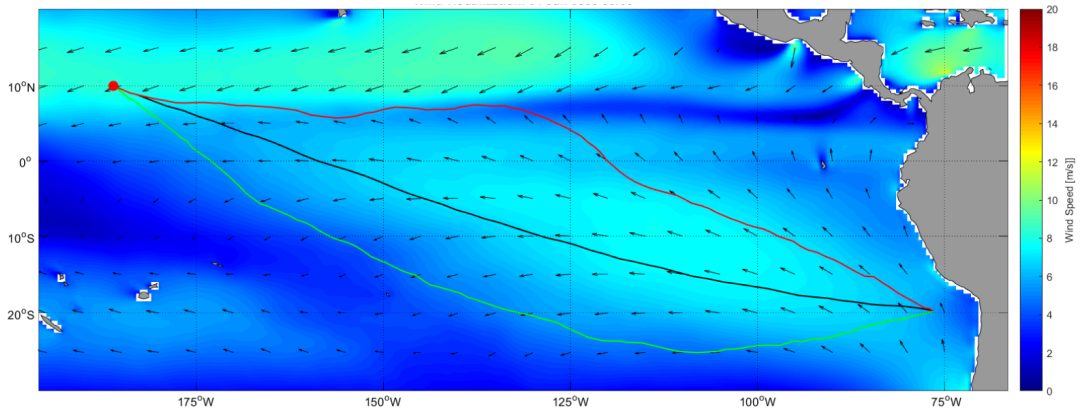

Figure D.3: Monthly averaged wind: December

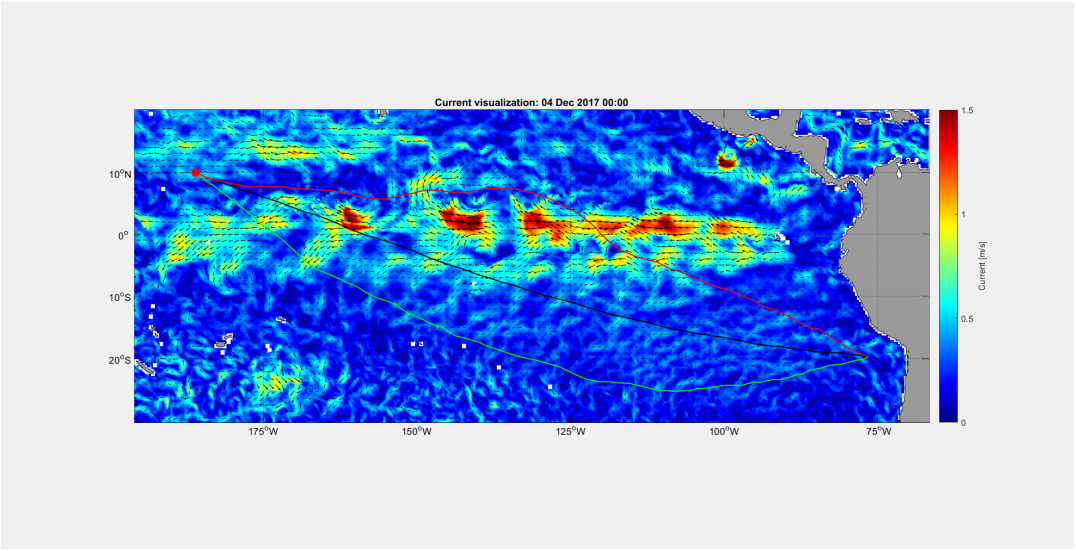

(a) Current

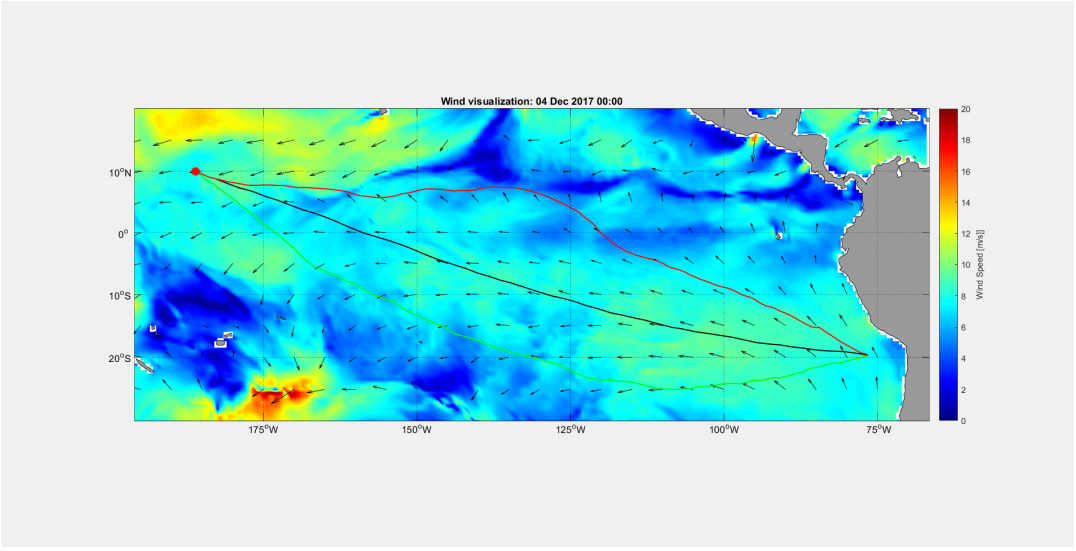

(b) Wind

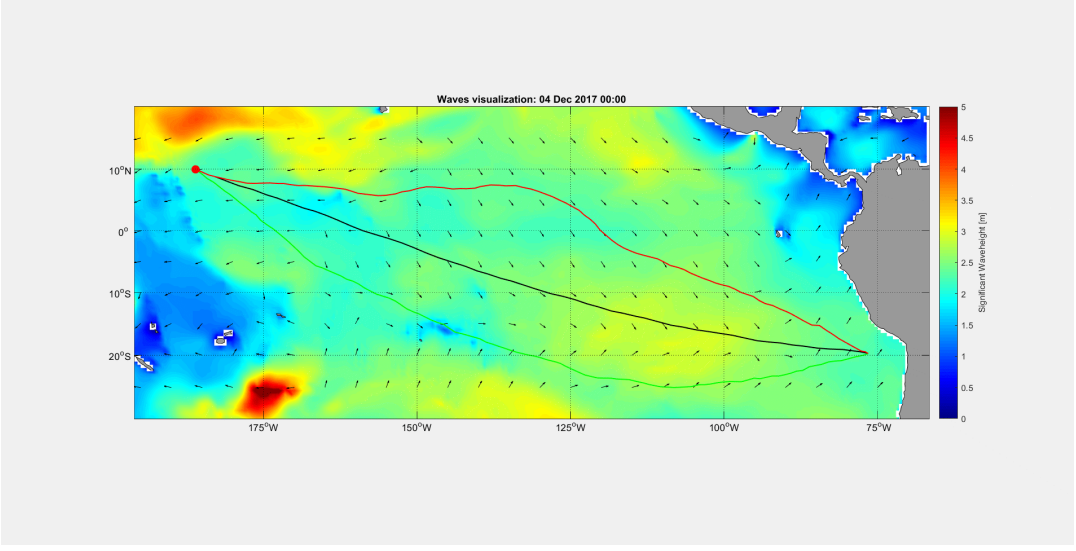

(c) Waves

Figure D.4: Hindcast overview on 04 Dec 2017.

D.2. Day-by-Day Progress

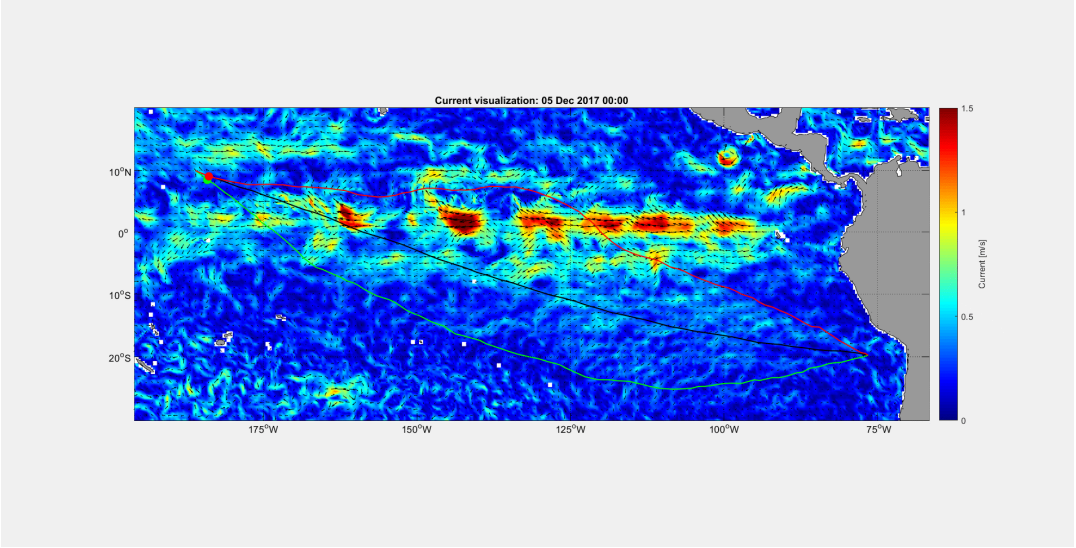

(a) Current

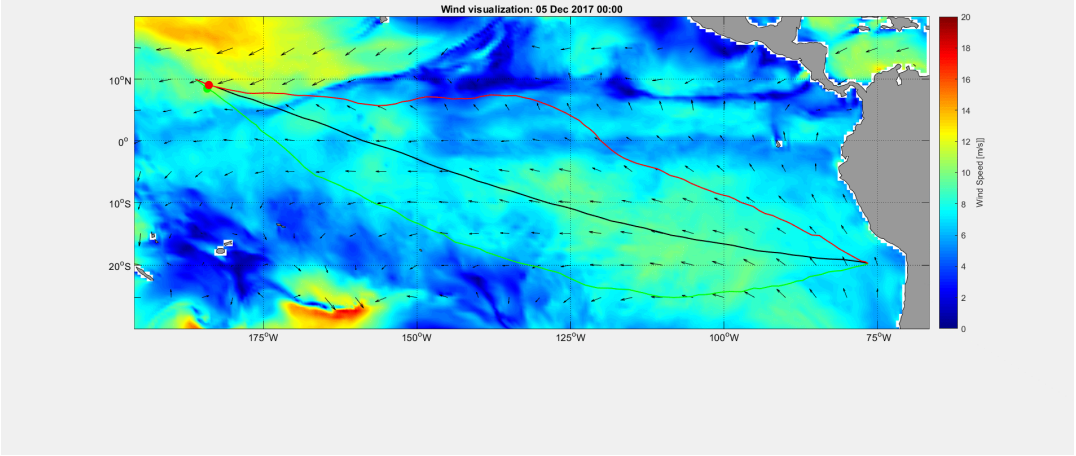

(b) Wind

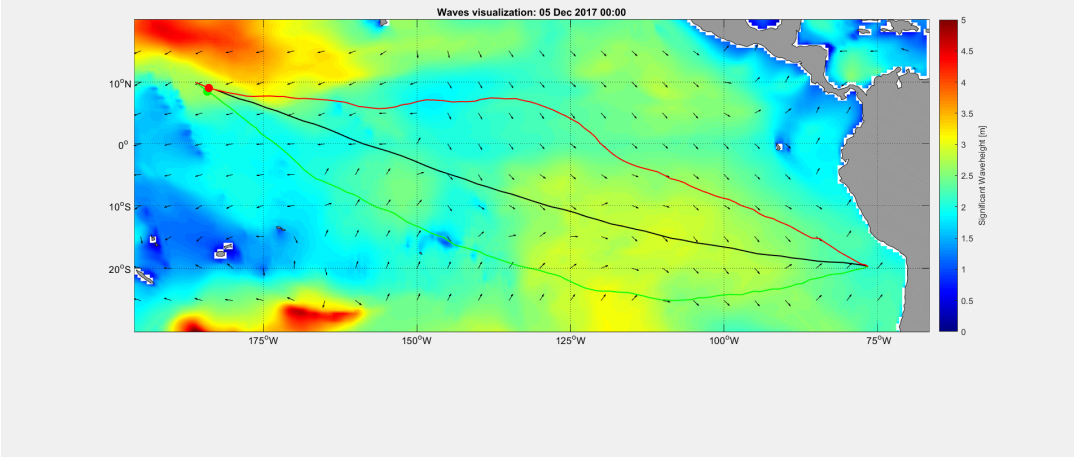

(c) Waves

Figure D.5: Hindcast overview on 05 Dec 2017.

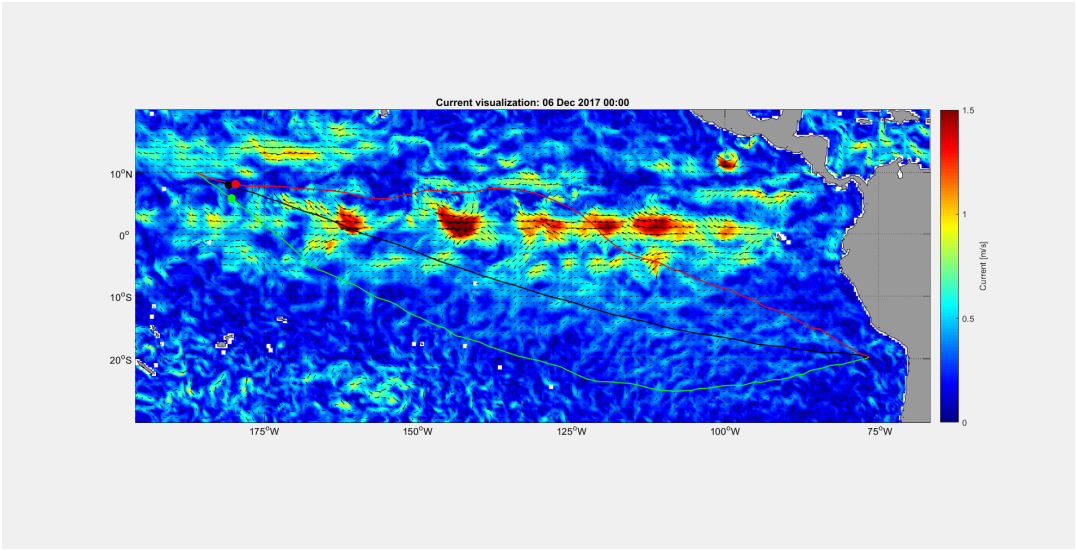

(a) Current

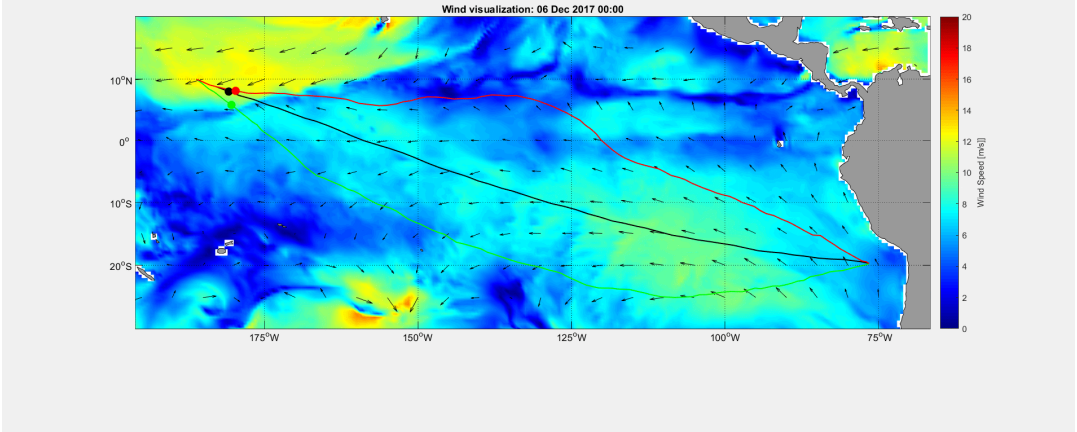

(b) Wind

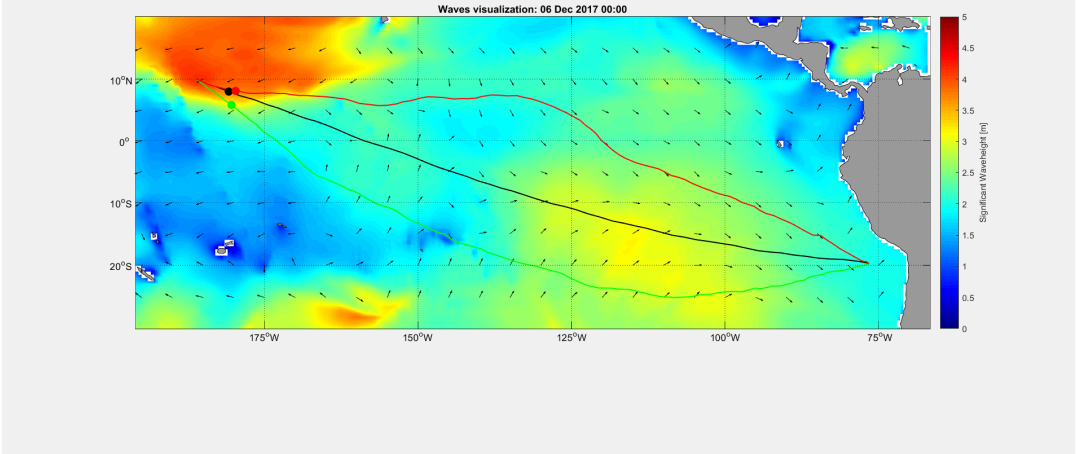

(c) Waves

Figure D.6: Hindcast overview on 06 Dec 2017.

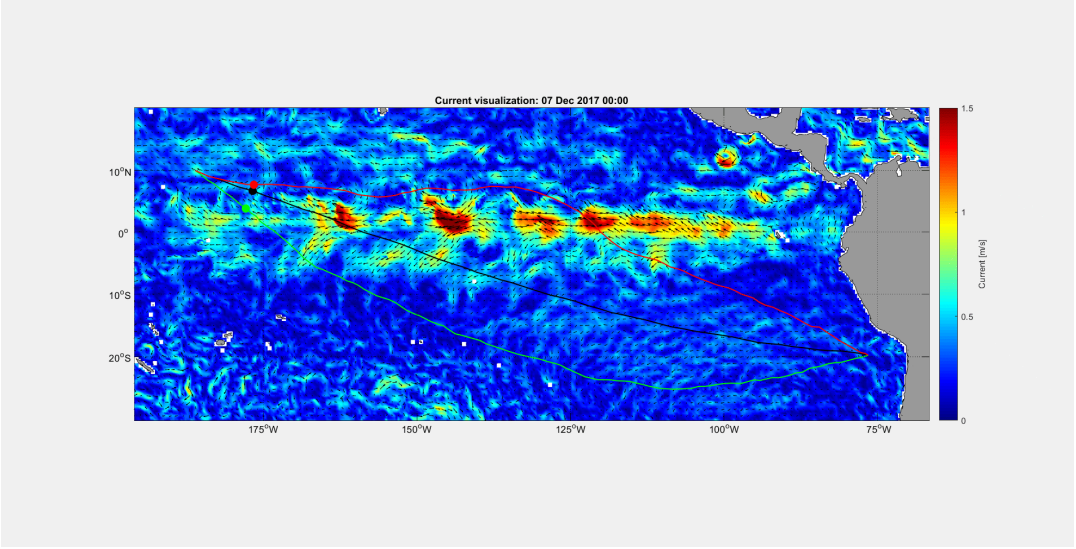

(a) Current

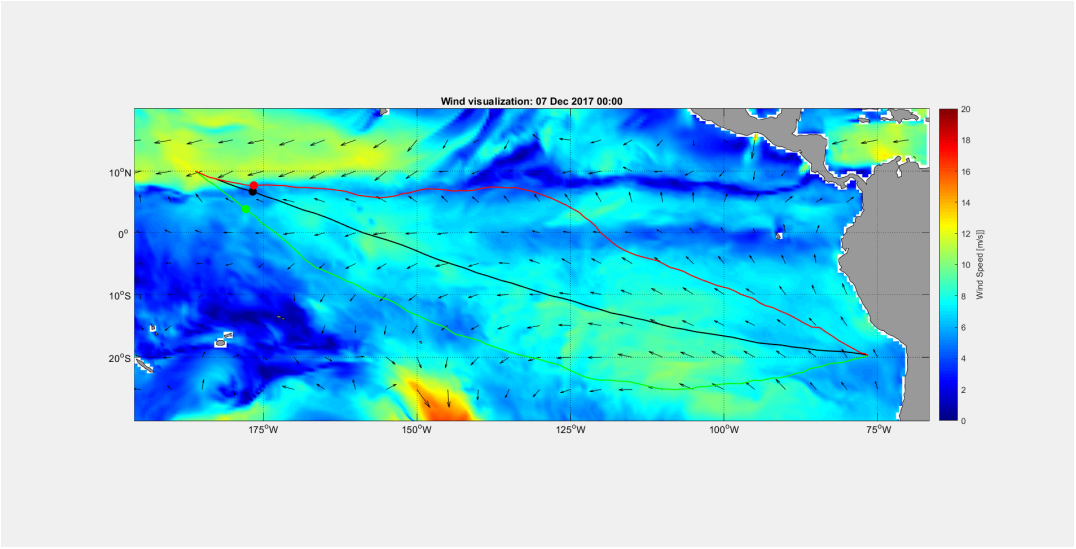

(b) Wind

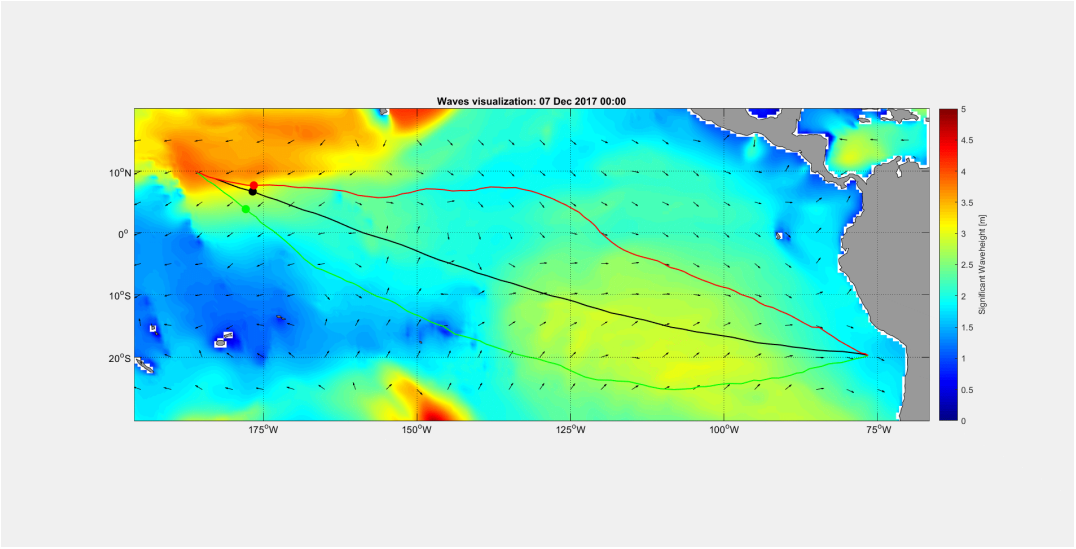

(c) Waves

Figure D.7: Hindcast overview on 07 Dec 2017.

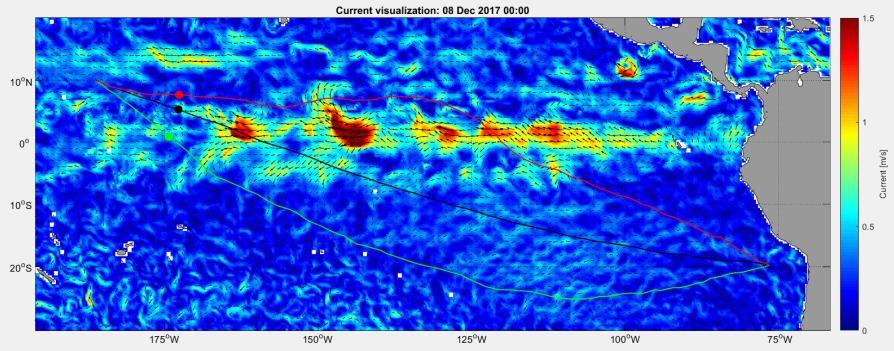

(a) Current

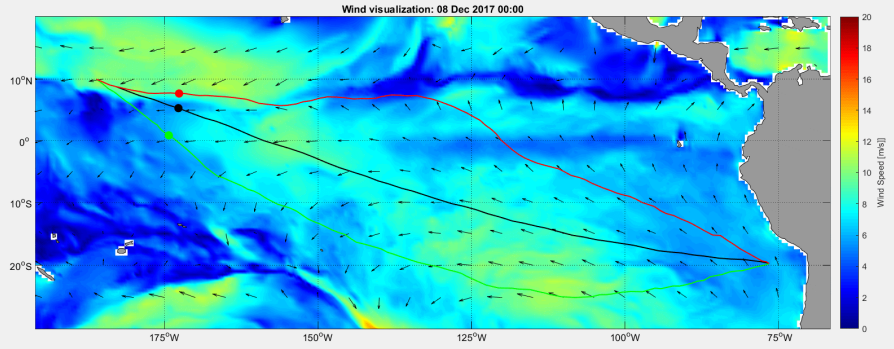

(b) Wind

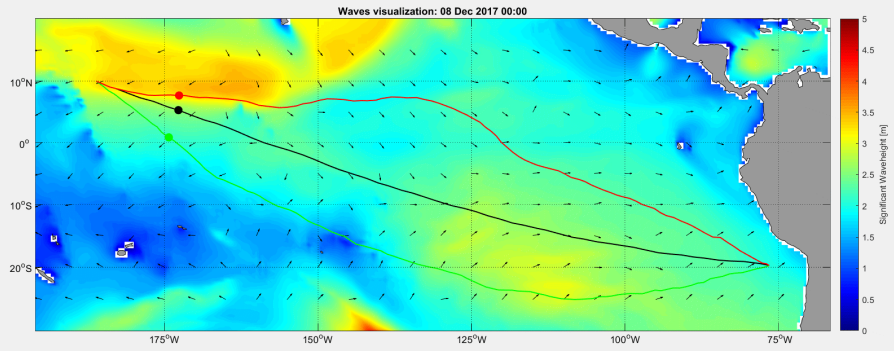

(c) Waves

Figure D.8: Hindcast overview on 08 Dec 2017.

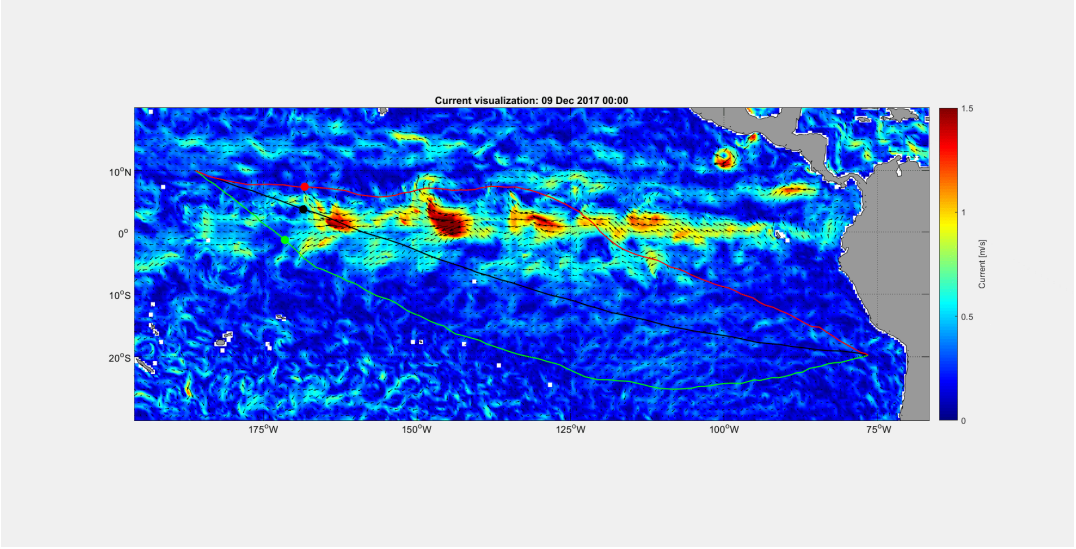

(a) Current

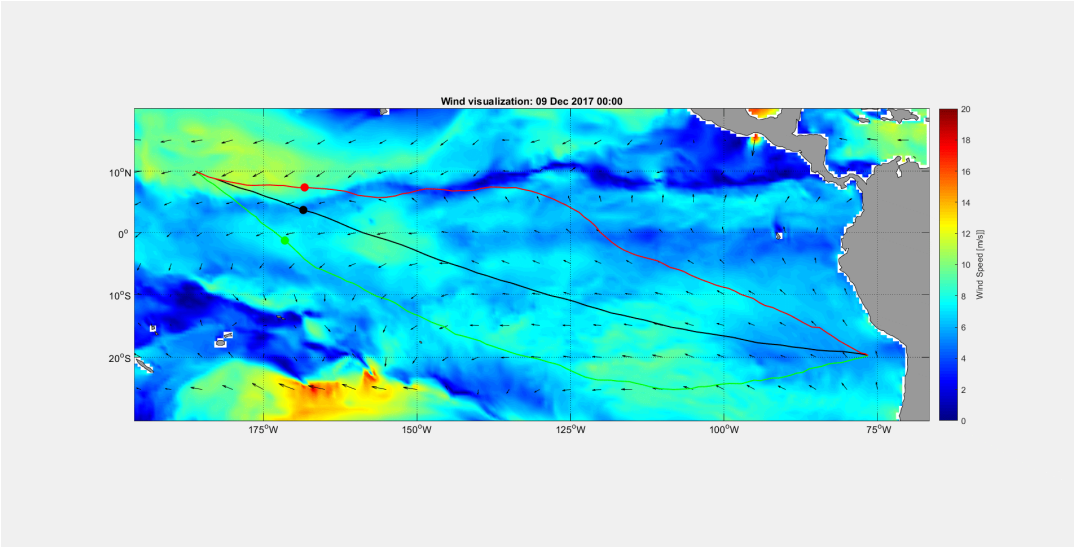

(b) Wind

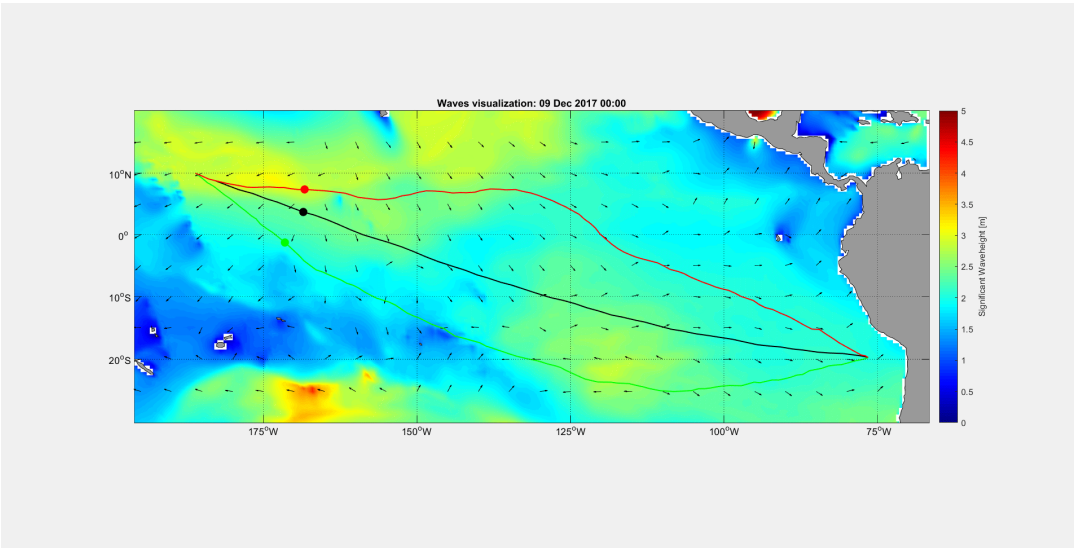

(c) Waves

Figure D.9: Hindcast overview on 09 Dec 2017.

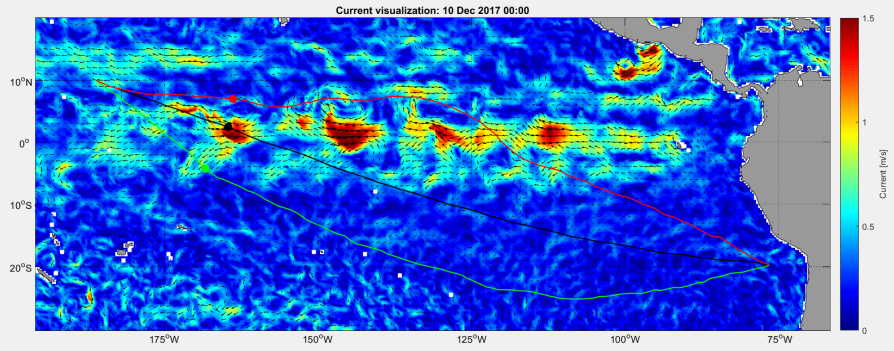

(a) Current

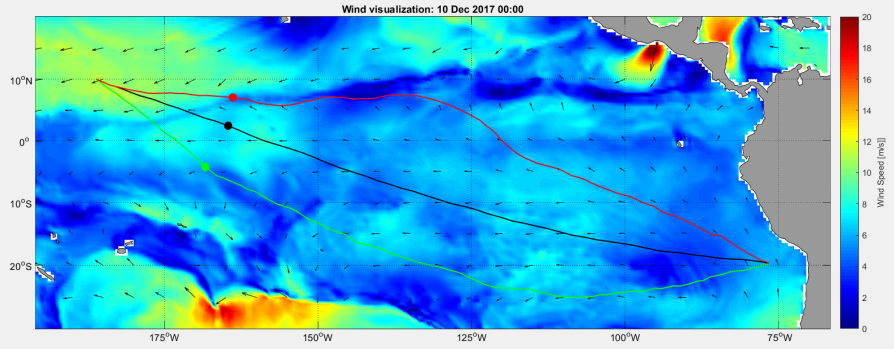

(b) Wind

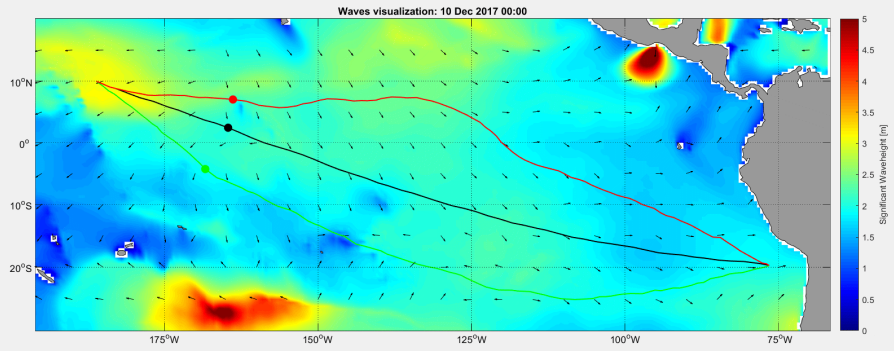

(c) Waves

Figure D.10: Hindcast overview on 10 Dec 2017.

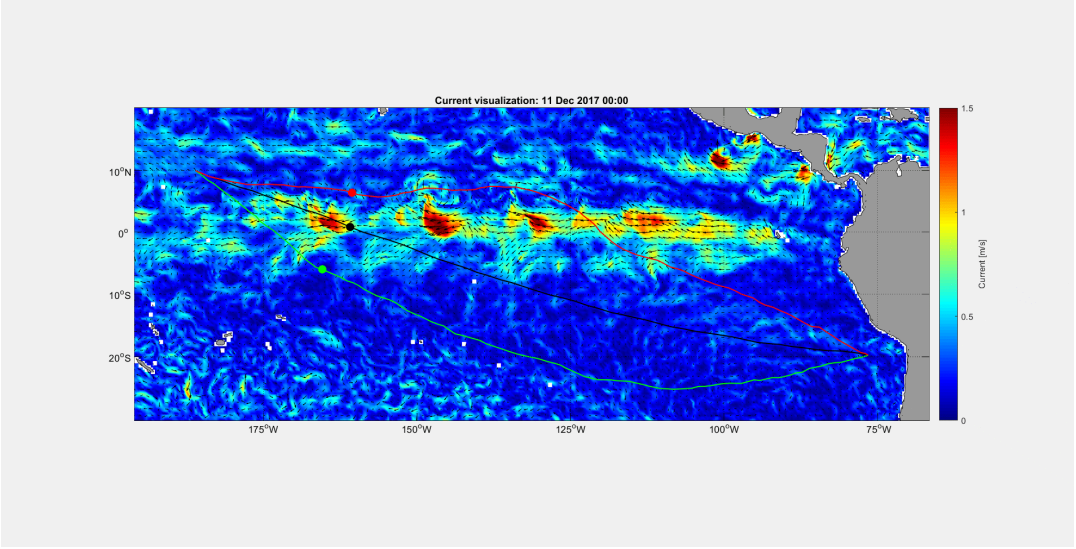

(a) Current

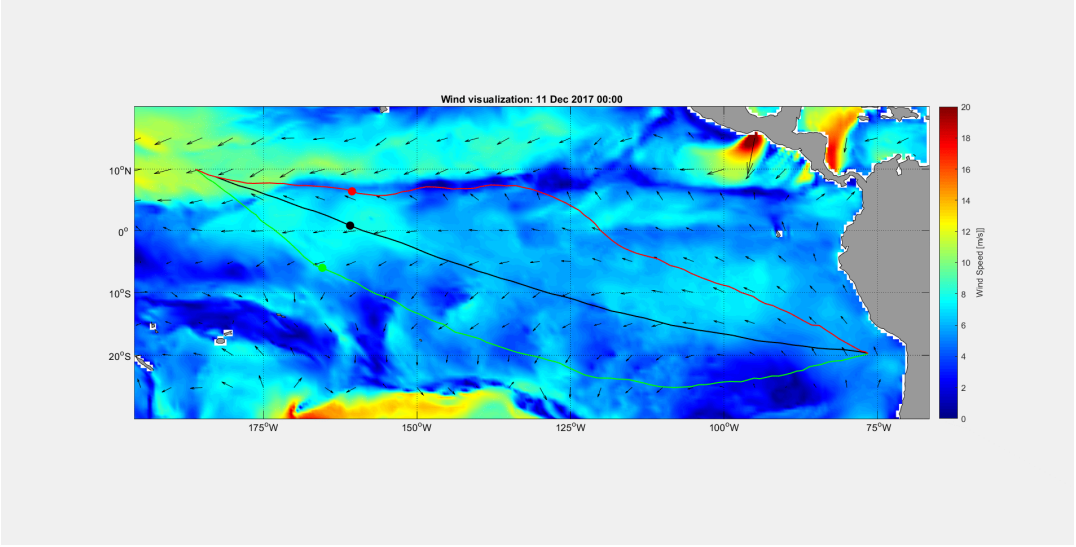

(b) Wind

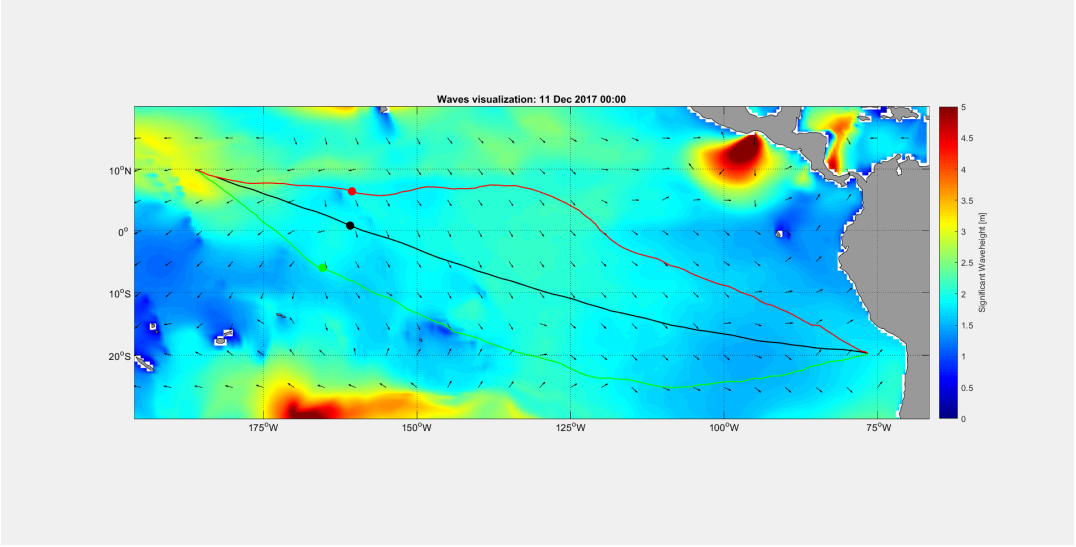

(c) Waves

Figure D.11: Hindcast overview on 11 Dec 2017.

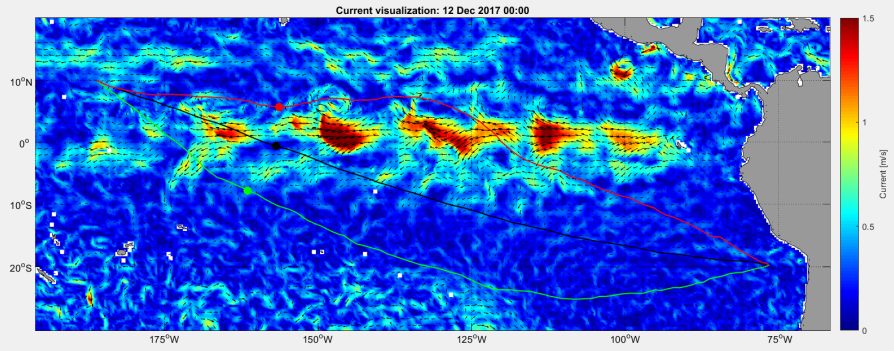

(a) Current

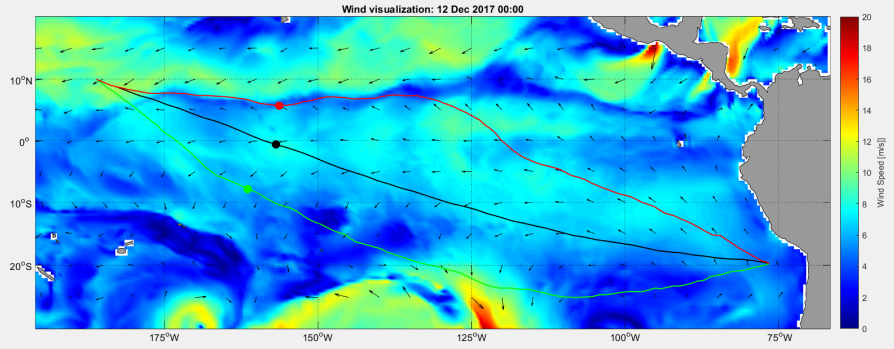

(b) Wind

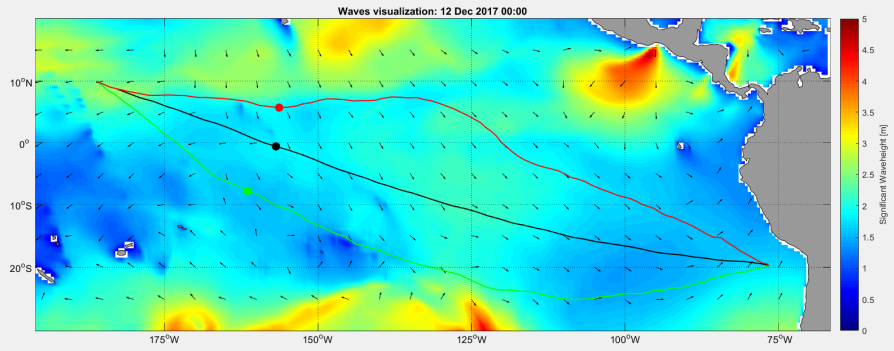

(c) Waves

Figure D.12: Hindcast overview on 12 Dec 2017.

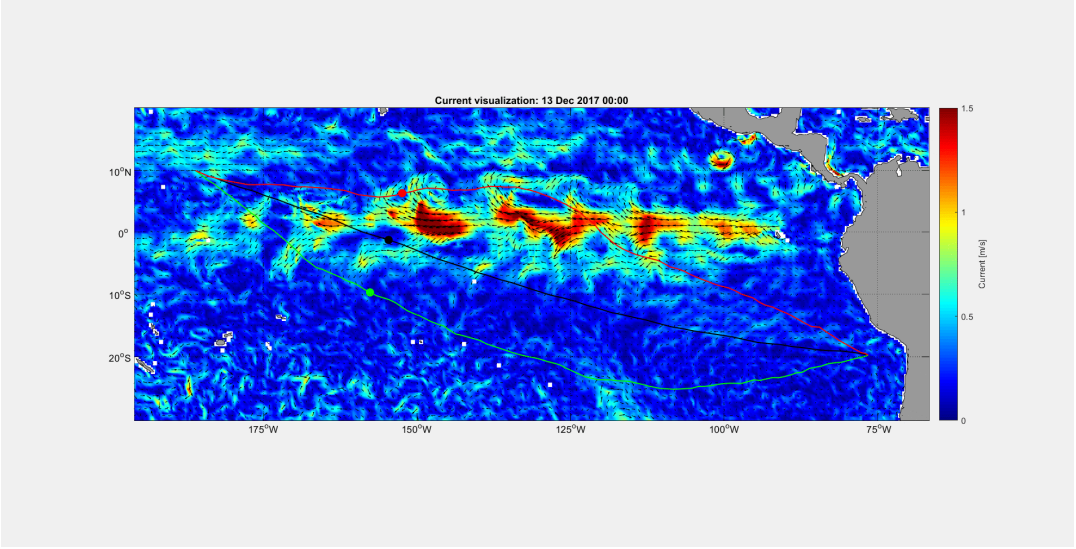

(a) Current

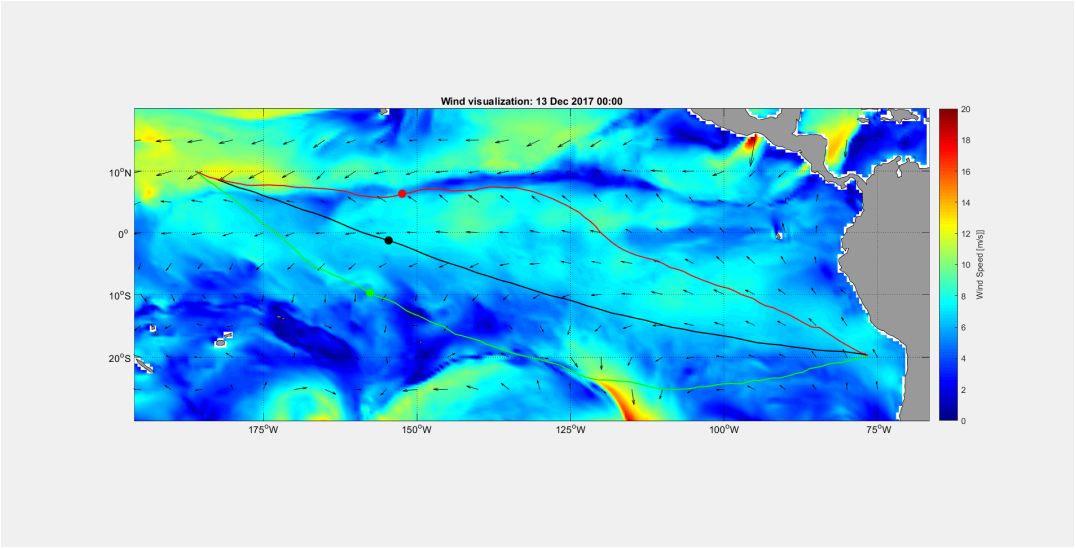

(b) Wind

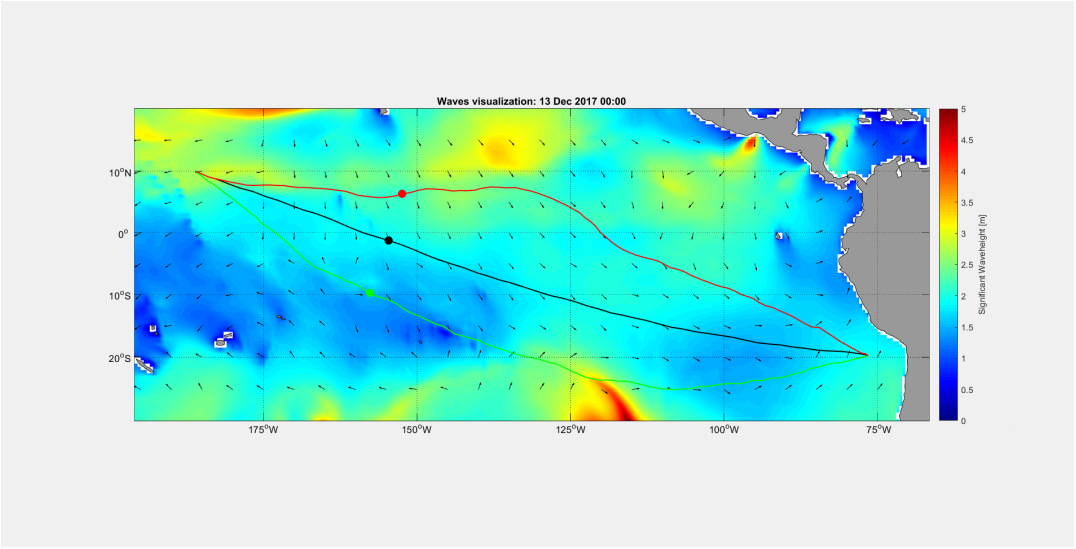

(c) Waves

Figure D.13: Hindcast overview on 13 Dec 2017.

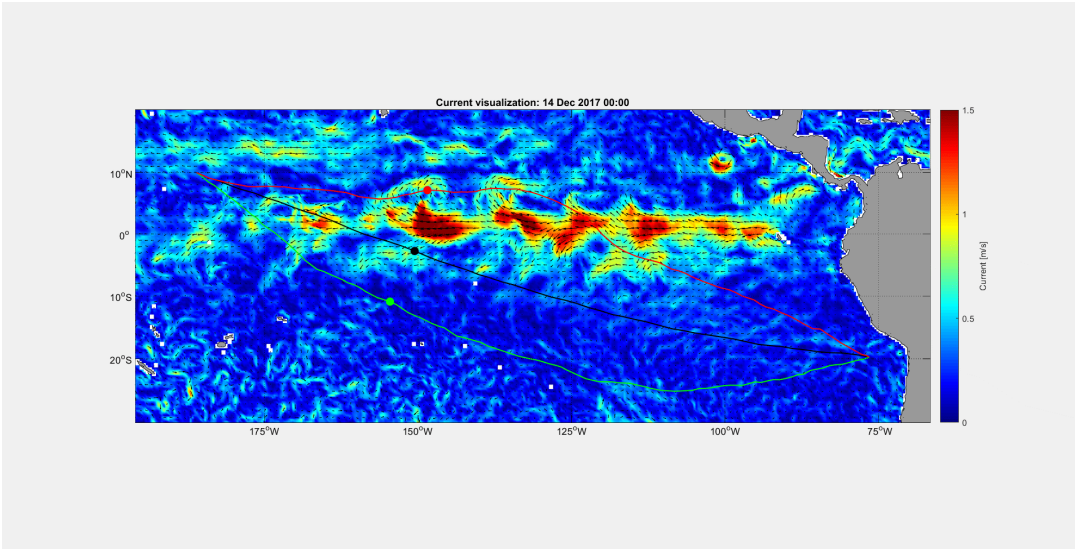

(a) Current

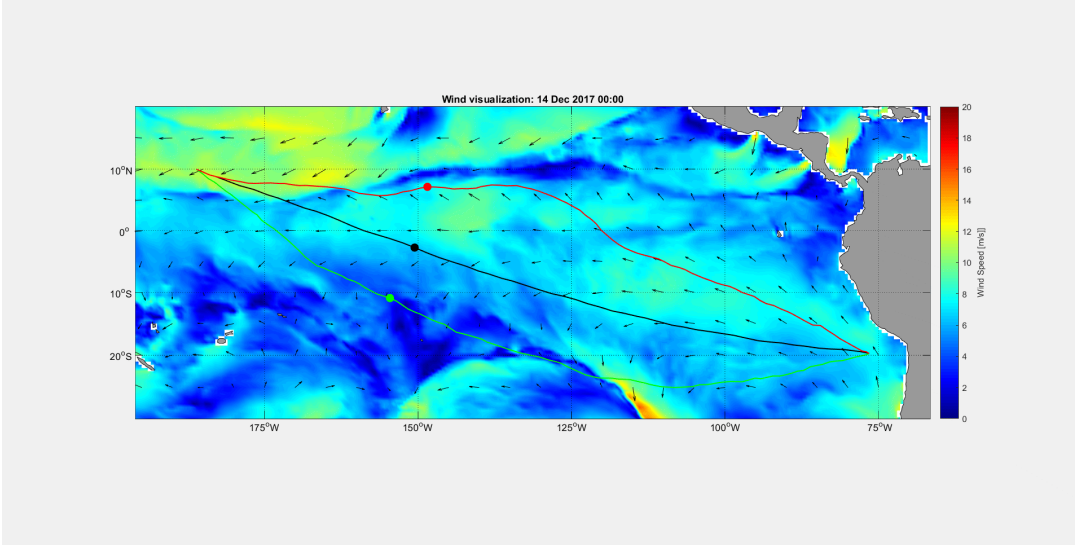

(b) Wind

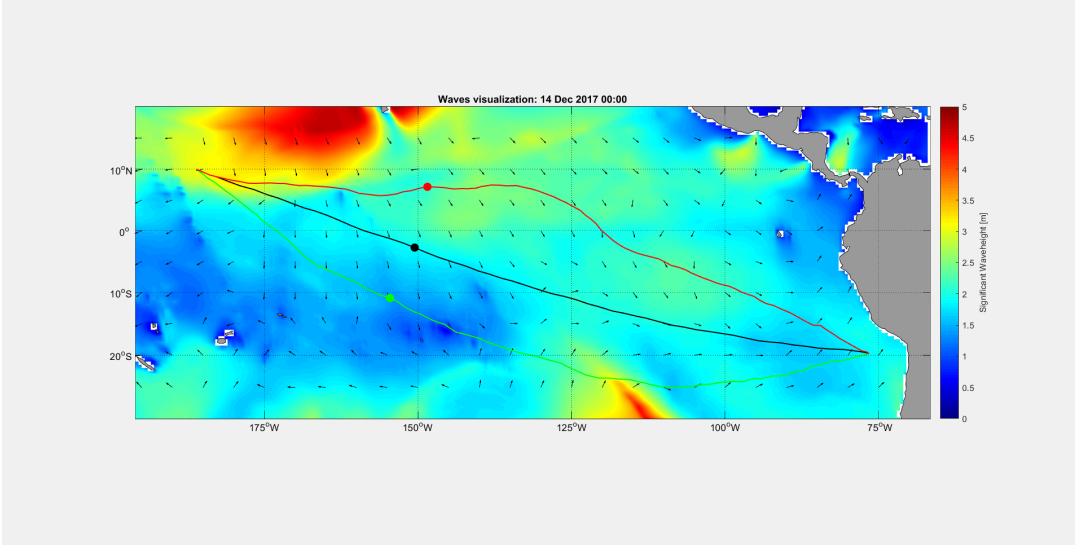

(c) Waves

Figure D.14: Hindcast overview on 14 Dec 2017.

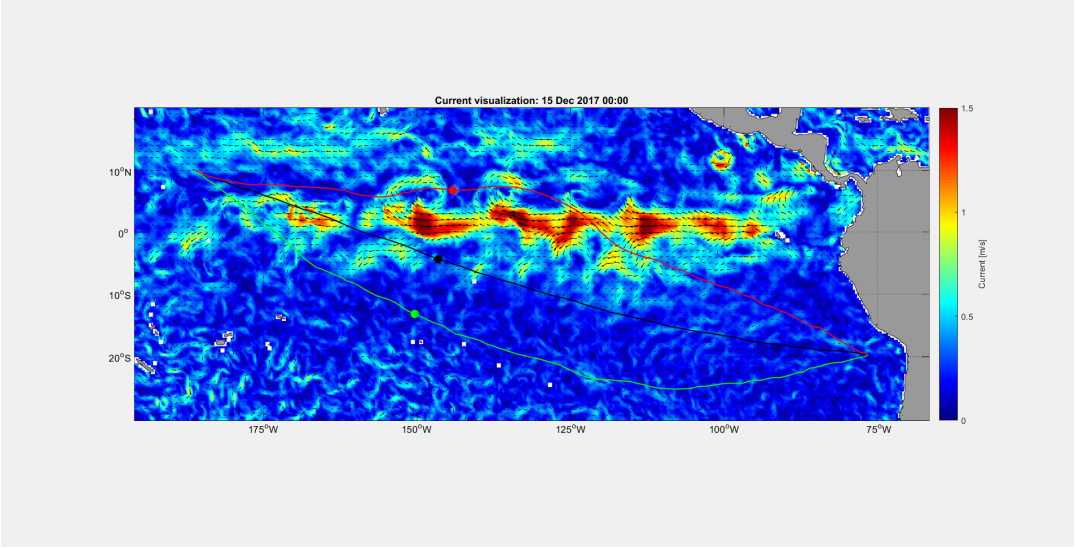

(a) Current

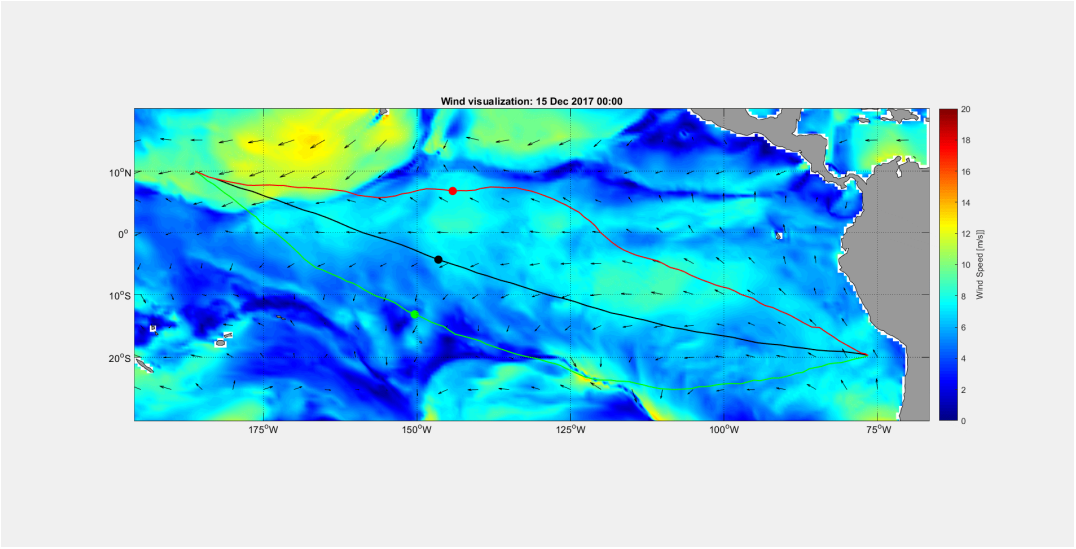

(b) Wind

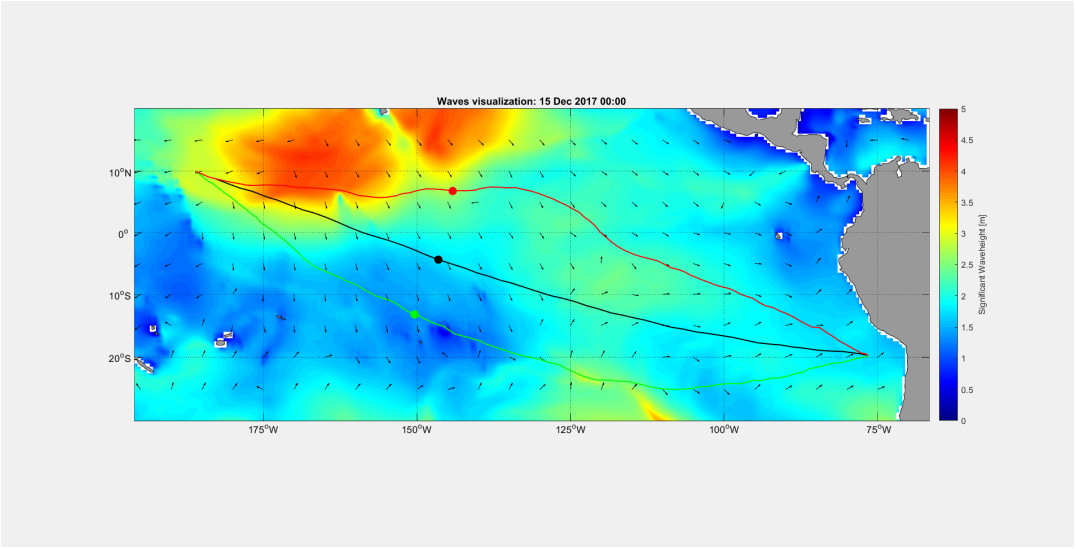

(c) Waves

Figure D.15: Hindcast overview on 15 Dec 2017.

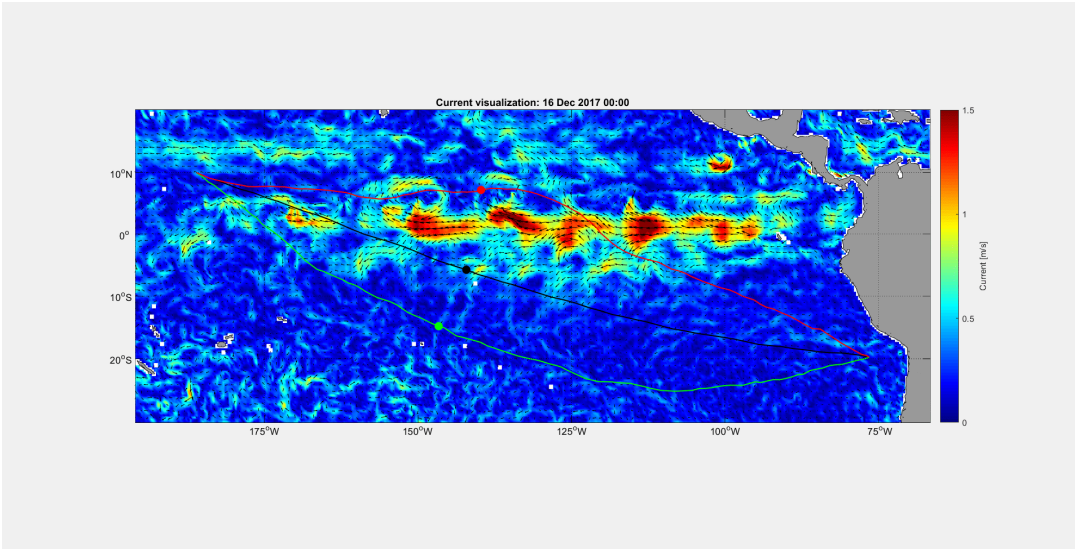

(a) Current

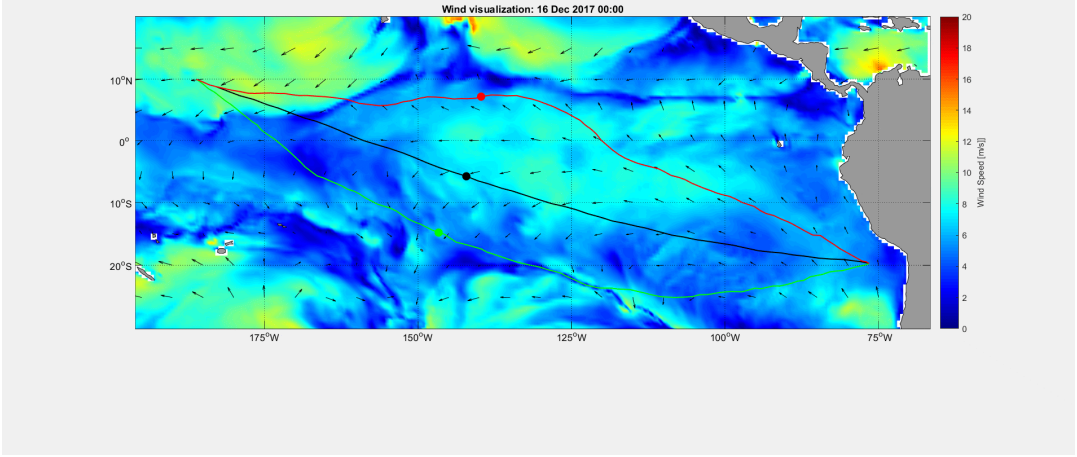

(b) Wind

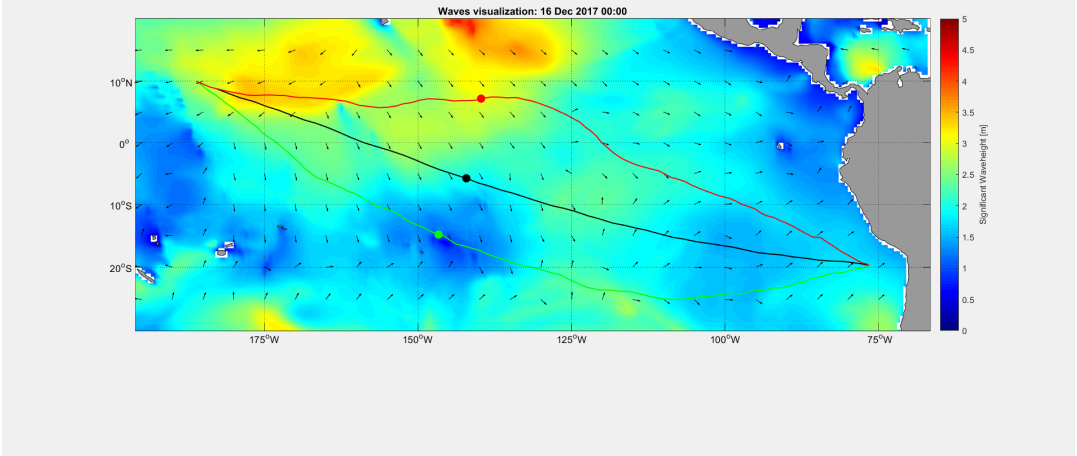

(c) Waves

Figure D.16: Hindcast overview on 16 Dec 2017.

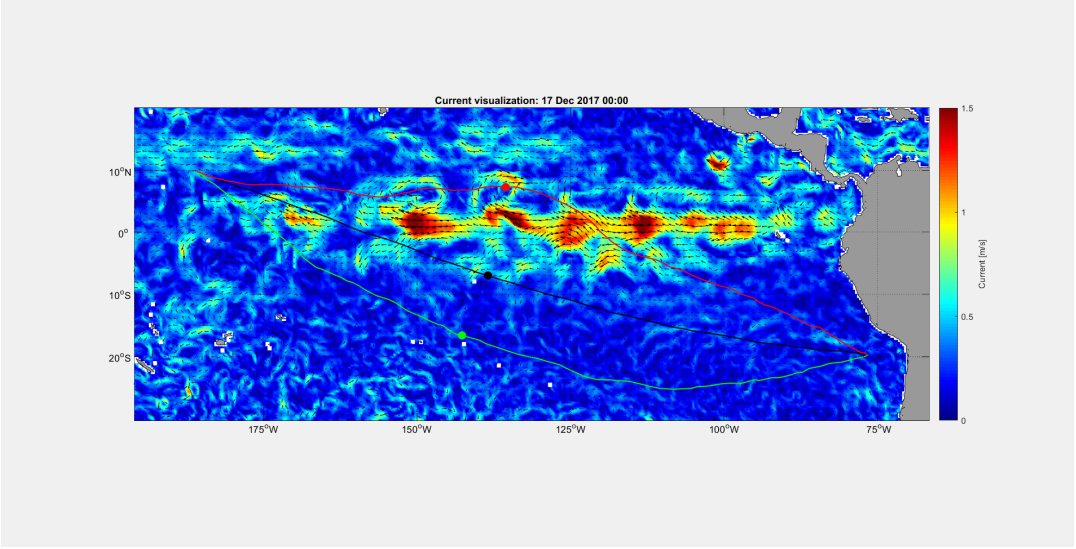

(a) Current

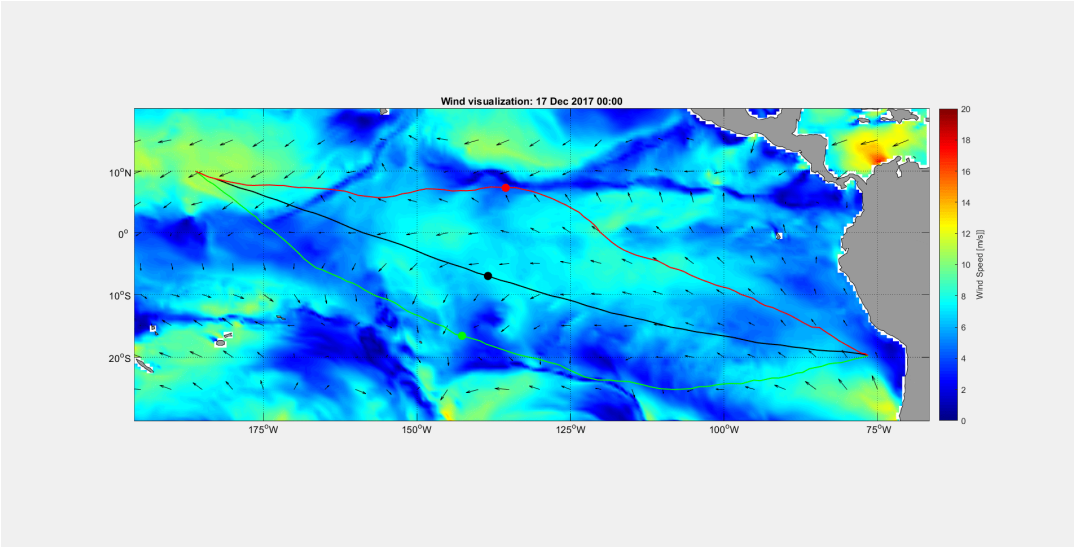

(b) Wind

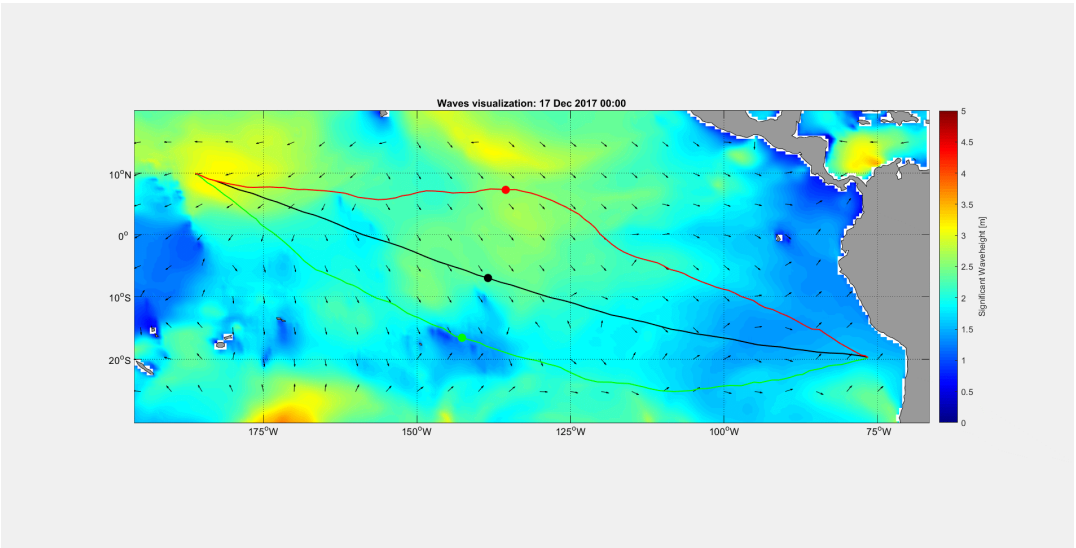

(c) Waves

Figure D.17: Hindcast overview on 17 Dec 2017.

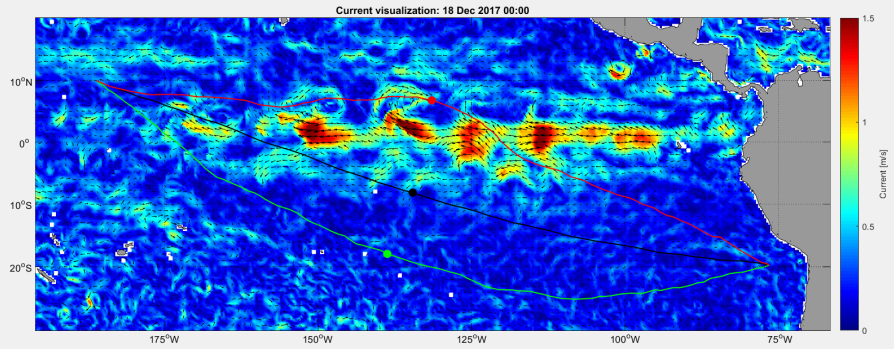

(a) Current

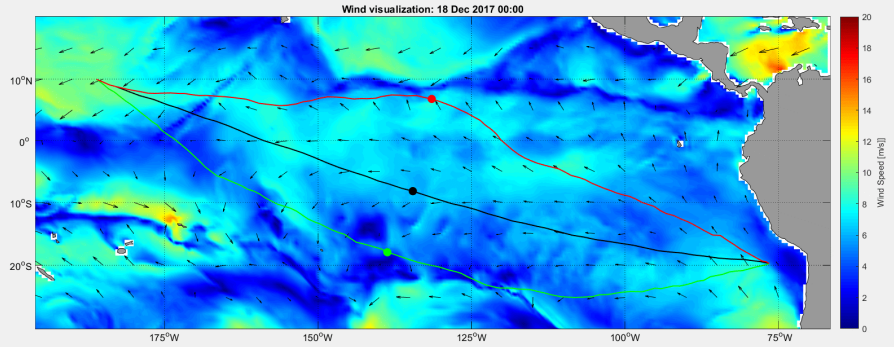

(b) Wind

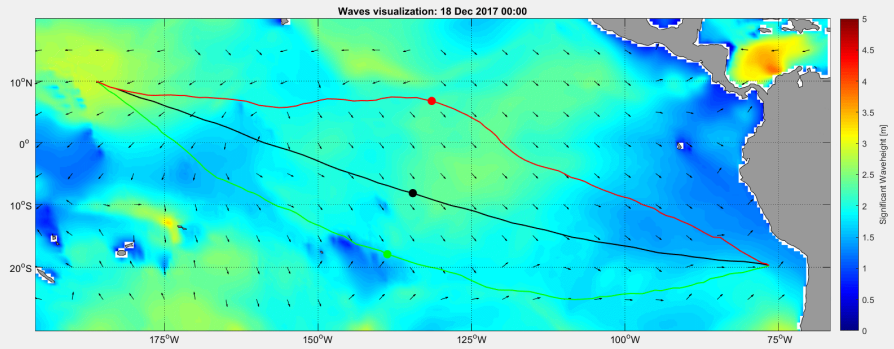

(c) Waves

Figure D.18: Hindcast overview on 18 Dec 2017.

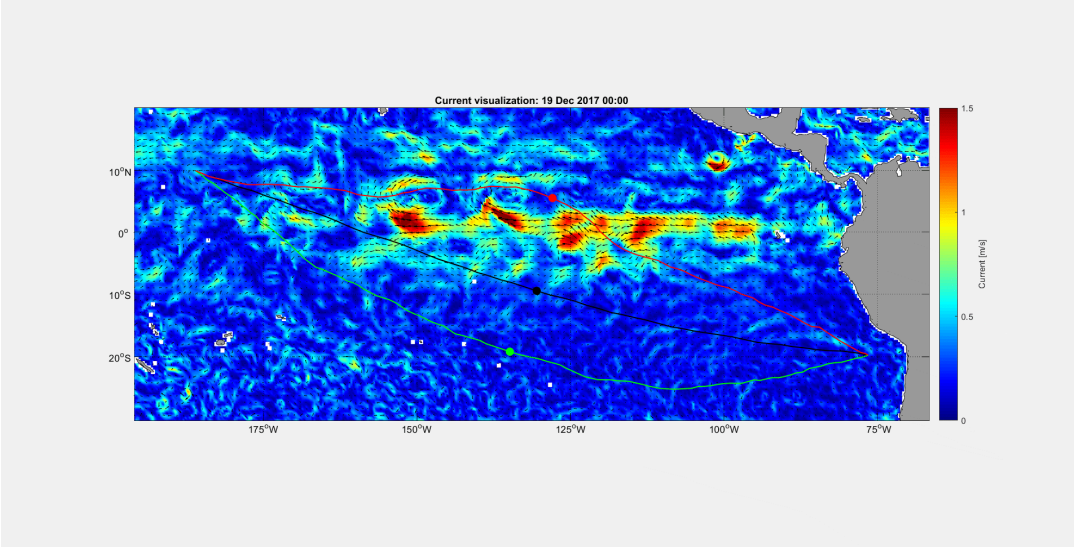

(a) Current

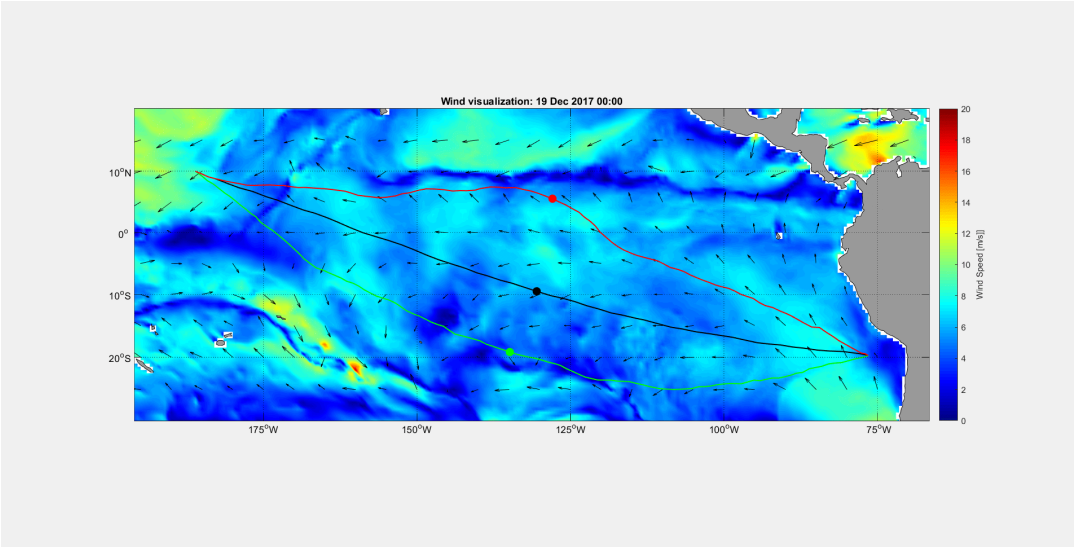

(b) Wind

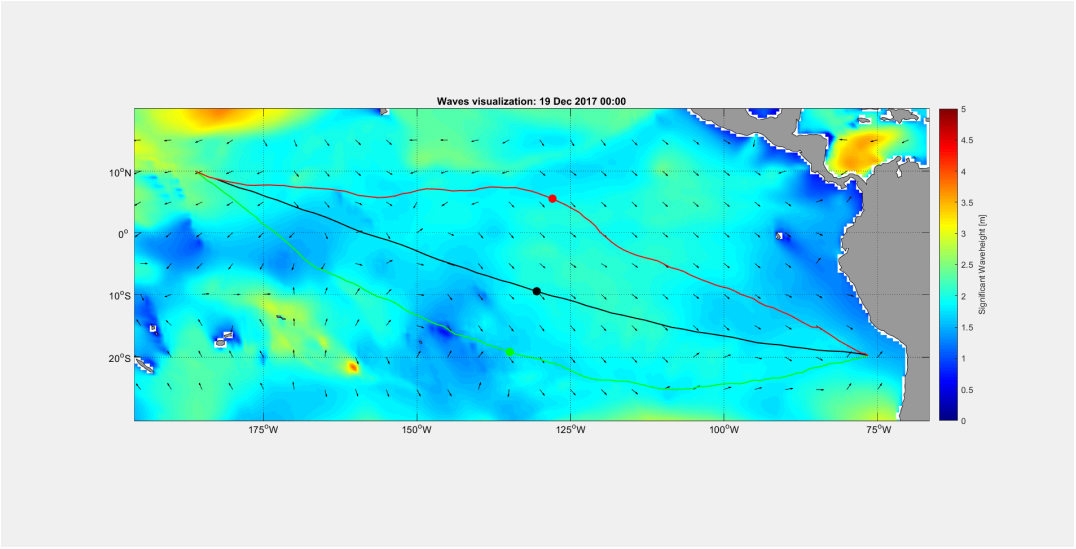

(c) Waves

Figure D.19: Hindcast overview on 19 Dec 2017.

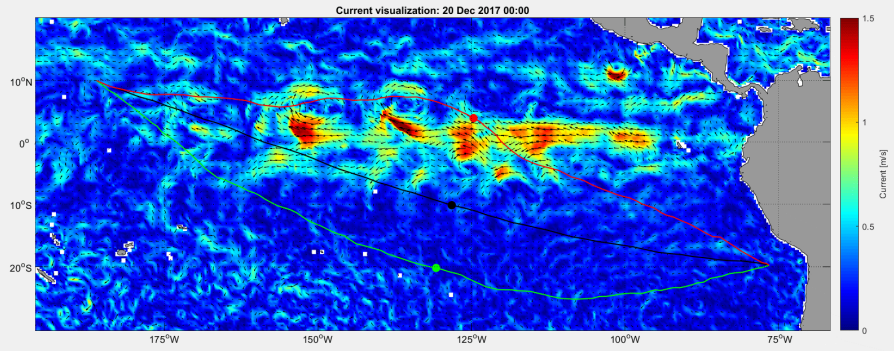

(a) Current

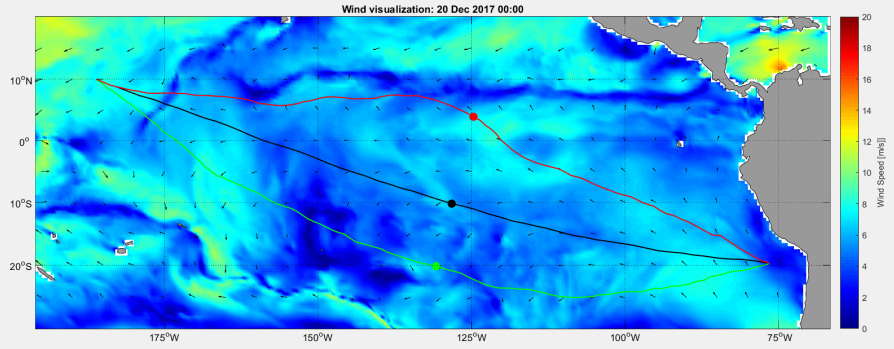

(b) Wind

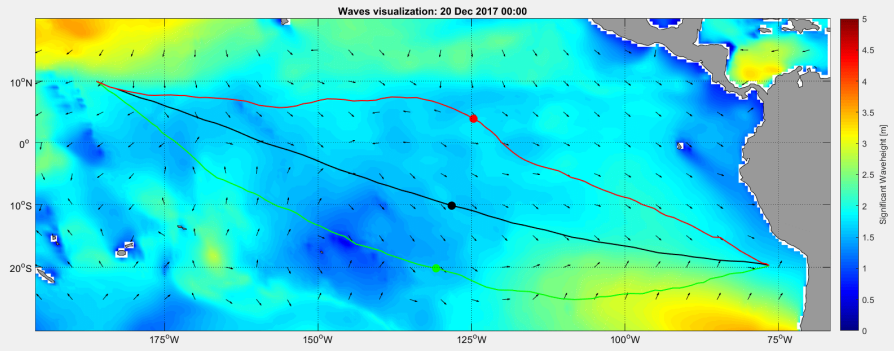

(c) Waves

Figure D.20: Hindcast overview on 20 Dec 2017.

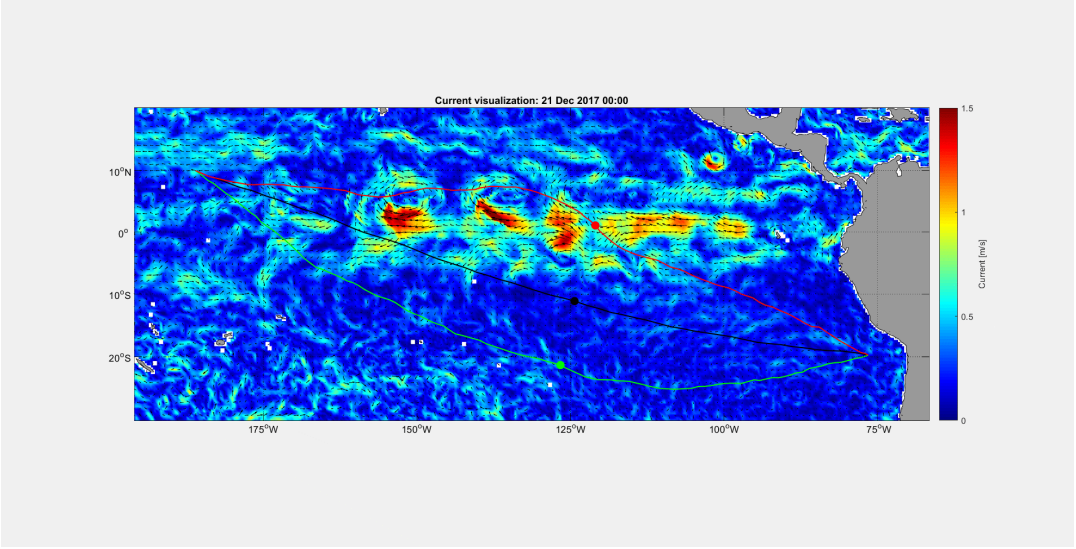

(a) Current

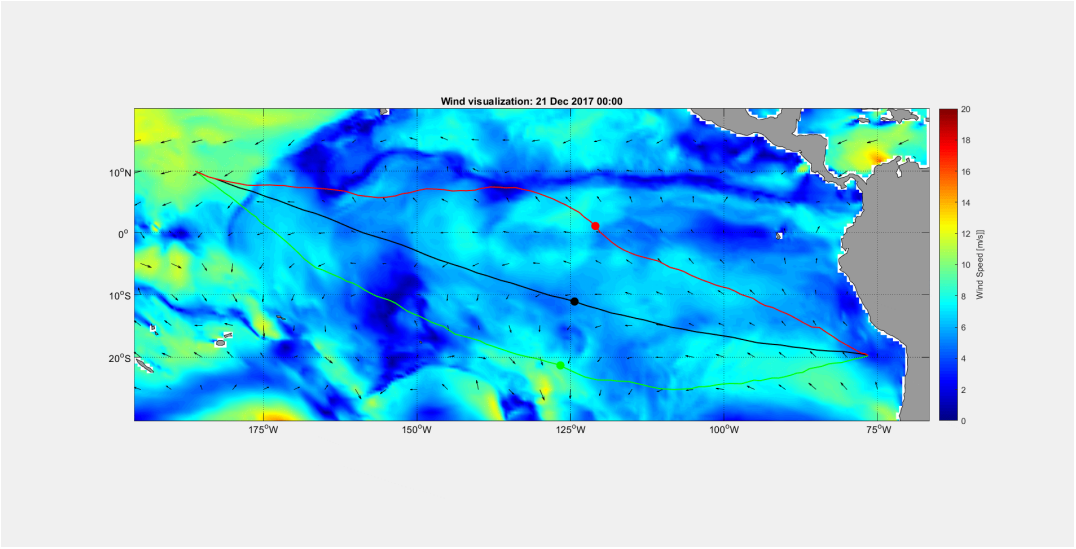

(b) Wind

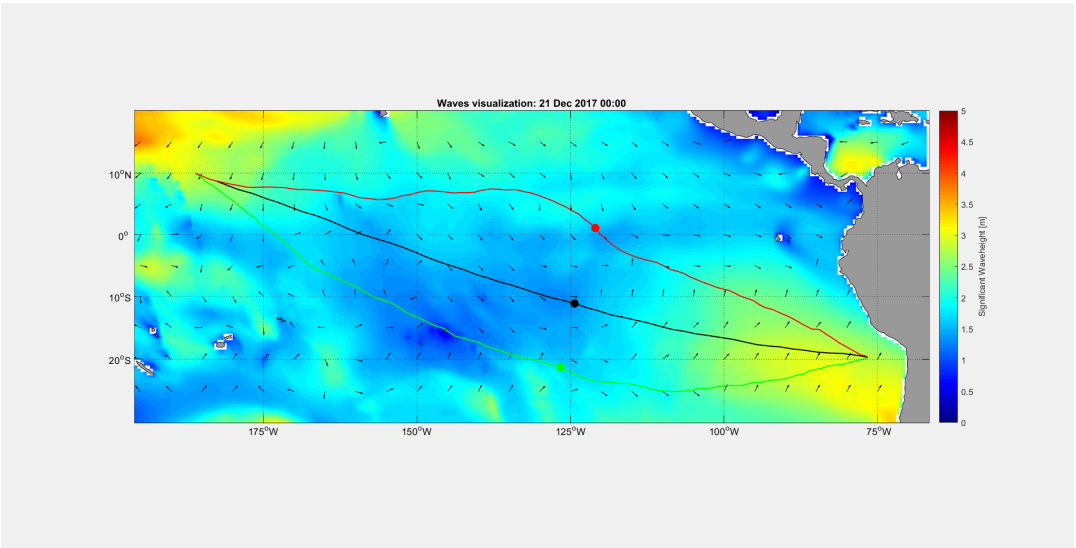

(c) Waves

Figure D.21: Hindcast overview on 21 Dec 2017.

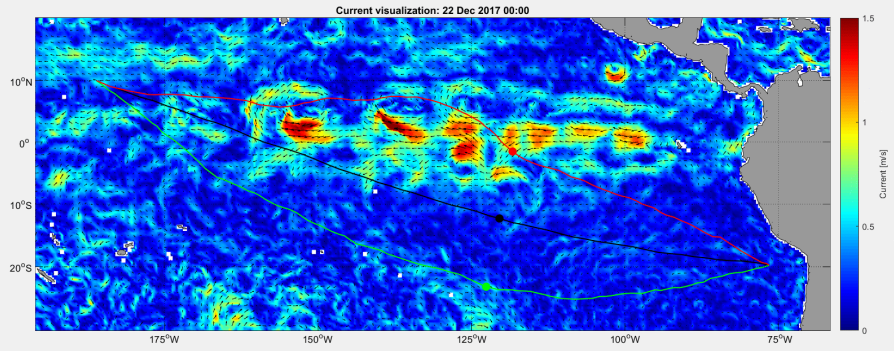

(a) Current

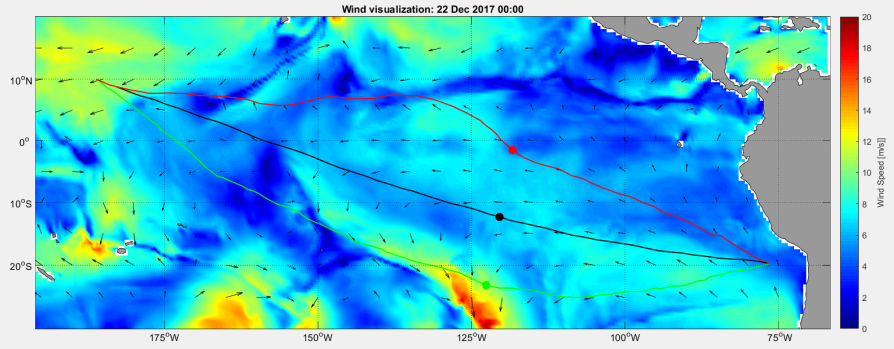

(b) Wind

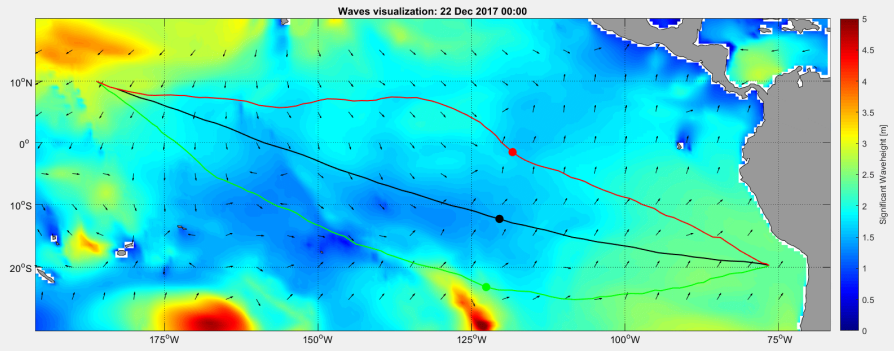

(c) Waves

Figure D.22: Hindcast overview on 22 Dec 2017.

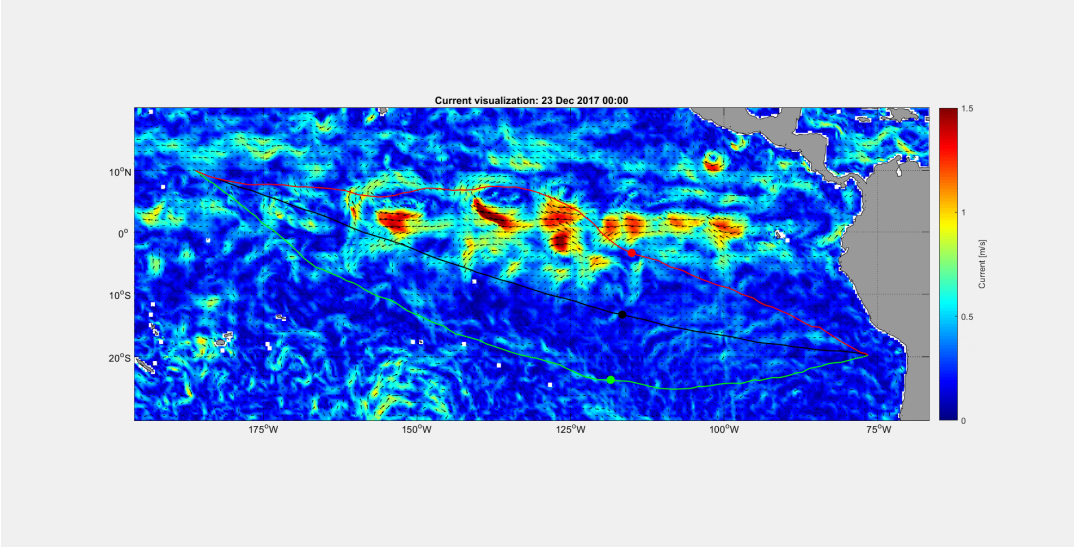

(a) Current

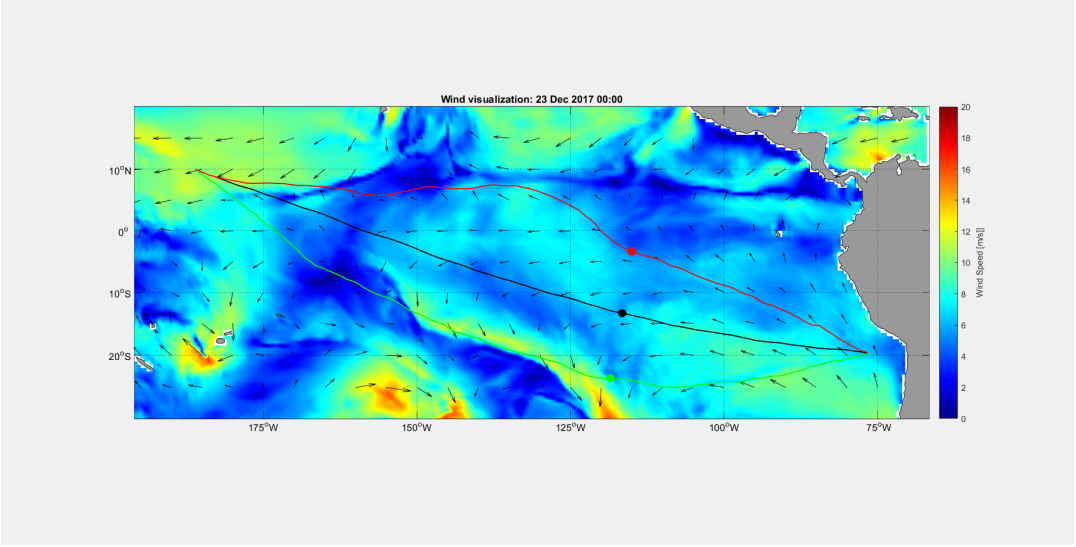

(b) Wind

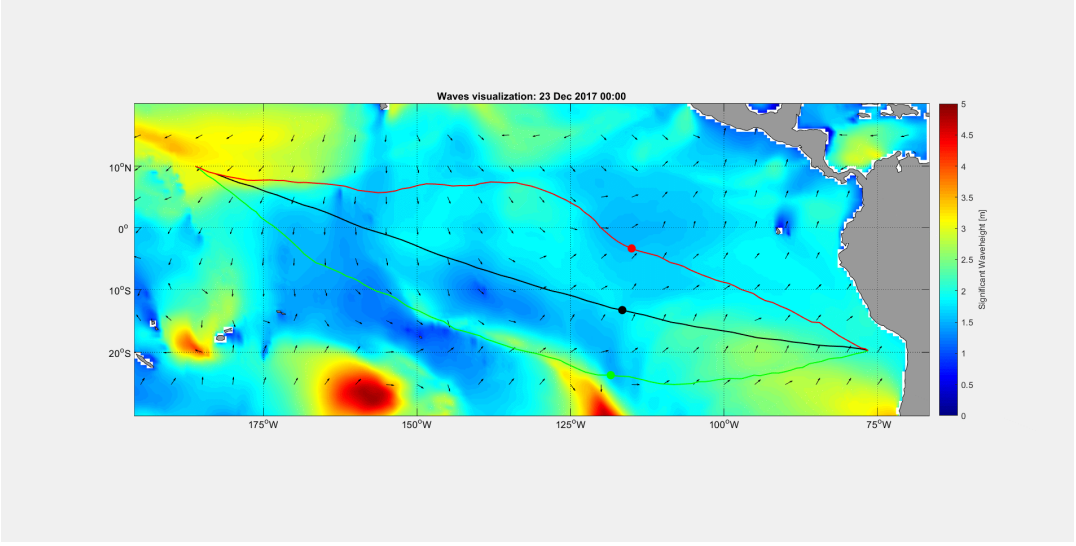

(c) Waves

Figure D.23: Hindcast overview on 23 Dec 2017.

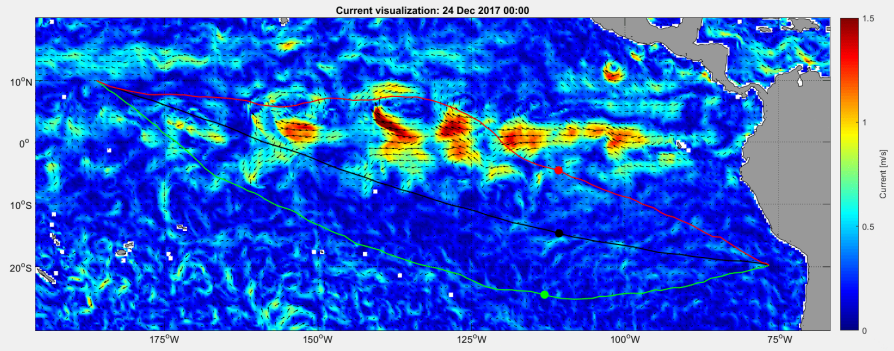

(a) Current

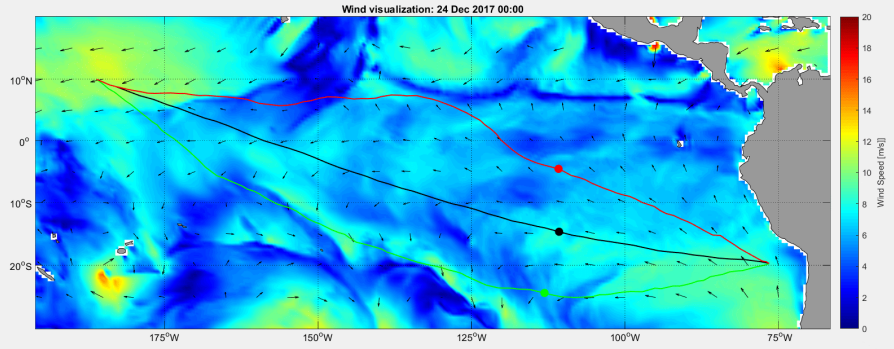

(b) Wind

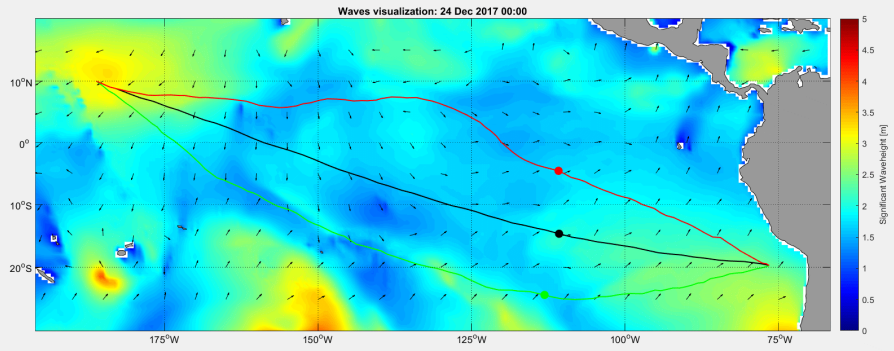

(c) Waves

Figure D.24: Hindcast overview on 24 Dec 2017.

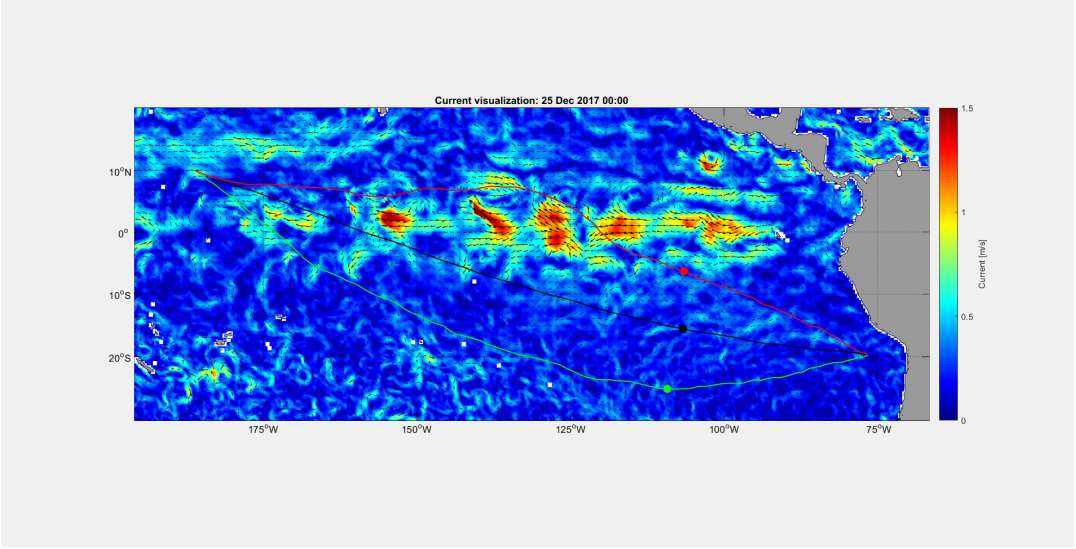

(a) Current

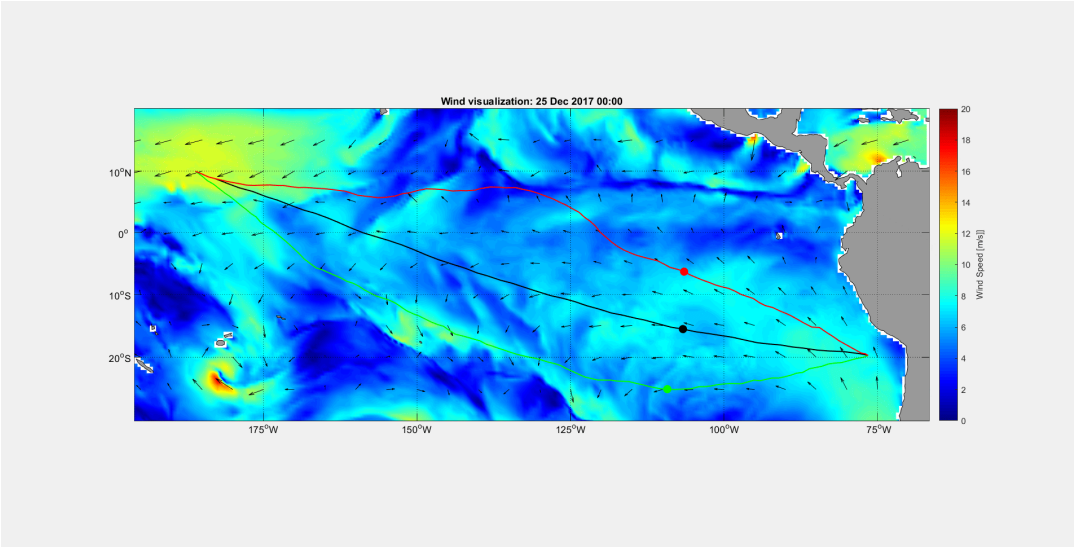

(b) Wind

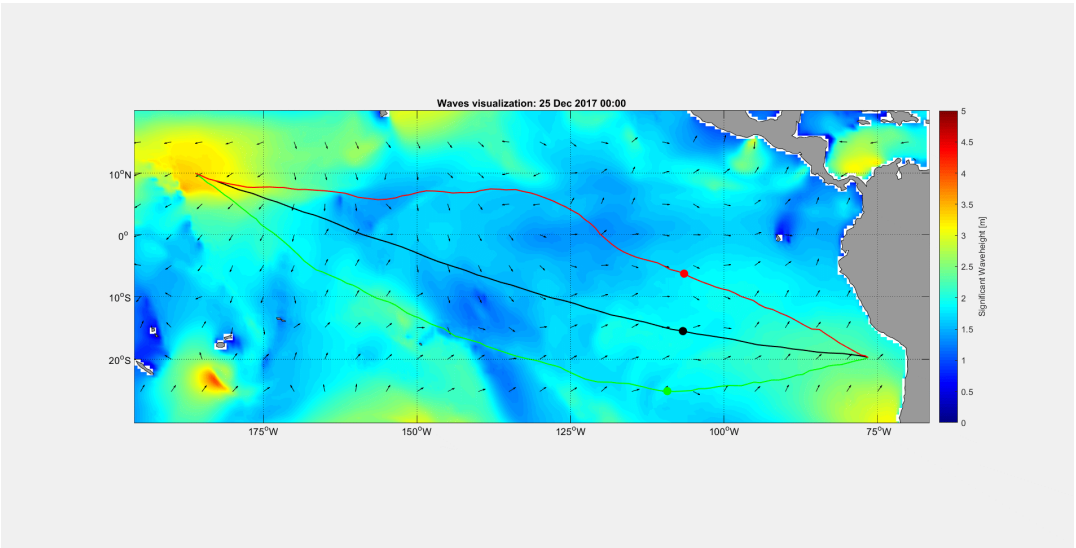

(c) Waves

Figure D.25: Hindcast overview on 25 Dec 2017.

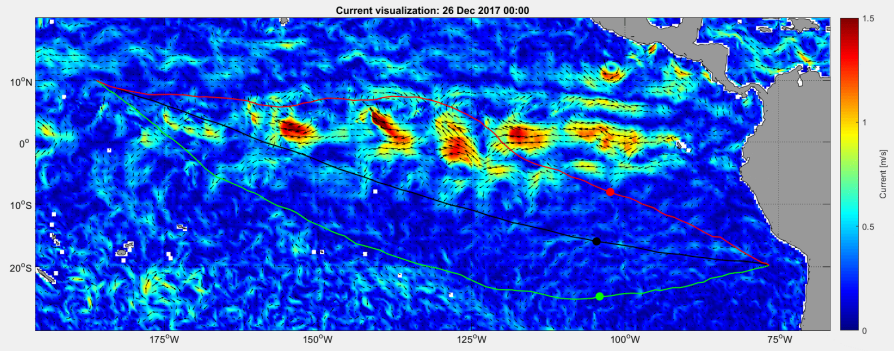

(a) Current

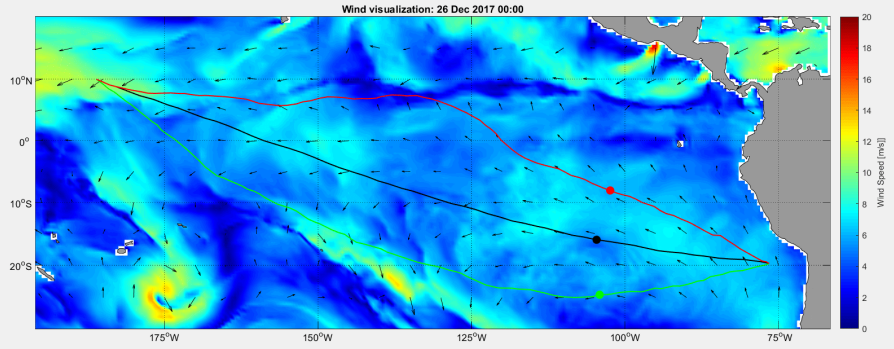

(b) Wind

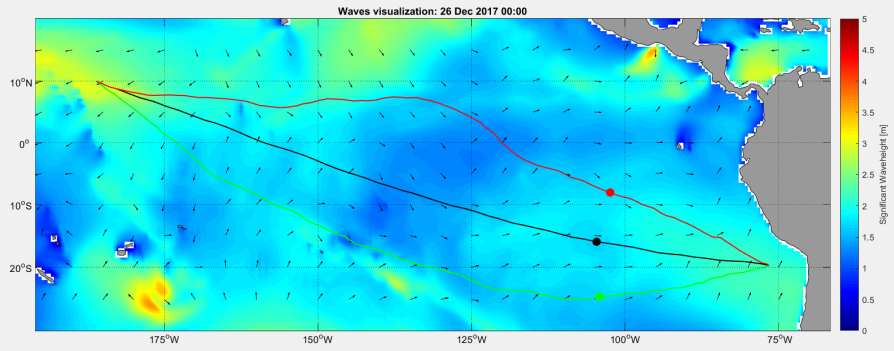

(c) Waves

Figure D.26: Hindcast overview on 26 Dec 2017.

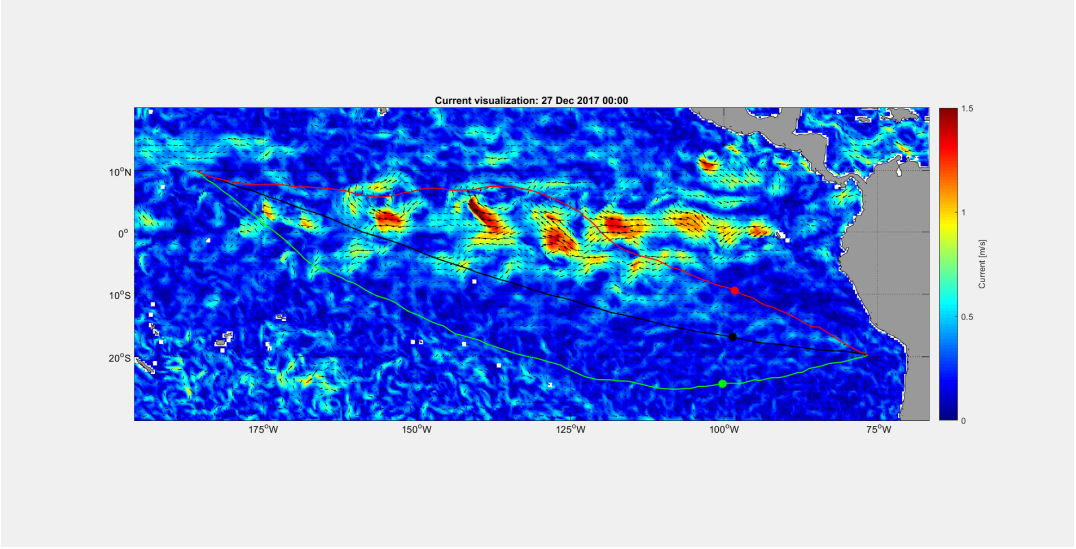

(a) Current

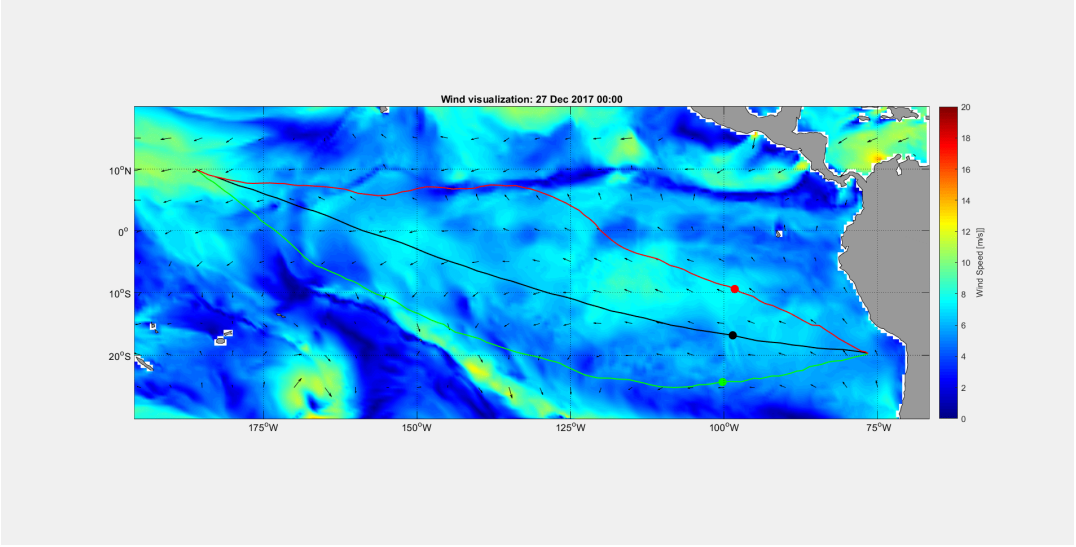

(b) Wind

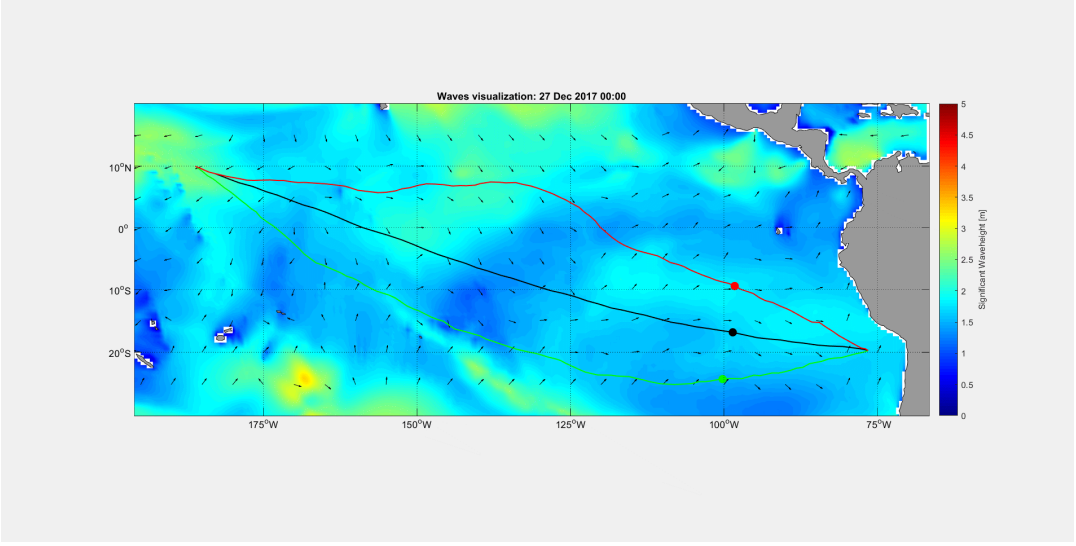

(c) Waves

Figure D.27: Hindcast overview on 27 Dec 2017.

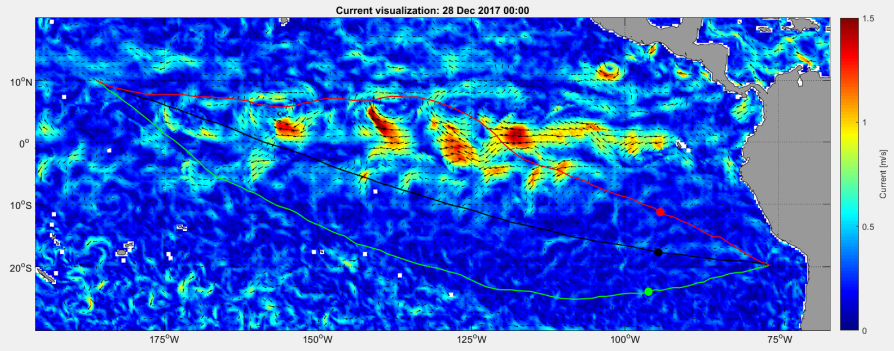

(a) Current

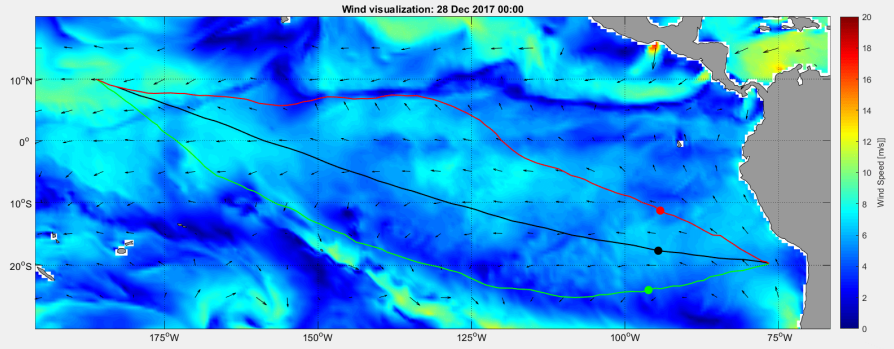

(b) Wind

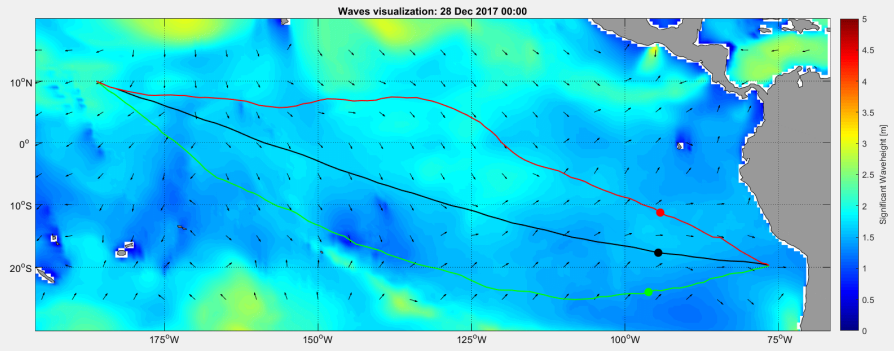

(c) Waves

Figure D.28: Hindcast overview on 28 Dec 2017.

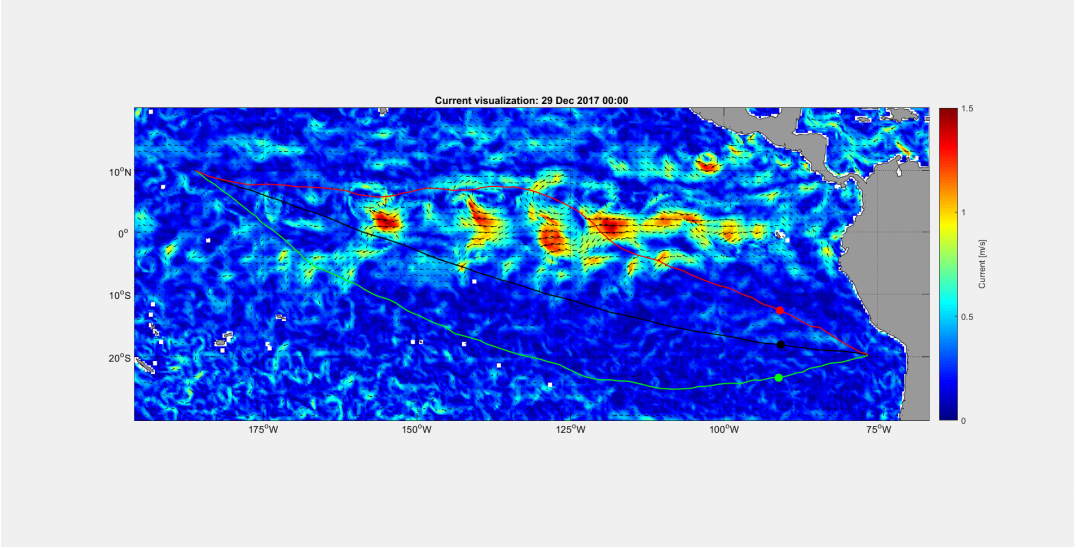

(a) Current

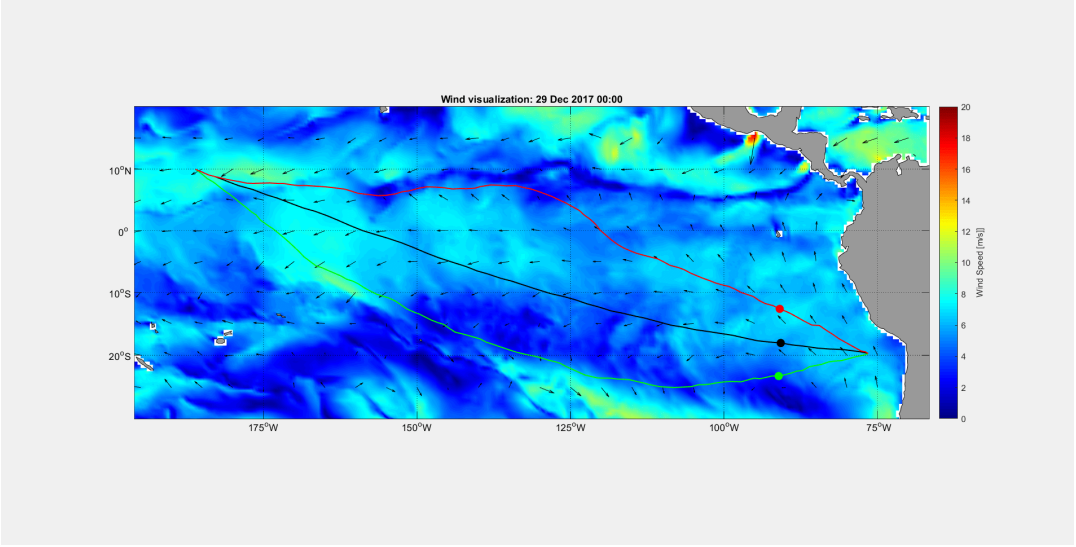

(b) Wind

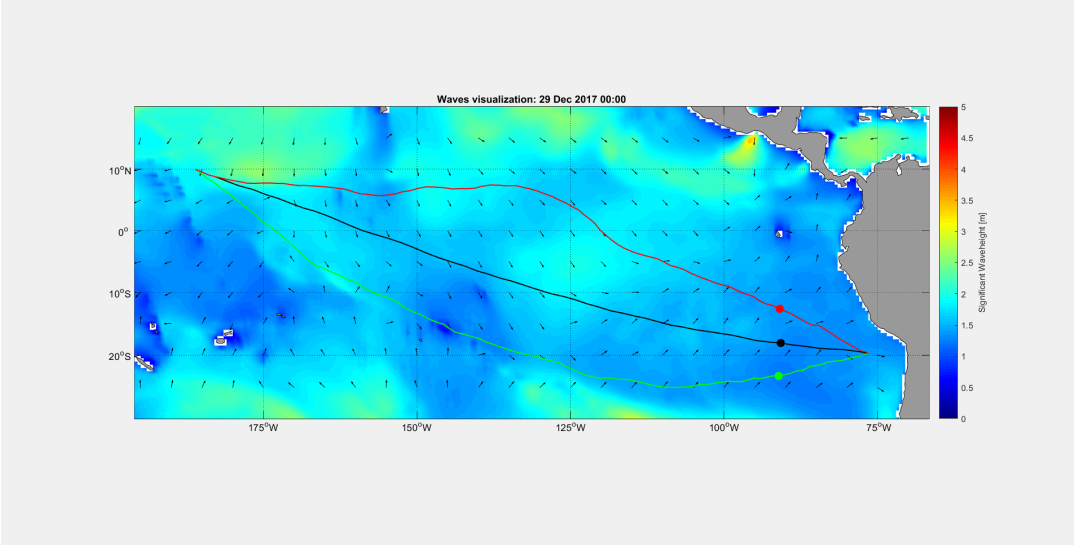

(c) Waves

Figure D.29: Hindcast overview on 29 Dec 2017.

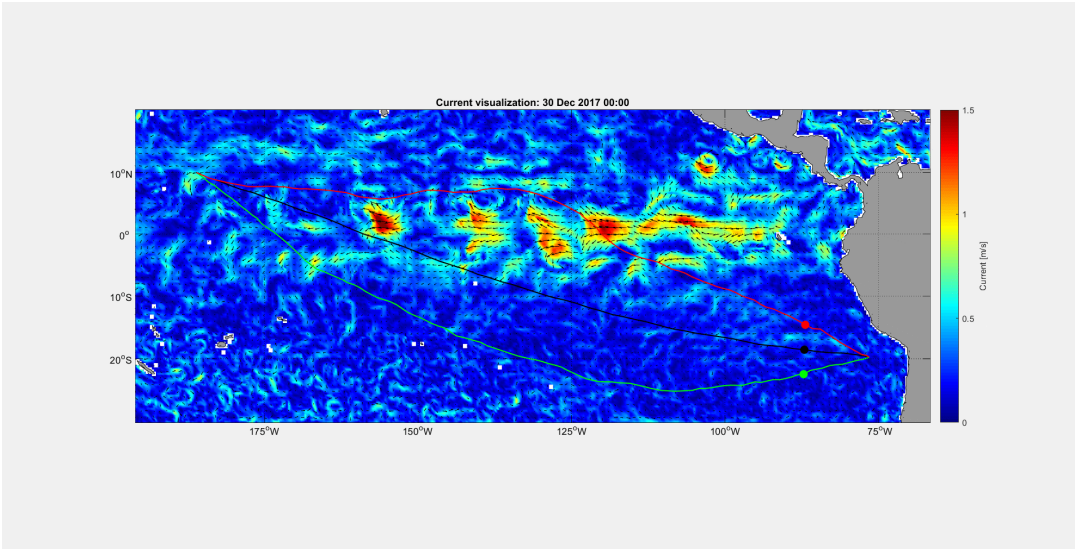

(a) Current

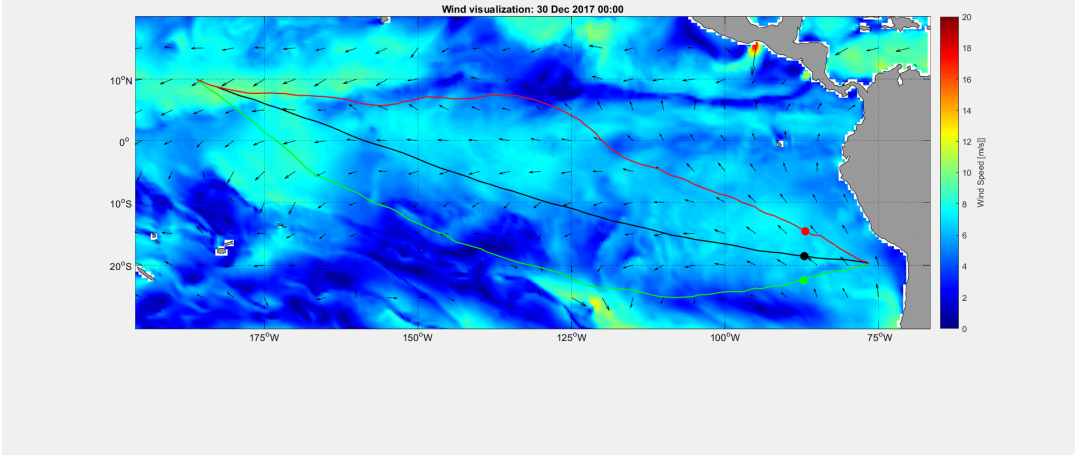

(b) Wind

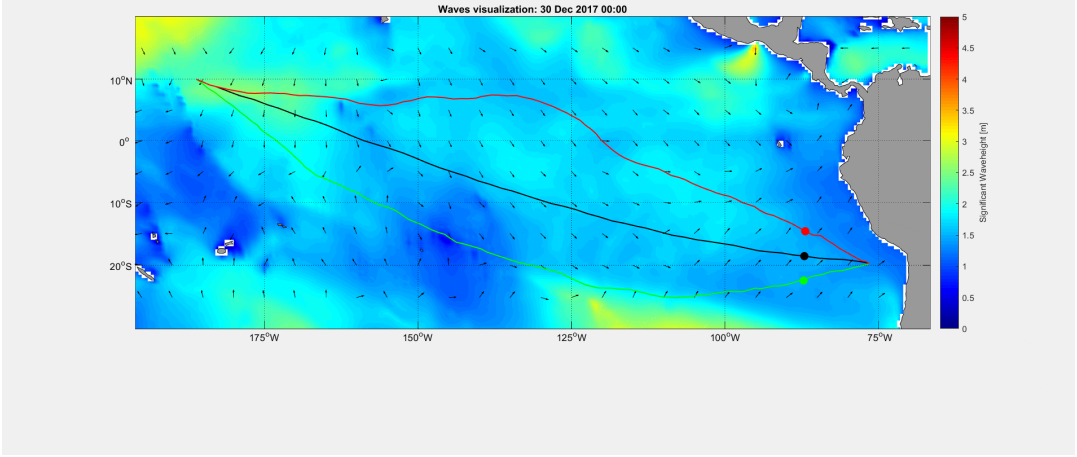

(c) Waves

Figure D.30: Hindcast overview on 30 Dec 2017.

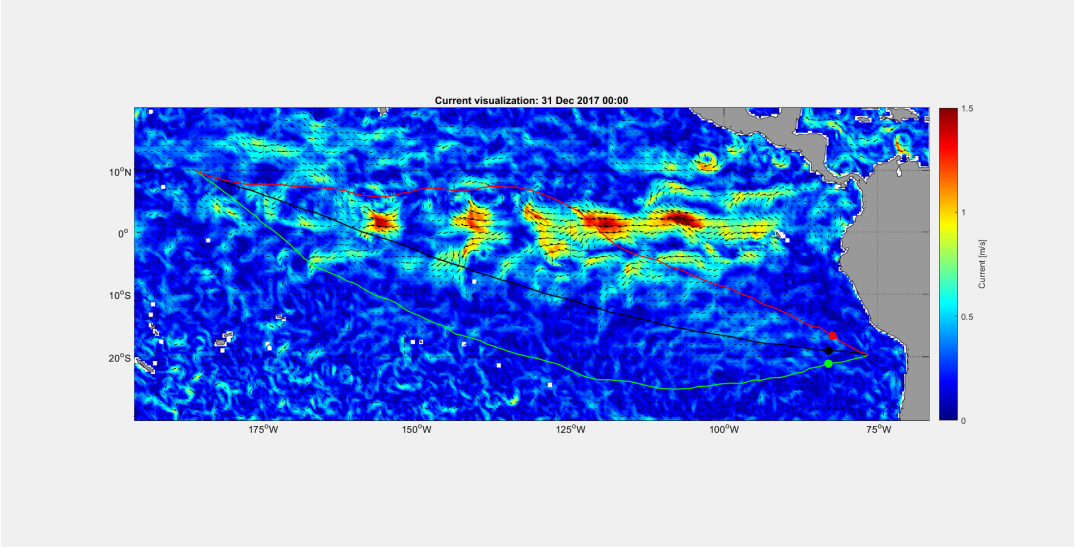

(a) Current

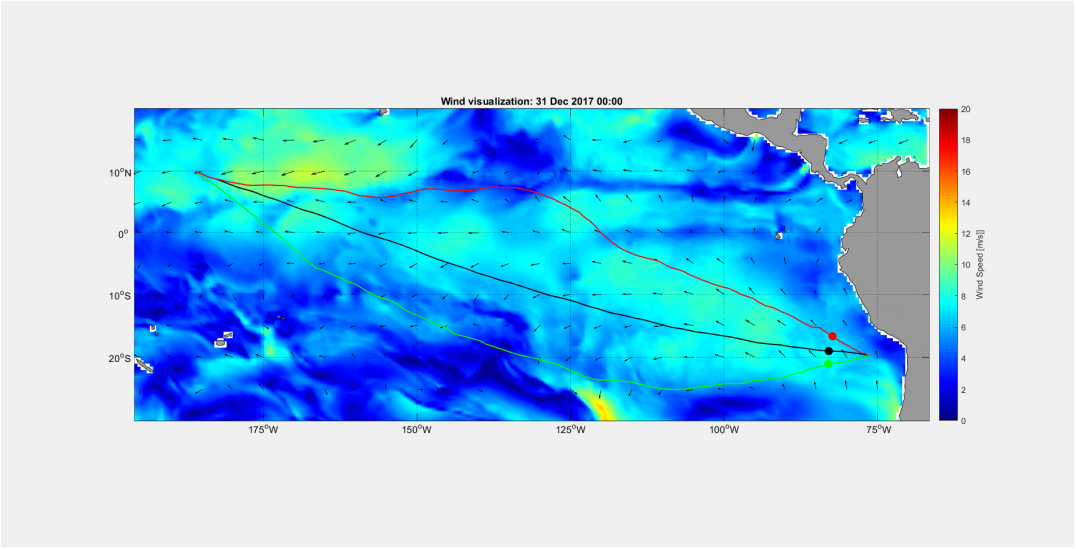

(b) Wind

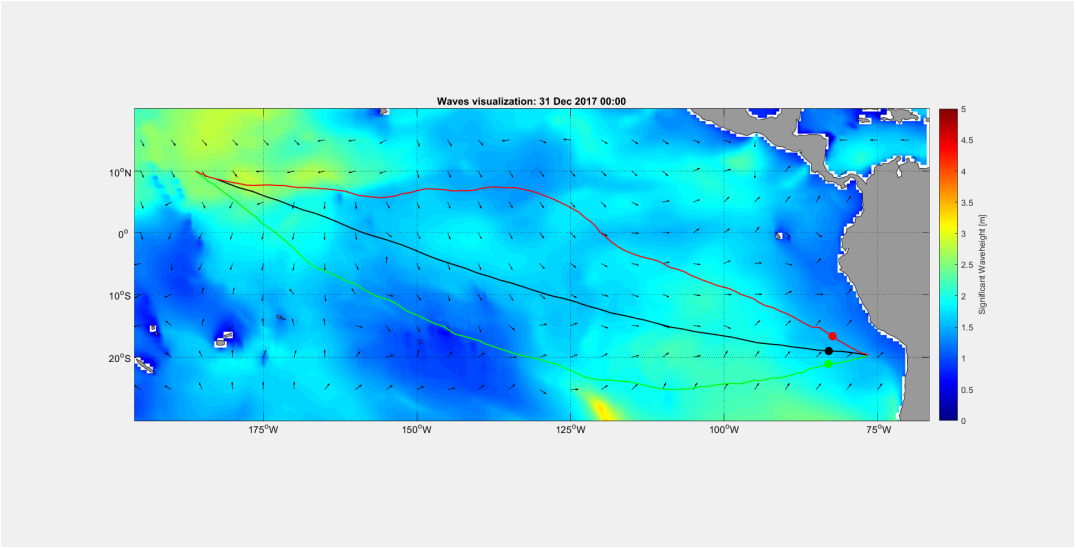

(c) Waves

Figure D.31: Hindcast overview on 31 Dec 2017.

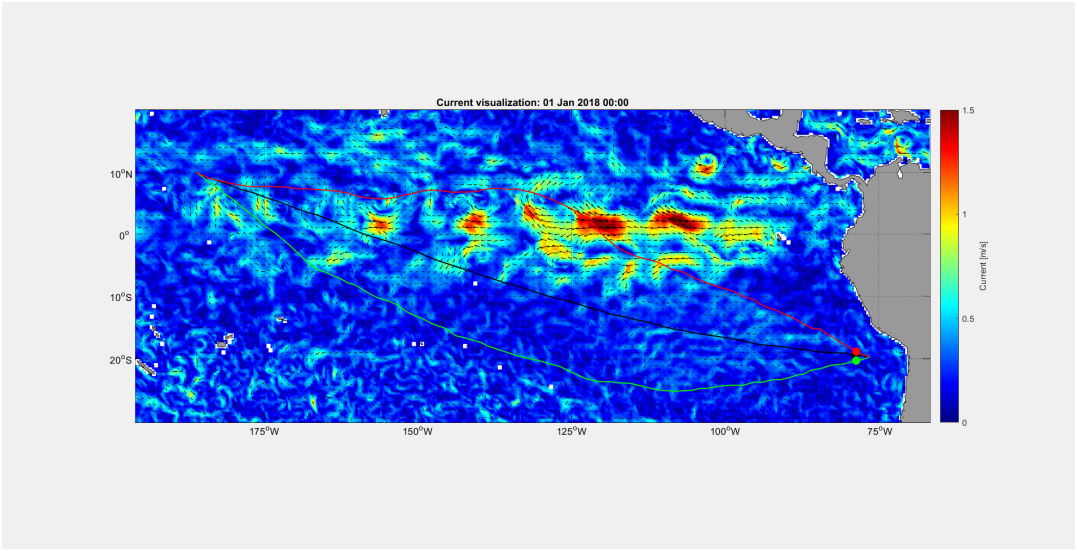

(a) Current

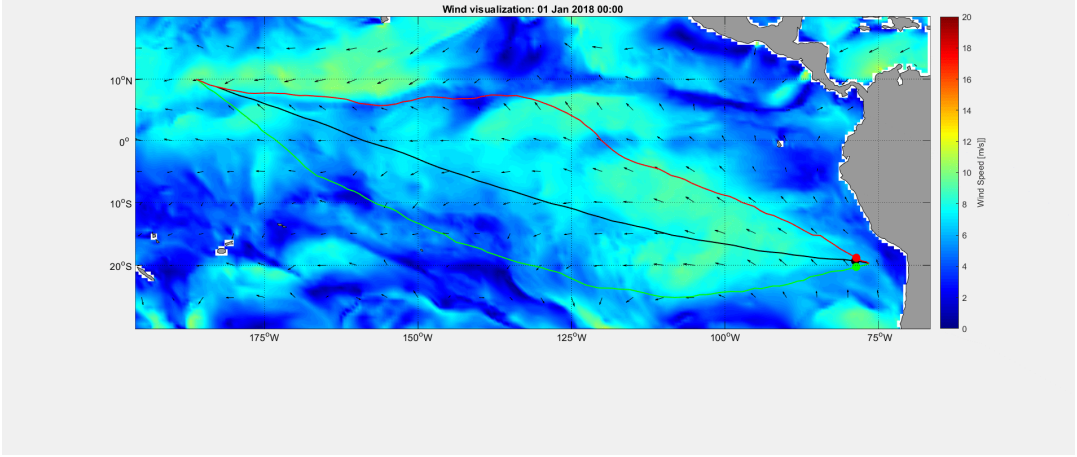

(b) Wind

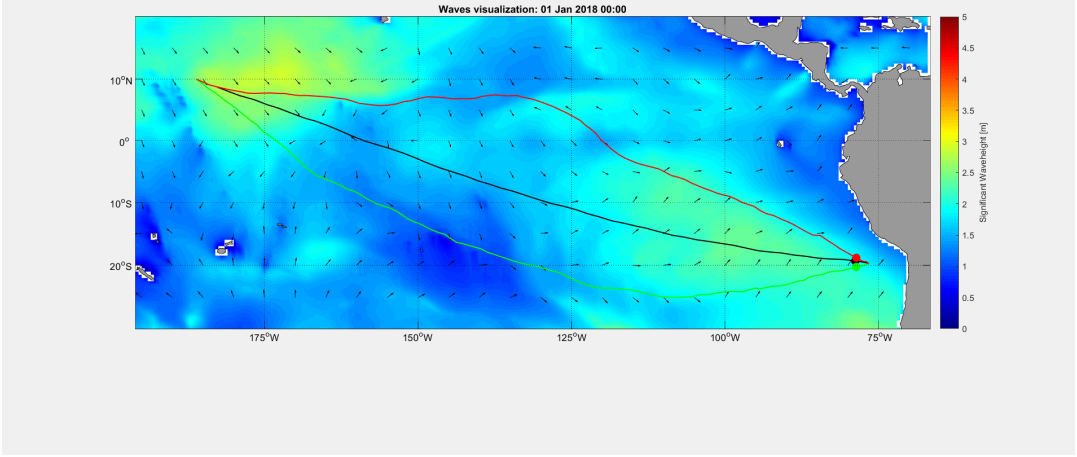

(c) Waves

Figure D.32: Hindcast overview on 01 Jan 2018.

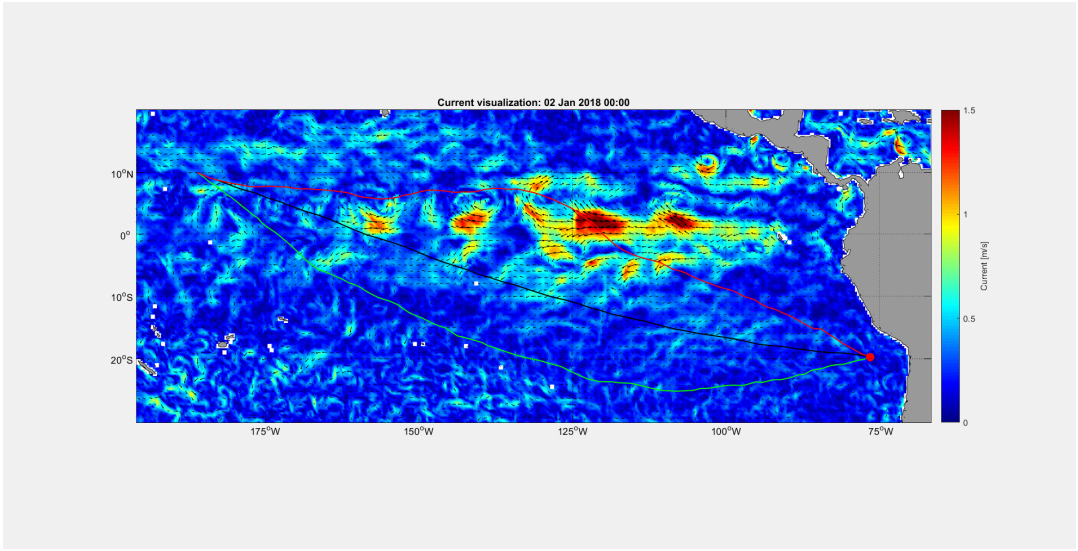

(a) Current

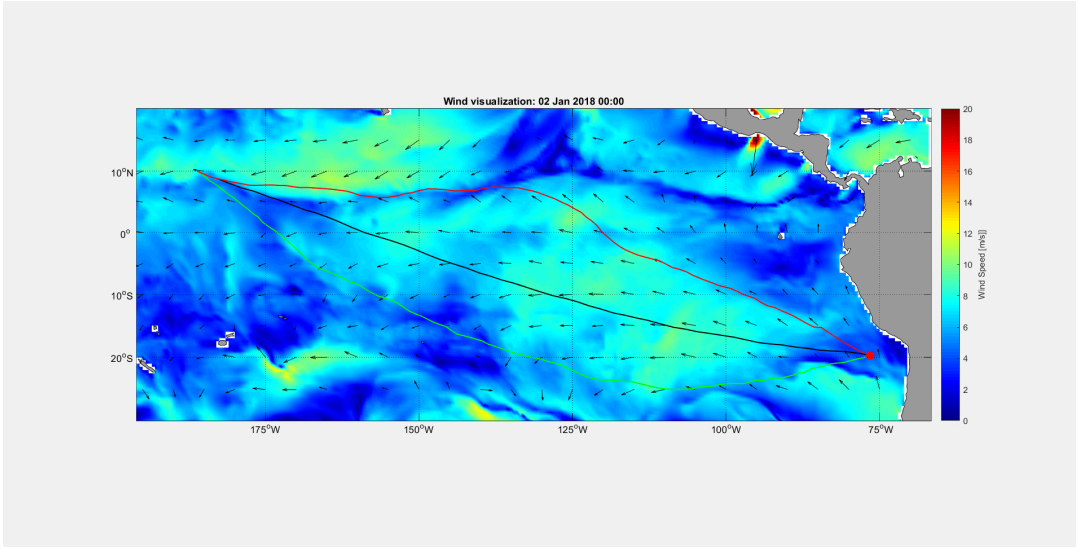

(b) Wind

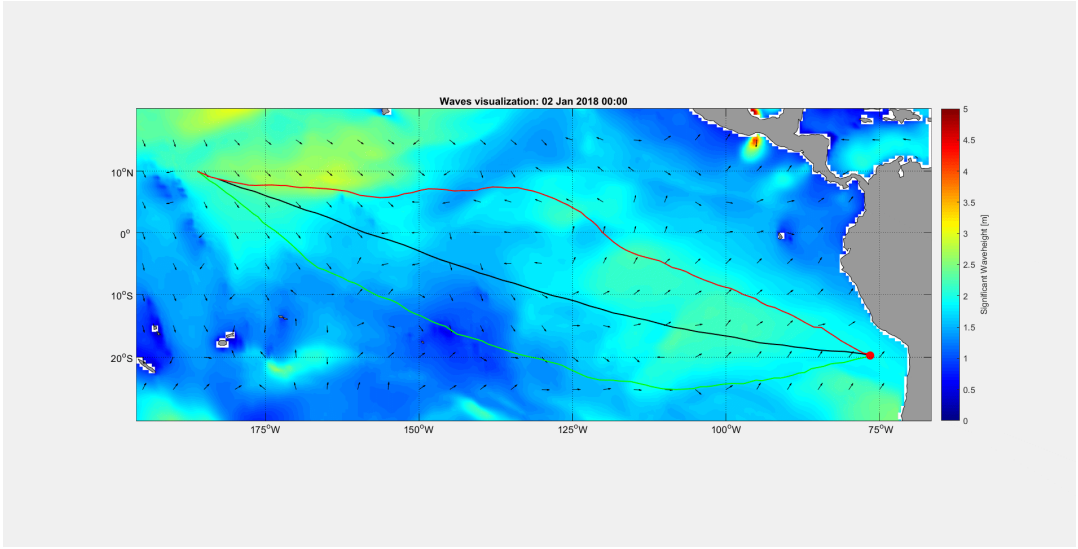

(c) Waves

Figure D.33: Hindcast overview on 02 Jan 2018.

Bibliography

[1] F. Aendekerk. Fleet performance monitoring: Documentation. software, CMB Technologies, 2017.

[2] F. Aendekerk. Fleet performance monitoring (fpm). software, CMB Group, 2017.

[3] F. Aendekerk. Land sea colormap, 2017. https://nl.mathworks.com/matlabcentral/fileexchange/63590-landseacolormap-m- (Accessed on 30/06/2017).

[4] Hossein Arsham and Miodrag Lovric. *Bartlett's Test*, pages 87–88. Springer Berlin Heidelberg, Berlin, Heidelberg, 2011. ISBN 978-3-642-04898-2. doi: 10.1007/978-3-642-04898-2_132. URL `https://doi.org/10.1007/978-3-642-04898-2_132`.

[5] Cygwin Authors. Cygwin version 2.5.2. website, 2017. https://www.cygwin.com/ (Accessed on 02/10/2017).

[6] Z. Bar-Yehuda. Plot google map. https://nl.mathworks.com/matlabcentral/fileexchange/27627-zoharby-plot-google-map (Accessed on: 03/06/2017).

[7] F. Beauducel. GREATCIRCLE and LOXODROME: "As the crow flies" and rhumb line path, distance and bearing. https://nl.mathworks.com/matlabcentral/fileexchange/37652-greatcircle-and-loxodrome—as-the-crow-flies–and-rhumb-line-path–distance-and-bearing (Accessed on 21/09/2017).

[8] R. Bellman. *Dynamic Programming*. Princetom University Press, Princeton, NJ, 1957.

[9] V. Bertram. *Practical Ship Hydrodynamics*, volume 1. Butterworth-Heinmann, 2000. p. 113.

[10] N. Bialystocki and D. Konovessis. On the estimation of ship's fuel consumption and speed curve: A statistical approach. *Journal of Ocean Engineering and Science*, 1:157–166, 2016.

[11] S.J. Bijlsma. *On minimal-time ship routing*. PhD thesis, TU Delft, 1975.

[12] W.E. Bleick and F.D. Faulkner. Minimal-time ship routing. *Journal of Applied Meteorology*, 4:217–221, 1965.

[13] W. Blendermann. Parameter identification of wind loads on ships. *Journal of wind engineering and industrial aerodynamics*, pages 339–351, October 1994.

[14] Roy Campe et al. Cmb staff. Personal interviews.

[15] National Geophysical Data Center. *2-minute Gridded Global Relief Data (ETOPO2) v2*. National Geophysical Data Center, NOAA, 2006. accessed on: 17/06/2017.

[16] E.P. Chassignet, H.E. Hurlburt, et al. U.s. godae: Global ocean prediction with the hybrid coordinate ocean model (hycom). *Oceanography*, 22(2):64–75, 2009.

[17] Companie Maritime Belge. The history of cmb, 2017. https://www.cmb.be/en/history (Accessed on: 07/12/2017).

[18] W. W. Daniel. Hypothesis testing of the difference between two population means, 1999. http://www.kean.edu/ fosborne/bstat/07b2means.html (Accessed on: 04/03/2018).

[19] C. de Wit. Proposal for low cost ocean weather routeing. *Journal of Navigation*, 43(3):428–439, 1990.

[20] E.W. Dijkstra. A note on two problems in connexion with graphs. *Numerische Mathematik*, 1:269–271, 1959.

[21] G.K. Harrell D.R. Lanning et al., editors. *Proceedings of the 2014 ACM Southeast Regional Conference Article No. 30: Dijkstra's Algorithm and Google Maps*, 2014. ACM New York.

[22] W. Ebisuza et al. Wgrib2: Wgrib for grib2 files. software, 02 2017. http://www.cpc.ncep.noaa.gov/products/wesley/wgrib2/index.html (Accessed on 02/10/2017).

[23] R.A. Fisher. *Statistical Methods for Research Workers*. Oliver and Boyd, Edinburgh, 1925.

[24] National Centers for Environmental Protection. Global real-time ocean forecast system, 2017. http://polar.ncep.noaa.gov/global/ (Accessed on 01/10/2017).

[25] Special Committee for Powering Performance Prediction of 25th ITTC 2008. Performance, propulsion 1978 ittc performance prediction method. *ITTC - Recommended Procedures and Guidelines*, (7.5-02.03-01.4), 2008.

[26] P. Frana. An interview with edsger w. dijkstra. *Communications of the ACM*, 53(8):41–47, 2010.

[27] C. Estacio Gomez. Estimacion de la resistencia por el metodo de holtrop y mennen. excel file, 2005. https://www.scribd.com/document/361758248/Metodo-de-Holtrop-Menen (Accessed on: 24/10/2017).

[28] The CMB Group. Mineral nippon. www.cmb.be, 2017. Accessed on: 31/03/2017.

[29] N. Gupta, K. Mangla, et al. Applying dijkstra's algorithm in routing process. *International Journal of New Technology and Research*, 2(5):122–124, 2016.

[30] M.R. Haddara and C. Guedes Soares. Wind loads on maritime structures. *Maritime Structures*, 12(3): 199–209, 1999.

[31] H. Hagiwara. *Weather Routing of (Sail-Assisted) Motor Vessels*. PhD thesis, TU Delft, 1989.

[32] G.J. Haltiner and H.D. Hamilton. Minimal time ship routing. *Journal of Applied Meteorology*, 1:1–7, 1962.

[33] P.E. Hart, N.J. Nilsson, et al. A formal basis for the heuristic determination of minimum cost paths. *IEEE Transactions on Systems Science and Cybernetics*, 4(2):100–107, 1968.

[34] S. Hartjes, T. Hendriks, et al. Contrail mitigation through 3d aircraft trajectory optimization. In *16th AIAA Aviation Technology, Integration, and Operations Conference*, Delft, The Netherlands, 2016. Delft University of Technology.

[35] K.U. Hollenbach. Estimating resistance and propulsion for single-screw and twin-screw ships. *Ship Technology Research*, 45(2), 1998.

[36] J. Holtrop. A statistical re-analysis of resistance and propulsion data. *International Shipbuilding Progress*, 31(363):272–276, 1984.

[37] J. Holtrop and G.G.C. Mennen. A statistical power prediction method. *International Shipbuilding Progress*, 25(290):253–256, 1978.

[38] J. Holtrop and G.G.J. Mennen. An approximate power prediction method. *International Shipbuilding Progress*, 29(335):166–170, 1982.

[39] B. Hooi. Tracing infectious diseases using generic and spatial data. mathesis, Stanford University, 2014.

[40] International Tank Towing Committee. Homepage. website, 2017. www.ittc.info (Accessed on 21/08/2017).

[41] R. Isherwood. Wind resistance of merchant ships. *Transactions of the Royal Institution of Naval Architects*, 114:327–338, 1972.

[42] ISO/. Ship and marine technology speed and power performance by analysis of speed trial data. Technical Report 15016, International Organisation for Standardization, 2015.

[43] ITTC. Full scale measurements, speed and power trials, analysis of speed/power trial data. techreport, ITTC, 2005.

[44] ITTC. Recommended procedures and guidelines - resistance test. techreport 3, ITTC, 2011.

[45] R.W. James. Application of wave forecasts to maritime navigation. Technical report, NAVAL OCEANOGRAPHIC OFFICE NSTL STATION MS, 1957.

[46] D.R. Jones, C.P. Perttunen, et al. Lipschitzian optimization without the lipschitz constant. *Journal of Optimization theory and application*, 79(1):157–181, 1993.

[47] M.B. Klompstra. *Time Aspects in Games and in Optimal Control*. PhD thesis, TU Delft, 1992.

[48] A.J. Kreitner. Heave, pitch and resistance of ships in a seaway. *Transactions of INA*, 1939.

[49] N. Kristensen. Weather routing: Sensitivity to ensemble wind and current input. Master's thesis, University of Oslo, 2010.

[50] W.H. Kruskal and W.A. Wallis. Use of ranks in one-crterion variancec analysis. *Journal of the American Statistical Association*, 47(260):583–621, 1952.

[51] E. Larsson and M.H. Simonsen. Direct weather routing. mathesis, Chalmers University of Technology, 2014.

[52] S. Luo, N. Ma, et al. Evaluation of resistance increase and speed loss of a ship in wind and waves. *Ocean Engineering and Science*, 1(3):212–218, 2016.

[53] G. Mannarini et al. Visir-i: small vessels - least-time nautical routes using wave forecasts. *Geosci. Model Dev.*, 9:1597–1625, 2016.

[54] Marintek. ShipX. software, Marintek, 2017. https://www.sintef.no/en/software/shipx/ (Accessed on 17/08/2017).

[55] Maritime Safety Office. *World Port Index*. NATIONAL GEOSPATIAL-INTELLIGENCE AGENCY, Springfield, Virginia, 26 edition, 2017.

[56] F.J. Massey. The kolmogorov-smirnov test for goodness of fit. *Journal of the American Statistical Aassociation*, 46(253):68–78, 1951.

[57] M.F. Maury. *Physical Geography of the Sea*. Harper & Brothers, 1855.

[58] K. Minsaas. Grunnlag for fartsprognoser [in norwegian]. techreport, Narubtej, Trondheim, Norway, 1982.

[59] NOAA. Oscawr one-third degree current hindcast, . Database access: ftp://podaac-ftp.jpl.nasa.gov/allData/oscar/preview/L4/oscar_third_deg (Latest access: 14/10/2017).

[60] NOAA. Multi_1 wind and wave hindcast, . Database access: ftp://polar.ncep.noaa.gov/pub/history/waves/multi_1/ (Latest access: 09/10/2017).

[61] NOAA. Wavewatch iii, model description, 2016. http://polar.ncep.noaa.gov/waves/wavewatch/ (Accessed on 20/06/2017).

[62] NOAA. Weather forecast database, 2017. http://www.ftp.ncep.noaa.gov/data/nccf/com/rtofs/prod/rtofs.20171001/ (Accessed on 01/10/2017).

[63] noaanews. Noaa completes weather and climate supercomputer upgrades, 2016. http://www.noaanews.noaa.gov/stories2016/011116-noaa-completes-weather-and-climate-supercomputer-upgrades.html (Accessed on: 31/08/2017).

[64] J. Nurmi. Achieving the optimum 'green' level by minimising exhaust emissions. the future of ship design - part 2. deltamarin/journal. *The Naval Architect. RINA*, pages 30–34, 2001.

[65] OCIMF. *Prediction of wind and current loads on VLCCs*. Witherby, London, 1994.

[66] D. Ostrowski et al. Comparative analysis of the algorithms for pathfinding in gps systems. In *The Fourteenth International Conference on Networks*, pages 102–108. The International Academy, Research and Industry Association, 2015.

[67] N.A. Papadakis and A.N. Perakis. Deterministic minimal time vessel routing. *Operations Research*, 38(3): 426–438, 1990.

[68] R. Pawlowicz et al. M_map: A mapping package for matlab, 2014. https://www.eoas.ubc.ca/rich/map.html (Accessed on 20/12/2016).

[69] A. Persson. *User Guide to ECMWF forecast products.* ECMWF, 1.2 edition, 2015.

[70] Q. Gong qnd L.R. Lewis et al. Pseudospectral motion planning for autonomous vehicles. *Journal of Guidance, Control and Dynamics*, 32(3):1039–1045, 2009.

[71] R. Quintana-Diaz. Mt54005 individual research assignment: The cmb group. Technical report, Delft University of Technology, 2017.

[72] A.V. Rao, Benson D.A., et al. Algorithm 902:gpops, a matlab software for solving multiple-phase optimal control problems using the gauss pseudospectral method. *ACM Transactions on Mathematical Software*, 37(2):22.1–2.39, 2010.

[73] H. Raven, A. van der Ploeg, and L. Eca. Towards a cfd-based prediction of ship performance - progress in predicting full-scale resistance and scale effects. Technical report, Maritime Research Institute Netherlands (MARIN), 2008.

[74] B. Schlining. nctoolbox, 2013. https://github.com/nctoolbox/nctoolbox (Accessed on 28/06/2017).

[75] B. Schlining et al. Compatibility with matlab compuler, 10 2016. https://github.com/nctoolbox/nctoolbox/issues/90 (Accessed on 01/10/2017).

[76] Ship&Bunkers. Average bunker prices, 2018. https://shipandbunker.com/prices/av (Accessed on 19/03/2018).

[77] MeteoGroup Shipping. Spos onboard: Ship performance optimisation system. https://www.meteogroup.com/product/spos (Accessed on 22/10/2017).

[78] Propulsion Specialist Committee of 23rd ITTC: Procedures for Resistance and Propeller Open Water Tests. Resistance uncertainty analysis, example for resistance test. *ITTC - Recommended Procedures and Guidelines*, (7.5-02.02-02), 2002.

[79] B. Sridhar, H.K. Ng, et al. Aircraft trajectory optimization and contrails avoidance in the presence of winds. *JOURNAL OF GUIDANCE, CONTROL, AND DYNAMICS*, 34(5):1577–1583, 2011.

[80] K. Subramani. Correctness of dijkstra's algorithm. LCSEE, West Virginia University, Morgantownm WV.

[81] J. Szlapczynska and R. Smierzchalski. Adopted isochrone method improving ship safety in weather routing with evolutionary approach. *International Journal of Reliability*, 14:635–645, 2007.

[82] The MathWorks, Inc. Matlab compiler documentation. https://nl.mathworks.com/products/compiler.html, 2016b.

[83] The MathWorks, Inc. Matlab ginput documentation. https://nl.mathworks.com/help/matlab/ref/ginput.html, 2016b.

[84] The World Bank. Co2 emissions (metric tons per capita), 2014. https://data.worldbank.org/indicator/EN.ATM.CO2E.PC?end=2014&locations=BE&start=1960&view=chart (Accessed on 19/03/2018).

[85] H.L. Tolman. The numerical model wavewatch: a third generation model for the hindcasting of wind waves on tides in shelf seas. Technical Report 89-2, Communications on Hydraulic and Geotechnical Engineering, Delft University of Technology, 1989. ISSN 0169-6548.

[86] H.G. Visser. *Course AE4447 Aircraft Performance Optimization: Foundations of Dynamic Optimization.* TU Delft, 2014. p. 43-139.

[87] S. Wei and P. Zhou. Development of a 3d dynamic programming method for weather routing. *TransNav, the International Journal on Marine Navigation and Safety of Sea Transportation*, 6(1):79–85, 2012. ISSN 2083-6473.

[88] A. Weintrit and T. Neumann, editors. *Methods and algorithms in navigation; marine navigation and safety of sea transportation.* CRC Press, 2nd edition, 2011. p. 182.